Ross Burdis, MEng.

BIOFABRICATION STRATEGIES TO GUIDE THE SELF-ORGANISATION OF BIOMIMETIC CARTILAGE AND OSTEOCHONDRAL TISSUES

Trinity College Dublin, March 2021

A thesis submitted to the University of Dublin in partial fulfilment of the requirements for the degree of

Doctor in Philosophy

Supervisor: Prof. Daniel J. Kelly

Internal Examiner: Prof. Conor T. Buckley

External Examiner: Prof. Tim Woodfield

Declaration

I declare that this thesis has not been submitted as an exercise for a degree at this or any other university and it is entirely my own work.

I agree to deposit this thesis in the University's open access institutional repository or allow the library to do so on my behalf, subject to Irish Copyright Legislation and Trinity College Library conditions of use and acknowledgement.

Ross Burdis

Dublin, March 31st, 2021

Summary

Current clinically available treatments for synovial joint damage fail to promote functional tissue regeneration. To date, the only treatment strategy which consistently results in a hyaline cartilage repair involves autologous transplantation of osteochondral plugs from a non-load bearing site. As such, it offers superior clinical outcomes compared to other approaches, but is associated with donor-site complications. Tissue engineering has long sought to fill the clinical need for an effective treatment strategy for damaged or diseased synovial joints. However, despite sustained efforts, traditional tissue engineering approaches have failed to produce implants that recapitulate the complex compositional and structural features of osteochondral tissues. Scaffold-free approaches in tissue engineering seek to mimic processes that occur during native tissue development to create more biomimetic grafts. This includes the use of cellular aggregates, microtissues and organoids as 'biological building blocks' for the engineering of more complex tissues and organs. The use of modular tissue-units offers many advantages over traditional approaches, including scalability and the capacity to individually optimise the constituent cellular/tissue-units. To engineer anatomically accurate tissues of scale suitable for tissue engineering and regenerative medicine applications, novel bioprinting modalities can be used to spatially pattern such biological building blocks and direct how cellular condensations or microtissues fuse and self-organise. With this in mind, the overall aim of this thesis was to leverage novel biofabrication and bioprinting strategies to direct cellular self-organisation towards the engineering of biomimetic osteochondral tissue analogues at a clinically relevant scale.

To achieve this objective, chapter 3 of this thesis investigated novel methods for generating numerous cell-aggregates and microtissues. A hydrogel microwell platform, which represented an ideal medium-high throughput technology suited to spheroid biofabrication at a clinically relevant scale, was developed. As such, it underpinned future studies which aimed to optimise the microtissue building blocks and apply them as a means of engineering a larger macro-tissue. Within this work, the capacity to form various spheroid phenotypes was also demonstrated. Specifically, cartilage microtissues and vascular spheroids were generated using the same microwell system by varying the cell type used. Both spheroid phenotypes were shown to be 'functional' after biofabrication and harvesting. In this context, functionality was demonstrated by the cartilage microtissues fusing to form a unified macro-tissue, or by endothelial sprouting between adjacent vascular spheroids to create pervasive microvascular networks. These preliminary proofs-of-principle studies supported the hypothesis that spheroids can be used to generate precursor tissues for organs of the musculoskeletal system. Within chapter 3, a novel stirred-tank bioreactor was also designed and fabricated with a view to develop a more scalable process. Efforts to generate cartilage microtissues in dynamic conditions

were less successful, resulting in the suppression of chondrogenesis and an osteogenic phenotype within dynamically cultivated microtissues. In spite of this, the bioreactor functioned properly and could represent an effective method for generating bone microtissues.

As previously discussed, bioprinting offers a means of precisely depositing biologics during biofabrication. Consequently, bioprinting has been employed to try to impart spatial organisation to engineered cartilages. In chapter 4, bioprinting was investigated as a method of depositing progenitor cells into an environment designed to guide self-organisation towards the generation of a stratified articular cartilage. After bioprinting, the progenitor cells formed high-density condensations within a polymer framework. During chondrogenic cultivation, these condensations self-organised into a highly biomimetic articular cartilage, guided by the boundary conditions proved by the supporting framework. The quality of this engineered cartilage could be enhanced further by culturing in dynamic conditions. Here, bioreactor culture resulted in near-native levels of cartilaginous matrix deposition and anisotropic organisation of the collagen network. This work established a strategy to bioprint biomimetic articular cartilage, *via* self-organisation of mesenchymal progenitor cells, within an instructive novel joint fixation device.

In chapter 5, hydrocortisone was identified as a factor, within endothelial growth media (EGM), capable of inducing a potent improvement in the chondrogenic potential of heterogeneous mesenchymal stem/stromal cells (MSCs) populations. Using the hydrogel microwell platform, EGM/hydrocortisone was shown to significantly improve the initial aggregation of MSCs and subsequent matrix accumulation within cartilage microtissues. This work directly impacts scaffold-free tissue engineering as reliable MSC chondrogenesis and the deposition of a substantial extracellular matrix (ECM) is essential to form tissues of scale. The findings of this chapter also impact the broader field of tissue engineering, as modifications to existing MSC chondrogenic induction protocols which enhance the quality of engineered cartilages could increase their clinical impact.

Generating scaffold-free cartilages at a clinically relevant scale can be challenging. Furthermore, current fixation method for securing engineered cartilage *in situ* do not provide an ideal solution and failures and complications are not uncommon. As such, chapter 6 demonstrated that a thick and homogenous stable cartilage macro-tissue could be bioassembled *via* the spontaneous self-organisation of early-cartilage microtissues. This engineered cartilage exhibited promising biochemical and mechanical properties and, by using a hybrid approach, could exhibit collagen fibre orientation that mimicked native articular cartilage. The efficacy of this engineered tissue as a treatment for focal chondral lesions was evaluated in a large animal preclinical defect model. Here, implantation of the self-organised cartilage, using the novel fixation device developed in chapter 4, did not result in a significant improvement in healing compared with an existing treatment modality.

Nevertheless, histological evidence from chapter 6 indicated that defect stabilisation and, in particular, regeneration of the subchondral bone are fundamental to successfully resurfacing injured synovial joints. As such, it was hypothesised that an osteochondral strategy could be an effective fixation method and improve the therapeutic impact of the self-organised cartilage. Chapter 7 investigated using developmentally inspired cartilage microtissues as organ-seeds for the biofabrication of a biphasic osteochondral implant. Two phenotypically distinct cartilage microtissue populations were bioassembled into a single implant; firstly a layer of stable articular surface and secondly an underlying osseous region consisting of islands of hypertrophic cartilage microtissues as precursors for bone formation. Treatment of clinically relevant osteochondral defects using this engineered implant resulted in immediate joint resurfacing, and after 6 months the restoration of a near-normal articular surface.

In conclusion, this thesis explores two overarching biofabrication strategies for engineering osteochondral tissues. By integrating novel biofabrication techniques and existing bioprinting methods, this work has demonstrated the capacity to guide self-organisation towards the formation of biomimetic, spatially organised engineered cartilage at a clinically relevant scale. Additionally, the capacity to leverage modular biofabrication approaches to generate developmentally inspired implants has been demonstrated. The therapeutic efficacy of such approaches suggests that such approaches are poised to make a significant clinical impact for the treatment of damaged and diseased synovial joints.

Contents

Chapter 1.
1 Introduction

1.1 The Clinical Problem

Hyaline cartilage is the highly specialised connective tissue found at the articulating surfaces of all long bones [1]. It exhibits a biochemical composition and structural hierarchy which relate directly to its unique biomechanical properties and function [2–5]. Healthy articular cartilage exists as part of a functional unit with subchondral bone, whereby the intimate contact between the two tissues forms the osteochondral junction [6]. Understanding of this complex interface is constantly evolving, and contact between un-calcified cartilage and subchondral bone, as well as direct transport pathways between vascular channels from the subchondral bone into the calcified cartilage, are now known to exist [7,8]. This mounting evidence of cross-talk between the two tissues of the osteochondral unit suggests that subchondral bone plays a central role in the homeostasis of normal articular cartilage, and damage induced changes in the subchondral bone can contribute significantly to the multifactorial progression of joint degeneration [9–17]. As such, many now consider that to fully treat damaged and disease to the articular cartilage also requires consideration of the entire osteochondral unit [10,12,18]. Therefore, excessive disruption of the subchondral bone plate during surgical intervention must also be carefully considered, from mechanical [19], and biological [10,11,20] standpoints, to avoid creating a degenerative state. Conflicting evidence relating to the most effective method for treating chondral and osteochondral lesions means that future treatment strategies must be carefully designed to consider the complexity of the osteochondral unit, and maximise their therapeutic potential.

Currently, early clinical treatments for damage to the articular surface fail to provide a complete solution. In general, common therapeutic strategies such as microfracture and autologous chondrocyte implantation (ACI) result in a mechanically inferior fibrocartilage repair tissue, which limits its longevity and associated clinical outcomes [21–24]. To date, autologous osteochondral transplantation (AOT) is the only treatment that results in a hyaline cartilage repair tissue. As such, it has been shown to outperform aforementioned clinical joint repair strategies [24,25]. However, it requires donor tissue and involves the creation of additional defects [26]. With this in mind, there is an urgent need for novel early treatment strategies that can provide effective joint resurfacing *via* a hyaline cartilage repair tissue and prevent the cascade of deleterious event associated with early joint damage and the progression of osteoarthritis.

1.2 Developmentally Inspired Musculoskeletal Tissue Engineering

Tissue engineering (TE) aims to regenerate a tissues or organs, which have lost functionality due to damage or disease. Despite sustained efforts, in the context of musculoskeletal TE, traditional approaches have failed to recapitulate the structure, composition and functional properties of the target tissue. In particular, engineering articular cartilage *in vitro* with a native-like organisation has been difficult. Numerous attempts have been made to encourage the formation of a stratified cartilage using 'top-down' TE that have involved heterogeneous cell populations [27], biochemical and mechanical gradients [28,29], multi-layered instructive scaffolds [30–32], modulation of environmental gradients [33], as well as mechanical stimulation [34]. More recently, rapid developments in additive manufacturing technologies has given rise to bioprinting, which gives user-defined control over the positioning of cells, biomaterials and biologics [35,36]. As such, bioprinting has been proposed as a method of imparting spatial organisation during biofabrication and yield a more biomimetic engineered cartilage [37,38]. Although bioprinting has been successfully employed to recreate some of the zonal features seen in native articular cartilage [39–41], complete recapitulation of many structural features, including the 'Benninghoff' arcade-like collagen structures, which are crucial to AC's function remain elusive. This may be due to the use of supporting hydrogel bioink in many bioprinting strategies, which can limit the capacity of cells to interact and (re)model the engineered tissue. In light of this, scaffold-free approaches have emerged as a branch of developmental engineering (DE) in which key processes that take place during the target tissues native development are re-enacted *in vitro*, as a means of generating highly-biomimetic engineered constructs [42].

Whilst scaffold-free approaches have been used to successfully engineer stable cartilage [43–51], bone-precursor [52–55], and bony tissues [56–60], they are not without their limitations. Specifically, in the absence of a 'bulking' biomaterial, such strategies are inherently difficult to scale and require large numbers of progenitor cells. Nutrient transfer limitations can also impede the development of highly-cellular constructs [61,62], which has motivated further investigations into first engineering scaled-down, micro-sized scaffold-free cell or tissue units, which are later used as 'biological building blocks' for the engineering of larger tissues. Aggregate engineering is one example of this model [63]. Here, the building blocks are typically spherical (spheroids) and can be broadly characterised into: 1) cellular aggregates, which are a condensation of undifferentiated stem or progenitor cells, 2) microtissues, where the body of cells has been driven towards a specific phenotype by exposure to differentiating factors, and 3) organoids, which are typically generated using embryonic stem cells (ESCs) or induced pluripotent stem cells (iPSCs) capable of forming complex, functional, and multi-layered tissues that closely mirror the structures and arrangements found in native organs. Collectively, spheroidal systems maintain the potent biological advantages associated

with scaffold-free approaches [64–67]. To date, such approaches have been used to heal large bone defects [54], engineer mechanically competent human cartilage [68], and treat osteochondral lesions [69]. Importantly, they are also amenable to high-throughput biofabrication [70–72] and have been discussed as organ seeds within modular bioassembly strategies, which include bioprinting, for organogenesis [73–77]. As such, aggregate engineering could offer a route towards engineering highly-biomimetic osteochondral tissues at a clinically relevant scale. Furthermore, implantation of these grafts could address the current clinical need for treatment strategies which restore the articular surface of synovial joints with a hyaline repair tissue.

1.3 Thesis Objectives

Emerging self-organisation strategies have the potential to overcome many of the challenges that have faced engineering biomimetic osteochondral tissues. Specifically, mirroring key events that occur during embryonic and postnatal development has been proven as a potent method for creating near-native cartilage *in vitro*. Despite this relative success, clinical translation of many developmentally inspired approaches is limited. There are numerous reasons for this, including the challenge of engineering tissues at a clinically-relevant scale and designing biofabrication strategies suited to realising clinical translation of promising *in vitro* tissues. Furthermore, the most effective strategy (chondral only versus osteochondral) for treating early joint disease and damage remains unclear. As such, the overarching objective of this thesis was to explore two approaches, namely 1) directed self-organisation and 2) microtissues as biological building blocks, for engineering scalable chondral and osteochondral tissues for the treatment of critically-sized chondral and osteochondral defects. To realise this goal, this thesis will address the following aims:

1.3.1 Aim 1: Design and validate novel methods for the biofabrication of cell-aggregates and microtissues

Novel methods for spheroid formation and cultivation will be developed as part of designing an effective engineering strategy for the biofabrication of (osteo)chondral tissues using these microtissues as biological building blocks. Specifically, a hydrogel microwell system intended as an ideal platform for the biofabrication of microtissues will be designed and validated in chapter 3. Additionally, an in-house stirred-bioreactor will be evaluated as a means of enhancing the cultivation of cartilage microtissues with a view to develop a more scalable process.

1.3.2 Aim 2: Engineer a highly biomimetic articular cartilage via directed self-organisation

Guiding the self-organisation process has been shown to direct stratification within a developing cartilage [41,78]. However, properly recreating the complex zonal-architecture of the collagen network seen within native articular cartilage remains elusive. As such, chapter 4 investigates if coupling a novel scaffold assembly with inkjet bioprinting can direct the self-organisation of MSCs

towards a highly-biomimetic cartilage. In particular, this study will aim to capture features of native cartilage, such as the 'Benninghoff' collagen arcades, rarely reported in literature and establish a method for bioprinting truly biomimetic articular cartilage.

1.3.3 Aim 3: Engineer high-quality cartilage microtissues in a medium-high throughput fashion

Whilst DE can be an effective strategy for creating biomimetic tissues, the absence of an interstitial scaffold or hydrogel places an onus on the cell's capacity to synthesise large quantities of extracellular matrix to generate tissues of scale. As such, methods which consistently produce high-quality cartilage microtissues could aid the scalability of such strategies. Based on a serendipitous discovery that Endothelial Growth Medium (EGM) enhanced mesenchymal stem/stromal cell (MSC) aggregation and chondrogenic capacity in animal derived MSCs, chapter 5 seeks to leverage this finding to develop a simple method for improving the chondrogenic capacity of heterogeneous MSC populations. In particular, this study aims to elucidate the driving factor(s) within EGM, and implement the factor(s) as a means of improving current chondrogenic culture regimes and generating high-quality cartilage microtissues.

1.3.4 Aim 4: Evaluate the efficacy of articular cartilage engineered using microtissues as a treatment for focal chondral lesions

Biofabrication of a stable cartilage using numerous cartilage microtissues as biological building blocks could be a way of treating focal cartilage defects. However, implantation of such self-organised cartilages can be challenging. To this end, chapter 6 first aims to evaluate if a stable cartilage can be generated *via* the spontaneous self-organisation of early-cartilage microtissues. This chapter will also explore the capacity of such engineered tissue to regenerate focal cartilage defects, using a novel implant developed in chapter 4 as a means of fixation within the synovial joint. The efficacy of this approach will be assessed using a large-animal preclinical model of focal chondral defects.

1.3.5 Aim 5: Assess a developmentally inspired osteochondral implant as a means of resurfacing articular joints

Emerging evidence suggests that developmentally inspired approaches are an effective method for forming bony and cartilaginous tissues. However, generating phenotypically distinct tissues within a monolithic implant can be challenging. As such, modular biofabrication approaches such as microtissue engineering, could offer a means of creating biphasic implants by combining two separately cultivated microtissue populations. Chapter 7 will explore the possibility to use the microwell platform to cultivate phenotypically distinct cartilage populations. Additionally, *via* novel bioassembly methods these tissue-specific populations will be combined into a single implant

intended for osteochondral repair. The efficacy of the engineered implant will be tested in a large-animal preclinical model for osteochondral lesions.

Chapter 2.
2 Literature Review

2.1 Introduction

The overarching goal of tissue engineering (TE) is the complete regeneration of a tissue or organ whose function has been impaired by injury or disease. Early failures in the field of TE has motivated increased interest in mimicking the natural processes that regulate cell fate and tissue development. This process, often termed developmental engineering [79,80], aims to recapitulate key features of the different stages of normal development as a means of engineering tissues or organs with biomimetic composition, structure and function. Developmental engineering looks to move away from some of the early concepts associated with the 'tissue engineering triad', which centred around the selection of cell type, soluble morphogens, and a scaffold substrate to control *in vitro* tissue formation. Here, the quality of the engineered tissue ultimately depends on the aptness of these three selected components, however due to their strong interdependence, altering one component of the triad commonly influences the effectiveness of the other components. Consequently, this approach tends to initiate a perpetual cycle of empirical attempts to find an adequate solution [79]. Instead, developmental engineering commonly focuses on the use of 'scaffold-free' systems, shifting the aim towards creating precursor tissues *in vitro* that are primed to follow a concerted progression *in vivo,* resulting in restoration through recapitulation of the target tissues native developmental programme.

Without a scaffold material, developmentally inspired TE seeks to leverage the cell's own ability to synthesis a biomimetic extracellular matrix (ECM) under the direction of appropriate exogenous cues – both soluble factors and biophysical signals generated by cell-cell and cell-ECM interactions. These biological processes typically involve cell condensation, proliferation, differentiation, matrix production and tissue maturation [42]. The principles of cellular self-assembly and self-organisation underpin scaffold-free approaches in TE. The former has been defined as a system in which order results from disorder in a spontaneous manner, without the introduction of external force or energy, resulting in a closed system [81]. In contrast, self-organisation can be defined as a process in which order appears as a result of external energy or forces being input into the system [81]. In the context of TE, the spontaneous arrangement of cells *via* cell-to-cell interactions as a means of minimising free energy is considered self-assembly. Typically, this process involves a non-adherent substrate, and a sequential set of phases that closely mirror native tissue formation. Self-organisation approaches include cell aggregate engineering where external forces generated by centrifugation is used to facilitate the aggregation of cells, and can involve processes like 3D bioprinting to impart direct cell positioning [42,73,82]. Tissue fusion is a collective term for a number of important events that occur during embryonic development to form organ structures [83]. It is the process by which two or

more isolated cell populations make contact and adhere, resulting in the initially discrete 'fusing units' forming a union [83]. Whilst cell-cell contact is an important feature of both self-assembly and self-organisation, unlike self-assembly, self-organisation involves tissue fusion processes (cell-to-matrix contact, matrix-to-matrix contact and ECM remodelling). In the context of TE, during this time two previously separate cell populations within engineered microtissues are brought together to form a continuous neotissue [81]. Routinely, both approaches (self-assembly or self-organisation) result in a tissue that has gross morphological, structural similarities, and comparable functional properties to native tissue, by virtue or recreating fundamental processes that occur *in vivo* [81].

One field positioned to benefit from this paradigm shift is musculoskeletal TE. To date, complete *in vitro* biomimicry of musculoskeletal tissues such as bone, cartilage and the osteochondral unit has not been achieved using traditional TE methods. Given that the tissues of the musculoskeletal system rely heavily on function through form, the modest clinical impact of the field of musculoskeletal TE is perhaps unsurprising given its failure to recapitulate the structure and composition of native tissues. This review will focus on the use of cellular aggregates, microtissues and organoids as 'building blocks' for TE strategies [74], and specifically how emerging biofabrication and bioprinting techniques are being used with such cellular structures to engineer tissues and organs of the musculoskeletal system. This review defines a 'cellular aggregate' as a body of undifferentiated stem or progenitor cells, while a 'microtissue' is defined as a body of cells that have been driven towards a specific phenotype *in vitro* by exposure to differentiating factors. As such, a microtissue exhibits a specific tissue phenotype and contains tissue specific ECM components. 'Organoids' are commonly generated from embryonic stem cells (ESCs) or induced pluripotent stem cells (iPSCs) grown in a 3D culture, were they self-organise into complex, functional and multi-layered tissues. As such, organoids are unrivalled in forming cellular and tissue arrangements analogous to those found in organs. Despite their great potential as tissue mimetics, organoids have limited sizes and reproducibility issues that limit their wide spread application in basic research and regenerative medicine [73,82]. However, because organoids can be produced in relatively large numbers they have the potential to be used as modular building blocks and/or embryonic seeds for scaled-up organ engineering [75]. The review will first describe how cellular aggregates, microtissues and organoids have been used for the engineering of bone, prevascularised constructs, cartilage, and osteochondral tissues. It then explore how cellular aggregates, microtissues and organoids can be used as 'building blocks' within emerging

biofabrication processes to engineer scaled-up constructs suitable for tissue engineering and regenerative medicine applications.

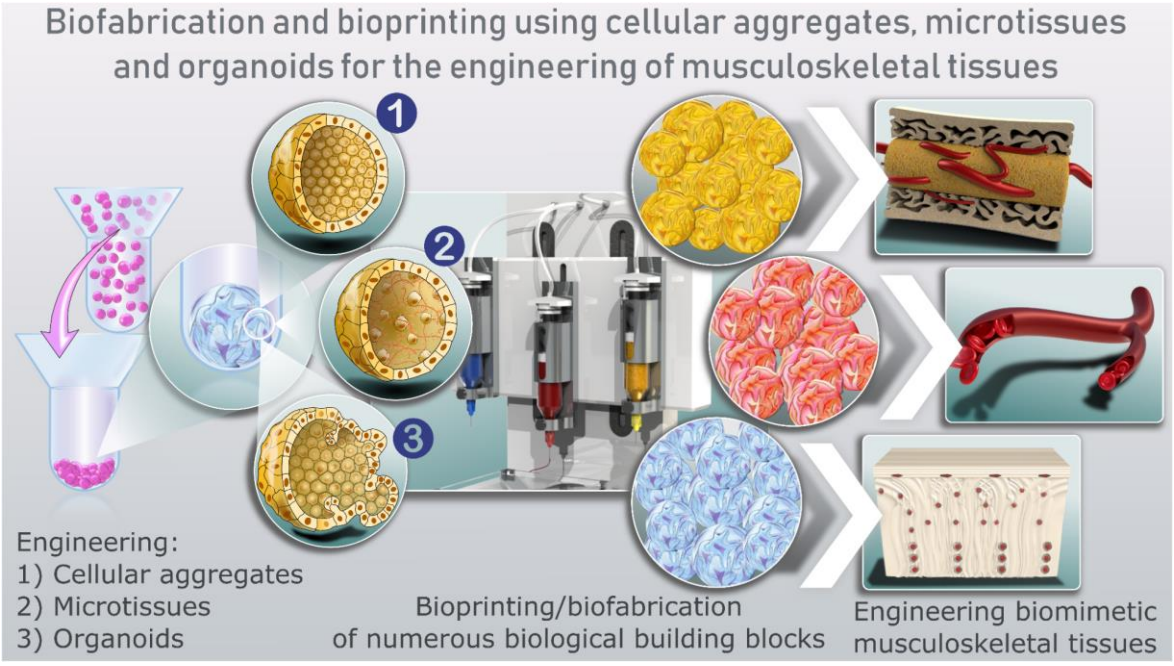

Figure 2.1 *Graphical abstract demonstrating a process for the biofabrication and bioprinting of cellular aggregates, microtissues and organoids for engineering musculoskeletal tissues.*

2.2 Cellular aggregates, microtissues and organoids for bone regeneration

Cell-based bone TE strategies can be broadly classified into those that attempt to recapitulate the process of either intramembranous or endochondral ossification. The latter approach, which involves the engineering of a cartilage soft callus *in vitro* for bone repair, can be considered a developmentally inspired TE strategy as it attempts to recapitulate key aspects of long bone development [84,85]. Remodelling of an engineered cartilage anlage has proven to be an effective method for recapitulating bone organogenesis ectopically [52,53]. However, generation of a similar functional bone organ, complete with marrow cavity, vasculature, and resident cell populations, at an orthotopic site is challenging, as is scaling such TE strategies to treat larger sized defects. This has motivated the development of TE strategies that seek to combine numerous cartilaginous microtissues together into a single construct primed for endochondral bone formation (Figure 2.2A). This section will review the use of immature cellular aggregates, cartilage microtissues (sometimes referred to as 'callus organoids' [54]) and osteogenic microtissues (that recapitulate an intramembranous ossification pathway) for the regeneration of large bone defects.

Cartilage microtissues for bone tissue engineering

Pellet culture is a well-established method for chondrogenic differentiation of mesenchymal stromal/stem cells (MSCs) [86]. Recognising that cartilaginous tissues engineered using MSCs have an inherent tendency to proceed along an endochondral pathway [85,87], cartilage pellets have also been used as part of strategies to regenerate large bone defects [88]. Van de stok and colleagues implanted 6 cartilage pellets (2 mm – 3 mm ø), each containing 2×10^5 human MSCs (hMSCs), into 6 mm long femoral defects in rats. Pre-implantation, the chondrogenic pellets were rich in proteoglycans and collagen types II and type X, the latter indicative of a hypertrophic cartilage phenotype. The pellets promoted complete bridging of the defect, as early as 4 weeks post-implantation. Once the defect had been filled with a mineralised tissue, remodelling of this *de novo* bone over the following 8 weeks restored the gross architecture of the native long bone (formation of a bony cortex and medullary canal). However, this result was heavily donor-dependent, occurring in only one of the three human cell donors investigated. The variance in healing capacity may derive from differences in the chondrogenic capacity of each donor. It appeared that the more chondrogenic the donor cells, i.e. the more cartilaginous ECM deposited *in vitro*, the better the bone healing observed *in vivo*, however further studies are required to validate such a conclusion. It remains unclear what level of chondrogenic differentiation and ECM deposition must be achieved *in vitro* to ensure predictable and robust endochondral bone formation *in vivo*.

The importance of cartilage microtissue scale for endochondral bone tissue engineering

A well-documented limitation of high-density cell systems and cell laden scaffolds is their susceptibility to inhomogeneous deposition of matrix components and core-necrosis, which can translate to implant failure *in vivo* [61,62]. A simple approach to address this challenge is to reduce the number of cells within a spheroid or microtissue, which has been shown to improve neotissue formation without the need for complex culture regimes incorporating bioreactors for perfusion or mechanical stimulation [66]. Interestingly, simply by reducing cell numbers within an aggregate, early chondrogenic differentiation can be initiated without soluble exogenous cues. Moreover, genes involved in the development of cartilage and endochondral ossification were strongly upregulated in lower cell number aggregates in the presence of transforming growth factor beta 1 (TGF-β_1). As a proof of concept, the authors compared traditional homogenous cell seeding of a scaffold to seeding with multiple cellular aggregates. Despite the total cell number being four times lower in the latter, the cartilaginous tissue formed within a collagen scaffold using cellular aggregates was more homogenous. Additionally, a necrotic core observed in the traditional approach was absent in the aggregate system [66].

Recent work by Nilsson Hall *et al.* [54] took the concept of downscaling spheroids a step further, reducing the cell number per aggregate to 250 cells to limit the size of the developing microtissue to <150 µm in an attempt to mitigate diffusion limitations of signalling molecules. The study leveraged emerging knowledge on the resident bone cell subpopulations that contribute greatest towards native callus formation during fracture healing. As such, they employed human-periosteum-derived cells (hPDCs), as opposed to bone marrow derived stem/stromal cells (bmMSCs) that are more commonly used for endochondral bone TE, for the formation of self-assembled cartilage microtissues. The authors used gene niches, identified from the native autonomous control of transitional zones in a developing growth plate, as a metric for determining the developmental stage of their microtissues. The phenotype displayed within late pre-hypertrophic cartilage spheroids during their *in vitro* differentiation lead to their definition as 'callus organoids'. In the context of developing callus organoids, a selected panel of developmentally inspired markers served as a means of directly assessing tissue development during the *in vitro* culture. These efforts culminated in a marked improvement in the reliability of *in vivo* outcome and provided support for the hypothesis that diffusion related challenges, which hinder tissue maturation within larger bone tissue engineered constructs, can be avoided by downscaling the cartilage rudiments to microtissues. Specifically, more consistent and complete bone formation resulted from ectopic (subcutaneous) implantation of constructs assembled from multiple smaller microtissues compared with more traditional macro-scale, self-assembled constructs (Figure 2.2B). This effective mineralisation of the cartilage rudiment and subsequent maturation into a bone organ ectopically was also reproducible within an orthotopic bone defect model, where the healing process mirrored that of normal fracture healing (Figure 2.2C & 2.5C). Taken together, the results clearly demonstrated the potential of modular pre-cursor microtissues, or callus organoids, to self-organise into a larger, functional bone organ. Additionally, the results strongly support the putative increased regenerative capacity of some understudied adult skeletal stem cell populations. The study exemplifies the developmental engineering paradigm, and offers a blueprint for how the design process can be implemented effectively in TE. Despite their relative success, Nilsson Hall and colleagues [54] recognise the need to continue work towards scalability of microtissues and organoids. In alignment with our own views, they identified a need for automated systems capable of generating the vast number of microtissues/organoids needed to create centimetre scale grafts, the risk inadequate vascularisation poses to the success of the highly metabolically demanding self-organised tissues, as well as the central role bioprinting is poised to take in structuring multicomponent tissues and organs.

Immature MSC aggregates for bone tissue engineering

Implantation of immature hMSC aggregates (also termed 'condensations'), coupled with the pro-chondrogenic cue TGF-β_1, has been shown to promote the regeneration of critically sized bone defects through formation of a cartilage intermediate *in vivo* [89]. Interestingly, bone regeneration was further enhanced by imparting some physiological load, *via* compliant fixation plates, onto the developing cartilage within the defect. Such mechanical loading was found to extend the cartilaginous phase of the endochondral ossification process, and was associated with improved repair and consistent bridging of the defect [89]. This work helps to establish the importance of mechanical cues in regulating the progression of developmentally inspired bone regeneration approaches, particularly when implanting 'unprimed' stem/stromal cell condensations within an orthotopic defect.

The regenerative potential of immature MSC condensations can also be improved through the addition of an engineered microvasculature. Rivron *et al.* identified hedgehog (Hh) proteins, specifically Sonic hedgehog (Shh), as predominant morphogenic factors that are reactivated during fracture healing and neovascularisation. Motivated by this observation they generated multicellular spheroids containing hMSCs and human umbilical vein endothelial cells (HUVECs), and exposed the aggregates to exogenous Shh protein which was found to induce the formation of patent microvascular lumen within the spheroid *in vitro* in a dose dependent manner. This engineered vasculature anastomosed with host vasculature and resulted in a significantly higher number of perfused vessels *in vivo*. Furthermore, this enhanced vascular network contributed towards the formation of mature bone tissue *in vivo* [90]. It is easy to envisage how such multicellular aggregates could be used as the building blocks to generate large engineered bone, complete with a perfusable vasculature. Section 3 of this review (see below) provides further details of how cellular aggregates and microtissues can be used to engineer such vascular networks within musculoskeletal tissues. Taken together, these results emphasise the importance of biomechanical or biochemical cues, as well as the use of supporting cells, to control the *in situ* development and therapeutic impact of constructs generated using cellular aggregates and spheroids.

Osteogenic microtissues for bone tissue engineering

The direct osteogenic differentiation of MSC aggregates represents a promising strategy for bone TE, however cells may undergo rapid phenotype reversion upon the withdrawal of soluble factors [57]. This presents a significant challenge for bone TE, as in spite of significant *in vitro* priming, implanted MSCs could contribute minimally to the regeneration of a bone defect. The provision of relevant ECM proteins has been proposed as a means of providing continued instruction and sustaining, *in vivo*, the osteogenic phenotype imposed *in vitro* [56,57]. Such a cell-instructive ECM is generated *in vitro* within osteogenic spheroids or microtissues, thereby generating a feedback loop which maintains their

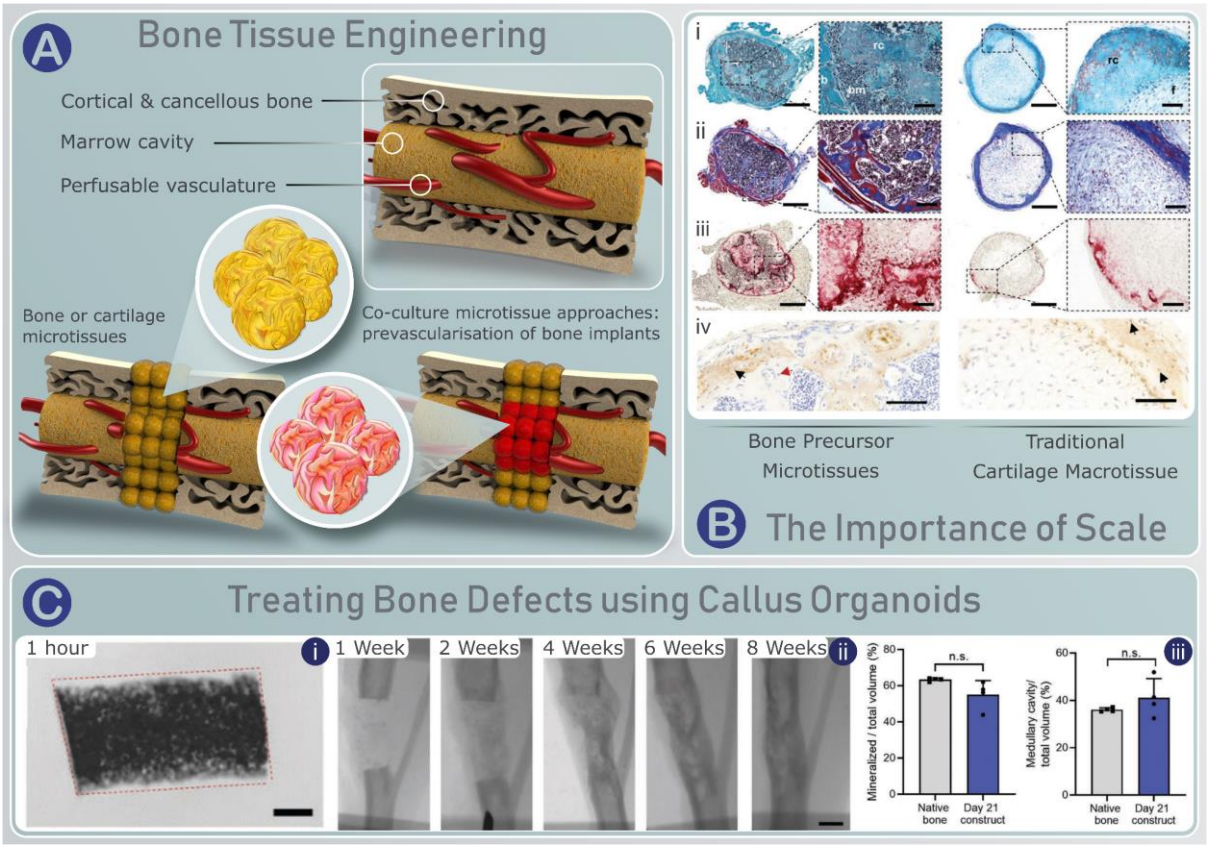

Figure 2.2 *A) Schematic representation of how microtissues can be utilised in bone tissue engineering. Bone precursor microtissues can be used alone, or in combination with vascular microtissues to generate prevascularised bone implants. B) The importance of scale when engineering cartilage precursors for endochondral bone tissue engineering. Histological comparison of bone precursor microtissues and a traditional cartilage macrotissue for bone tissue engineering via endochondral ossification, 4 weeks after ectopic implantation. i) Safranin O, ii) Masson's Trichrome, iii) tartrate-resistant acid phosphatase (TRAP), and iv) Human osteocalcin (hOCN) staining. Collectively, histological staining indicated that cells (positive hOCN staining) within the implanted bone precursor microtissues contributed towards the generation of a ossicle, with trabecular struts, active remodelling (positive TRAP staining for osteoclast activity), and bone marrow. In contrast, a traditional cartilage macrotissue only mineralised at the periphery of the implant and is filled with fibrous tissue, with little to no evidence of a bone marrow cavity. Scale bars = 500 µm (overview), and 100 µm (zoom & iv). C) The same precursor microtissues can be used to heal a murine, critically-sized long bone defect. i) Brightfield image 1 hour after assembling numerous microtissues into a single construct (Scale Bar = 1 mm). ii) X-ray images of the tibia defect treated with the microtissue construct (i) healing over 8 weeks (Scale bar = 1 mm). iii) Comparing the native tibia to the healed defect 8 weeks after implantation using ex vivo nano-CT quantification of mineralised volume (% of total volume) and the medullary cavity (% of total volume), (unpaired t-test). Figures B & C were adapted from [14].*

osteogenic potential through cellular interactions with cell-secreted proteins. Murphy *et al.* provided experimental support for this hypothesis, linking the increased and persistent osteogenic phenotype of MSCs within a spheroidal or microtissue system, upon removal of soluble cues, to cell-ECM engagements mediated by integrins such as $\alpha_1\beta_2$ [56]. Given that osteo-induced MSC aggregates retain their differentiation markers better than single cells, a number of studies have investigated if

such microtissues can act as a direct replacement for individual MSCs within biomaterial constructs for bone formation *in vivo* [58,59]. Furthermore, the angiogenic and osteogenic potential of such microtissues can be enhanced by hypoxic pre-treatment of the MSCs during their monolayer expansion; such environmental culture conditions were shown to improve viability and upregulate vascular endothelial growth factor (VEGF) expression without inhibiting the osteogenic differentiation of the cells. Furthermore, these pre-conditioned osteogenic microtissues significantly improved healing within critically sized bone defects when compared with those treated with individual MSCs [60].

2.3 Cellular aggregates and microtissues for engineering vascular networks

Supporting angiogenesis and strategies to prevascularise engineered tissues

Engineering a supporting vascular network is integral to the regeneration of all vascularised tissues and organs, including musculoskeletal tissues such as bone and muscle. In this context, cellular aggregates have been used to indirectly support the process of angiogenesis during tissue regeneration, while vascular microtissues have been used to prevascularise engineered constructs prior to implantation. In the context of the former approach, MSC aggregates have been shown to be potent drivers of neovascularisation through paracrine secretion of angiogenic factors such as VEGF and hepatocyte growth factor (HGF) [91,92]. Additionally, cell aggregates have demonstrated improved cell survival rates in ischemic environments due to the cells within the aggregate being naturally preconditioned to hypoxic conditions and the upregulation of hypoxia induced survival factors such as, hypoxia-inducible factor 1-alpha (HIF1α) and anti-apoptotic factors [91]. Improving the survival of grafted cells is an important feature in the context of scaled-up TE, where apoptosis due to oxygen deficiency within constructs in a physiological environment presents a significant challenge. The expression of these secreted angiogenic growth factors has been quoted as being 20- to 145- fold higher when compared to monolayer culture, and their effects so pronounced that conditioned media from spheroid culture is alone sufficient to accelerate wound healing [93].

Despite this potency, sprouting new blood vessels from the surrounding host vasculature and their subsequent ingrowth into the engineered tissue graft is a complex, multifactorial process which requires significant time [94]. Consequently, for large grafts where implanted cells cannot survive solely by diffusion from the proximal host vasculature, prevascularisation of the engineered tissue or the inclusion of cellular aggregates with the potential to differentiate directly into vascular endothelial cells, represents a promising strategy for rapidly developing an adequate blood supply (Figure 2.3A). This process accelerates vascularisation by anastomosing a microvascular network, typically preformed *in* vitro, with the immediate host vasculature through inosculation. Spheroids generated using cells derived from human adipose tissue have been shown to partially differentiate into vascular

endothelial cells [92], as well as contributing directly to newly forming blood vessels within an implanted scaffold [92,95]. In a direct comparison with a traditional single cell approach, MSCs from spheroids were found to contribute twice as much to developing microvessels (~ 40% of cells in *de novo* vessels were identified as coming from the implanted spheroids, vs ~ 20% from single cell implants). Moreover, these developing vessels made a marked contribution to the overall vascularisation of the implanted scaffold by combining with invading host-vessels *via* inosculation [95]. Cellular aggregates generated using a co-culture of HUVECs and MSCs have also been shown to support the development of microvascular networks *in vitro* due to sprouting between individual aggregates (Figure 2.3Bi & 2.5B) [96,97]. When encapsulated within a collagen/fibrin hydrogel, such co-cultured spheroids have supported the formation of a more pervasive prevascular network compared to seeding co-cultures of monodispersed cells (Figure 2.3Bi & ii). Additionally, this approach yielded a significant increase in the expression of osteogenic genes [96]. This suggests that the inclusion of vascular co-cultures can aid not only in overcoming diffusion limitations through prevascularisation, but also enhance the differentiation of MSCs in applications where the target tissue is natively vascularised, such as bone. However, the mechanism of this synergistic interplay is currently undetermined and requires further investigation.

As previously discussed, successful examples of engineering tissues on a clinically relevant scale has been scarce. Generally, successful cases are limited to tissues with low metabolic demands, those that are naturally hypoxic, are low in cell number, and are relatively thin (< 2 mm) and as such, at the limit of simple diffusion [98]. By extension, cellular aggregates or spheroids are high cell-density systems, and their size (diameter) is constrained by diffusion, with various 'maximum' diameters quoted throughout the literature. As aggregates/spheroids have been successfully prevascularised using HUVECs co-cultured with various cell types (bone marrow derived MSCs [99], human fibroblasts [100], human osteoblasts [101,102], human myofibroblasts [103]), a strategy of prevascularising each microtissue subunit is an attractive means of prevascularisation and potentially a route towards engineering organs with a rapidly perfusable vasculature. For example, it has been shown that prevascularised tissues of scale can be engineered by 'coating' multiple microtissues with HUVECs which migrate throughout the microtissues forming a prevascular network. Individually prevascularised microtissues can self-organise into a larger macrotissue, and unlike non-vascularised implants, connect with the host vascular network, resulting in the preformed capillary-like network being perfused with host erythrocytes [103]. In summation, these findings suggest that spheroids contribution's to vascularisation can go beyond their significant paracrine effects and reach into vasculogenesis, acting as individual vascular units capable of spontaneously developing new microvascular networks *in situ*.

Engineering larger vessels using microtissues

At present, the size of many vascularised engineered tissues is of the millimetre scale. As such, the microvascular networks previously discussed can be effective means of overcoming diffusion limitations associated with high cell-density systems. However, as such engineered tissues approach the centimetre scale (i.e. clinically relevant in humans), the need for a larger, immediately-perfusable vasculature increases. *In vitro* work with centimetre scale, functional tissues biofabricated from spheroidal building blocks has demonstrated that maintaining viability, and the consequent functionality of the engineered tissue, is only achievable with perfusable lumen within the body of the construct [104]. In light of this, engineering macroscale vessels, using vascular microtissues, which are amenable to integration within other spheroidal based musculoskeletal developmental engineering approaches is important for scalability (Figure 2.3).

The principles of self-assembly and self-organisation have been used to engineer vascular constructs at a macroscopic scale. Gwyther *et al.* [105] have demonstrated a scalable method for generating vascular tubes from aggregates of smooth muscle cells. The technique involved seeding a high density cell suspension into a non-adherent annular well. After 48 hours, the cells had spontaneously aggregated into a torus, contracting around the central post of the agarose well. The internal diameter of the rings (2, 4, and 6 mm) could be tuned by altering the size of the post, and the thickness of these tissues increased in accordance with the deposition of ECM components. Even without exogenous growth factors, individual rings were mechanically robust after only 8 days in culture, displaying mechanical properties that were favourable compared to traditional cell and hydrogel approaches. Furthermore, discrete rings could be manually aligned on a silicone mandrel, which fused together to form a continuous vascular tube (> 2 mm in length). Despite this relative success, it should be noted that a cell line was employed in this study. The notable increase in proliferative capacity of a cell line compared to a primary cell source could account for the rapid generation of ECM components, tissue growth, and resultant mechanical properties reported. A more recent study employed a similar self-assembly method to form vascular tissue rings from human induced pluripotent stem cell (hiPSCs) derived smooth muscle cells [106].

In the context of engineering functional tissues *via* prefabricated building blocks, it is important to consider the mechanical properties of the individual components. In the context of vascular tissue

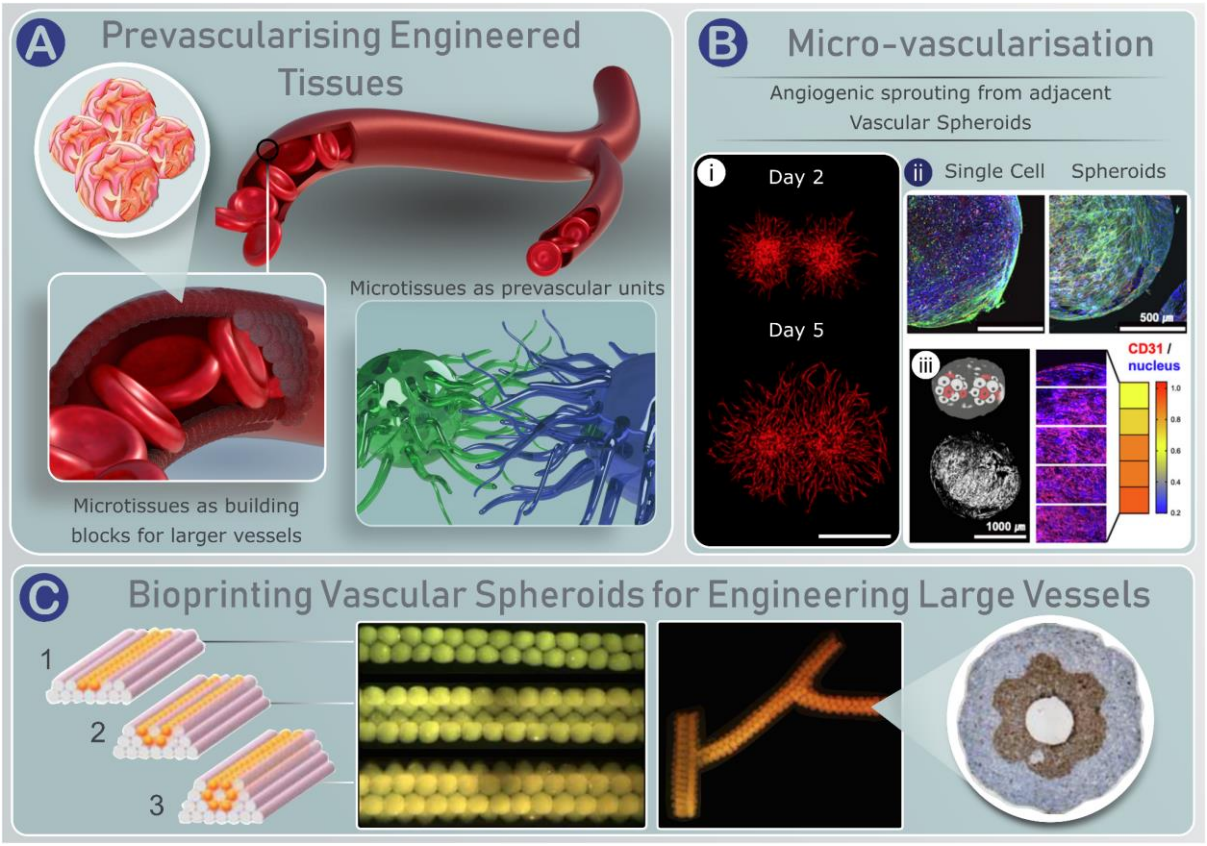

Figure 2.3 *A) Schematic of different approaches for prevasularising engineered tissues with blood vessels at different scales. The first uses vascular spheroids for engineering large blood vessels. The second employs spheroids as individual vascular units to form a prevascular network through endothelial sprouting. B) Vascular spheroids for prevascularisation. i) Adjacent HUVECs spheroids can sprout outwards and create a microvascular network (Scale Bar = 1 mm) [34]. ii) MSC and HUVEC co-cultures can form vascular spheroids and be seeded within a hydrogel. Within this environment, these vascular units undergo angiogenic sprouting and form prevascular networks (iii) (Blue – DAPI, Green – f-actin, Red – CD31), Scale Bar = 500 µm (ii) and 1 mm (iii) [33]. C) Spheroids can be bioprinted and self-organise into large, unified, and branched vessels. Bioprinting can be used to create tubular structures from spheroids (left-centre), it also allows to create connected bifurcations within the tubular structures (centre-right). Over time, initially discrete spheroids fuse to form a unified vascular tissue. Finally, bioprinting can spatially localise phenotypically distinct spheroid populations to form double-layered vascular walls. Here, spheroids expressing smooth muscle α-actin (brown) have been localised centrally within the bioprinted vessel (right) [47].*

engineering, burst pressure is an important criteria. Achieving burst pressures approaching those of native vessels has come from fusing individual cell/tissue sheets [107,108]. Such cell/tissue sheets may be more suited to engineering functional vascular tissues than spheroids, because they can easily form continuous tubes, requiring only one fusion point. Several methods of self-organising cell sheets have been proposed. Some involve stacking sheets, and through the incorporation of HUVECs, permit prevascularisation of the developing 3D tissue [109]. Others have mimicked the concentric layers of native vessels, by rolling cells sheets comprised of distinct cells types [107]. Despite their inferior mechanical properties (e.g. burst strength), strategies relying on cellular aggregates or spheroids offer

a distinct benefit over the aforementioned method as they allow the fabrication of branched macro-vascular structures. Norotte *et al.* [110] demonstrated that multicellular spheroids and cylinders can be used to biofabricate tubular structures as well as vessel-like structures with several bifurcations from a larger tubular structure (Figure 2.3C). Efforts towards bioprinting microtissues for bone regeneration could benefit from this work, for example, by integrating such bioprinted vessels within a population of bone precursor microtissues.

2.4 Microtissues as building blocks for engineering articular cartilage

Numerous iterations and combinations of the three aforementioned elements of the 'tissue engineering triad' have been explored in attempts to engineer cartilage grafts mimicking the complex structure, composition and biomechanics of native articular cartilage [5]. These efforts have resulted in a number of different cell- (e.g. matrix-assisted autologous chondrocyte transplantation) and/or scaffold-based TE approaches reaching the clinic [111–113]. The relatively limited clinical success of many of these approaches has motivated further research in embryonic and postnatal developmental processes that can potentially be leveraged to improve cartilage TE [114]. Early developmentally inspired approaches utilised non-adherent surfaces to coax the self-assembly of articular chondrocytes and the production of a neocartilage *in vitro* [115]. Although scaffolds for cartilage engineering, arguably the most widely researched aspect of the traditional paradigm, can provide several benefits they are not without their limitations [81]. As such, 'scaffold-free' approaches, unencumbered by the constraints imposed by a scaffold material or hydrogel, free the cells to self-assemble and self-organise (Figure 2.4A). It is believed that through the generation of their own microenvironment, the limitations associated with scaffold-based TE (shielding from biophysical and biomechanical cues, toxicity and/or immunogenicity of the scaffold or degradation products, poor synchronisation between neotissue formation and material degradation, phenotype alteration, and restricted cell-cell communication [81,115]) can be circumvented. Additionally, the processes of self-assembly and self-organisation offer their own benefits for functional articular cartilage TE. These biological advantages centre on recreating keystone events that occur throughout the mesenchymal condensation during skeletogenesis, from the production of physiologically relevant cell adhesion proteins (neural cadherin (N-cadherin) and neural cell adhesion molecule (N-CAM)), to recapitulating specific and appropriate cell-ECM interactions and growth factor mediated signalling events associated with limb bud development [64]. As a result, such scaffold-free approaches can more effectively recreate the sequential events of mesenchymal condensation during limb bud development. Moreover, it is seen as a crucial step in reliably committing undifferentiated stem/progenitor cells towards a stable chondrogenic lineage *in vitro*, and the subsequent development of tissue which is biochemically and biomechanically comparable to that of early developing cartilage [43,44,64].

Lessons from cellular self-assembly for engineering stable cartilage

Considering the broader fields of self-assembly and self-organisation can assist in the development of high-quality engineered cartilage when using cellular aggregates and microtissues. Several groups have successfully leveraged self-assembly *in vitro* to generate a highly bio-mimetic engineered cartilage (Figure 2.4Bi) [45,46]. Additionally, others have demonstrated that MSCs self-assembled into discs or micromasses, as opposed to pellets used in traditional MSC chondrogenic assays [86], can elicit a more robust chondrogenic response [47,48,116]. Of particular note in this field is the work of Athanasiou and colleagues who have successfully used self-assembled cartilage discs as a platform to investigate the influence of growth factors [45,49,117], enzymatic treatment [45,50,117], and mechanical stimuli [51] on the development and maturation of scaffold-free cartilage tissue. Additionally, others have shown that spatiotemporally exposing self-assembled cartilage discs to physiologically inspired soluble cues can promote the generation of a spatially organised tissue [46]. Furthermore, this TE strategy supported the development of phenotypically stable tissues, where the *in vitro* engineered stratified tissue was resistant to uncontrolled endochondral ossification *in vivo*, retaining its physiological zonal organisation in a subcutaneous murine mode (Figure 2.4Bii). As such, this work affirmed the putative benefit of recapitulating aspects of native cartilage development in the pursuit of maturing hMSCs into a stable and organised cartilage tissue. However, in spite of these promising findings, there are several challenges with translating such approaches to preclinical and human clinical applications [111,118]. For example, engineering anatomically defined tissues with comparable thickness to human articular cartilage is challenging using established self-assembly approaches. Fixation of these cartilage discs *in situ*, or their integration with an osseous phase with sufficient integration to withstand the substantial shear and compressive forces within a joint presents a significant challenge. Complications during surgical fixation of scaffold-free cartilage have been discussed elsewhere [111]. Attempts to secure self-assembled neo-cartilage discs using fibrin glue with extensive joint immobilisation (6 weeks) have demonstrated significant graft failure (50% of implant remaining in place) after 24 weeks *in vivo* [119].

Engineering organised articular cartilage using microtissues

Using cellular aggregates or cartilage microtissues as building blocks may address many of the challenges of engineering anatomically defined cartilaginous tissues of scale suitable for human clinical use. For example, it has been demonstrated that MSC aggregates, cultured for 5 days in the presence of TGF-β_3 to generate cartilage microtissues, can fuse under external pressure to form a homogenous cartilage matrix [68]. In addition, the developing cartilage successfully integrated with an underlying bone scaffold in both a simple plug configuration as well as in a large, anatomically accurate implant. Similar to the tissue that forms in self-assembled discs, the study demonstrated that

by mimicking some of the features present in the embryonic milieu, a cartilage with physiologic stratification of matrix components (glycosaminoglycan (GAG), collagen type- II and X, lubricin) in native tissue can be engineered when employing cartilage microtissues as building blocks (Figure 2.4C & 2.5A). Furthermore, the engineered tissue possessed biomechanical properties (compressive modulus >800 kPA and friction co-efficient <0.3) approaching those of native cartilage after only 5 weeks of chondrogenic cultivation [68]. Limitations with this approach include its manual nature, requiring the external pressure of a polydimethylsiloxane (PDMS) mould to force the formation of a homogenous tissue. Given that spontaneous fusion of the cell aggregates was not achievable without these constraints, difficulties may arise when adopting this methodology to patient-specific geometries. A potential explanation for the limited spontaneous fusion could be the spheroid size (~ 1mm in diameter) employed, although a relationship between spheroid size and/or cellularity and their capacity to spontaneously fuse was not elucidated. Furthermore, it remains unclear if such approaches lead to the development of articular cartilage with native-like anisotropy in its collagen network. Others have mirrored these findings and have observed that an upregulation of numerous chondrogenic markers during cellular self-assembly does not cause a concomitant formation of a stratified collagen organisation [42,45,47]. Studies that have attempted to guide collagen organisation in self-assembled tissue have primarily utilised mechanical constraints or polymeric boundary conditions, demonstrating that improvements in collagen organisation correlate with more biomimetic compressive properties [41,78]. In the future it is possible to envision the use of automated 3D bioassembly strategies that enable the precise localisation of microtissues [120] within carefully designed 3D printed scaffolds that function to guide their fusion and growth, ultimately directing the spatial organisation of the engineered tissue. Here care must be taken to ensure that such guiding scaffold structures to not negatively interfere with the fusion and remodelling of the microtissues. Alternatively, microtissues could be combined with preformed collagen-based scaffolds that already emulate the arcade structure of articular cartilage. In one example of such an approach, collagen threads were woven in a zig-zag pattern to form tubular structures that mimic the collagen organisation in articular cartilage. Two compacted collagen sheets were then sandwich between these tubes, stabilising the configuration prior to cross-linking the collagen. The patent cylindrical pores (1 mm) that remained were populated with cell pellets (1,000,000 MSCs, 0.6 ± 0.2 mm in diameter) which had been cultured for 3 days in expansion medium. Once seeded into the scaffolds, spheroids were cultured chondrogenically and supported robust deposition of sGAGs and type II collagen, ultimately resulting in an increase in the apparent Young's modulus (by 60%) compared to the un-seeded scaffold. The construct demonstrated substantial elastic properties and a compressive modulus approaching that of naïve native articular cartilage [121]. Given the reliance native cartilage has on

the spatial organisation of it macromolecular network, finding an efficacious and reproducible approach for generating spatial organisation within self-assembled cartilage is essential.

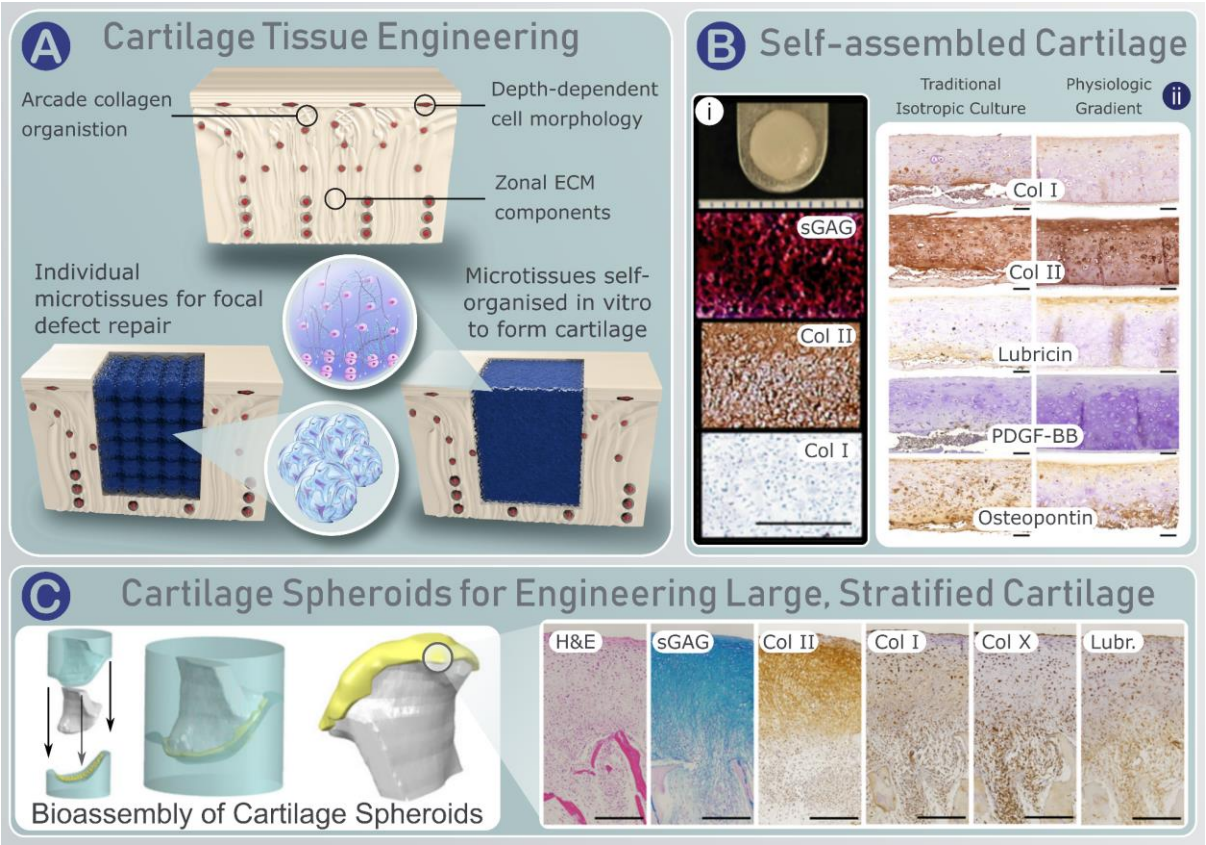

Figure 2.4 *A) Microtissues for cartilage tissue engineering. Individual cartilage microtissues can be employed directly within a defect, or allowed to first self-organise in vitro into a spatially organised tissue before implantation. B) Lessons from engineering a stable cartilage phenotype via self-assembly. i) Gross morphology and histology of self-assembled neo-cartilage treated with TGF-β and chondroitinase-ABC. Histologically, a stable, uniform and rich cartilage matrix is formed (positive staining for sGAG, collagen type II), scale bar = 200 µm [57]. ii) Recapitulating the spatiotemporal gradients present during native cartilage development have been shown as a means of spatially organising an engineered cartilage. Here, self-assembled human cartilage with physiologic organisation demonstrated more stability in vivo compared to a similar self-assembled cartilage that had been cultivated in traditional isotropic chondrogenic conditions. Histologically, the deposition of collagen type I, loss of collagen type II, absence of superficial lubricin expression, invasion of preosteoclasts/osteoclasts (Platelet-derived growth factor-BB (PDGF- BB)), and extensive osteopontin expression is indicative that cartilage cultured traditional isotropic culture conditions was more prone to undergo endochondral ossification in vivo, when compared to a more zonally organised engineered tissue (Scale bar = 100 µm) [58]. C) Cartilage spheroids can be fused to engineer large, anatomically-shaped and stratified cartilage. Cartilage spheroids were bioassembled on top of an anatomically shaped bone scaffold by pressing the scaffold into the spheroids using a two-piece silicone mould (left). After 5 weeks of chondrogenic cultivation, spheroids had fused and generated a stable cartilage tissue with zonal organisation (Scale bar = 500 µm) [68].*

The importance of cartilage microtissue scale for articular cartilage tissue engineering

The use of larger cartilaginous spheroids for cartilage TE have been associated with certain limitations, specifically an intrinsic heterogeneity in cell phenotype due to diffusional gradients within such tissues. These gradients can affect not only cell morphology, but also cause distinct regions of matrix deposition within a single spheroid. Specifically, the production of collagen I superficially, collagen I,II, and X in the middle regions of the aggregate, and an absence of matrix within the core due to apoptotic or dead cells have been reported [62]. As such, the validity of high cell density spheroidal models for cartilage regeneration have been questioned [62]. The formation of chemical gradients and suboptimal culture conditions in these larger aggregates can account for many of the aforementioned issues. While measuring gradients in cellular aggregates is challenging, levels of oxygen, nutrients like glucose, and growth factors exist within such structures and their contribution to the spheroid microenvironment has been discussed as impacting cellular properties and behaviours [122,123]. To date, most studies investigating transport phenomena in spheroids has been completed using non-MSC populations [124]. Since different cell types consume nutrients at different rates, have different packing densities and porosity which alter the rate of diffusion [124–126], leveraging these findings is challenging. Nevertheless, MSC spheroids formed using 15,000, 30,000 and 60,000 cells (with diameters of 352 µm, 502 µm, and 706 µm respectively) showed a significant decrease in cellular metabolism, specifically glucose consumption, as cellularity and spheroid size increased. Since there was only a 10 % gradient in oxygen from the outer diameter to the core in the largest spheroid, it was hypothesised that cells were adaptively reducing their biosynthetic output to avoid generation of a hypoxic core in larger spheroids [124]. Additionally, a 400 µm diameter has been identified as the upper limit for spheroid size to avoid core hypoxia and cell death as a result of limitations in the diffusive length of nutrient transport [127]. Hence, the development of scaled-down versions of the progenitor aggregates is emerging as a logical alternative [66]. To this end, studies have sought to create high-throughput methods for generating small (<200 µm) microtissues from a few hundred articular chondrocytes [128,129]. The archetypical single cell scaffold-based approach has been directly challenged using microtissues generated using human periosteum-derived stem cells. *In vitro*, the small (50 – 250 cells, 60 µm – 120 µm in diameter) microaggregates underwent a more pronounced downregulation of stemness markers and a subsequent nuclear translocation of Sox9 and upregulation of Sox9 associated genes compared to single cells over 7 days of *in vitro* culture. Additionally, over 21 days of chondrogenic culture micro-aggregates containing 50, 100, and 250 cells significantly enhanced chondrogenic gene expression and cartilage specific ECM accumulation compared to single cells. Furthermore ectopic implantation of un-primed micro-aggregates (no exposure to the chondrogenic morphogens such as TGF-β) elicited a more rapid and intense formation of cartilage when compared histologically to primed (+ TGF-β) single cell constructs. As might be

expected, this difference was amplified if the microaggregates were also exposed to TGF-β during the 6 day *in vitro* preculture, forming cartilaginous microtissues [129,130]. However, given the potential negative impacts of using growth factors in therapeutics, the capacity to outperform traditional single cell approaches in the absence of exogenous factors emphasises the potent potential of aggregation techniques to steer stem cell fate both *in vitro* and *in vivo*. Additionally, by scaling-down cartilage microtissues, they can become compatible with current extrusion based bioprinting methods that have been used for the structuring of single-cell-laden hydrogels for several years [71].

To date, orthotopic implantation of such cartilage microtissues has been scarce. However, promising defect regeneration from larger spheroids treatments in the clinical environment (chondrosphere®) [42,131,132] suggests that the improvements seen *in vitro* by down-scaling spheroid size can lead to further improvements. Additionally, much of the work previously undertaken with self-assembled cartilage can be directly translated to applications where microtissues are intended as 'building blocks' for generating an engineered cartilage. All of these approaches have sought to improve the quality of the neotissue formed *in vitro*. Consequently, the addition of boundary conditions to drive collagen anisotropy [41,78,121], enzymatic treatment to re-balance the sGAG:Collagen ratio [45,50], ECM substrate materials [133], the inclusion of growth factor eluting biomaterial micro-spheres [134], or the use of cartilage progenitor cells [135–137] can all potentially be used to enhance the functional development of articular cartilage engineered using microtissues. Despite this, issues generally associated with cartilaginous spheroids, such as the aberrant cellular morphology and phenotype observed in the peripheral regions of such tissues, may impact the quality of the overall tissue generated when numerous microtissues are brought together to generate a single tissue of scale. With this in mind, and given the aforementioned challenges with achieving spontaneous fusion of adjacent cartilage spheroids [68,138], significant thought must be given in each case to ensure that the microtissues are fit for purpose. In summation, robust chondrogenesis is achievable by recapitulating the mesenchymal condensation observed during cartilage development. Furthermore, the organisation of this developing tissue can be modulated, at least in part, by the introduction of cues to guide the self-organising tissue. This provides encouragement that a mature, biomimetic cartilage tissue for the biological resurfacing of damaged and diseased joints is within reach using cartilage microtissues as biological building blocks.

2.5 Osteochondral tissue engineering

Self-organised progenitor cell aggregates have also been used to generate constructs to treat osteochondral defects [69,139–142]. In one such study, cell aggregates generated using adipose derived stem/stromal cells were fused to create cylindrical scaffold-free implants. These undifferentiated constructs were then used to treat osteochondral defects created in the patella-femoral groove of mini-pigs. Macroscopically, the treatment groups appeared to have filled with an

abundance of cartilaginous tissue, whereas the tissue filling the empty defects appeared to be more fibrous and depressed from the defect surface. However, no significant differences in the quality of repair was observed between the control and experimental groups at either the 6- or 12-month time-points. Histologically, the repair tissue at the apical surface of the treated defect appeared filled with fibrocartilage and regeneration of the subchondral bone occurred *via* an endochondral pathway. In contrast, empty defects were entirely filled with fibrous tissue, with little to no regeneration of the osseous or chondral regions visible 12 months post-operatively [69]. Although microscopic scoring indicated a significant improvement in healing, there are several features of this early work worth noting. First, defects were created in a relatively low-load bearing site within the joint; it would be of interest to observed how such an immature, predominantly cellular, construct would respond to a more biomechanically demanding environment such as the femoral condyle. Additionally, although this treatment resulted in an improvement over the untreated control, this approach failed to consistently promote complete hyaline cartilage repair. Despite this, the study also raises interesting questions into the mechanisms by which the cells within the undifferentiated spheroids are guided, by the surrounding environment, towards regenerating the distinct osteochondral tissues. Additionally, it provides encouragement that long-term regeneration of osteochondral tissues can be enhanced by the use of scaffold-free tissue engineering strategies, although direct comparisons with scaffold-based approaches are required to better understand the relative benefits of both.

2.6 Biofabrication strategies

As the platform technologies, hardware capabilities, and biomaterial science associated with bioprinting expands so does its scope. Traditionally, bioprinting involved the precise, user-defined spatial deposition of a single-cell suspension encapsulated within a bioink in three-dimensions. However, the remit of bioprinting is now extending towards the deposition of cellular aggregates, microtissues and organoids in hopes of bioprinting complex organ-units using these organoids as embryonic seeds [75]. The rapidly expanding toolbox available to bioprinting labs has pushed the boundaries of the 'biofabrication window' significantly from when print fidelity was predominantly defined by the shear thinning nature of the deposited cell-laden biomaterial (bioink) [143]. Martin *et al.* have recently proposed two prospective methods for 'organogenesis by design', which combine the paradigms of self-organisation and bioprinting [75]. The first, leverages bioprinting to impose geometric design and sizes to direct a pool of printed stem/progenitor cells towards a developing organoid. When compared to traditional symmetrical, spherical self-assembly, the self-patterning of the bioprinted cells can potentially be guided through the user-defined micro-patterning. Alternately, bioprinting can be utilised in a bottom-up approach whereby numerous small organoid units, created prior to the printing process from stem/progenitor cells, are deposited in a spatio-temporal fashion to drive subsequent development. In this scheme, the patterning imposed during bioprinting is

intended to instruct the formation of more complex, large-scale organogenesis from the smaller intermediate organ progenitor building blocks [75]. Within this section, an up-to-date insight into novel and emerging bioprinting/biofabrication strategies employed for the development of functional tissues and organs from high-density cell aggregates and microtissue precursors will be provided, with a focus on the technological advancements that have facilitated significant progress in the field.

Embedded bioprinting of cellular aggregates in supporting baths

Until recently, bioprinting millimetre scale structures with acceptable fidelity has been limited to polymer-rich bioinks [144]. However, the inherent opposing requirements of a bioink mean that these dense bioinks offer limited biomimicry and ultimately restrict tissue development. 3D bioprinting within a suspension media has emerged as a platform for patterning lower viscosity, biomimetic bioinks with excellent resolution and fidelity [144]. Microgel support baths have emerged as a means of supporting the deposition of both individual cells as well as cell spheroids [145,146]. These support baths, which act as liquid-like solids (LLS), are formed of granular hydrogel microgels tightly packed within cell culture medium [145]. Post-extrusion, the microgels provide physical support for single cells as well as cellular aggregates, whilst offering unrestricted diffusion of nutrients, waste, and other molecules by virtue of the interstitial spaces between the microgels and their high (>99% w/w) liquid composition [145]. This approach has demonstrated exceptional resolution and print fidelity, capable of reproducing personalised tissues and organs (Figure 2.5D) [147]. Additionally, similar methods have been used to support both bone and cartilage by bioprinting cellular condensations and then maintaining them in long term culture within mechanically stable support medium [146]. In this study, human stem cells were the only component of the bioink. As such, they were able to coalesce *via* transmembrane proteins and differentiate along specific musculoskeletal lineages generating specific matrix components unhindered by an interstitial hydrogel. To achieve this, photoreactive groups were added to alginate micro-particles, which allowed the support bath to be cross-linked post-printing generating a mechanically stable substrate for extended culture.

Sacrificial writing into functional tissue (SWIFT)

The sacrificial writing into functional tissue (SWIFT) technique effectively inverts the aforementioned 'support bath' paradigm, whereby a sacrificial ink is printed into a slurry-support bath comprising predominantly of cellular spheroids [104]. As such, SWIFT demonstrates that by coupling a carefully selected ECM and 'organ building blocks' (OBBs), a support bath that displays strong shear-thinning behaviour with appropriate yielding ahead of the translating nozzle and self-healing in its wake, analogous to the microgels used in traditional embedded printing techniques is possible (Figure 2.5Ei & ii). Interestingly, in the absence of densely packed OBBs, the ECM solution alone does not exhibit the necessary rheological properties to support embedded 3D printing. At physiological temperatures,

the ECM undergoes marked stiffening, fixing the geometry imposed within the OBBs by the sacrificial ink as it is evacuated (figure 2.5Eiii). This methodology was leveraged to generate networks of perfusable tubular features embedded within the construct, which serve as template for vascular channels within the construct which could exceed 40 mm in length and 4 mm in thickness. In doing so, the authors successfully maintained cell viability within the extraordinarily dense (0.5 billion cells) living matrix *via* perfusion of hyper-oxygenated (95% O_2) culture media through the printed channels. Furthermore, attempts were made to endothelialise the lumen with HUVECs. Although a confluent layer of endothelial cells across the entire lumen was not achieved, the results suggest that HUVECs have the capacity to adhere to the fusing EBs and remain in place during perfusion. Patent channels were printed into various OBBs: compacted embryonic bodies (EBs), cerebral organoids, and cardiac spheroids, without disrupting the complex architectures present within the developing organoids [104].

Aspiration-assisted bioprinting (AAB) of spheroids

Although different support baths may provide an effective substrate for bioprinting microtissues as minimal units for organogenesis, the precise control over their positioning in the 3D space has presented significant challenge. The aspiration-assisted bioprinting (AAB) technique represents a promising approach to address this challenge [97]. In this method, spheroids are positioned using the minimal aspiration force (critical lifting pressure) to overcome gravity, buoyance force, hydraulic drag, and the thermodynamic barrier at the interface, whilst maintaining cell viability above 80%. Application of this approach has been demonstrated in both scaffold based and scaffold-free situations. AAB has also been investigated as a method for engineering osteochondral tissues. Retention of osteogenic and chondrogenic spheroid phenotypes was maintained following bioprinting and translated into fusion of the distinct spheroids with the histomorphological characteristics of an osteochondral interface [148].

Fluid-based singularisation

Given the complexity of engineering biological interfaces such as the osteochondral unit, bioassembly of numerous different microtissues into a single implant capable of self-organising into an organ precursor will not be without its challenges. To this end, unique micro-fluidic systems merged with bioprinting methods are emerging as effective means of spatially organising spheroids for osteochondral tissue engineering applications. Advanced bioprinting methods have also yielded the biofabrication of a biphasic, hemi-spherical constructs intended for osteochondral resurfacing (Figure 2.5Eiv). Here, a novel fluid-based singularisation module was employed to accurately insert individual spheroids (cell- or biomaterial-based) into the pores of a thermoplastic polymer scaffold. Automated deposition of the pre-differentiated microtissues or chondrocyte laden microgels did not impact long-

term viability, fusion of adjacent µtissues, or cell phenotype, resulting in the formation of cartilage specific ECM proteins over 28 days of *in vitro* culture [120].

The Kenzan method

Alternatively, spheroids can be spatially organised using the 'Kenzan' method. Here, pre-assembled spheroids are robotically aspirated, like above, and subsequently impaled on a micro-needle array, which serves as a temporary support. The distance between the needles (commonly 500 µm) is such that adjacent spheroids can interact and secrete a supporting matrix [149]. In the absence of a supporting biomaterial, the Kenzan method has been shown as an effective method for assembling numerous spheroids to form live vascular tubes measuring 5 mm in diameter and 2 cm in height [150], cartilage constructs for the treatment of focal defects (3 mm ⌀ x 1 mm) [151] and cylindrical osteochondral implants measuring 5 mm ⌀ x 4 mm [141]. The latter aided in the regeneration (radiologically and histologically) of osteochondral defects in a preclinical animal model [141]. Despite this, several drawbacks unique to using the Kenzan method as a means of bioassembling spheroids have been identified. Predominantly, the inter-needle distance defines a relatively narrow range of spheroid diameters that will permit fusion and the development of a unified tissue. As such, it places an onus on generating optimal spheroids which, could prove challenging when considering the use of unknown cell combinations, and/or culture conditions/periods [149].

Bioprinted-assisted tissue emergence (BATE)

Bioprinted-assisted tissue emergence, or BATE [82], aims to leverage bioprinting to accurately control the initial spatial organisation and densities of organoid-forming stem cells to permit their spontaneous self-organisation into larger, centimetre scale, tissues. Here, a custom-built extrusion-mode printer was fabricated by combining a syringe pump with an inverted microscope. The microscope stage controller was used to define the spatial positions, while the syringe pump allowed extrusion of cell/organoid suspensions *via* a pulled glass capillary. Cells were deposited into a bath of hydrogel precursor material which, after printing was crosslinked at 37 °C to maintain the spatial positioning of the deposited biologics.

The study successfully demonstrated that bioprinting is an effective method of controlling the spatial deposition of stem cells onto a bioactive ECM substrate whilst maintaining their ability to form complex structures reminiscent of those within a mature organ through self-organisation (such as lumens, branched vasculature and tubular intestinal epithelia with *in vivo*-like crypts and villus domains). Additionally, bioprinting permitted spatial and temporal control over the introduction of support cells, which can have a potent modulatory effect on developing organoids, improving growth and development [82]. Although considerable precision is required from the bioprinting hardware,

this approach does not require the development of an overly complex bioprinting modality. Instead, the bioprinter is used as a means to accurately and precisely control experimental variables, such as cell density, initial tissue geometry and the proximity and positioning of co-deposited heterogeneous cell populations. As such, the influence these factors, and others (cell-matrix interactions and soluble factors), on the spontaneous cellular self-organisation into organoids can be robustly investigated. Interestingly, the development of the 'BATE' technique demonstrates that highly complex printing methodologies are not required to strictly define spatial control over organoid/spheroid deposition.

Instead, identifying and engineering appropriate conditions between the developing organoids and the surrounding environment can allow the printed cells to create the geometrical complexity of the final tissue, through post-printing remodelling and self-organisation. As such, it seems bioprinting is best suited as a tool, within a design strategy, to help define initial conditions and creating a favourable environment for the naturally programmed organoid building blocks as well as their relevant support cells to self-organise a specific tissue or organ [82].

2.7 Outlook

Leveraging cellular self-organisation within musculoskeletal tissue engineering holds tremendous promise for generating constructs that mimic the native tissue's composition and structural organisation. This can be enabled by the use of novel biofabrication techniques that provide precise control over the location of cellular aggregates or microtissues in 3D space. In this paper we have summarised the many advantages of using aggregates, microtissues and organoids as building blocks for generating large, biomimetic musculoskeletal tissues. In common with other scaffold-free tissue engineering strategies, such approaches can promote the development of a more biomimetic tissue as the cells are free to interact and self-organise. Moreover, tissue engineering with microtissues is an inherently scalable process. This benefit comes from first engineering scaled-down microtissues that inherently overcome nutrient transport limitations and yield more consistent lineage commitment and ECM deposition. Once combined, these microtissues have exhibited the capacity to act as functional building-blocks for the biofabrication of larger tissues *via* self-organisation and remodelling into functional grafts.

Despite this promise, some deficiencies with current strategies remain. Robust fusion between proximal microtissues can prove challenging, and failure to form a continuous tissue can compromise the effectiveness of the construct. Additionally, achieving significant tissue maturation *in vitro* may be unobtainable within reasonable culture times, and hence a truly 'scaffold-free' approach to engineering a mechanically functional musculoskeletal tissue may be unfeasible. Within the musculoskeletal system, tissues are often placed under significant physiological loads. In this review we have highlighted that modular assembly of microtissues alone may not be sufficient to

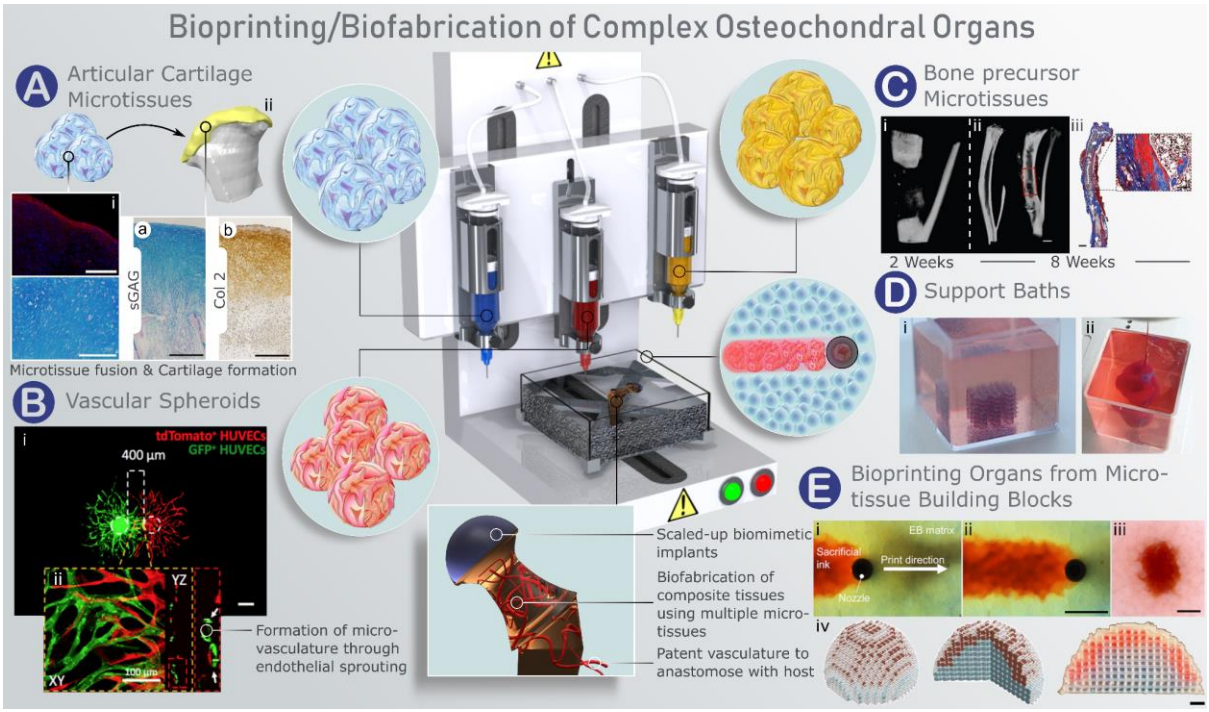

Figure 2.5 *Bioprinting/Biofabrication of complex osteochondral organs. A) Articular cartilage microtissues. i) Individual cartilage microtissues can fuse to form a homogenous cartilaginous tissue [68]. Positive tenascin deposition at the periphery of two fusing units (Red) indicates successful union between cartilage microtissues (Top), and homogenous sGAG deposition results from the successful self-organisation of the developing cartilage tissue (Bottom) (Scale bar = 200 µm). ii) Large, anatomically shaped cartilage can be engineered via fusion of cartilage microtissues. This engineered cartilage stains positively for canonical articular cartilage markers, sGAG (a) and collagen type II (b) (Scale bar = 500 µm). B) Vascular spheroids. i) Bioprinted HUVEC spheroids demonstrate angiogenic sprouting behaviour, forming capillary networks between adjacent spheroids after 7 days (Scale bar = 400 µm) (ii – High magnification at the interface region in the XY and YZ planes) [34]. C) Bone precursor microtissues. Implantation of developmentally inspired callus organoids into critically sized bone defects enables the regeneration of the long bone with similar morphological properties of the native organ [14]. i) Nano-CT 3D rendered image at 2 weeks post implantation, ii) native bone (left) and treated tibia after 8 weeks (right) (scale bar = 1mm). iii) Masson's Trichrome staining of the treated defect after 8 weeks indicating full bridging of the defect with cortical bone and the presence of a mature marrow cavity (Scale bars = 1 mm and 100 µm, overview and high-magnification respectively). D) Support Baths. i) A multi-layered woodpile structure printed within a support bath, demonstrating high print resolution and fidelity. ii) A heart printed within a support bath, complete with key anatomical structures such as, hollow left and right ventricles [94]. E) Bioprinting organs from microtissue building blocks. i-iii) SWIFT [41]. (i,ii)Time lapse of printing a sacrificial ink (red) via embedded 3D printing within a live matrix of embryonic bodies (EB) (Scale bar = 1 mm). iii) Cross-section of the channel imposed within the matrix of spheroids by the sacrificial ink, which following evacuation of the sacrificial material was perfusable (Scale bar = 500 µm). iv) Illustration of computer-aided design (CAD) models of the bioassembly of phenotypically distinct spheroid within a scaled-up hemispherical construct for osteochondral joint resurfacing (left). A proof-of concept image (right) where hydrogel microspheres, stained red and blue to represent chondrogenic and osteogenic phases of the osteochondral implant respectively, have been bioprinted within a polymer support framework (Scale bar = 2 mm) [71].*

generate a mechanically functional tissue, and reliance on a supporting scaffold material may still exist until *in situ* maturation has occurred [42,74]. Modular biofabrication approaches, such as the self-organisation of individual microtissues, alleviate, in part, the interdependence between tissue formation and scaffold properties that occurs *in vitro* as the biological components of an implant can be individually optimised prior to their combination with the selected scaffold. Interestingly, scaffolds and microstructural devices could provide a valuable platform to help direct developing microtissues and self-organising constructs [73]. If properly designed and implemented, a careful balance between engineered guidance and dynamic remodelling within developing tissues can be provided. Resulting instructive boundaries and degrees of freedom can yield control over self-organisation that better recapitulates that seen in embryonic development [73]. Implementation of successful tissue guidance could have significant impact for the engineering of spatially complex tissues such as articular cartilage, where controlling the architecture of the collagen network remains a key challenge in the field.

In addition to generating structured, mechanically robust tissues, another key challenge facing the biofabrication of large self-organised tissues is vascularisation. An adequate nutrient supply is a pre-requisite for the delivery of nutrients and oxygen to large-scale engineered tissues and organs. While several methods have attempted to form networks of small vessels/capillaries with the hope of mitigating diffusional limitations, generating a perfusable, large-scale vascularised network is yet to be realised *in vitro* [73]. The emerging bioprinting strategies outlined in this review and elsewhere are positioned to address some of the hurdles associated with scalability and vascularisation [152]. In particular, bioprinting offers a means of directing the process by which microtissues fuse and self-organise into structurally complex tissues. Additionally, it serves as a platform technology to allow the accurate combination of multiple different microtissue phenotypes, independently generated, in a single construct within the confines of a user-defined architecture. Such approaches could also be combined with other techniques such as cell sheet engineering, that have also been applied in orthopaedic tissue engineering [153].

The generation of anatomically accurate implants, such as large osteochondral grafts that comprise cartilaginous, bony, and vascular tissues, is achievable by leveraging recent developments in the fields of biofabrication and bioprinting. Microtissues are an appealing method for large-scale, automated biofabrication of human tissues and organs, but bioprinting must be carefully employed to direct their fusion and self-organisation in a programmable manner [152,154]. This will require further developments in bioprinting hardware to address the challenges outlined above and to ensure the successful clinical application of such bioprinted implants in regenerative medicine. Realising automated, high-throughput methods for forming vast numbers of microtissues with various phenotypes, bioassembly of these pre-cursors into continuous functional units capable of progressing

along a specific (e.g. developmentally inspired) pathway, and creating *in vitro* conditions and external cues that promote the development of structurally organised and mechanically functional tissues will require sustained efforts and convergence between several disciplines. In addition, convergence of different biofabrication technologies will likely be required to achieve these ambitious goals and to enable the scalable, efficient and cost-effective engineering of such tissues and organs.

In conclusion, it is becoming increasingly apparent that following a developmental engineering process can facilitate the engineering of biomimetic tissues recapitulating key biological features at various scales. Using cellular aggregates, microtissues or organoids as biological building blocks within such bioprinting platforms will be central to future efforts in this field of research. Such bioprinted tissues are poised to transform the field of regenerative medicine in the decades ahead.

Chapter 3.
3 Novel Methods

3.1 Microtissue Platform

3.1.1 Introduction

A particular focus of this thesis was on scaling-down self-organised tissue-units towards microtissues. The overarching aim was to use these microtissues as building blocks to engineer consistent and scalable macro-tissues by leveraging the potent biological advantages associated with mimicking key developmental processes [67,81]. Scaling-down traditional cartilage spheroids has been discussed as a means of combining spheroid culture with existing bioprinting strategies [71,155], and has been shown to outperform traditional approaches using homogenous cell seeding of scaffolds in terms of MSC commitment towards a chondrogenic lineage and their capacity to form cartilaginous tissues *in vivo* [130]. Importantly, microtissues are also a logical means of mitigating some of the shortcomings associated with using larger cartilage spheroids [66]. Specifically, cartilage microtissues can help to mitigate the diffusion gradients within the tissue and can alleviate heterogeneity of cell phenotype and matrix production associated with traditional chondrogenic assays [54,62,66]. While this thesis primarily focused on cartilage engineering, others have explored the use of spheroids/microtissues for generating other tissues, such as vascular structures [72,96,110]. Since spheroidal tissue-units have been proposed as 'biological building-blocks' for organogenesis [152], identifying a methodology suited to generating such tissue/organ seeds, expressing the necessary phenotype, for engineering tissues/organs of the musculoskeletal system is essential.

Multiple methods have been described in the literature to produce multicellular spheroids [156]. An ideal platform for generating microtissues has been defined as a scalable process, which can create standardised spheroids with uniform shape, size and fortitude to be used in biofabrication processes such as bioprinting [152]. Additionally, the platform must not incur biological damage during microtissue production and/or prevent their capacity for subsequent tissue fusion. Finally, it must also accommodate the generation of diverse microtissues with unique phenotypes and complementary composite structures [152]. At present, well plates with patterned bases designed to facilitate the formation of spheroids in a high-throughput fashion exist commercially (AggreWell™, Stemcell). However, the plates are single-use, and their shallow well-design results in technical challenges when generating microtissue cohorts of equal size. Additionally, they come at a considerable cost (8.25× the price of a conventional 6-well plate). Alternative, lower-cost hydrogel platforms have recently been made commercially available (MicroTissues® 3D Petri Dish®, Sigma) which offer a more reusable platform than the aforementioned single-use 'all-in-one' plates. Despite

addressing some of the economic limitations, these hydrogel-moulding alternatives fail to satisfy the medium-to-high throughput demands of scaled-up biofabrication. Additionally, the fabrication procedure can be laborious and microwell array design unintuitive. Within the literature, existing microwell platforms involve the use of various non-adherent polymers [142,157–160] and hydrogels [54,60,70–72,129,130,161,162] as substrate materials. The design and methodology employed in these systems varies greatly. Consequently, some methods are conceived as platforms for high-throughput screening rather than biofabrication purposes [162], whilst others, albeit effective and well-designed, are highly complex [158,160], which limits their universal uptake. Some suitable methods for generating large numbers of microtissues for the biofabrication of musculoskeletal tissue have been proposed [70–72]. However, this approach involves unnecessary manual manipulation of the hydrogel microwell mould, and could be significantly simplified by a direct-moulding approach.

There is an increasing interest in generating microtissues in medium/high-throughput fashions for engineering tissues of scale. Given the inadequacies of current commercial and academic microwell platforms, this study sought to design a new platform for the fabrication of hydrogel microwells for use in cell-aggregate and microtissue-based biofabrication strategies. Specifically, the aim was to create a re-usable, cost-effective, simple, and functional microwell platform for generating numerous cell-aggregates and microtissues intended as biological building blocks for musculoskeletal applications. To achieve this aim, this work leverages 3D printing and novel cell-culture procedures. Collectively, the efforts yield a flexible hydrogel platform that supports cell-aggregation of various cell types, the lineage commitment of stem/stromal cells and ultimately the formation of a tissue-specific ECM.

3.1.2 Materials and Methods

Bone Marrow Stem/Stromal Cell (BMCS) Isolation and Expansion: Goat BMSCs (gBMSCs) were harvested under sterile conditions from the sternum of skeletally mature, female, Saanen goats. Briefly, excised bone marrow was cut into small pieces using a scalpel. The marrow pieces were then gently rotated for 5 minutes in high glucose Dulbecco's modified eagle's medium (hgDMEM) GlutaMAX supplemented with 10 % (v/v) FBS, 100 U/mL penicillin, 100 µg/mL streptomycin (all Gibco, Biosciences, Dublin, Ireland) and 5 ng/mL FGF2 (Prospect Bio) (XPAN) to help liberate the cellular components. The culture medium was then aspirated and passed through a 40 µm cell sieve prior to counting and plating at a density of $57 \times 10^3/cm^2$ and expanded under physioxic conditions (37 °C in a humidified atmosphere with 5 % CO_2 and 5 % pO_2) for improved chondrogenic differentiation. Following colony formation, gBMSCs were trypsinised using 0.25 % (w/v) Trypsin Ethylenediaminetetraacetic acid (EDTA). gBMSCs for microtissues were expanded from an initial density of 5000 cells/cm^2 in XPAN medium under physioxic conditions until P3. gBMSCs were initially used to validate the capacity of the microwells to support initial cell-aggregation and subsequent growth under chondrogenic culture conditions, while human BMSCs (hBMSCs; see below) were used for the formation of vascular spheroids.

Human BMSC (hMSC) isolation: hMSCs were isolated from unprocessed human bone marrow (Lonza) on the basis of plastic adherence. Briefly, unprocessed bone marrow was plated at 2.5×10^5 cells/cm^2 (estimated approx. 4000-5000 MSCs/cm^2) in XPAN medium and expanded under physiological oxygen conditions (37 °C in a humidified atmosphere with 5 % CO_2 and 5 % pO_2). Following colony formation, hBMSCs were trypsinised using 0.25 % (w/v) Trypsin Ethylenediaminetetraacetic acid (EDTA), hBMSCs were expanded in XPAN under physioxic conditions (5 % pO_2) and used at P3.

Human Umbilical Vein Endothelial Cell (HUVEC) Expansion: GFP-expressing HUVECs (Lonza, Walkersville, MD) were cultured at 2500 cells/cm^2 in Endothelial growth media (EGM), which is composed of Endothelial Cell Basal Medium-2 (EBM) (Lonza) supplemented with MV Microvascular Endothelial Cell Growth Medium-2 BulletKit™ (Lonza), at 37 °C in a humidified atmosphere with 5 % CO_2 and 20 % pO_2. HUVECs were used at P4.

Cartilage Microtissue formation: Key features of the design process involved in creating the novel method for forming microtissues is discussed in the results section of this chapter. Generic details pertaining to the formation of the microtissues are described herein. The microwell stamps were sterilised using ethylene-oxide (EtO) gas prior to use.

Cells were seeded into the microwells by pipetting an appropriate density into each well. After seeding, plates were centrifuged at 700 × g for 5 minutes to collect cells at the bottom of each well. Plates were then incubated in XPAN described previously. For establishing conditions for forming

cartilage microtissues, two culture conditions were initially explored. The first involved 7 days of cultivation in XPAN medium, the second included a switch to chondrogenic differentiation media (CDM) after the first 4 days in XPAN. CDM consisted of hgDMEM GlutaMAX supplemented with 100 U/ml penicillin, 100 µg/ml streptomycin (both Gibco), 100 µg/ml sodium pyruvate, 40 µg/ml L-proline, 50 µg/ml L-ascorbic acid-2-phosphate, 4.7 µg/ml linoleic acid, 1.5 mg/ml bovine serum albumin, 1 X insulin–transferrin–selenium, 100 nM dexamethasone (all from Sigma), 2.5 µg/ml amphotericin B and 10 ng/ml of human transforming growth factor-b3 (TGF-b3) (Peprotech, UK) at 37 °C in a humidified atmosphere with 5 % CO_2 and 5 % pO_2.

Cartilage macrotissue self-organisation: After 7 days, microtissues were harvested, counted and seeded into agarose wells. The well was created using sterile 2 % (w/v) agarose cast into a 12 well plate. The central agarose well was 2 mm in diameter and 1.5 mm in depth. The number of microtissues seeded to create each construct was determined as a function of the microtissue volume and the volume of the final construct. As such, the following equation was used:

$$Number\ of\ microtissues = \frac{Volume\ of\ the\ construct\ \times 0.74}{Volume\ of\ the\ microtissue}$$

Where,

$$Volume\ of\ the\ microtissue = \frac{4}{3}\pi r^3$$

and 0.74 is the packing efficiency, or packing factor. For this study the volume of the construct chosen was determined using 2 mm diameter and a depth of 1 mm. After seeding the microtissues into the central agarose well, CDM was added slowly to prevent disruption of the microtissues. The developing cartilages were maintained in CDM and physioxic conditions for 3 weeks. Media was exchanged every 2-3 days.

Vascular Spheroid Formation, Fibrin Hydrogel Formulation & Seeding: For the generation of vascular spheroids, HUVECs (either alone or in combination with hMSCs) were seeded into the microwells as a homogenous cell suspension at an appropriate concentration to create spheroids contain 1×10^3 cells. Microwells were centrifuged at 600 × g for 5 minutes and plates were then incubated in EGM, described previously, in physiological oxygen conditions (37 °C in a humidified atmosphere with 5 % CO_2 and 5 % pO_2) for 24 h to allow for spheroid formation.

The capacity to form functional vascular spheroids was evaluated using a fibrin based hydrogel. Previously, a similar hydrogel has been modified using a gelatin carrier method which was adapted from Kang et al. [163], and shown to support the formation of prevascular networks [164]. Briefly, formulation of the fibrin hydrogel/bioink involved the addition of hyaluronic acid (Sigma) to high glucose Dulbecco's Modified Eagle Medium (hgDMEM) (Gibco, Biosciences) at a concentration of

3 mg/mL and overnight stirring at 37 °C to ensure complete dissolution. 10 % (v/v) glycerol (Sigma) was then added and the solution was stirred for 1 h at room temperature. Gelatin type A (175g bloom) (Sigma) was added at a concentration of 40 mg/mL and stirred for 2 h at 37 °C until fully dissolved. Before use, Fibrinogen (Sigma) was added to this carrier gel at a concentration of 30 mg/mL and stirred for 2 h at 37 °C. Vascular spheroids were seeded into the hydrogels at a density of 300 spheroids per 50 µL of hydrogel, in accordance to similar studies within literature [96].

To enhance vascularisation, EGM was supplemented with 50 ng/mL of human vascular endothelial growth factor (hVEGF, Peprotech). After 7 days of culture in physiological oxygen conditions (37 °C in a humidified atmosphere with 5 % CO_2 and 5 % pO_2), prevascularised constructs were evaluated using confocal microscopy. For immunocytochemical analysis hydrogels were fixed with 4 % PFA for 30 minutes, permeabilised in 0.5 % Triton in PBS for 15 minutes and stained with Rhodamine red Phalloidin (5U/mL; 165nM; Thermo Fisher) for 1 h. Cells were washed and counterstained with DAPI (4',6-diamidino-2-phenylindole; 1µg/mL; Sigma) for 15 minutes and imaged using a Leica SP8 scanning confocal microscope. Representative images are presented as maximum projections of z-stacks.

Histological Evaluation: Samples were fixed using 4 % paraformaldehyde (PFA) solution overnight at 4 °C. After fixation, samples were dehydrated in a graded series of ethanol solutions (70 % - 100 %), cleared in xylene, and embedded in paraffin wax (all Sigma-Alrich). Prior to staining tissue sections (5 µm) were rehydrated. Sections were stained with hematoxylin and eosin (H&E), 1 % (w/v) alcian blue 8GX in 0.1 M hydrochloric acid (HCL) (AB) to visualise sulphated glycosaminoglycan (sGAG) content and counter-stained with 0.1 % (w/v) nuclear fast red to determine cellular distribution, and 0.1 % (w/v) picrosirius red (PSR) to visualise collagen deposition (all from Sigma-Aldrich). Stained sections were imaged using an Aperio ScanScope slide scanner. Sections stained with PSR were imaged using polarised light microscopy (PLM) to visualise collagen fibre orientation. Immunohistochemistry was performed for collagen type I (Abcam ab90395 1:400), collagen type II (Santa Cruz sc52658 1:400), and collagen type X (Abcam ab49945 1:200) as previously described [165].

Image Quantification and Statistical Analysis: Diameter measurement of growing microtissues were taken from microscope images (4x) using ImageJ software. Statistical analysis was performed using GraphPad Prism software (GraphPad Software, CA, USA). Analysis of differences between two groups at one timepoint was done using a standard two-tailed t-test. For two or more groups over multiple time-points a two-way analysis of variance (ANOVA) was performed. Numerical and graphical results are presented as mean ± standard deviation unless stated otherwise. Significance was determined when $p < 0.05$.

3.1.3 Results and Discussion

Stamp Design and Fabrication

The stamps, which acted as positive moulds for the microwell pattern, were designed using Solidworks® CAD software. Each microwell measured 1 mm in diameter (ø), with a total well depth of 1.5 mm, which comprised of a 1 mm deep cylindrical section and a domed end which was 0.5 mm deep (Figure 3.1B). The top of each microwell was chamfered asymmetrically, 0.5 mm × 1 mm (width × depth). As this approach was intended for use within a scalable biofabrication strategy, the platform needed to maximise the number of microtissues generated. Here, a 6-well plate was selected as it gives the largest culture surface-area of the standard well-plates. The individual positive microwell moulds were patterned onto the stamp that was designed to fit into the individual wells of a 6 well-plate, creating 401 microwells at the bottom of each well. Again, microwells were patterned onto the stamp to fill the surface with only whole microwells and to also avoid creating flat-spots around the perimeter of the well (Figure 3.1B).

The design of the individual microwells was motivated by other microwell platforms described in literature [54,70–72,156,157]. Each microwell needed to have a round-bottom to encourage the formation of a uniform, spherical aggregate [154]. Additionally, each microwell needed to be sufficiently deep to prevent the interaction of neighbouring aggregates/microtissues, and to ensure easy handing during cell-culture. Creating shallow wells results in the inadvertent fusion between adjacent microtissues [54], which creates an inhomogeneous population. Generating consistent microtissues has been described as essential both for generating a homogenous phenotype throughout the population, as well as for efficient deposition using extrusion-based bioprinting [71]. To facilitate this the top of each microwell was sloped, with no ‘flat-spots’ between adjacent microwells. This ensured the collection of all of the cells within suspension, maximising the efficiency of the technique and reproducibility of the spheroids. Other microwell designs reported in literature which have flat surfaces between adjacent wells have resulted in the collection of cells outside of the microwell [157].

A STL file for the part was then prepared for printing using Preform 2.16.0 software (Formlabs, Massachusetts, United States); a 50 µm layer height was used for every mould. Positive moulds were fabricated using a Form 2 stereolithography printer (Formlabs, Massachusetts, United States). Completed parts were processed post-printing in accordance with the manufacturer’s guidelines. Briefly, parts were washed in propan-2-ol (Sigma Aldrich) to clear any uncured resin, following which they were exposed to UV light (405 nm, 9.1 W) (Form cure, Formlabs, Massachusetts, United States) for 30 minutes at 60 °C to ensure complete crosslinking. Selecting SLA printing as the manufacturing method resulted in excellent resolution. The positive moulds of the final part were uniform and highly

reproducible (Figure 3.1C). The surface finish of the individual microwell moulds was also excellent with no obvious roughness or irregularities, making them an ideal positive pattern for the hydrogel (Figure 3.1C iii).

The process for fabricating the hydrogel microwells (Figure 3.1D) involved first pouring molten agarose (4 % (w/v), 80 °C) into the wells of a 6-well plate. Before the stamps were inserted into the molten hydrogel, they were sprayed 2-3 times with sterile DiH_2O using an atomiser spray-bottle. The fine water droplets deposited on the moulding surface of the stamp worked to overcome the surface tension created between the viscous hydrogel solution and the surface of the stamp. As such, it ensured accurate recreation of the positive mould and prevented the formation of bubbles at the stamp-hydrogel interface by allowing the hydrogel to easily flow through the tortuous architecture. Each stamp was held in place using a holder, which ensured the stamps were held at a fixed height and at 90° to create consistent microwells in each macro-well and between well plates. After the hydrogel has cooled and solidified, the holders and mould could be removed, leaving behind the hydrogel microwells within the well plate. This direct-patterning approach proved an effective way of modifying 6-well plates in a cost-effective, reproducible, and re-usable manner. Since the positive-mould for the microwells was a stamp, the moulding process described within this study was simplified from previous systems. Frequently, microwells are cast in a separate positive mould, before being manually removed and inverted into the well-plate [70,72,142,161]. By directly moulding the agarose within each well this system minimised the risk of human error, as well as the unnecessary manual manipulation of the hydrogel microwells during fabrication.

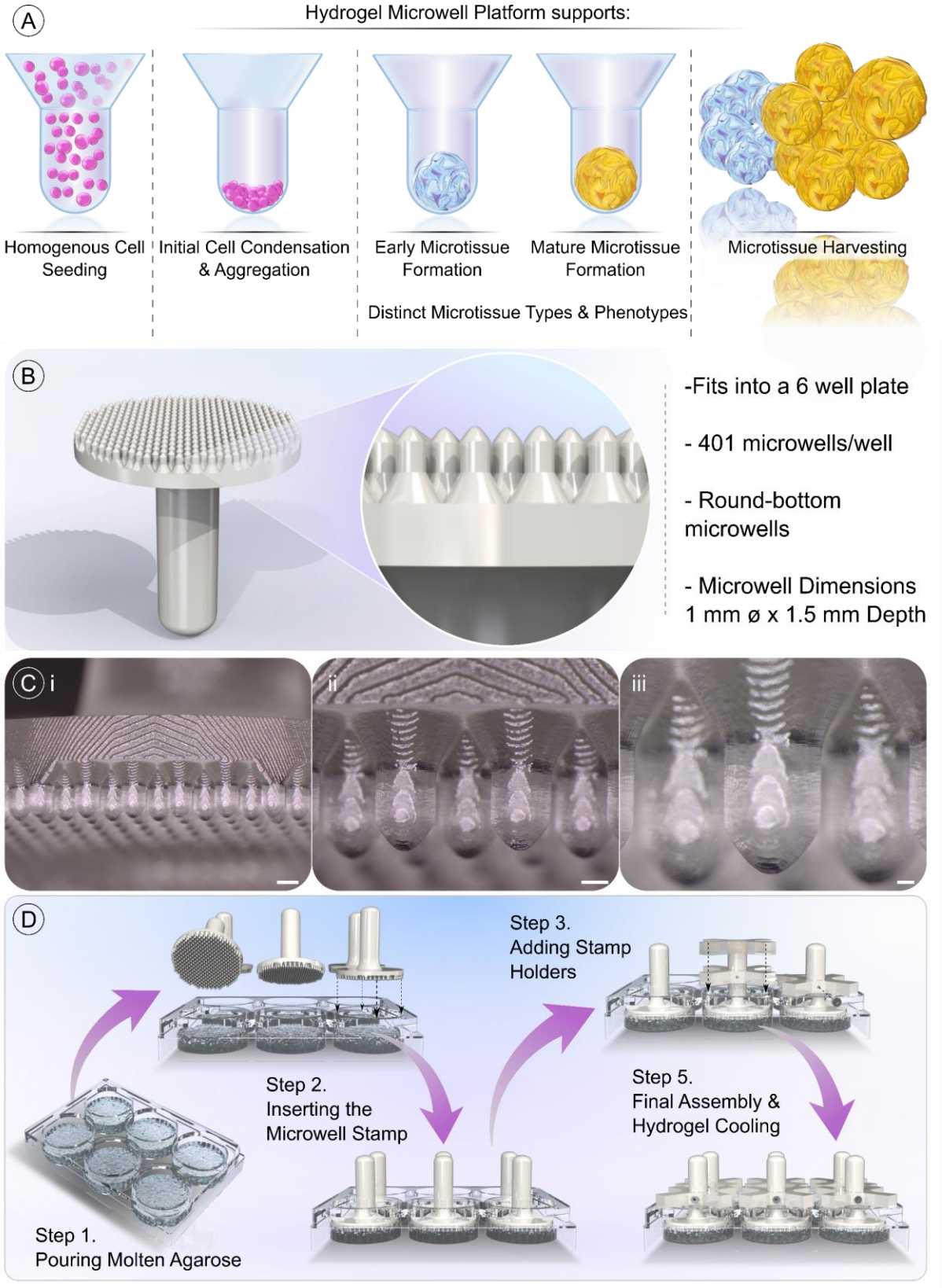

Figure 3.1 *Design and Fabrication of a novel microwell stamp and protocol for hydrogel microwell generation. A) Cartoon of the cellular processes the hydrogel platform would need to support to be effective. B) Schematic of stamp design and key features. C) Macro/micro-images of the 3D printed stamp. (Scale Bars: i) 1 mm, ii) 500 µm, iii) 200 µm) D) Schematic of the microwell moulding process.*

Early Validation of Microwell Platform for Generating Cartilage Microtissues

To assess if the microwell system developed herein was capable of supporting the processes outlined in Figure 3.1A, gBMSCs were seeded into the macro-wells at different densities to create cell aggregates with a range of starting cell numbers (1×10^3, 2×10^3, 4×10^3, 8×10^3, and 16×10^3). At day 2, microscopic images indicated that cell-aggregates could be generated within the hydrogel microwells at all densities (Figure 3.2A). Additionally, by simply varying the cell-number, the size of the cell-aggregate/microtissue could be altered, with aggregate size increasing with the initial cell number (Figure 3.2B). Quantification of aggregate diameter also indicated the methodology for seeding the microwells, coupled with their design, created highly reproducible cell-aggregates (Figure 3.2B).

To determine culture conditions for creating sizable microtissues for use as biological building blocks, two culture regimes were initially compared. The first involved 7 days of cultivation in XPAN medium. Here, with the exception of the 1×10^3 and 2×10^3 cells per microtissue groups, a significant

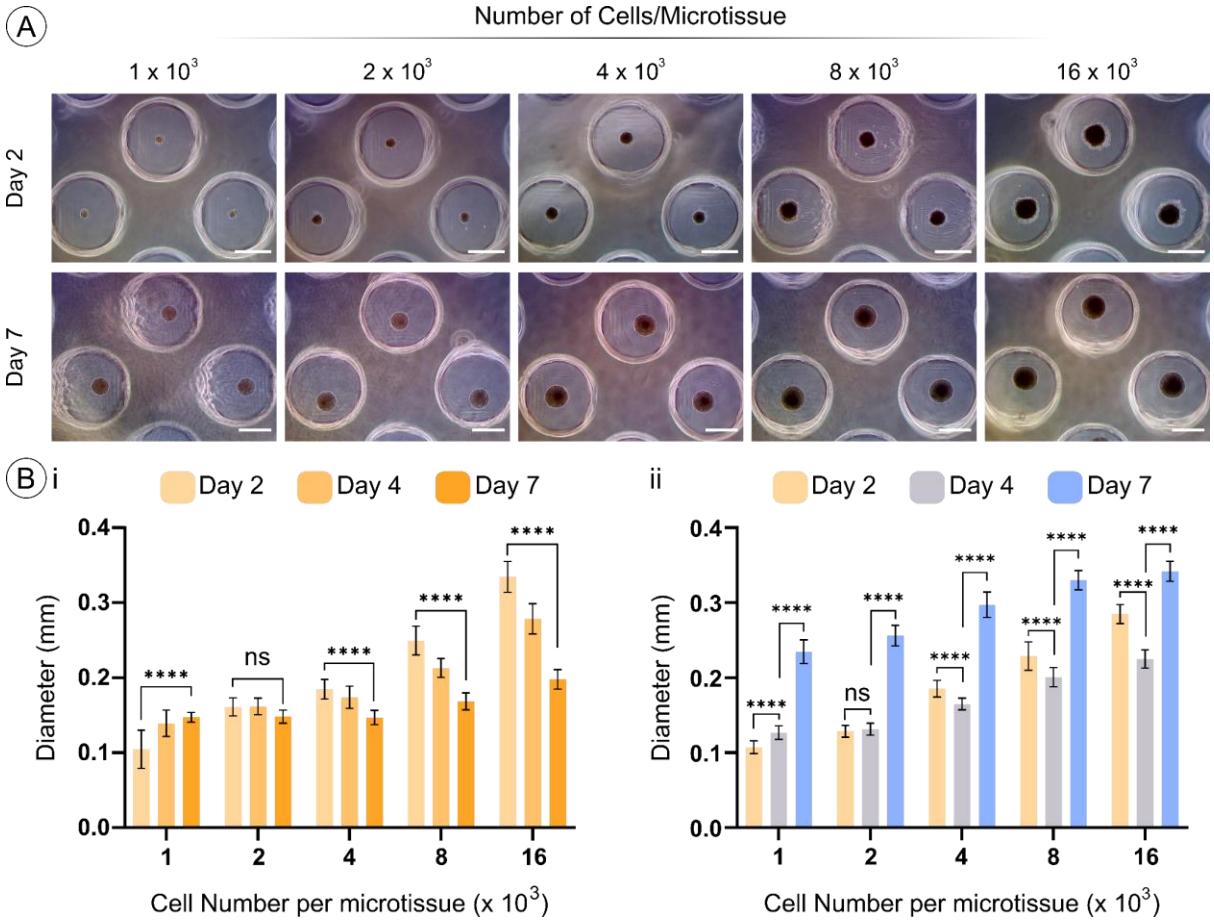

Figure 3.2 *Early validation of hydrogel microwell platform. A) Microscopic images of cell aggregation of MSCs after 2 days, and the growth of the microtissues after 3 days of chondrogenic induction (Day 7). (Scale Bar = 500 µm). B) Quantification of cell aggregates/microtissues diameter. i) Cell aggregates cultivated in XPAN for 7 days. ii) Early cartilage microtissues cultivated in 4 days of XPAN followed by 3 days in CDM. * Denotes significant differences when tested using an ordinary two-way ANOVA, with Tukey multiple comparison test (N = 12, Mean ± SD).*

contraction of the cell-aggregate was observed over the 7 day cultivation. The resulting spheroids generated by cultivation in XPAN medium were was too small (<200 µm) to be feasibly used for generating tissues of scale (Figure 3.2B i). For the second condition, aggregates were maintained in XPAN for 4 days, followed by stimulation with CDM for a further 3 days. By day 7, the microtissues was grown significantly from day 4 (Figure 3.2A & B ii), suggesting that they could be further used as building blocks for the generation of cartilage microtissue.

To evaluate the capacity of these early cartilage microtissues to self-organise into a cartilage macrotissue, sufficient numbers of microtissues were placed into a non-adherent agarose well to fill

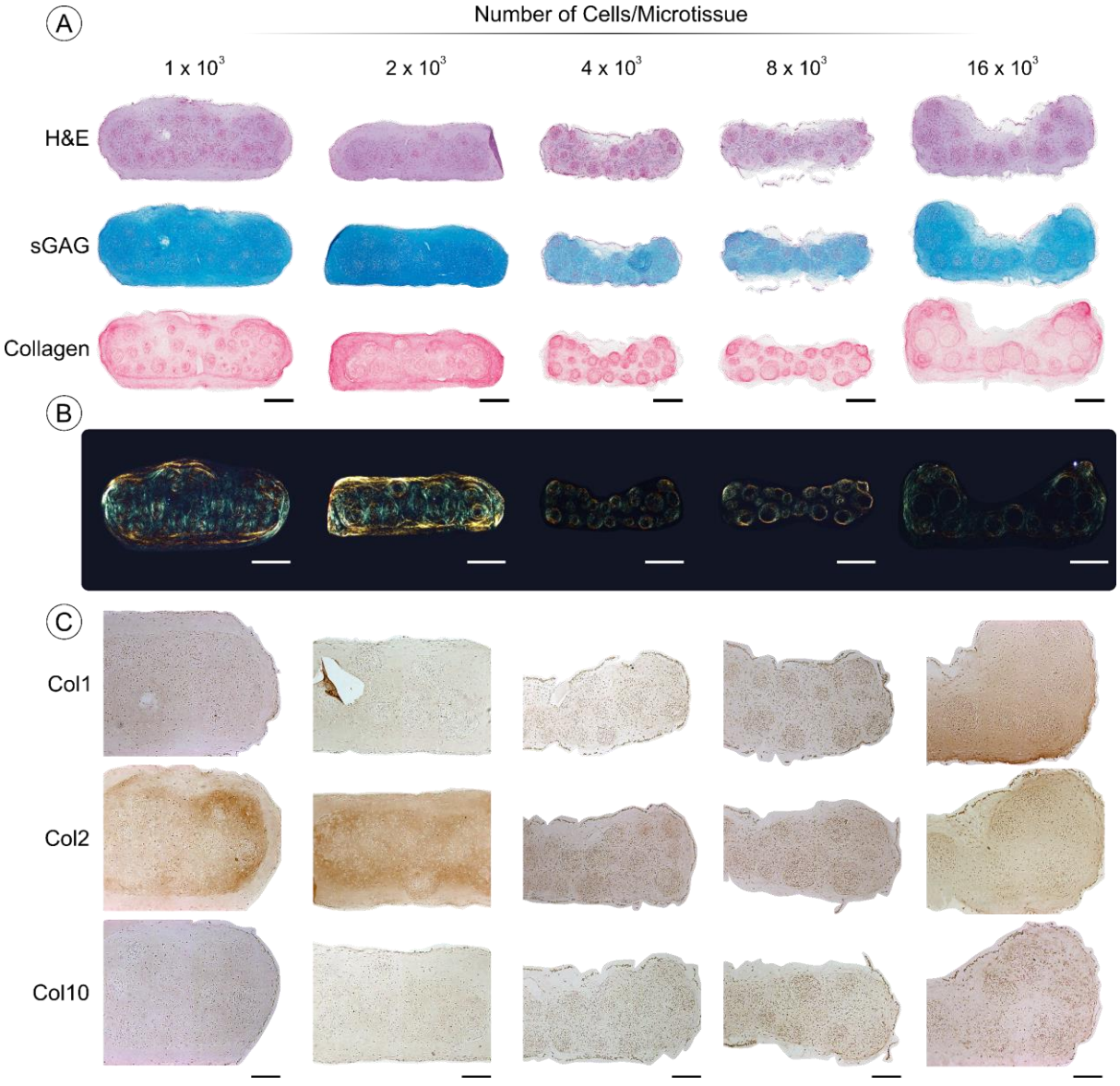

Figure 3.3 *Early validation of microtissues generated within the hydrogel platform to fuse into a homogenous cartilage. A) Histological panel for canonical cartilage matrix components after 21 days of chondrogenic culture. (Scale Bar = 400 µm). B) Polarised light microscopy for visualising the collagen arrangement. (Scale Bar = 500 µm). C) Immunohistochemistry panel for collagen types I, II, and X after 21 days of chondrogenic culture. (Scale Bar = 200 µm).*

2 mm ø × 1 mm. Over 21 days of chondrogenic culture, the initially discrete tissue-units fused and created a cartilage tissue. The quality of the cartilage, determined *via* histology, seemed to vary significantly depending on the initial cell density which was employed (Figure 3.3). Specifically, it appeared that using a larger number of smaller microtissues (lower number of cells per microtissue) yielded a tissue that was more homogenous (Figure 3.3A), cartilaginous (Figure 3.3A & C), and organised (Figure 3.3B) compared to using a relatively low number of larger and more cellular microtissues. This early work on self-organising cartilage microtissues served to validate that, the hydrogel microwell platform developed within this chapter was suitable as a means of generating large numbers of microtissues for use in biofabrication/bioassembly strategies. In particular, MSCs within cell-aggregates could be differentiated into early-cartilage microtissues, with the growth of these microtissues during chondrogenic induction yielding spheroids which were sufficiently large (> 200 µm) to be used for bioassembly. These early findings suggest that harvesting and re-seeding the cartilage microtissue seeds did not prevent the formation of a cartilage phenotype within the self-organised macro-tissue. Furthermore, it would appear that using a greater number of smaller, less cellular microtissues appeared to yield a superior engineered macro-cartilage after 21 days of cultivation.

Differences in nutrient diffusion and cellular consumption rates within the engineered cartilages could help to explain this observation. Specifically, chondrocyte oxygen consumption has been linked to glucose consumption whereby, in low glucose conditions near anoxic conditions can arise [166]. This 'Crabtree' effect could be influencing the more cellular engineered cartilages where low glucose levels drive the consumption of oxygen and create extreme hypoxic conditions within the construct and inhibit ECM synthesis. Moreover, cell viability, matrix production and mechanical functionality of engineered cartilages using MSCs has been shown to be compromised by glucose and oxygen deprivation [167]. In particular the work by Farrell *et al.* indicated that glucose deprivation was the principle limiting factor in construct maturation [167]. In a similar traditional hydrogel based tissue engineering approaches, the accumulation of matrix macromolecules during chondrogenic cultivation has been coupled with a 42% reduction in diffusivity [168]. As such, the compounding effects of matrix deposition and high glucose consumption rates in more cellular engineered cartilages could explain their poor ECM accumulation and maturation. Additionally, acidic conditions (pH 6.4) generated through the addition of lactic acid has been shown to significantly inhibit sGAG production [169]. In this context, cartilage macrotissues engineered using less cellular microtissues may accumulate less acidic waste metabolites, leading to superior matrix accumulation. Future work within this thesis will look to optimise the cultivation and self-organisation regimes employed, with a view to creating a scalable engineered AC suitable for joint repair.

Hydrogel Microwell Platform Supports the Formation of Vascular Spheroids

As part of the microwell platform development, the capacity for the system to support the aggregation of HUVECs, as well as co-cultures of HUVECs and hMSCs, for the generation of vascular spheroids was also assessed (Figure 3.4A). After 24 hours, the vascular spheroids could be harvested from the wells without dissociating (Figure 3.4B). Furthermore, seeding the 3:1 and 1:1 MSC:HUVEC vascular spheroids into a fibrin-based hydrogel, that has been shown to support vascularisation [164], resulted in HUVEC sprouting and the generation of a microvascular network. There was an apparent improvement in the pervasiveness of this vascular network by increasing the number of hMSCs within the vascular spheroids (Figure 3.4C).

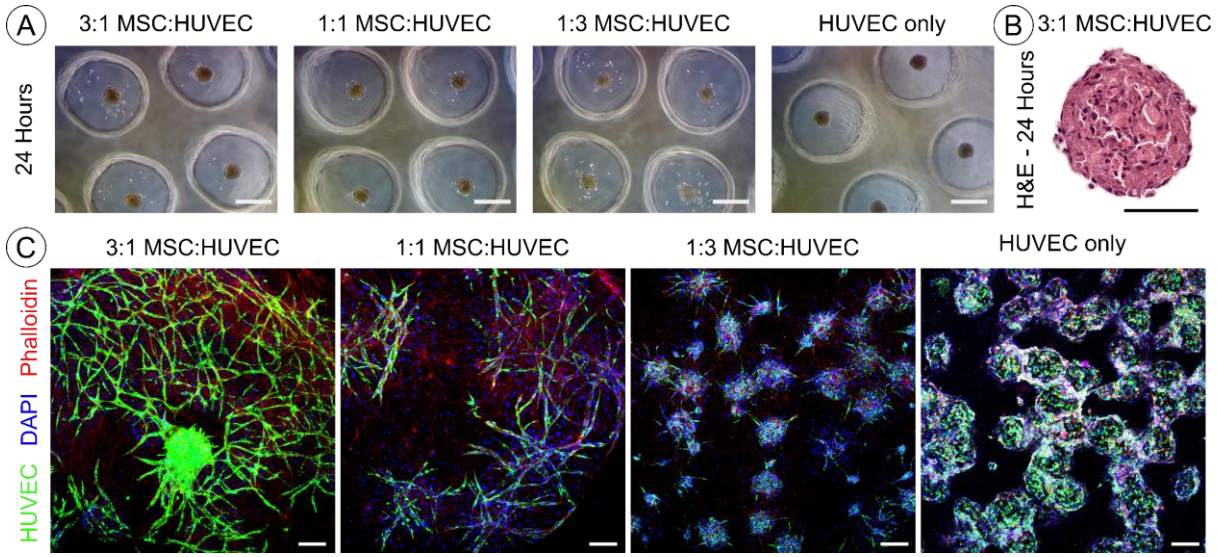

Figure 3.4 *Generation of vascular spheroids for prevasacularisation. A) Vascular spheroids formed after 24 hours using different co-culture ratios of hMSCs & GFP-HUVECs (1 × 10^3 cells/spheroid). (Scale Bar = 500 µm). B) H&E Staining of a 3:1 (hMSC:HUVEC) vascular spheroid after 24 hours. (Scale Bar = 100 µm). C) Immunocytochemistry for the visualisation of pre-vascular network formation within the fibrin based hydrogel. (Scale Bar = 150 µm)*

A well-documented challenge associated with engineering vascularised musculoskeletal tissues, such as bone, at a clinically relevant scale are the increasing nutrient demands. To combat this, multiples strategies for vascularising engineered tissues have been proposed, including pro-angiogenic growth factors and the inclusion of channels within engineered constructs [170–175]. Such approaches rely on the ingrowth of host vasculature from the defect site surrounding the engineered tissue/construct. This process of angiogenesis is relatively slow [94], and can be ineffective for large engineered implants. As such, strategies to 'prevascularise' an engineered tissue have been developed. Here, forming a microvascular network within the implant *in vitro* is proposed as a rapid method of perfusing engineered tissues *in vivo via* anastomosis of an engineered microvasculature with host vessels [176,177]. Typically, generating a microvascular network *in vitro* involves a homogenous suspension of endothelial cells (with or without supporting mural cells such as

fibroblasts or MSCs) within an appropriate hydrogel [164]. However, the use of spheroids in microvascular engineering has also been proposed [72], where they have been shown to outperform single-cell approaches *in vitro* and *in vivo* [95,96]. As part of this work, albeit in its infancy, the microwell platform has been shown to support the formation of vascular spheroids. Furthermore, like with early-cartilage microtissues, these vascular spheroids can be harvested and re-used as vascular seeds for the biofabrication of a microvascular network. These preliminary results provides evidence that the hydrogel microwells developed within this chapter can be an important tool in strategies that aim to biofabricate musculoskeletal tissues of scale using the bioassembly of phenotypically distinct microtissue populations.

3.1.4 Conclusion

Taken together, the results in this study demonstrate the successful design and implementation of a novel microwell platform technology for the high-throughput fabrication of microtissues. The platform satisfies the key criteria for the ideal spheroid/microtissue biofabrication platform, specifically a scalable process capable of generating standardised microtissues which exhibit a specific phenotype and which are also capable of fusion into large macro-tissues. Importantly, this work fits into a larger biofabrication scheme, as the ability to harvest these tissue-units and use them as seeds for engineering musculoskeletal tissues (cartilage and vasculature) has been demonstrated.

3.2 Novel Bioreactor Design

3.2.1 Introduction

Bioreactor systems have been used for the generation of mesenchymal stem/stromal cell (MSC) aggregates from single-cell suspensions, in so called 'dynamic collision-based assembly', but attempts to leverage similar dynamic conditions for the prolonged cultivation of MSC aggregates have been limited [156,178]. In tissue engineering strategies, where numerous MSC aggregates/microtissues are intended as biological building blocks for organogenesis, many current approaches for spheroid biofabrication have been described as 'not scalable' as they are unable to generate the necessary quantity of spheroids for organ biofabrication [154]. To this end, microwells are often discussed as one of the few truly 'high-throughput' technologies, capable of generating a sufficient numbers of organ-seeds [154]. However, complications during extended culture periods, such as interactions between adjacent spheroids creating an inhomogeneous population, constrained tissue growth/development due to nutrient limitations, and diminishing spheroid yield, means that they may not be represent an ideal solution. Despite these shortcomings, cell aggregates formed in static conditions within microwell arrays are far more reproducible than those generated in dynamic conditions and, as such, are better suited to biofabrication applications [154,156,178]. Therefore, combining bioreactors for spheroid cultivation after formation in a microwell platform has been proposed as a means of improving scalability [54], without compromising spheroid quality.

Efforts to follow static aggregate formation with dynamic cultivation have predominantly used undifferentiated MSC aggregates [179–182]. Here, dynamic cultivation of MSC aggregates has been associated with active proliferation, mitigation of core necrosis, and the maintenance of stemness [178]. However, seeding pre-formed aggregates into gentle dynamic systems, such as orbital shakers, results in amalgamation and fusion of the initially discrete units [179]. In the context of biofabrication, the homogeneity of a spheroid/microtissue population is essential for retaining the ability to create user-defined tissue geometries. As such, more aggressive dynamic systems like stirred-tank reactors, which have been used for the culture of MSC aggregates [183], could be used to maintain single-spheroids during dynamic cultivation. Here, undifferentiated MSC aggregates cultured in such systems using expansion medium have been shown to coalesce during culture [184], although it remains unclear whether differentiated MSCs within microtissues behave differently [182].

Motivated by the reported benefits of culturing undifferentiated MSCs in dynamic systems, coupled with the known benefits of bioreactor culture in tissue engineering [185]. This study aimed to evaluate if bioreactor culture would enhance the engineering of homogenous cartilage microtissues the cultivation of microtissues. Specifically, the aim was to determine if the putative mass-transfer benefits of bioreactor culture [185] would mitigate the diffusion related challenges reported in static

spheroidal culture [178,183], and ultimately improve the quality of the engineered microtissue. Additionally, this work aimed to elucidate if bioreactor culture could be used to alleviate the problems associated with long-term microwell culture, specifically spheroid-spheroid and spheroid-microwell interactions, and well as constrained spheroid growth/development due to nutrient limitations. To evaluate this, a simple bioreactor was designed and fabricated. This novel bioreactor was intended as an accessible and cost-effective alternative to more complex equivalents and if effective, could be easily implemented within a larger biofabrication strategy using microtissues as biological building blocks. Within this chapter, protocol/engineering decisions were motivated by the primary goal of maintaining the suitability of spheroids for subsequent biofabrication processes. As such, the culture conditions were tailored towards avoiding the aggregation of the initially discrete spheroids seeded into the bioreactor. To this end, the bioreactor was intended as a step in a biofabrication strategy facilitating the medium-long term cultivation of spheroids. In this context, the bioreactor needed to be simple and easily implemented. Therefore, the decision was made to design a stirred bioreactor rather than a more complex and potentially problematic perfusion system.

3.2.2 Materials and Methods

Stirred Bioreactor Hardware Design and Fabrication: The framework for the bioreactor was designed using Solidworks® CAD software, converted into g-code using Ultimaker Cura 4.8, and fabricated from PLA using an Ultimaker 3+ (Ultimaker B.V.). In total, there were 6 modular components that constituated the frame. The individual pieces of the framework were designed to slot into eachother to ensure good alignment. To further secure the framework, M3 brass threaded inserts (Radionics, Ireland) were press fit into the framework at pre-defined locations and the modular component of the frame were screwed in place. Built into the base-plate of the frame was a slot for the culture vessel to ensure centralisation of the propeller. Within the back-plate, housing for an ILS OSLONeye LED mini-spotlight (Intelligent LED Solutions, Radionics) was included. This was situated behind the culture vessel and allowed for visualisation of the spheroids during cultivation. Within the top-plate, positions for stainless steel bearings (RS Pro, Radionics) were included. A flexible beam coupling (Radionics) was used to connect the NEMA-17 stepper motor and the stainless steel drive shaft. IP68 cable glands (Radionics) were used to seal the wiring that entered the motor housing. Components of the lid seal were designed using Solidworks® CAD software, converted into g-code using Preform 2.16.0 software and the part was fabricated using a Form 2 stereolithography printer (both Formlabs, Massachusetts, United States).

Stirred Bioreactor Electronics & Motion Control: A control box was assembled to house electronic components responsible for controlling the motor and LED. An Arduino Uno (Figure s3.1A i) powered by a 12V DC supply (Figure s3.1A ii) was used as a microprocessor to send control signals to a DM542 2-Phase Stepper Motor Driver (Figure s3.1A iii) powered by a 24V DC supply (Figure s3.1A iv). The stepper driver output was connected to a Nema-17 stepper motor, which was mounted in the bioreactor chassis and used to rotate the propeller shaft. A circular LED array (ILS OSLONeye LED mini-spotlight) driven by a constant current LED driver (Figure s3.1A v) and controlled by a switch on the front panel of the control box. An LCD display (Displaytech 162D-CC-BC-3LP) (Figure s3.1A vi) was used to communicate information on RPM at the front panel of the control box. Code was written in Arduino IDE software to set the RPM of the motor in discrete increments of 30 from 0 – 180 RPM using a 10 KΩ potentiometer on the front panel of the control box (Figure s3.1B). The front panel also contained 2 single pole single throw (SPST) switches to control motor rotation direction and turn the LED on/off, in addition to a 1 KΩ potentiometer to control contrast on the LCD display. The rear panel of the control box contains a power lead to plug into a mains electrical outlet, a power switch to turn on mains power inside the control box, and a control lead containing all wires to control the motor and LED (Figure s3.1C). A DB9 connector is wired to the end of the control lead to plug into and interface with the bioreactor.

Cell Culture and Cartilage Microtissue Formation: gBMSCs were isolated and expanded as previously described in §1.2 of this chapter. Briefly, isolated gBMSCs were expanded in high glucose Dulbecco's modified eagle's medium (hgDMEM) GlutaMAX supplemented with 10 % (v/v) FBS, 100 U/mL penicillin, 100 µg/mL streptomycin (all Gibco, Biosciences, Dublin, Ireland) and 5 ng/mL FGF2 (Prospect Bio) (XPAN) under physioxic conditions (37 °C in a humidified atmosphere with 5 % CO_2 and 5 % pO_2) until P3. Cartilage microtissues were formed within hydrogel microwells that had been pre-soaked in EGM. A cell suspension was seeded into these microwells as previously described in §1.2 of this chapter to generate microtissues containing 4×10^3 gBMSCs. After 2 days of chondrogenic induction, cartilage microtissues intended for further cultivation were harvested, counted, and moved into the stirred bioreactor. Within the bioreactor, they were cultured in an equivalent volume of CDM to those that remained in static conditions within the agarose microwells - 0.535×10^6 cells/mL. The propeller speed was set to 150 RPM, as this was determined as the minimum speed required to maintain the spheroids in suspension. Both cohorts of microtissues were cultured in physioxic conditions, and media was exchanged every 2-3 days.

Histological and Biochemical Analysis: After 14 days of chondrogenic cultivation, microtissues were harvested, washed in saline and fixed using 4 % paraformaldehyde (PFA) solution overnight at 4 °C. After fixation, samples were dehydrated in a graded series of ethanol solutions (70 % - 100 %), cleared in xylene, and embedded in paraffin wax (all Sigma-Alrich). Prior to staining tissue sections (5 µm) were rehydrated. Sections were stained with hematoxylin and eosin (H&E), 1 % (w/v) alcian blue 8GX in 0.1 M hydrochloric acid (HCL) (AB) to visualise sulphated glycosaminoglycan (sGAG) content and counter-stained with 0.1 % (w/v) nuclear fast red to determine cellular distribution, 0.1 % (w/v) picrosirius red (PSR) to visualise collagen deposition, and 1 % (w/v) alizarin red (AR) (pH 4.1) to determine mineral deposition *via* calcium staining (all from Sigma-Aldrich). Stained sections were imaged using an Aperio ScanScope slide scanner and thickness measurements obtained using Aperio Imagescope.

Samples for biochemical evaluation were washed in PBS after retrieval. A papain enzyme solution, 3.88 U/mL of papain enzyme in 100 mM sodium phosphate buffer/5 mM Na2EDTA/10 mM Lcysteine, pH 6.5 (all from Sigma–Aldrich), was used to digest the samples at 60 °C for 18 h. DNA content was quantified immediately after digestion using Quant-iT™ PicoGreen ® dsDNA Reagent and Kit (Molecular Probes, Biosciences). The amount of sGAG was determined using the dimethylmethylene blue dye-binding assay (Blyscan, Biocolor Ltd., Northern Ireland), with a chondroitin sulphate standard read using the Synergy HT multi-detection micro-plate reader (BioTek Instruments, Inc) with a wavelength set to 656 nm. Total collagen content was determined using a chloramine-T assay to measure the hydroxyproline content and calculated collagen content using a hydroxyproline-to-collagen ratio of 1:7.69 [186]. Briefly, samples were mixed with 38 % HCL (Sigma)

and incubated at 110 °C for 18 h to allow hydrolysis to occur. Samples were subsequently dried in a fume hood and the sediment reconstituted in ultra-pure H_2O. 2.82 % (w/v) Chloramine T and 0.05 % (w/v) 4-(Dimethylamino) benzaldehyde (both Sigma) were added and the hydroxyproline content quantified with a trans-4-Hydroxy-L-proline (Fluka analytical) standard using a Synergy HT multi-detection micro-plate reader at a wavelength of 570 nm (BioTek Instruments, Inc).

3.2.3 Results and Discussion

Bioreactor Design and Fabrication

The aim of this study was to design a stirred bioreactor, suited to the medium-long term culture of cartilage microtissues. As such, there were several design criteria that needed to be satisfied. The bioreactor needed to operate reliably, both mechanically and biologically, throughout culture. Specifically, the culture vessel needed to remain as a sterile environment for prolonged culture periods (≥ 14 days). This presented a challenge given the moving parts involved with a stirred bioreactor. To overcome this, a lid seal assembly was proposed which would prevent the intrusion of particulate contaminants during operation (Figure 3.5B). The 3-part assembly included a sealing nut, two O-rings, and a magnetic couple (Figure 3.5B ii-iv). Collectively, the sealing nut and O-rings was a conduit for the propeller shaft to enter the culture vessel without creating a direct route for contaminants. Central to this function was the magnetic couple, which served a dual function. Primarily, it connected the propeller shaft to a drive shaft, but by including a skirt that covered the lid-seal nut it also created a physical barrier to particulates. Importantly, this protective function did not

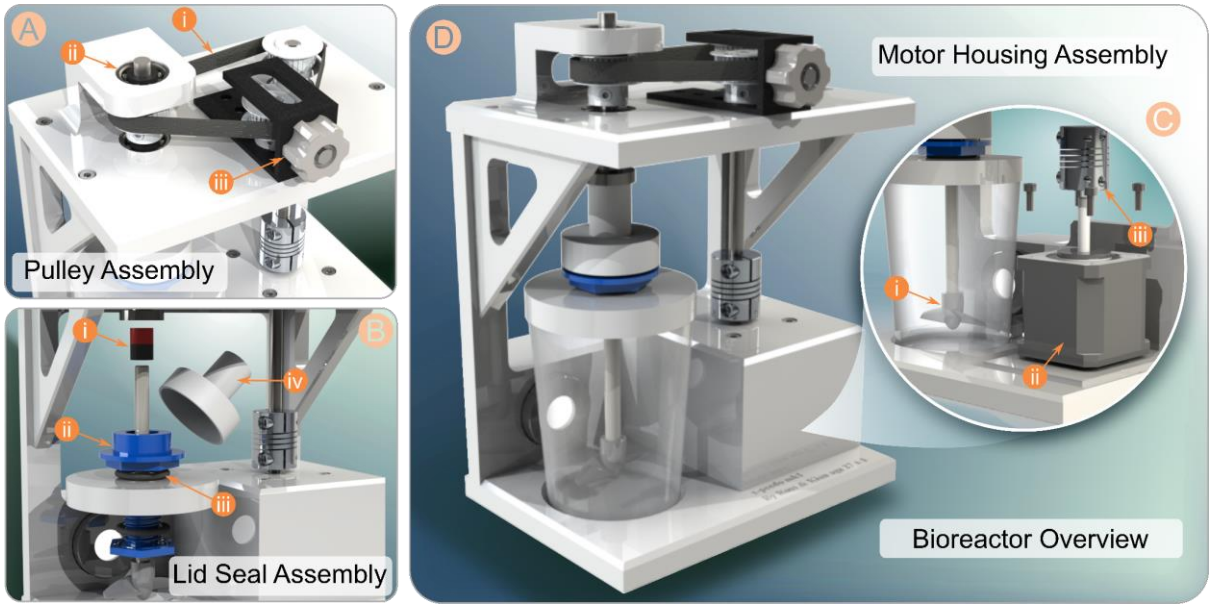

Figure 3.5 *Schematic representations of the stirred bioreactor and key features. A) The pulley assembly, was used to allow the motor to be housed alongside the culture vessel. Conversion of drive to the propeller shaft used three pulleys and a belt (i). Bearings (ii) ensured the drive and propeller shafts ran smoothly and a tension wheel (iii) attached to one of the three pulleys allowed the adjustment of the belt tension to maintain drive efficiency. B) In order to maintain sterility within the culture vessel during operation, a lid seal assembly was designed and implemented. A magnetic couple was used to connect the propeller shaft to drive shaft (i & iv). This allowed for quick release when detaching the culture vessel during media exchanges. The housing for the magnet (iv) had a skirt, which fit over the upper half of the lid seal (ii) to prevent particulates from falling into the culture vessel. Two O-rings (iii) were used to create an air-tight finish when the lid seal was tightened. C) The propeller (i) was driven by a small stepper motor (ii) which was housed in a sealed environment next to the culture vessel. A flexible beam coupling (iii) was used to connect the stepper motor and the drive shaft. D) A schematic of the complete assembly.*

impeding actuation and allowed for gas exchange between the culture vessel and the environment. Additionally, the magnetic couple made removal of the culture vessel from the bioreactor quick and simple without compromising the sterility of the system. Collectively, this mechanism proved effective during acellular pilot-studies where culture media pH (as indicated by phenol-red) remained within an acceptable range and there was no indication of contamination during simulated use and media changes (Data not shown).

This work aimed to provide an accessible platform for the dynamic cultivation of microtissues. To achieve this, the framework for the bioreactor was designed to be fabricated using common commercially available 3D printers (Ultimaker 3+ and Form2). The simple design and assembly was motivated by the need for a bioreactor that can be easily and economically implemented within biofabrication strategies targeted towards generating musculoskeletal tissues of scale. Other custom bioreactors described in the literature for the cultivation of aggregated MSCs require machined parts and custom glassware [183]. Although commercially available stirred bioreactors are widely available, they are expensive. Simple single-use culture vessels alone (without the motorised platform for actuation) can cost €106, and €661 for a reusable version (Corning®). Moreover, these systems are magnetically driven, which means motorised magnetic plates have to be introduced into an incubator. Instead, the bioreactor designed within this study offers an affordable (< €200) all-in-one solution with a small footprint. Furthermore, by having an external control unit for the bioreactor, adjustments to the bioreactor setting without disrupting the incubator environment are possible.

In summation, this chapter describes the design and production of a novel stirred-tank bioreactor, which can be fabricated using simple additive manufacturing technologies that are widely available in tissue engineering labs. Moreover, the bioreactor is a fraction of the cost of commercially available systems without compromising quality and basic functionality. Given the need to employ bioreactors within scalable strategies for organ biofabrication [154], this stirred-tank reactor has the potential to be a valuable asset in academic biofabrication strategies in the future.

Validation of Stirred Bioreactor for the Generation of Cartilage Microtissues

The feasibility of using a stirred bioreactor as a means of generating a large number of high-quality, homogenous cartilage microtissues was investigated as part of this study. Microtissues were first generated in the microwells for 2 days. The quality of the cartilage ECM generated after another 14 days of chondrogenic cultivation within the dynamic cultivation conditions was compared (histologically and biochemically) to a static control where the microtissues remained within the hydrogel microwells (Figure 3.6). Histologically, static cartilage microtissues were much larger, and stained intensely for sGAG and collagen. In contrast, those cultured dynamically stained weakly for sGAG and collagen. Negative staining for mineral deposition within the cartilage microtissues cultured

within the microwells was expected and suggested a stable phenotype. Surprisingly, dynamic cultivation of microtissues within the stirred bioreactor resulted in diffuse positive mineral staining (Figure 3.6A). Biochemically, there was a statistically higher biosynthesis of sGAG from cells within microtissues cultivated in static conditions, but there was no statistical differences in collagen production per cell (Figure 3.6B).

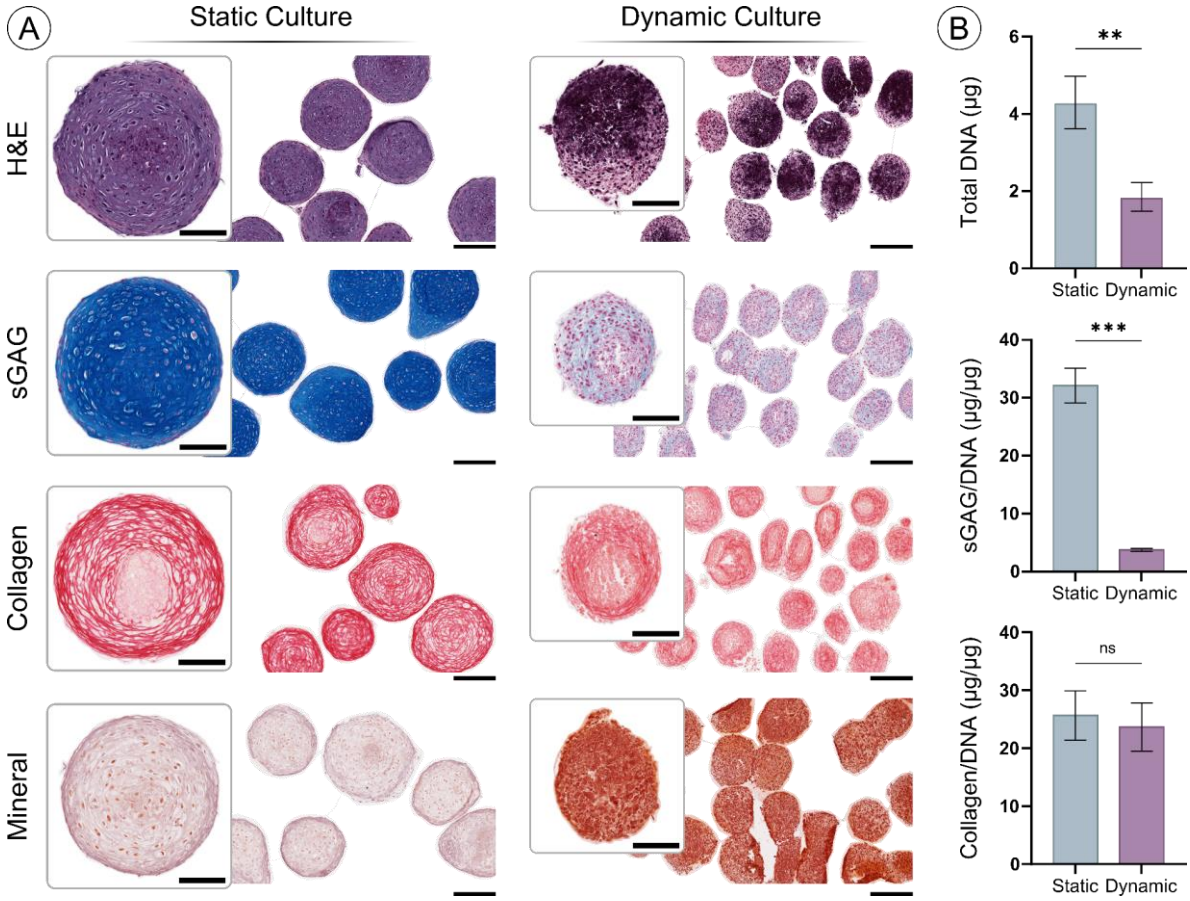

Figure 3.6 *Histological and biochemical evaluation of cartilage microtissues after 14 days of chondrogenic cultivation. A) Histological panel for microtissues cultured within the hydrogel microwells (Static Culture) or within the stirred bioreactor (Dynamic Culture). (Scale Bars; Overview = 200 µm, Zoom = 100 µm). B) Biochemical quantification of the microtissues, levels of DNA as well as sGAG and collagen normalised to DNA content are provided. * Denotes significant difference when tested using a two-tailed, unpaired Welch's t-test, $p<0.05$ (N = 3, Mean ± SD)*

In this study, dynamic conditions within the stirred bioreactor appeared to interfere with chondrogenesis. Despite cultivation in CDM and physioxic (5% pO_2) conditions, there was an uncharacteristic absence of sGAG and diffuse mineralisation within the dynamically cultured microtissues. In the context of chondrogenesis, dynamic conditions (rotational bioreactor) have resulted in an enhanced biosynthetic output of chondrocytes [187], whilst culturing MSCs under similar conditions has resulted in a suppression of chondrogenesis [188]. Here, shear stresses exerted on MSCs was proposed as a contributing factor in dynamic culture not supporting a chondrogenic phenotype [188]. Studies which have used cartilage spheroids to investigate if fluid induced shear has

undesirable effects on chondrogenic differentiation have shown that flow-perfusion reduces chondrogenesis and can upregulate osteogenic markers in MSCs [189]. Similarly, and in agreement with the findings of this study, dynamic culture has resulted in a reduction in sGAG accumulation when using goat BMSCs when compared to static conditions [190]. Although aggregates have been proposed as 'shielding' the inner cell mass from shear forces during dynamic culture [178], the poor chondrogenesis seen within the dynamic condition could be attributed to excessive shear forces generated within the bioreactor.

Another explanation for the aberrant chondrogenesis in dynamic culture could be changes in oxygen tension within the culture vessel whereby, increased oxygen transport in dynamic culture may explain the concurrent reduction in chondrogenesis and increased expression of osteogenic markers within the microtissues. Oxygen tension is a known to be a potent regulator of MSC fate [191–195]. Specifically, lower oxygen tensions are closely coupled with the induction and commitment of MSCs towards a chondrogenic lineage [191,193,195]. Since, dynamic culture conditions will increase the effective pO_2 despite culturing in physioxic conditions, the oxygen tension within the stirred bioreactor may have surpassed optimal conditions for robust chondrogenesis. Moreover, local oxygen gradients within engineered cartilages have been shown to regulate the biosynthetic output of MSC. Specifically, regions of lower oxygen concentration within larger constructs, enhances localised sGAG, and to a lesser extent collagen deposition, in static conditions [196]. As such, the environment at the bottom of the hydrogel microwells could create local hypoxic conditions, favourable for chondrogenesis. This preferential environment could, in part, be accentuating the difference in sGAG production seen between the two culture regimes.

Although it is difficult to decouple the influence of fluid-flow induces shear and oxygen tension on chondrogenesis within this study, these results suggest that dynamic culture should be employed cautiously. Further reduction of the ambient oxygen tension (from 5 % to 3 % O_2) has been shown to facilitate chondrogenesis in dynamic conditions [197], and could be employed here to combat the poor chondrogenesis seen within dynamically cultivated cartilage microtissues. Alternatively, alteration of the stirring speed could help to reduce the putative negative effects fluid-shear has on chondrogenesis. In this study, a stir speed of 150rpm was chosen as the minimum speed necessary to maintain a single-spheroid suspension. Given the emphasis on generating spheroids suited to use as biological building blocks within a biofabrication strategy, this work opted to not reduce the stir speed at the expense of creating a potentially detrimental high-shear environment. Since little evidence exists on the effect of stirred bioreactor culture on differentiated MSCs within spheroids, determining the quality of cartilage microtissues following a relatively aggressive dynamic culture regime was an important finding. While regime alterations or bioreactor system changes could be made, the risk of spheroids coalescing fundamentally limits the application of dynamic systems in generating large

numbers of microtissues for the biofabrication for cartilage. Alternatively, given the promising results using perfusion culture for engineering clinically relevant bone [198,199] and the mineralisation observed in dynamically cultured microtissues, could suggest bone as a more relevant target-tissue for microtissues cultivated in stirred bioreactors. Similar osteogenic spheroids have been used effectively for bone healing [200], demonstrating the potential for mineralised spheroids, like the ones identified in this chapter, in bone tissue engineering applications.

3.2.4 Conclusion

Cultivation of cartilage microtissues in dynamic conditions failed to improve the quality of the cartilage microtissues. Instead, dynamic cultivation appeared to interfere with chondrogenic induction, favouring as osteogenic phenotype. Despite designing a suitable stirred-tank bioreactor, the results of this study indicate that superior cartilage microtissues are formed in static conditions. Hence, future studies within this thesis will use the hydrogel microwell platform for the medium-long term cultivation of cartilage microtissues.

Chapter 4.

4 Bioprinting of Biomimetic Self-organised Cartilage with a Supporting Joint Fixation Device

4.1 Introduction

Articular cartilage (AC), is the primary bearing material within the joint and provides a low friction, highly wear-resistant surface, mediating load-transmission to the underlying bone [2,3,201]. The capacity of AC to endure decades of extensive loading without succumbing to wear and fatigue is predominantly due to its unique composition and highly organised extracellular matrix (ECM). The architecture of the extensively cross-linked collagen network varies through the depth of the tissue, imparting mechanical properties uniquely suited to its function within the joint [2,3,202–209]. Engineering replacement tissues that recreate this unique spatial organisation, as opposed to the formation of a homogenous tissue, is believed essential to successful joint regeneration [201]. Traditionally, tissue engineering strategies involve homogenously distributing cells within a biomaterial scaffold or hydrogel. Consequently, AC engineered *via* traditional, 'top-down', approaches can fail to recapitulate the structural complexity of its native counterpart. Attempts to generate tissue stratification have included using zonally isolated chondrocyte populations [27], biochemical and mechanical gradients [28,29], multi-layered hydrogels and polymer scaffolds [30–32], re-cellularised AC explants [210], physical modulation of the environmental gradients [33], and the application of biologically relevant mechanical stimuli [34].

Bioprinting offers user-defined control over the spatial organisation of biomaterials, cells and other biologics during biofabrication [35,36]. As such, it has been explored as a means of engineering spatially organised AC [211]. For example, articular cartilage-resident chondroprogenitor cells (ACPCs) and mesenchymal stem/stromal cells (MSCs) have been localised *via* extrusion bioprinting to create zonal ECM profiles similar to those within the superficial and deep regions of native AC [39]. Alternatively, extrusion bioprinting has been employed to control cellularity in a depth dependant manner within collagen type II hydrogels [40]. Combining bioprinting with additive manufacturing as a multi-tool approach for the biofabrication of hybrid constructs has demonstrated that melt electro-written polycaprolactone (PCL) fibres can be used to reinforce bioinks. Through careful design of the polymer support, it is possible to engineer composites with native-like, depth dependent mechanical properties. Furthermore, such composites have been shown to effectively translate mechanical loads to encapsulated cells, supporting their robust chondrogenic differentiation [212]. Despite this relative success, complete recapitulation of many structural aspects of native AC, including the Benninghoff

arcade structure of the collagen network, are rarely reported. A potential explanation for this is the absence of active matrix (re)modelling during tissue maturation. Many biofabrication strategies aim to immediately recreate the biomechanical properties of mature native AC by spatial alterations to material composition and architecture, without sufficient consideration for how such material environments will impact the encapsulated cells. So, while many 3D (bio)printed constructs may be biomimetic in their design, they are generally not engineered to allow cells to actively interact, condensate, and self-organise their local ECM. An alternative to such 'top-down' biofabrication strategies to engineering functional AC, would be to deposit cells into an environment that encourages the self-organisation of a biomimetic tissue in a 'bottom-up' fashion.

AC development begins with the condensation of MSCs. Forming similar mesenchymal condensations *in vitro* has been a longstanding assay for chondrogenic differentiation [213]. Allowing cells to generate such a cartilage-like tissue in the absence of a biomaterial scaffold has formed the basis of numerous scaffold-free tissue engineering strategies. Furthermore, such scaffold-free methods have been combined with novel biofabrication and/or bioprinting strategies in an attempt to engineer more organised and functional grafts. For example, tissue strands, formed from cell-aggregates, have been bioprinted without the need for a delivery medium or supporting structure [214]. These scaffold-free strands supported robust chondrogenesis and could fuse after 1 week to form a cartilage with a compressive modulus of 1,094 ± 26.33 kPa. In the absence of an interstitial biomaterial, extensive cell-cell interactions were supported, which was associated with tissue maturation and biomimicry, whilst removing complications such as matching material degradation with neotissue formation [214]. Similar cartilage-tissue stands have been spatially orientated *via* bioprinting in an attempt to create a zonally stratified AC [215], whereas others have shown that cellular spheroids can be positioned using bioprinting to generate an osteochondral interface [148]. Predominantly, bioprinting scaffold-free bioinks has been done using extrusion-based methods [155]. Drop-on-demand (DoD) bioprinting technologies, such as inkjetting, have been used for numerous applications because of their simplicity, versatility, and precision [35,216]. In the context of cartilage tissue engineering, DoD bioprinting has been applied to biofabricate hybrid constructs consisting of electrospun PCL fibre and chondrocyte laden hydrogels [217], as well as for *in situ* cartilage repair [218]. Interestingly, by removing a permanent biomaterial from the deposited bioink, inkjet bioprinting can be used to generate a spatially organised cartilage [41]. Specifically, droplets of cell suspension (MSCs and chondrocyte co-culture) can be deposited into polymer microchambers where cells spontaneously aggregate and form chondrogenic spheroids. The boundary conditions imposed on the growing spheroids by the polymer microwells directed growth upwards and form a stratified cartilage tissue. Overall, this process was an effective means of imposing physical-cues, which encouraged spatial organisation within a self-organised system. However, the solid polymer base to

the microchambers, formation of a relatively thin cartilage layer, and the need for integrating this tissue onto an osseous implant to support bony fixation limits the approaches *in vivo* applicability.

Although using the subchondral bone for fixation of a scaffold or engineered tissue within the synovial joint is not uncommon [111], excessive disruption of the subchondral bone plate must be carefully considered, from mechanical [19] and biological [10,11,20] standpoints, to avoid creating a degenerative state. Alternative chondral fixation methods include press-fitting, suturing, adhesives, and orthopaedic pins [111,219]. Press-fitting results in low fixation strengths and is heavily reliant on accurately matching the defect geometry and the roughness of the subchondral bone [220–222]. Fibrin glue is widely used as a fixative due to its low cost, as well as its fast and intuitive application [111,222–225]. However, relatively low detachment loads and inadequate fixation have been reported [220]. Sutures, both transchondral and transosseous, can withstand demanding loads [220]. However, they incur iatrogenic damage, can create excessive and/or unbalanced tension within the implant, as well as being laborious and technically demanding [220,222]. Biodegradable pins have been used as methods of fixing polymer scaffolds *in situ* for autologous matrix-induced chondrogenesis (AMIC) and matrix-assisted chondrocyte implantation (MACI) [226,227]. Clinical application of bioresorbable pins tend to use soft scaffold materials; the application of the same pin for fixation of 3D printed polymer framework has resulted in significant damage during implantation and the loss of scaffold integrity [228].

This study seeks to address two key challenges in the field of AC tissue engineering. Firstly, the challenge of reliably fixing an engineered tissue into the synovial joint, and secondly the need for a reliable method for generating a thick, stratified and biomimetic AC. The aim of this study was to create a novel fixation device, which can also function to guide the self-organisation of MSC condensations and the subsequent development of a stratified AC. The goal was to create an implant that incurred minimal disruption to the subchondral bone, whilst providing adequate fixation. To achieve this, this study designed novel fabrication methods, bioprinting strategies, and culture regimes which, culminated in the biofabrication of a hybrid implant for resurfacing focal chondral defects.

4.2 Material and Methods

4.2.1 Bone Marrow Mesenchymal Stem/Stromal Cell (MSC) Isolation and Expansion

MSCs were isolated from the femoral shaft of 4 month old pigs under sterile conditions. They were expanded in expansion medium (XPAN) which, is composed of high glucose Dulbecco's modified eagle's medium (hgDMEM) GlutaMAX supplemented with 10 % v/v FBS, 100 U/mL penicillin, 100 µg/mL streptomycin (all Gibco, Biosciences, Dublin, Ireland) and 5 ng/mL FGF2 (Prospect Bio). All MSCs were expanded in physioxic conditions (37 °C in a humidified atmosphere with 5 % CO_2 and 5 % pO_2) for chondrogenic differentiation. After initial colonies had formed, MSCs were trypsinised, counted, and re-seeded at a density of 5,000 cells/cm^2 and expanded until the end of passage 2.

4.2.2 Implant Fabrication & Assembly

Implant design and fabrication: Implants were fabricated using fused deposition modelling (FDM). Here, implants were designed using BIOCAD (RegenHU, Switzerland) and fabricated using the thermopolymer printhead of a 3D Discovery multi-head bioprinting system (Regen Hu, Switzerland) using the machine parameters outlined in table 4.1. Implants were fabricated using polycaprolactone (PCL, Perstop) and stored in 70 % ethanol prior to assembly.

Table 4.1 *Machine Parameters for FDM of the implant*

Parameter	*Needle Gauge*	*Backpressure*	*Printhead Temperature*	*Tank Temperature*	*Feed Rate*	*Screw Speed*
Microwells	32 G	0.04 MPa	88 °C	80 °C	7.2 mm/s	5 rev/m
Pin	32 G	0.04 MPa	88 °C	80 °C	1.2 mm/s	29 rev/m

A

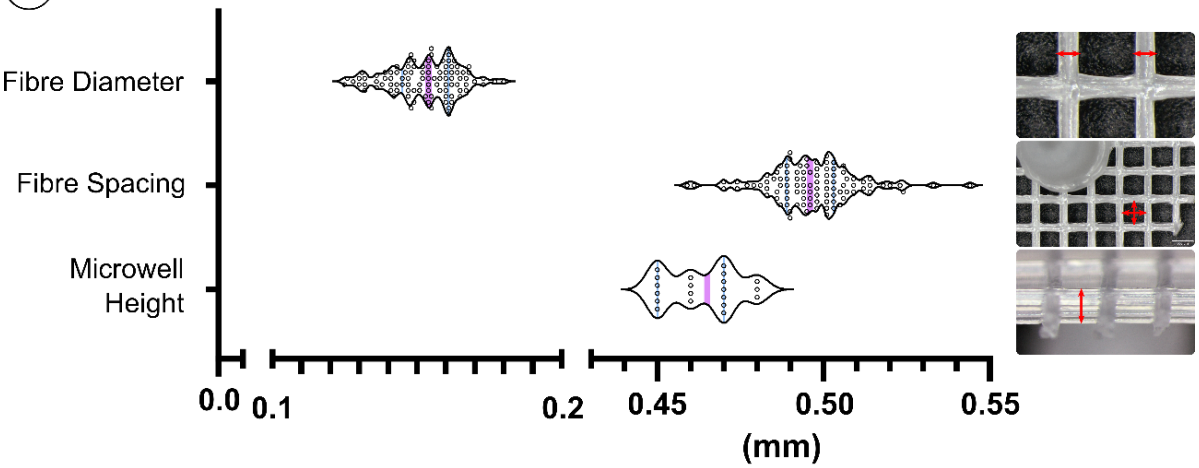

B

	Mean ± SD	Max	Min
Fibre Diameter	153 ± 12 µm	180 µm	125 µm
Fibre Spacing	497 ± 13 µm	544 µm	459 µm
Microwell Height	464 ± 11 µm	480 µm	450 µm

Figure 4.1 *Measurements of the microwell array from the fabricated implant. A) Graphical representation of the measurements of fibre diameter, fibre spacing, and microwell height. B) Key dimensions as mean ± SD as well as maximum and minimum values. (N = 20 for microwell height, N = 100 for fibre diameter and fibre spacing)*

Vacuum former: The vacuum former was designed using Solidworks (Figure 4.2), a STL file for the part was then converted into G-code using Preform 2.16.0 software and the part was fabricated using a Form 2 stereolithography printer (both Formlabs, Massachusetts, United States). The completed parts were processed post-printing in accordance with the manufacturer's guidelines. Briefly, parts were washed in propan-2-ol (Sigma Aldrich) to clear any uncured resin, following which they were exposed to UV light (365nm, 6W) for 30 minutes at 60°C to ensure complete crosslinking.

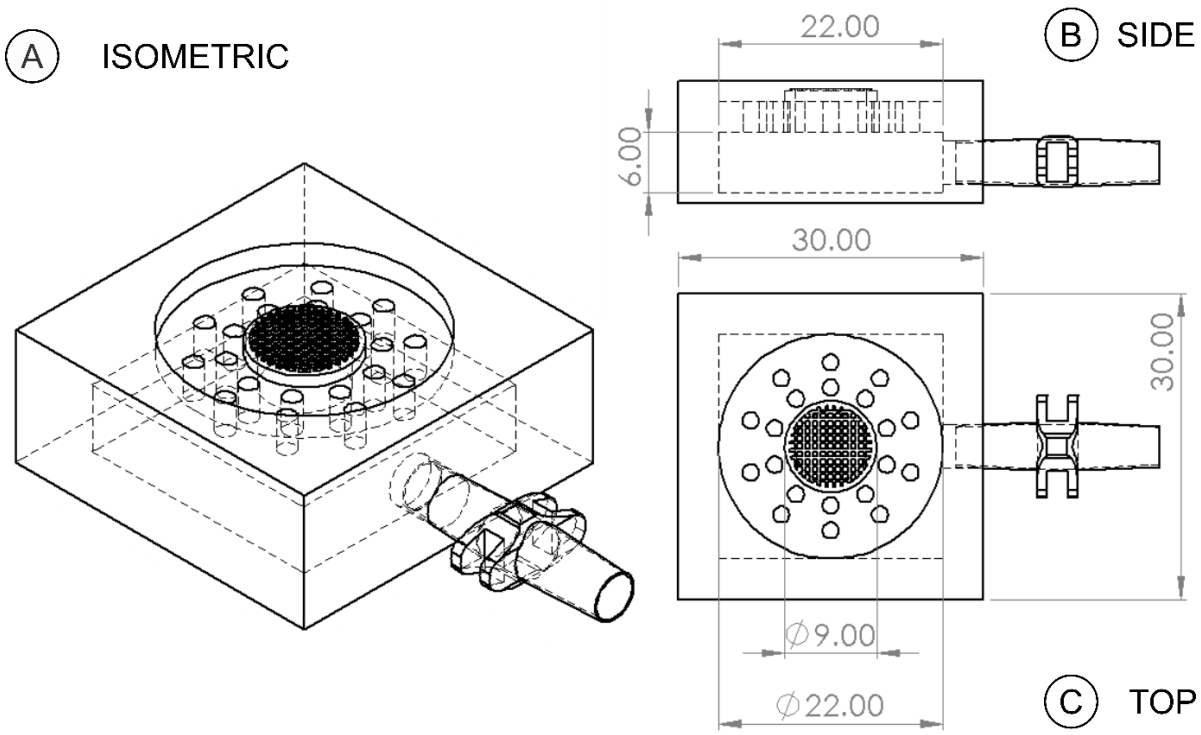

Figure 4.2 *Engineering drawings of the vacuum former. Isometric (A), side (B), and top (C) views are provided with overview dimensions provided in millimeters.*

Addition of the temporary base: The addition of the temporary base was carried out under clean, but not sterile conditions. First a square of paraffin film (Parafilm®, Sigma) was cut to size (30 mm × 30 mm). A piece of rubber elastomer (Blu tack®, Bostik) was then placed onto the back of the film. The elastomer was then rolled/pressed flat, ensuring complete contact with the film to a thickness of ~ 500 µm and diameter of ~ 22 mm. At the centre of the square, a 2 mm hole was punched into the rubber elastomer using a biopsy punch, care was taken to not damage or perforate the paraffin film. At the centre of the 2 mm hole, a 1 mm hole was punched through the paraffin film using a biopsy punch. The protective backing was then removed from the paraffin film and the implant pushed through the 1 mm centralised hole. Using a stereomicroscope (Zeiss) for guidance, this assembly was

positioned centrally on the vacuum former. A vacuum was applied using a mini diaphragm vacuum pump (VP 86, VWR) at maximum vacuum (100 mbar). After visual conformation of the temporary base moulding to the underside of the implant, the vacuum was released and the assembly was removed. Excess backing material was trimmed from the final implant using scissors and the implant was assessed visually under the stereomicroscope to ensure each microwell was properly sealed.

Implant Centralisation: Polylactic acid (PLA) inserts were designed using Solidworks. G-code for the inserts was created using Ultimaker Cura 4.8, and fabricated using an Ultimaker 3+ (Ultimaker B.V.). Inserts were designed to fit inside a 12 well plate (Corning), and to centralise the assembled implants during the bioprinting process.

Fully assembled implants and inserts were sterilised using ethylene oxide gas (EtO) for 12 hours (Anprolene, Andersen Products, USA) and allowed to air for a minimum of 24 hours prior to use. More details on implant design, fabrication, and assembly can be found in the results section.

4.2.3 Inkjet Bioprinting

All inkjet bioprinting was carried out under aseptic conditions using the cell-friendly inkjet printhead (CF300) as part of the 3D Discovery multi-head bioprinting system (Regen Hu, Switzerland).

Cell-free droplet optimisation: To optimise the droplet volume for bioprinting a standard curve was created. Droplet volume (µL) was varied as a function of valve opening time (µs) with a constant back pressure of 0.150 MPa. At various valve opening times (500 µs, 1,000 µs, 2,000 µs, 4,000 µs, 8,000 µs, and 10,000 µs) 100 droplets of DMEM were deposited and weighed, this was repeated 6 times for each valve opening time. The average volume dispensed per droplet (µL) was calculated as the weight recorded (mg) divided by the number of droplets dispensed (100). From this standard curve, valve opening times for 1×, 3×, and 9× microwell volumes were calculated and tested.

Inkjet Bioprinting: MSC suspensions were created at specific densities to yield 50×10^3 cells/microwell and 100×10^3 cells/microwell, or 4×10^6 cells/implant and 8×10^6 cells/implant respectively. MSCs were bioprinted in DMEM only to prevent the formation of bubbles during bioprinting. After deposition, implants were returned to the incubator at physioxic conditions and cells allowed to settle for 15 minutes. After which, 25 µL of XPAN was carefully added every 15 minutes to the bioprinted cells to provide nutrients and prevent drying during the first 2 hours. After 2 hours, XPAN was added to the well to cover the entire assembly. Implants were maintained in XPAN for the first two days of culture before chondrogenic induction. Chondrogenesis was initiated using Chondrogenic Differentiation Medium (CDM). CDM is comprised of hgDMEM GlutaMAX supplemented with 100 U/mL penicillin, 100 µg/mL streptomycin (both Gibco), 100 µg/mL sodium pyruvate, 40 µg/mL L-proline, 50 µg/mL L-ascorbic acid-2-phosphate, 4.7 µg/mL linoleic acid, 1.5 mg/mL bovine serum

albumin, 1× insulin–transferrin–selenium (ITS), 100 nM dexamethasone (all from Sigma), 2.5 µg/mL amphotericin B and 10 ng/mL of human transforming growth factor-b3 (TGF-β) (Peprotech, UK). Throughout the 4 week culture, implants were maintained in physioxic conditions (37 °C in a humidified atmosphere with 5 % CO_2 and 5 % pO_2).

4.2.4 Static and Dynamic Culture Regimes

The influence of static and dynamic culture conditions (Figure 4.3A) on the development of a self-organised cartilage was investigated in this study. In both culture regimes, the same number of implants were loaded per bioreactor which, always contained the same volume of CDM (80 mL). Implants were moved into the bioreactor upon chondrogenic induction (Day 2). In static conditions, the temporary base removed after 7 days of culture (5 days of chondrogenic culture) (Figure 4.3B). This process was carried out in sterile conditions and the implants returned to the static bioreactor afterwards, where the platform remained in the lowered position. The motivation for the 'early' removal of the base was to mitigate nutrient limitations in the static condition, permitting bi-directional nutrient exchange and tissue growth. Dynamic culture involved the continuous linear actuation of the stage, over 5 mm of travel at a frequency of 0.048 Hz (Figure 4.3A). Here, due to the enhanced nutrient exchange permitted by the dynamic conditions the temporary base was left on, in an attempt to better direct tissue growth and maturation. As such, the base was removed after 3 weeks in the dynamically cultured group (Figure 4.3B). Media (80 mL) was exchanged every 2-3 days for the duration of the 28 day study.

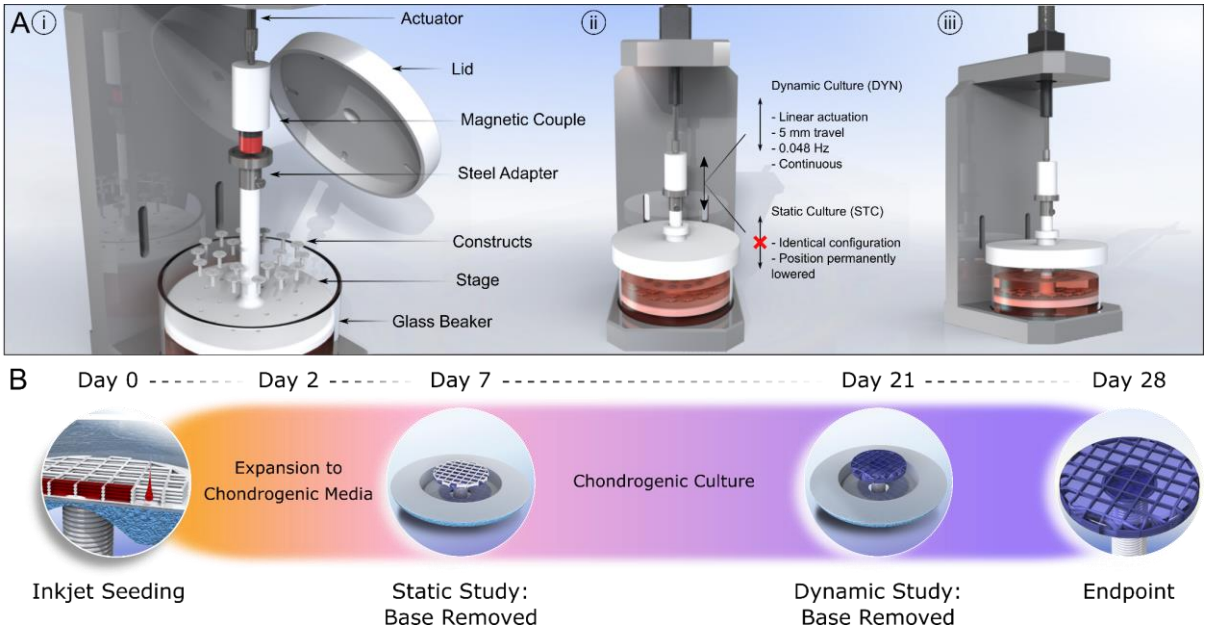

Figure 4.3 *Study design. A) Bioreactor configuration and culture conditions. i) Labelled schematic of the bioreactor assembly. ii) Description of the dynamic and static culture conditions. iii) Overview of the complete configuration. B) Timeline highlighting key milestones during the formation of a self-organised cartilage via inkjet bioprinting.*

4.2.5 Histological & Immunofluorescence Evaluation

Histological Evaluation: Samples were fixed using 4 % paraformaldehyde (PFA) solution overnight at 4 °C. After fixation, samples were dehydrated in a graded series of ethanol solutions (70 % - 100 %), cleared in xylene, and embedded in paraffin wax (all Sigma-Alrich). Prior to staining tissue sections (5 µm) were rehydrated. Sections were stained with hematoxylin and eosin (H&E), 1 % (w/v) alcian blue 8GX in 0.1 M hydrochloric acid (HCL) (AB) to visualise sulphated glycosaminoglycan (sGAG) content and counter-stained with 0.1 % (w/v) nuclear fast red to determine cellular distribution, 0.1 % (w/v) picrosirius red (PSR) to visualise collagen deposition, and 1 % (w/v) alizarin red (AR) (pH 4.1) to determine mineral deposition *via* calcium staining (all from Sigma-Aldrich). Stained sections were imaged using an Aperio ScanScope slide scanner and thickness measurements obtained using Aperio Imagescope.

Live/Dead Cell Assay: Cell viability was established using a live/dead assay kit (Invitrogen, Bioscience). Constructs were rinsed in PBS and incubated for 1 h in a solution containing 2 µM calcein and 4 µM of ethidium homodimer-1 (EthD-1). After incubation, the constructs were rinsed again and imaged with Leica SP8 scanning confocal microscope (485 nm and 530 nm excitation and 530 nm and 645 nm emission for calcein and EthD-1 respectively). All images are presented as maximum projection z-stack reconstructions analysing cell viability through the depth of the tissue (view is from the top).

Immunofluorescence Staining: Antigen retrieval was carried out by treating rehydrated samples with pronase (3.5 units/mL) (Merck) in a humidified environment at 37 °C for 25 minutes, followed by hylaronadase (4000 units/mL) (Sigma-Aldrich) in a humidified environment at 37 °C for 25 minutes. Non-specific sites were blocked using a 10 % goat serum and 1 % BSA blocking buffer for collagen type II and type X for 1 hour at room temperature. For collagen type I a 10 % donkey serum and 1 % BSA blocking buffer was used. Collagen type I (1:300, ab-90395, Abcam), collagen type II (1:300, ab 34712, Abcam), and collagen type X (1:300, ab 49945, Abcam) primary antibodies were incubated with the samples overnight at 4 °C. The secondary antibodies for collagen type I (1:300, ab 150075, Abcam), collagen type II (1:300, A11001, Life Technologies) and collagen type X (1:300, ab 150121, Abcam) were incubated with the samples for 4 hours at room temperature, followed by DAPI (2 µg/mL in PBS) for 10 minutes at room temperature. Samples were imaged the following day using a Leica SP8 scanning confocal microscope.

4.2.6 Polarised-light Microscopy & Collagen Alignment Quantification

Sections stained with PSR were imaged using polarised light microscopy to visualise collagen fibre orientation. Quantification of mean fibre orientation and dispersion was carried out using the 'directionality' feature in ImageJ software. Fibre coherency and colour maps were determined using the OrientationJ plugin [229]. The zones of the engineered tissue were defined as follows: the deep-

zone was characterised as tissue formed within the microwell, the middle-zone was tissue that formed over the microwells, and the superficial zone was the top ~10 % of the engineered tissue. Multiple sections were taken from the edge, quarter, and middle regions of 2 engineered samples. From these sections, 20 microwells were selected and evaluated at random. Data points presented graphically represent the quantification of the fibre directionality from the defined zones of the tissue within for each microwell. 95 % confidence ellipses presented in dispersion vs orientation plots were determined using the Real statistics resource pack add-in for excel.

4.2.7 Biochemical Evaluation

Samples were washed in PBS after retrieval and the wet-weight was recorded for samples which were cultured dynamically. A papain enzyme solution, 3.88 U/mL of papain enzyme in 100 mM sodium phosphate buffer/5 mM Na2EDTA/10 mM Lcysteine, pH 6.5 (all from Sigma–Aldrich), was used to digest the samples at 60 °C for 18 hours. DNA content was quantified immediately after digestion using Quant-iT™ PicoGreen ® dsDNA Reagent and Kit (Molecular Probes, Biosciences). The amount of sGAG was determined using the dimethylmethylene blue dye-binding assay (Blyscan, Biocolor Ltd., Northern Ireland), with a chondroitin sulphate standard read using the Synergy HT multi-detection micro-plate reader (BioTek Instruments, Inc) with a wavelength set to 656 nm. Total collagen content was determined using a chloramine-T assay to measure the hydroxyproline content and calculated collagen content using a hydroxyproline-to-collagen ratio of 1:7.69 [186]. Briefly, samples were mixed with 38 % HCL (Sigma) and incubated at 110 °C for 18 hours to allow hydrolysis to occur. Samples were subsequently dried in a fume hood and the sediment reconstituted in ultra-pure H_2O. 2.82 % (w/v) Chloramine T and 0.05 % (w/v) 4-(Dimethylamino) benzaldehyde (both Sigma) were added and the hydroxyproline content quantified with a trans-4-Hydroxy-L-proline (Fluka analytical) standard using a Synergy HT multi-detection micro-plate reader at a wavelength of 570 nm (BioTek Instruments, Inc).

4.2.8 Image Quantification & Statistical Analysis

The thickness of the engineered cartilage was measured using ImageScope software (Aperio). Statistical analysis was performed using GraphPad Prism software (GraphPad Software, CA, USA). Analysis of differences between two groups at one timepoint was done using a standard two-tailed t-test. For two groups over multiple time-points a one-way analysis of variance (ANOVA) was performed. Numerical and graphical results are presented as mean ± standard deviation unless stated otherwise. Significance was determined when $p < 0.05$.

4.3 Results

4.3.1 Design and Fabrication of a Novel Joint Fixation Device

Given the challenges associated with integrating engineered cartilage in place within a joint defect, this study first sought to design and fabricate a novel synovial joint fixation device. The implant was intended to work in conjunction with micro-drilling, a pre-existing treatment for focal chondral defects. During the micro-drilling procedure, small diameter hole(s) are used to perforate the subchondral bone plate and induce bleeding. The aim was to use one of these holes to fixate an engineered cartilage *in situ* within the joint. As such, the device design was centred on a pin which could be push-fit into a micro-drilling hole. At the head of the pin, a suitable platform for engineering a self-organised cartilage was created. To do so, a baseless microwell array was designed (Figure 4.4A). As previously discussed, a similar 'microchamber' approach has been shown as an effective method for generating a relatively thick and spatially organised engineered cartilage [41]. However, the solid polymer base of these microchambers represent a significant shortcoming. Hence, this study aimed to design a similar structure, but without a permanent base.

The implant was fabricated *via* FDM. Due to the constraints of FDM, the implant was fabricated inverted to avoid creating overhangs and maximise print fidelity. The microwells were designed and fabricated with no lateral porosity. It was hypothesised that these solid walls would operate as boundary conditions for the developing cartilage, directing the growth of the neotissue and the organisation of its collagen network (Figure 4.4Bi). When printing the pin, it was noticed that the extruded polymer spiralling along the length of the pin (Figure 4.4Bii). As this feature was not intentional, it was hypothesised to be a result of the forces exerted on the previous layer of semi-molten polymer as the subsequent layers are deposited above. Specifically, the circular print-path causes the extruded filament to drag and displace the subjacent layer off-axis, creating the spiral. The consistent melt temperatures, material flow rates, and printing speed mean that this unique feature can be effectively recreated between individual prints. Although an artefact of the fabrication method, these macroscopic undulations of the pins surface could help initial fixation, acting like the threads of a screw (Figure 4.4Bii). Moreover, this macroscopic features coupled with the microscopic surface topography created by individual printed layers, created a multi-scale surface topography that could prove beneficial in terms of osteointegration at the host site. In conjunction with designing a novel implant drilling protocols and surgical guides for implantation were also developed (Figure 4.4C). Collectively, these efforts resulted in the implant sitting dead-centre in the created defect and the surface of the polymer being marginally recessed from the articular surface (Figure 4.4D).

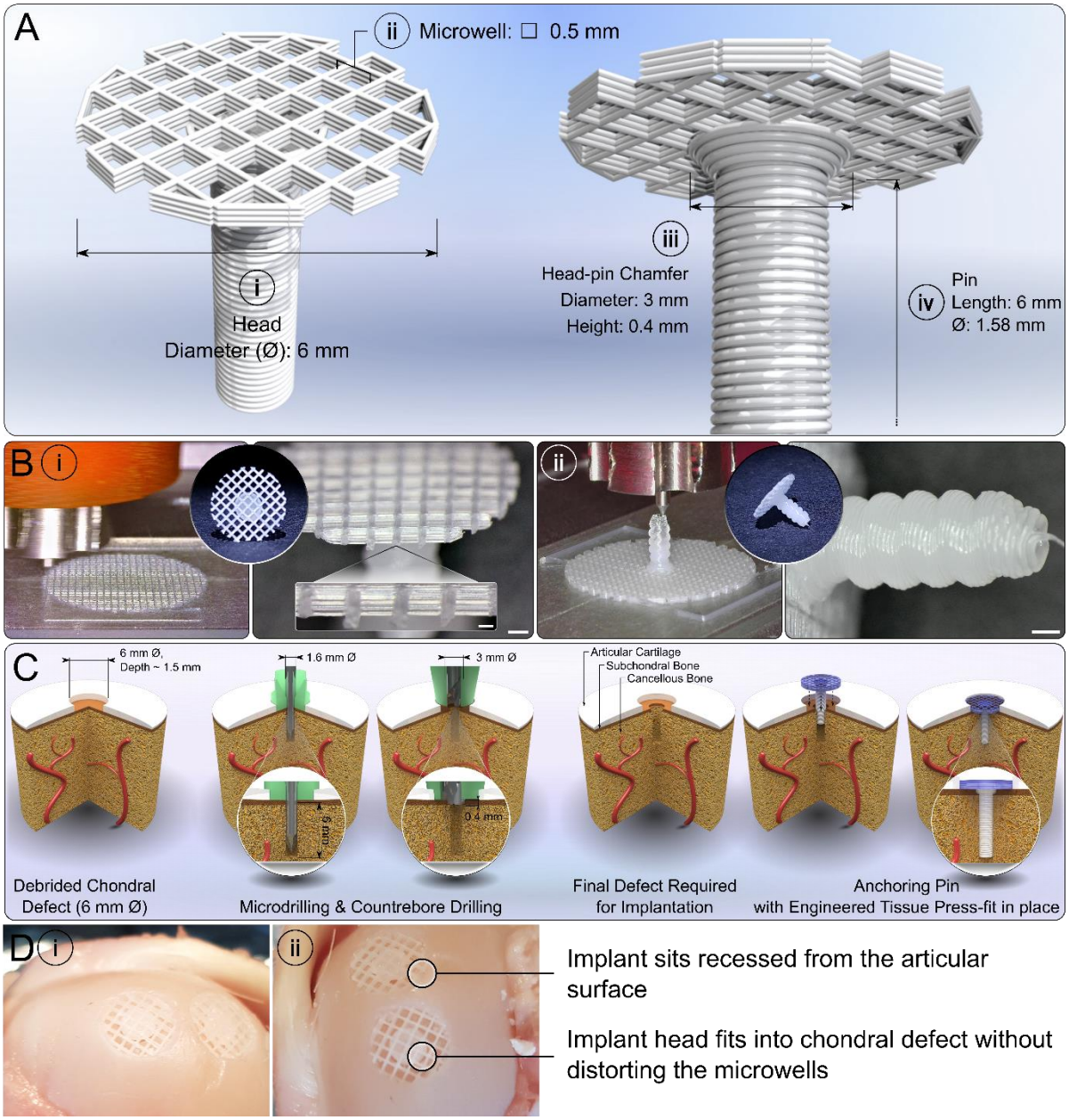

Figure 4.4 *Design, 3D fabrication, and implantation strategy for a novel cartilage-fixation device. A) Schematic representation of the proposed implant design. The implant is comprised of a 6 mm diameter head (i) which, is made-up of an array of bottomless microwells measuring 500 µm square (ii). Directly below is a small chamfer (iii) designed to maximise the interface between the head and the pin (iv). The pin has a small diameter (1.58 mm) and is intended to be press-fit into a micro-drilling hole (1.6 mm ⌀). B) Snapshots of implant fabrication via FDM. The implant was fabricated inverted, to prevent the need to print overhangs and improve print fidelity. The microwells (i) were printed with no lateral porosity, and fabrication of the pin (ii) resulted in the formation of a spiralled pattern. C) Schematic of the intended implantation procedure. Di & ii) Macroscopic images take of cell-free implants within a 6 mm chondral defect as a proof-of-concept of the implantation strategy. (Scale Bar: Bi Overview = 500 µm, Inset = 200 µm. Bii = 500 µm)*

4.3.2 Implant Assembly and Bioprinting Strategy

In order to bioprint a cell suspension into the microwell array, a temporary base was first designed. This presented a significant challenge as the base material needed to meet several criteria. Primarily, it would have to be hydrophobic (to avoid protein absorption and cell attachment), non-cytotoxic, be sufficiently flexible to conform to the underside of the microwells creating a water-tight seal, and be easily removed without damaging the implant, the engineered tissue, or leave unwanted residues. A paraffin film was selected as the material that best fitted these constraints. However, the film alone did not adhere strongly to the underside of the microwells, and therefore a rubber elastomer was used as a backing material to reinforce the paraffin film.

The shallow depth of the microwells (464 ± 11 µm) left little tolerance during the addition of the temporary base. If the base was assembled too loosely then it would not provide an adequate seal. Equally, if the base was 'over attached' then it would encroach into the vacancy of the individual microwells and prevent cell deposition. As such, manual addition of the base was insufficient and instead a custom-made vacuum former was designed (Figure 4.5A). The process for adding the temporary base was simple and reliable, forming an excellent seal below each microwell without impinging into the microwells (Figure 4.5B & C). Having established that the novel assembly methods for fabricating an implant suited bioprinting, holders were designed to centralise the implants within the wells of a well-plate (Figure 4.5C & D). This allowed tight control of the bioprinting process, permitting the accurate drop-on-demand deposition of a bioink into individual microwells

Inkjet bioprinting offers user-defined control over the deposition of picolitre volumes of bioink. As such, it represented the ideal bioprinting modality for cell-seeding the microwells. However, a trade-off between depositing low volumes, the need for spatially accurate bioprinting, and the large number of cells needed to generate tissues of scale created a challenge. Given the high cell-densities required, maintaining an acceptable level of cell-viability was prioritised. It was believed that maintaining an acceptable level of cell-viability using 50×10^3 cells or 100×10^3 cells in 0.115 µL (the theoretical volume of each microwell) of basal culture media during extrusion or post-printing was unlikely. Therefore, this study investigated several 'filling scenarios' which were designed to determine the maximum volume of bioink that could be deposited into each microwell before spatial resolution was lost (Figure 4.5D). The aim was to leverage the surface tension generated in each microwell to fill it with a maximum volume of bioink before it would spill into adjacent wells. To investigate this, the valve opening time of the inkjet printhead was varied to accurately control droplet volume. It was identified that 3 times the microwell volume (0.345 µL) was the optimal droplet volume to maintain print fidelity whilst maximising bioink volume (Figure 4.5E).

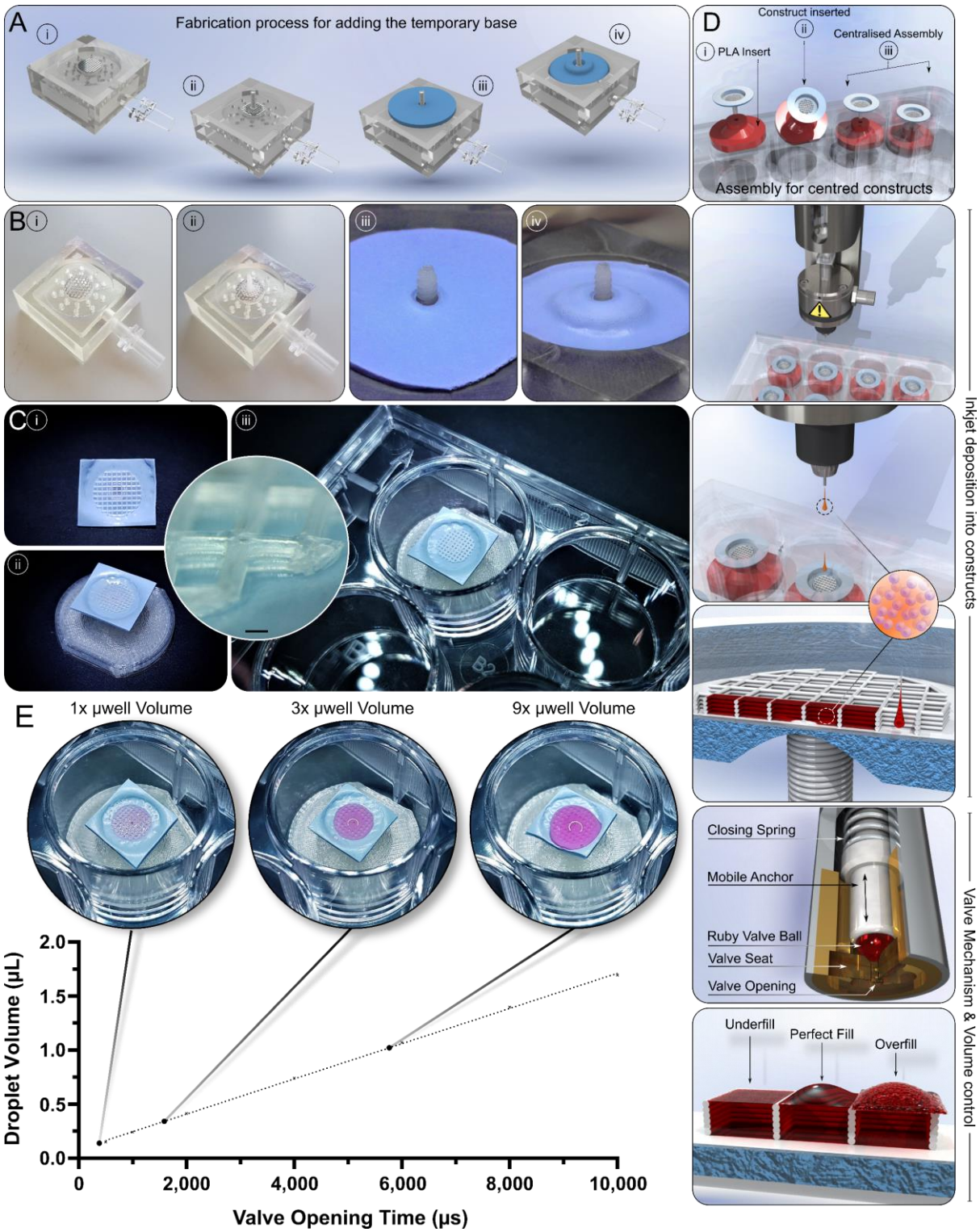

Figure 4.5 *Implant assembly and bioprinting methodology. A) A schematic representation of the process used to apply a temporary base underneath the microwell array. i) Custom vacuum former, ii) PCL implant positioned on the former, iii) temporary base added to the back of the implant, and iv) moulding of the temporary base using a vacuum. B) Image take of each of the five steps outlined within A). C) The final implant (i) and assembly required (ii) to hold the implant centrally within a well plate (iii). Inset shows the effective seal formed below a single microwell by the temporary base. D) Schematic timeline of the inkjet bioprinting process, including, the valve working mechanism and three microwell filling scenarios. E) Droplet volume is controlled as a function of valve opening time, macroscopic images of the three filling scenarios with the respective volume deposited per microwell and the valve opening time used to deposit that volume (N = 6, Mean ± SD). (Scale Bar = 200 µm)*

4.3.3 *Early Differences in MSC Conformation*

To gain an insight into early cellular viability and phenotype, tissues forming within the microwells were evaluated 7 days after bioprinting. Live/dead imaging indicated excellent cell viability regardless of the starting cell-density and showed a relatively even distribution of cells throughout the implant (Figure 4.6), demonstrating the success of the bioprinting and post-printing culture regime. In cross-section, the two cell densities resulted in two distinct cellular arrangements. MSCs within microwells containing 50×10^3 cells formed small condensations which collected in the corner of the microwells, forming interactions with aggregates of adjacent microwells through small gaps between the layers of the polymer walls. By doubling the number of cells in each microwell, a cell sheet was formed at the bottom of each well. Unsurprisingly, after only 5 days of chondrogenic induction the ECM generated within these early MSC condensations stained weakly for sGAG and collagen, and negatively for any mineral deposition (Figure 4.6). Despite being highly cellular, the contents of the microwells was well-integrated and the temporary base could be easily removed without the disruption of the structures or cell death.

4.3.4 *Self-organised Cartilage in Static Culture Conditions*

In static culture conditions the temporary base was removed after 7 days (5 days of chondrogenic culture). This decision was motivated by the knowledge that highly cellular systems are vulnerable to failure *via* nutrient limitations. As previously demonstrated, the resident cells and early-cartilage

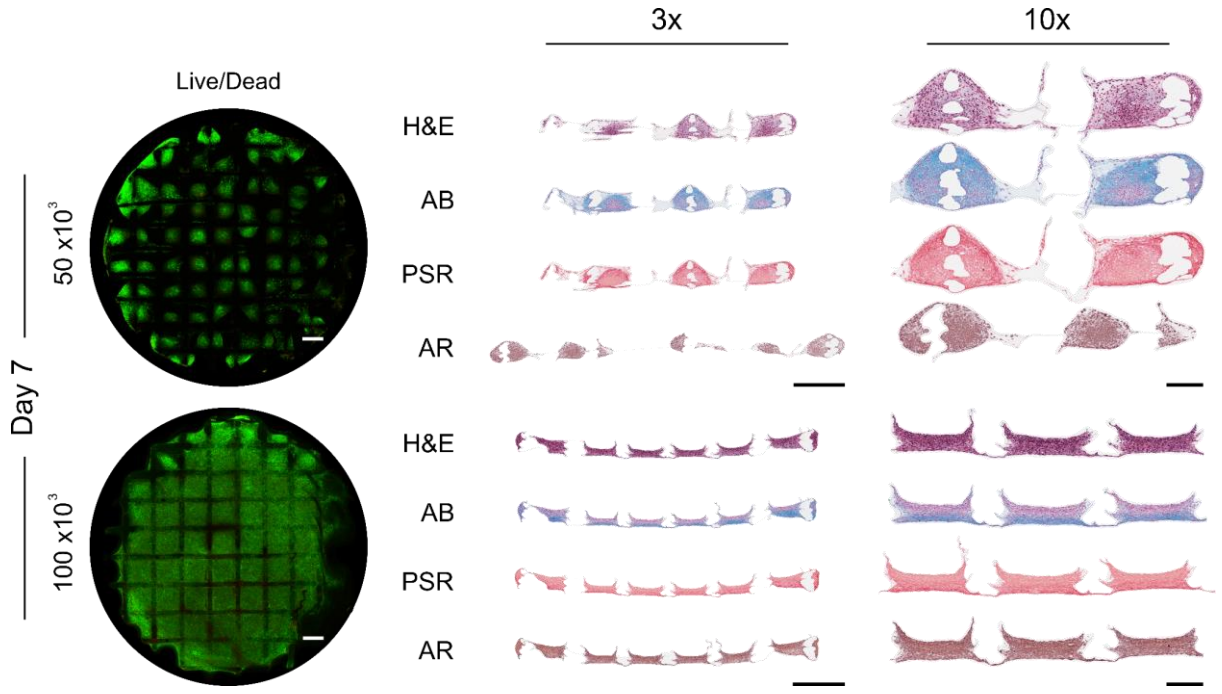

Figure 4.6 *Early differences in cellular arrangement. Live/dead and histological sections 7 days after bioprinting, including 5 days of chondrogenic induction. sGAG, collagen, and mineral are stained for by AB, PSR, and AR respectively. (Scale Bars: Live/Dead = 500 µm, 3× = 700 µm, 10× = 200 µm)*

tissue was well established after 7 days and the base could be removed under sterile conditions without significant disruption to the developing tissue.

After 4 weeks of chondrogenic cultivation, a white glossy tissue had formed in the head of the implant. Histologically, this self-organised was rich in cartilage-specific ECM components for both cell seeding densities (Figure 4.7). The tissue that formed using the lower starting cell-density had begun to grow over the confines of the microwells in several places throughout the implant. However, this overgrowth had not resulted in the formation of a thick and even cartilage surface (Figure 4.7Ai). Despite this, the tissue was extensively stained positive for sGAG and collagen. The deposition of these ECM component appeared consistent throughout the depth of the tissue and the span of the implant, generating a homogenous tissue with no signs of nutrient transport limitations promoting core necrosis. Early removal of the base had resulted in some bi-directional tissue growth, but tissue interconnection between adjacent microwells at the underside of the implant head was limited (Figure 4.5Aii). Some evidence of cartilage mineralisation was detected in some peripheral regions of the implant. The positive mineral staining occurred predominantly at the periphery of the middle section of the tissue and to a lesser extent in the quarter section (Figure 4.7Ai & ii).

Macroscopically, the higher starting density appeared to generate thicker and more opaque tissue (Figure 4.5B). These observations were confirmed histologically by the formation of substantial and consistent cartilage over the top of the microwell walls (Figure 4.7Bi). Like in the lower cell density, the cellular distribution and accumulation of cartilaginous ECM was homogenous throughout the self-organised cartilage. Evidence of growth below the microwells was also noted, however, this culminated in the formation of hemi-spherical tissue caps with no connection between the tissues of the neighbouring microwells formed (Figure 4.7Bii). Instead, vertical tissue growth was evident, resulting in the formation of a markedly thicker and more congruent tissue surface when compared to the 50×10^3 cells/microwell group. Similar evidence of cartilage mineralisation was apparent in the 100×10^3 cells/microwell group. However, it was far less pervasive than in the lower-density (Figure 4.7Bi & ii).

Although histological evidence indicated both groups supported a highly chondrogenic phenotype, the lower cell density appeared to stain more positively for both sGAG and collagen whilst being less cellular. These observations were confirmed biochemically, where despite containing significantly less DNA by day 28 (Figure 4.8A), the total sGAG and collagen detected in the 50×10^3 cells/microwell group was significantly higher than in the tissue formed using 100×10^3 cells/microwell (Figure 4.8B & C). Unsurprisingly, normalisation of the absolute amounts of sGAG and collagen to DNA quantity demonstrated that the biosynthetic output of the resident cells in the lower starting density was significantly higher (Figure 4.8D & E). In summation, these results indicated that although 100 ×

10^3 cells/microwell yields a thicker and more consistent self-organised cartilage, a significantly richer cartilaginous matrix can be formed by using half the starting cell number.

4.3.5 A Higher Initial Cell Density Yields Better Spatial Organisation

Whilst this study recognise the importance of robust chondrogenesis and the generation of significant amounts of ECM proteins, the spatial organisation of engineered AC is also essential to creating a biomimetic tissue. In particular, recreating the anisotropic arrangement of the collagen network seen in native AC is a longstanding challenge. Hence, PLM was used determine if there were differences in the collagen arrangement within the self-organised cartilages.

Some evidence of spatial organisation within the 50×10^3 cells/microwell tissue was apparent (Figure 4.9A). It appeared that confining tissue growth, using the microwell walls, drove vertical alignment of the collagen fibres within the deep- and, to a much lesser extent, the middle-zone of the engineered tissue. Superficially, collagen was arranged perpendicular to the deep fibres and parallel with tissue surface as expected. Visually, the self-organised cartilage engineered using 100×10^3 cells/microwell appeared to be more biomimetic (Figure 4.9B). In the superficial region of the tissue, the collagen orientation was similar to what was observed in the lower-density group, whereby the fibrils ran parallel with the apical surface. Due to the generation of a thicker tissue, the middle zone was more apparent throughout the implant. Within this middle zone, the collagen fibre closely resembled that of native tissue. Characteristic arcs of collagen fibres, transitioning from their perpendicular alignment in the deeper regions to more superficial regions of the mid-zone, were noted within this tissue. In the deep-zone, most fibrils also aligned perpendicular to the surface, although in general the arrangement here appeared less cohesive than in the mid-zone above and in the lower-density group.

Quantification of collagen fibril alignment in both groups corroborated these observations (Figure 4.10). In terms of mean fibre orientation, 100×10^3 cells/microwell yielded a far more biomimetic tissue. Throughout the implant (edge, quarter, and middle sections), a higher starting cell density resulted in a mean fibre orientation closer to those in native tissue in the middle and superficial regions. Additionally, in the middle and superficial zones of the 100×10^3 cells/microwell group exhibited a significantly higher level of fibre coherency, indicating greater collagen alignment within these specific zones and superior tissue organisation.

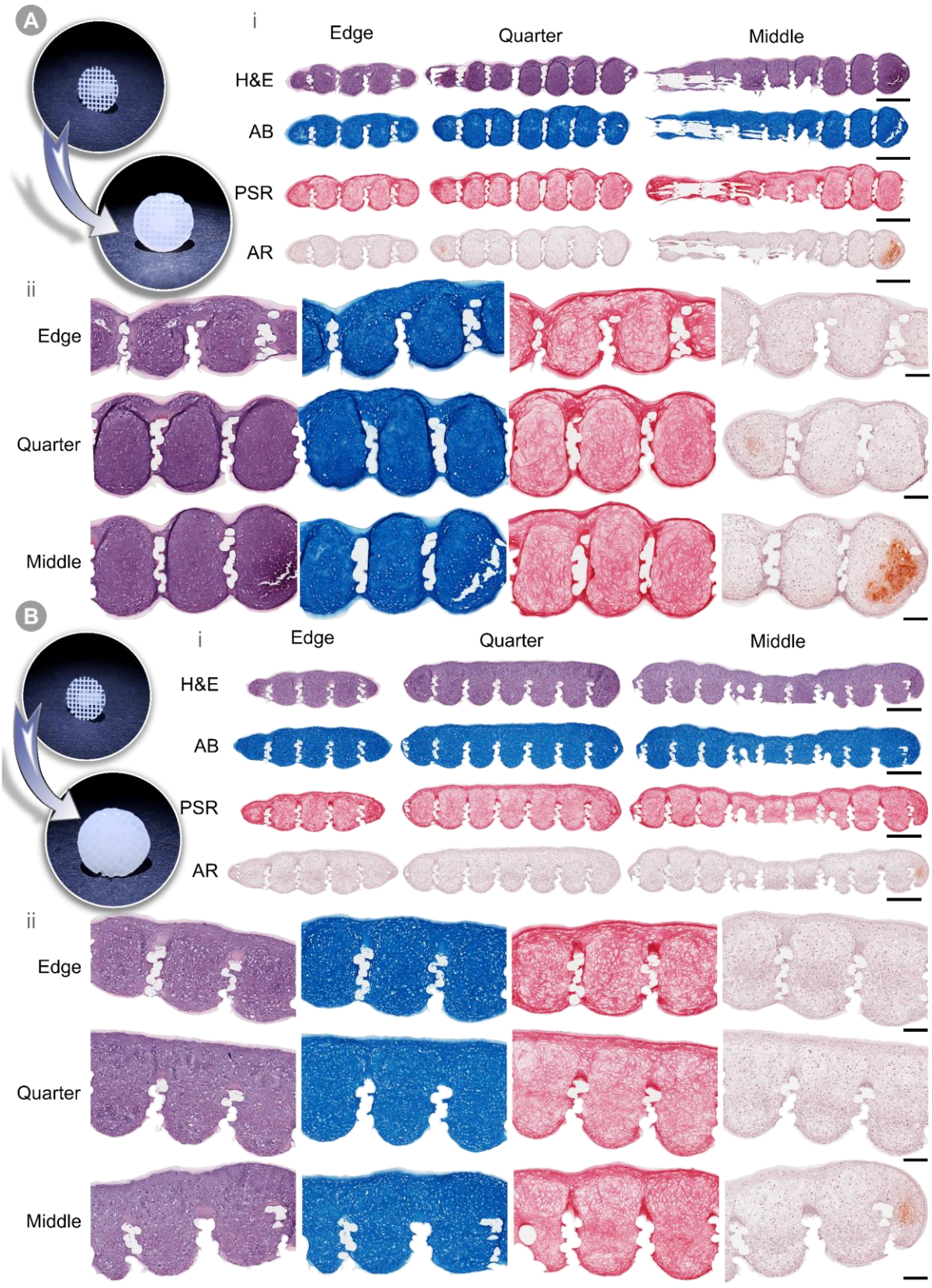

Figure 4.7 *Bioprinted, self-organised cartilage forms within the microwell array of the implant. A) Macroscopic and histological images of the 50 × 10^3 cells/microwell after 4 week of chondrogenic culture. i) 3× overview images of the engineered tissue, sections taken at the edge, quarter, and middle regions of the implant. ii) 10× images of three regions. B) Macroscopic and histological images of the 100 × 10^3 cells/microwell after 4 week of chondrogenic culture. i) 3× overview images of the engineered tissue, sections taken at the edge, quarter, and middle regions of the implant. ii) 10× images of three regions. (Scale Bars: Overview = 700 µm, Zoom = 200 µm).*

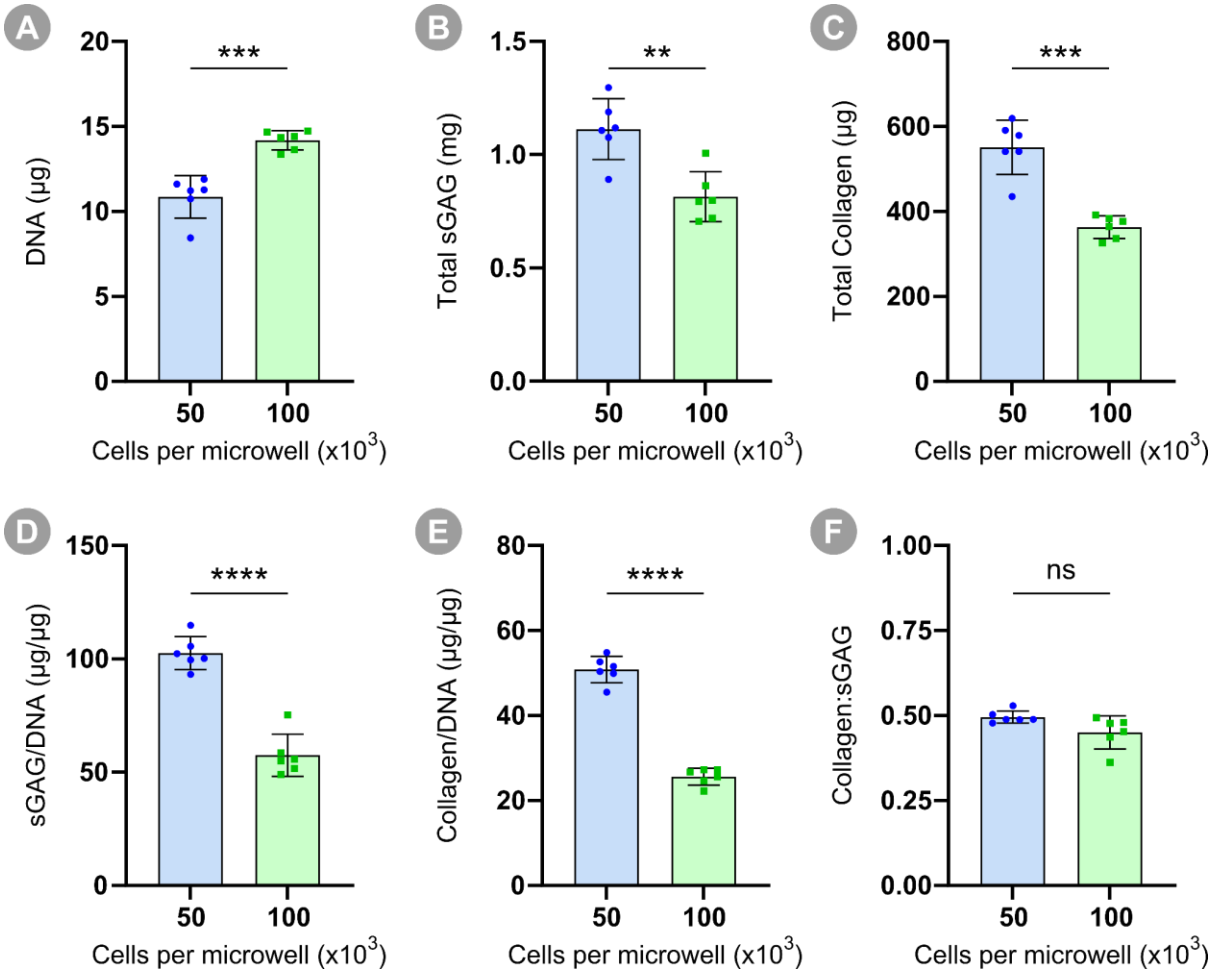

Figure 4.8 *50 × 10^3 cells/microwell result in a richer self-organised cartilage after 4 weeks of chondrogenic culture. A) After 4 weeks, 100 × 10^3 cells/microwell had significantly higher DNA levels. B & C) Total sGAG and collagen within the engineered tissue was significantly higher with the lower starting cell density. D & E) sGAG and collagen levels normalised to DNA were also significantly higher in the 50 × 10^3 cells/microwell group compared to the 100 × 10^3 cells/microwell group. F) The collagen to sGAG ratio within the engineered cartilage showed no significant differences. * denotes significance using a two-tailed, unpaired Welch's t-test, $p < 0.05$ (N = 6, Mean ± SD).*

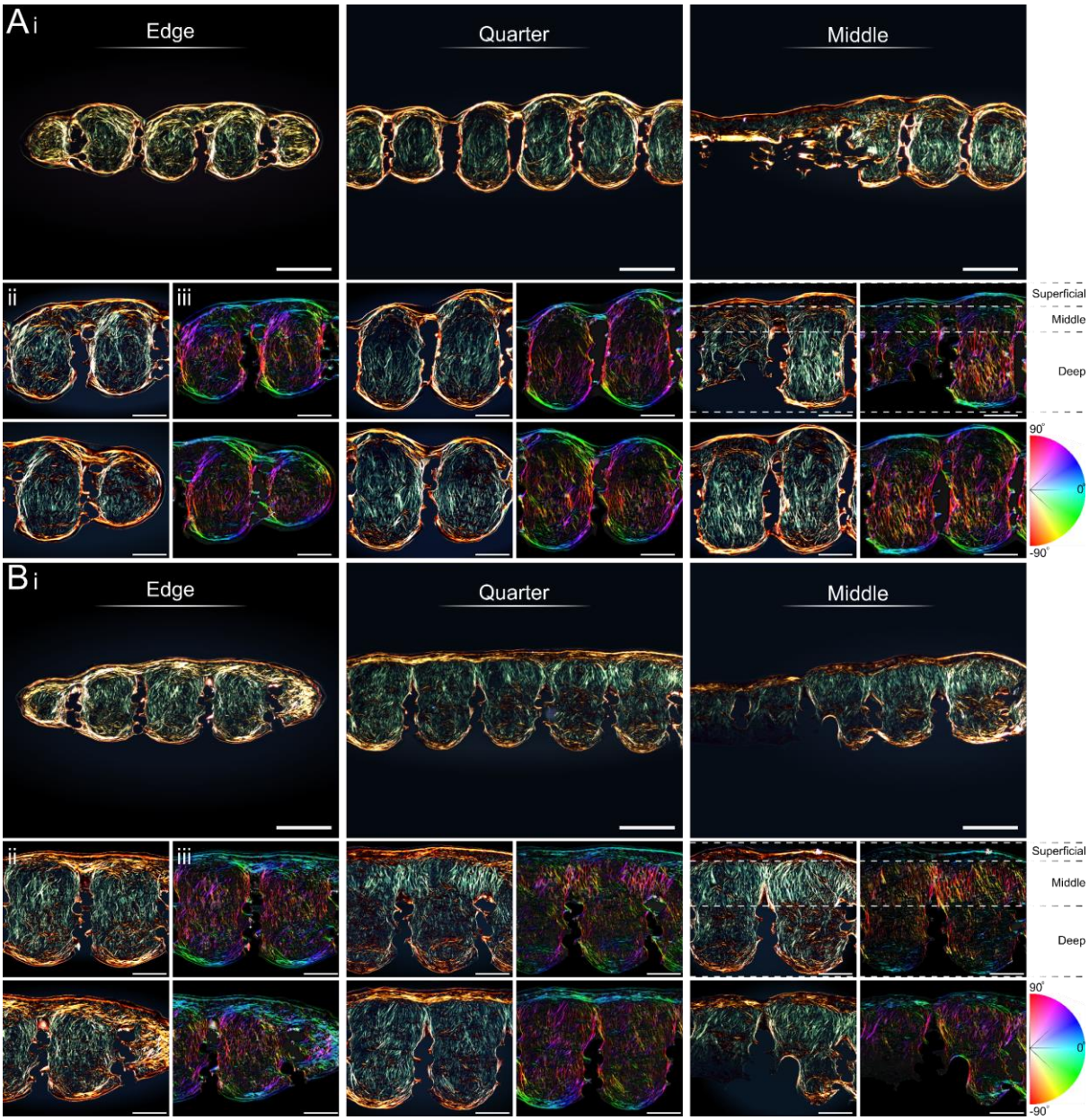

Figure 4.9 *Bioprinting 100 × 10^3 cells/microwell results in spatial organisation of the collagen network within the self-organised tissue. A) PLM of the cartilage engineered using 50 × 10^3 cells/microwell. B) PLM of the cartilage engineered using 100 × 10^3 cells/microwell. i) Overview of the implant. ii Top & Bottom) Two ROI taken at 10× magnification Images of two microwells. Quantification of collagen alignment was carried out at this magnification. iii) Colour map of the collagen network. (Scale Bar: Overview = 500 µm, Zoomed ROI = 250 µm)*

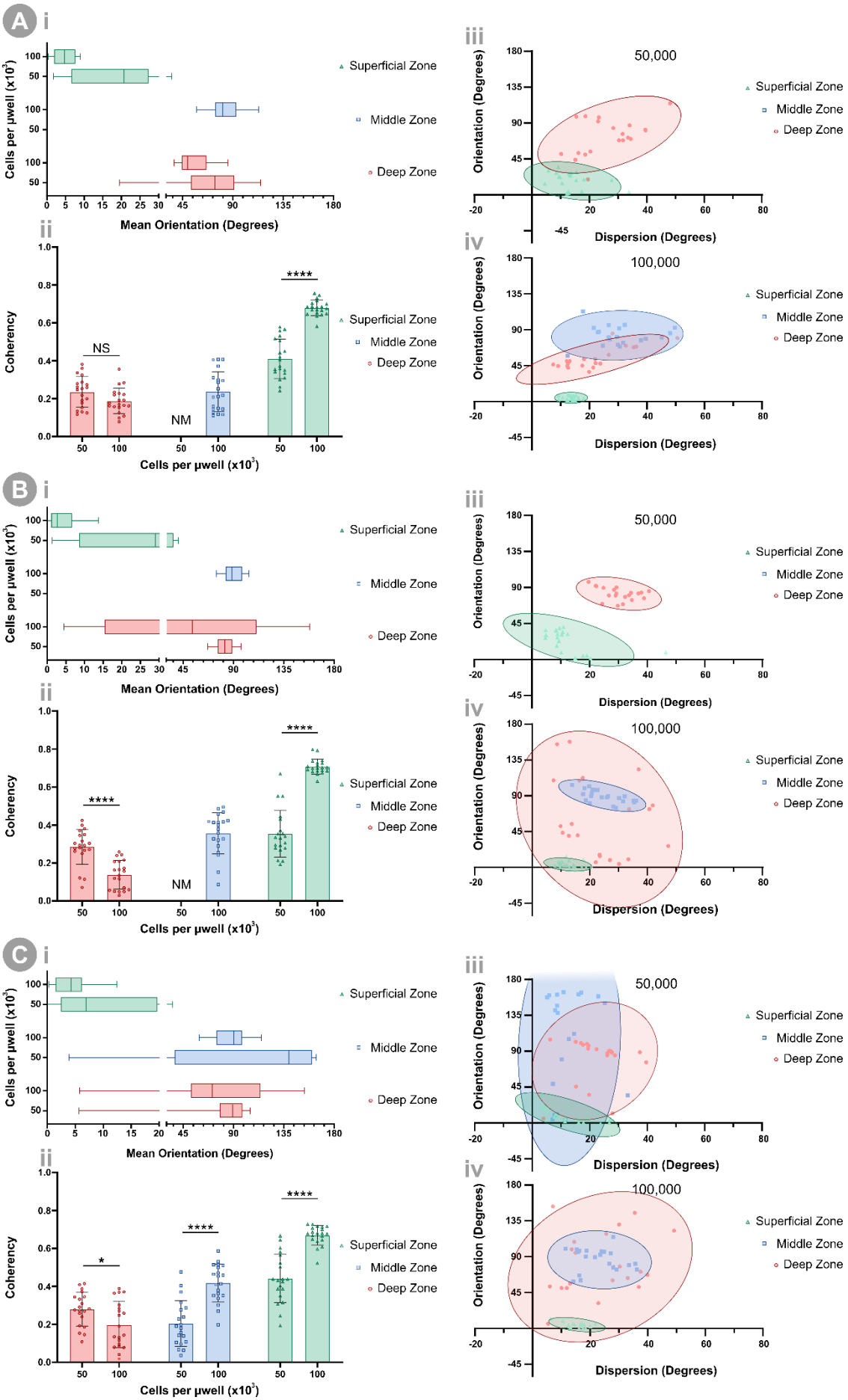
A
i
Cells per µwell (x10³)
Mean Orientation (Degrees)
Superficial Zone
Middle Zone
Deep Zone
ii
Coherency
NS
NM
****
Cells per µwell (x10³)
iii
50,000
Orientation (Degrees)
Dispersion (Degrees)
iv
100,000
B
C
*

Figure 4.10 *A biomimetic collagen architecture is engineered by using 100 × 10^3 cells/microwell. Quantification of the collagen fibre directionality within the self-organised tissue was carried out at; A) the edge region, B) the quarter region, and C) the middle region. Quantitative analysis included (i) determining the mean fibre orientation, (ii) the coherency of the fibres where, a value of 1 indicates fibres are aligned in the same direction, while a value of 0 indicates dispersion of fibres in all directions, (iii & iv) dispersion versus mean orientation. * denotes significance using a two-tailed, unpaired Welch's t-test, $p < 0.05$ (N = 20, Mean ± SD).*

4.3.6 Dynamic Culture Conditions Support the Engineering of Biomimetic Self-organised Cartilage

Having demonstrated that bioprinting 100 × 10^3 cells/microwell is an effective means of creating a promising collagen stratification, but compromises the biosynthetic output of the resident MSCs. It was hypothesised that nutrient limitations within the highly cellular system was responsible for the diminished production of cartilage ECM components. To this end, this chapter next explored whether dynamic culture could help alleviate these nutrient limitations and produce a rich cartilage matrix with a physiologic stratification.

After 4 weeks of dynamic culture, the tissue formed within the head of the implant was significantly thicker than previous attempts (Figure 4.11A & Table 4.2). Histologically, the neotissue had extensively over grown the microwell walls (Figure 4.11B). Additionally, a native-like cellular morphology and distribution was observed which had not been previously seen in the self-organised cartilage cultivated in static conditions (Figure 4.11C). Deposition of sGAG and collagen was uniform throughout, and unlike static conditions, there was no evidence of cartilage mineralisation when using dynamic culture. Biochemically, there was no significant difference in levels of DNA when comparing static and dynamic groups of the same cell-density. However, the biosynthetic output of the cells cultured dynamically was significantly higher. This culminated in a rich ECM, with total levels of sGAG and collagen reaching 2.81 ± 0.555 mg and 1026 ± 74.6 mg respectively. The incredibly robust chondrogenesis resulted in a tissue that exhibited native levels of sGAG (% WW) (Figure 4.11D) [230]. Moreover, an improvement in the spatial organisation of the collagen network within the engineered cartilage by culturing in dynamic conditions was observed (Figure 4.10). In particular, a highly biomimetic fibre orientation in all 3 zones of the engineered tissue, which closely matched those seen in native AC was seen.

Table 4.2 *Physical and biochemical properties for the engineered cartilages after 4 weeks. '*' Denotes a significant difference when compared to the 50 × 10^3 cells/microwell group and '&' denotes a significant difference when compared to the 100 × 10^3 cells/microwell (static), both when tested using a Brown-Forsythe and Welch One-way ANOVA, p < 0.05 (N = 6, Mean ± SD).*

	Thickness (µm)	*Total sGAG (mg)*	*Total Collagen (µg)*	*sGAG/DNA*	*Collagen/DNA*
50 × 10^3 STAT	801 ± 73.1	1.11 ± 0.134	551 ± 64.2	103 ± 7.25	50.8 ± 3.15
100 × 10^3 STAT	921 ± 32.0 *	0.814 ± 0.110 **	363 ± 26.4 ***	57.5 ± 9.30 ****	25.6 ± 1.94 ****
100 × 10^3 DYN	1389 ± 49.8 ****,&&&&	2.81 ± 0.555 ***,&&&	1026 ± 74.6 ****,&&&&	179 ± 22.7 ***,&&&&	66.1 ± 6.51 **,&&&&

For example, in the quarter section the mean fibre orientation in each zone for the engineered tissue versus native AC was as follows: 84.4° ± 12.4° and 90.5 ° ± 6.00° for the deep zone, 83.7° ± 8.20° and 89.4° ± 10.6° for the middle zone, and 5.22° ± 4.96° and 0.784° ± 0.764° for the superficial zone. Additionally, dynamic culture resulted in a significant improvement of the fibre coherency within the deep and middle zones. Although the mean orientation of fibres within the superficial zone was analogous to those seen in native tissue, there was a reduction in fibre coherency within this zone compared to static conditions. This could be explained, in part, by the greater tissue thickness and the incomplete development of the transitional zone (Figure 4.12B & C).

Finally, to determine tissue phenotype, immunofluorescence staining was undertaken to identify the collagen types present within the engineered cartilage (Figure 4.13). In static conditions, diffuse positive staining for collagen type II was apparent, as well as weak straining for collagen type I and type X in both cell densities. Interestingly, more cellular engineered cartilage (100 × 10^3 cells/microwell), expressed lower levels of both collagen type I and type X, indicative of a more stable phenotype. Dynamic cultivation of bioprinted cartilage yielded similar expression of collagen type II as observed in static conditions. However, dynamic conditions suppressed the expression of collagens type I and type X which were previously identified in static culture conditions. These results clearly demonstrate that a rich, biomimetic, and stable cartilage can be engineered *via* the guided self-organisation of MSCs. Moreover, the quality of this tissue can be significantly enhance by employing a dynamic culture regime (Figure 4.13 & Table 4.2).

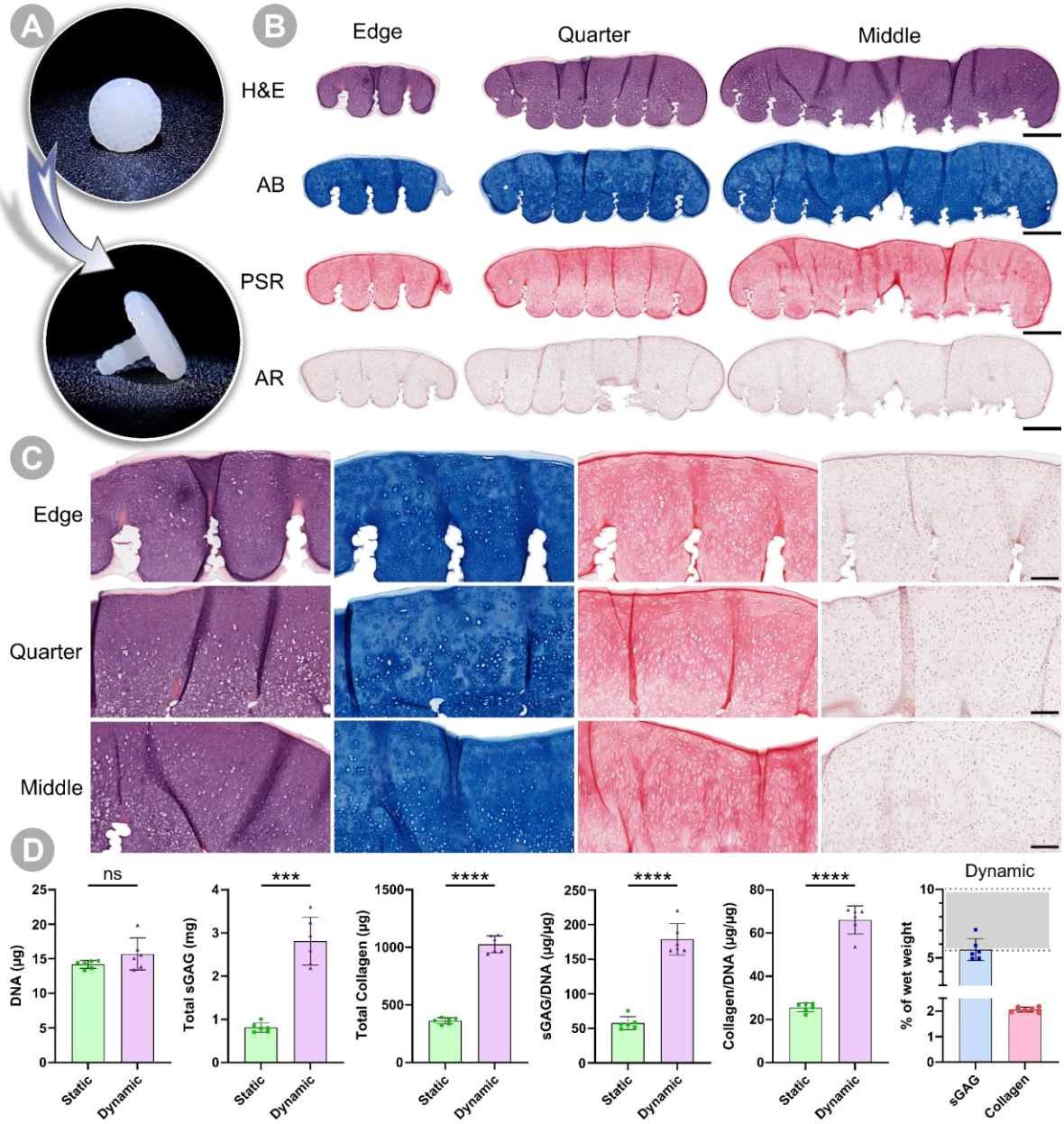

Figure 4.11 *Dynamic culture significantly enhances the quality of the self-organised cartilage. A) Macroscopic images of the 100 × 10^3 cells/microwell after 4 week of dynamic chondrogenic culture. B) 3× overview images of the engineered tissue, sections taken at the edge, quarter, and middle regions of the implant. C) 10× images of the three regions. D) Biochemical quantification of the engineered cartilage. Dynamic, chondrogenic culture conditions significantly increases the deposition of canonical cartilage matrix components when compared to static culture. The wet weight percentage of sGAG within the engineered tissue approached that found in native tissue (grey box) at the same time point. (Scale Bars: Overview = 700 µm, Zoom = 200 µm) * denotes significance using a two-tailed, unpaired Welch's t-test, $p < 0.05$ (N = 6, Mean ± SD).*

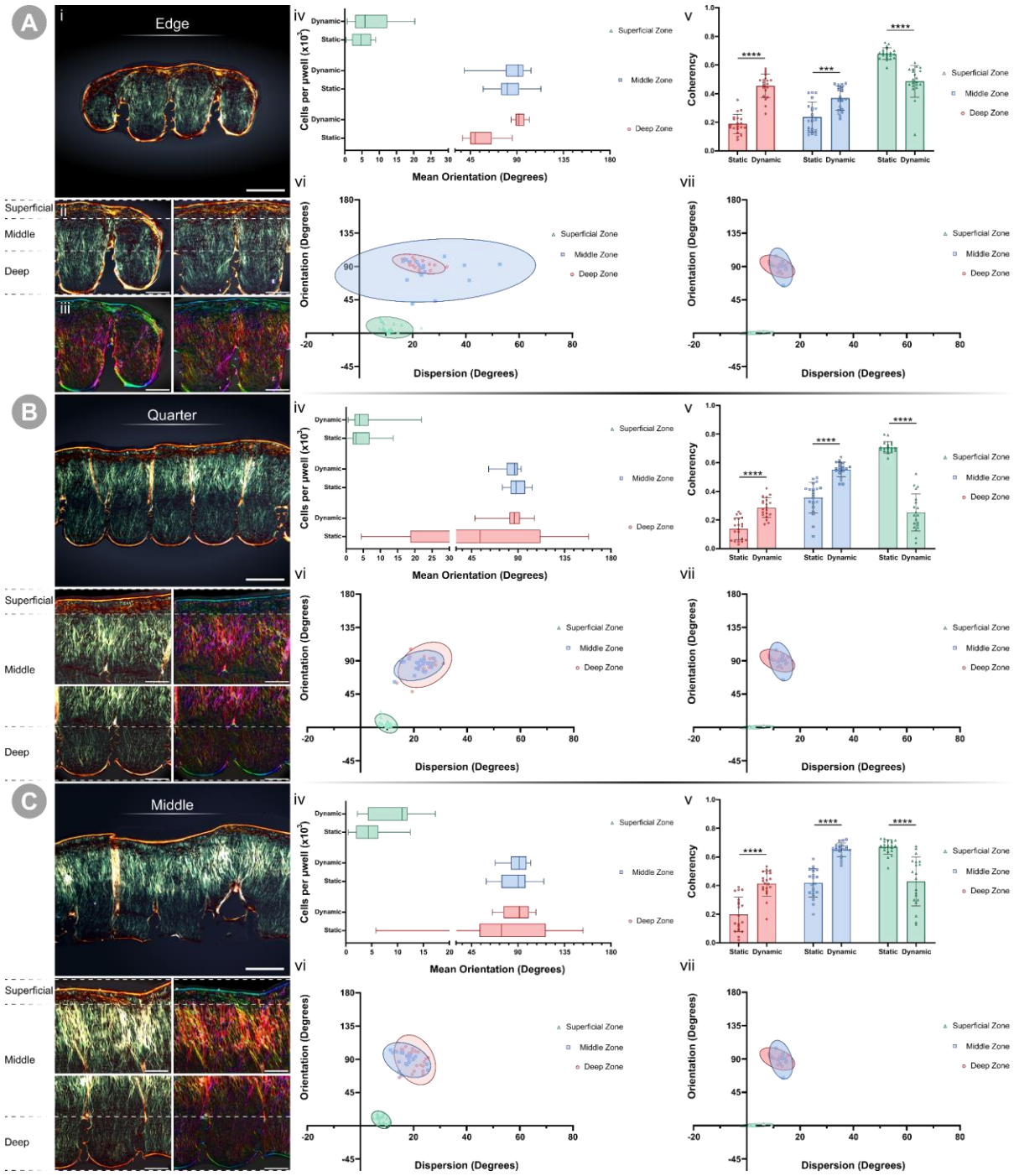

Figure 4.12 *Dynamic culture generates a tissue with a collagen architecture that closely matches native articular cartilage. Quantification of the collagen fibres within the self-organised tissue was carried out at; A) the edge region, i) Overview of the implant. ii Left & Right) Two 10x magnification Images of two microwells. iii) Colour map of the collagen network. B) The quarter region, and C) the middle region. For the quarter and middle regions, sections were divided into two due to the thickness of the tissue. 10x magnification Images and corresponding colour map are left & right. Quantitative analysis included (iv) determining the mean fibre orientation, (v) the coherency of the fibres where, a value of 1 indicates fibres are aligned in the same direction, while a value of 0 indicates dispersion of fibres in all directions, and (vi & vii) dispersion versus mean orientation, where vi) is the engineered tissue and vii) is native AC. (Scale Bars: Overview = 500 µm, Zoom ROI = 250 µm) * denotes significance using a two-tailed, unpaired Welch's t-test, $p < 0.05$ (N = 20, Mean ± SD).*

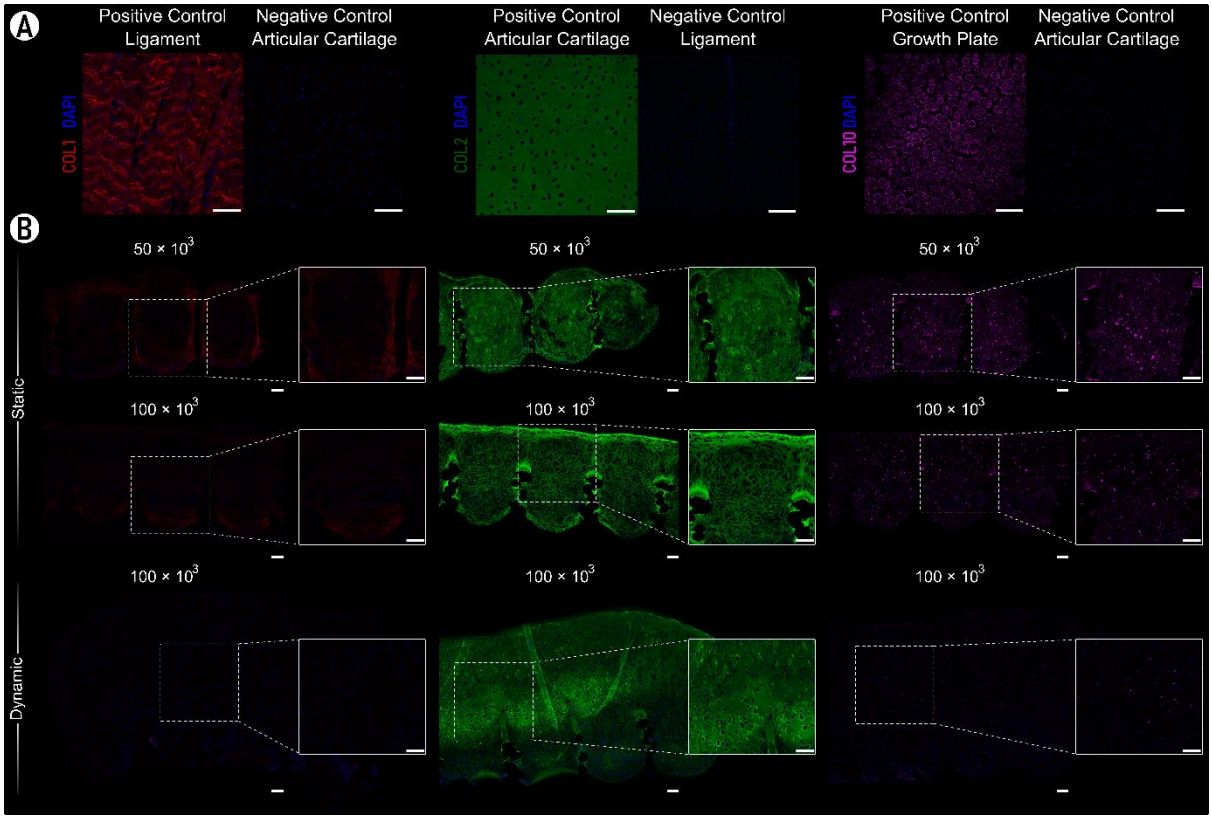

Figure 4.13 *Dynamic culture yields a stable cartilage phenotype. Immunofluorescence staining for collagen isotypes with nuclear staining using DAPI. A) Positive and negative controls for collagen type I (red), type II (green), and type X (magenta). B) Staining for collagen type I (red), type II (green), and type X (magenta) within engineered tissues indicated similar expression of collagen type II in all conditions after 4 weeks. However, levels of collagen type I and type X are lower in engineered cartilages that has been cultivated in dynamic conditions. (Scale Bar = 100 µm)*

4.4 Discussion

Within this chapter, a novel strategy for bioprinting of biomimetic cartilage grafts for the treatment of focal chondral defects was developed. This implant consisted of a microwell array intended to contain and guide a self-organising cartilage on top of a fixation pin fabricated using FDM that designed to anchor the graft into a synovial joint. As previously discussed, creating an osteochondral implant for the treatment of a chondral defect is often employed to secure an engineered scaffold or tissue *in situ* [111,231]. However, changes within injured subchondral bone have been linked with the initiation and/or propagation of a deleterious state within damaged joints [10,11,19,20], motivating the search for alterative, less detrimental approaches to fixing engineered cartilage to the subchondral bone [231,232]. Biodegradable pins are one fixation strategy with a relatively small footprint that have been used clinically [226,227]. However, they are not well suited to fixing stiffer 3D printed implants in place [228]. In light of this, an important finding of this study was designing an implant that integrated the 3D printed scaffold and the fixation pin into a single device. Since the fixation pin was designed to work in conjunction with micro-drilling, and hence minimise the iatrogenic damage to the subchondral bone, reliably creating a small diameter pin below the chondral scaffold was pivotal. FDM was found to an effective additive manufacturing method due to its resolution and amenability to creating complex monolithic parts. During implant fabrication the formation of a spiral along the pin was observed. Whilst this was as unanticipated addition, given that the surface feature could be reproducibly created during 3D fabrication it was believed that it could be a beneficial attribute. In particular, it was hypothesised that the spirals would act like threads on a screw and provide greater mechanical anchorage when the implant was press-fit in place. Additionally, the macroscale undulations coupled with the microscale topography formed by the printed layers serve to increase surface area, and create surface roughness. Creating a multiscale surface topography is frequently discussed as a central feature for improving osteointegration of implants [233,234]. In conjunction with designing and fabricating the implant, modification to the existing micro-drilling technique were also made as part of developing a new surgical approach. As such, this work provides a platform for the fixation of engineered cartilage within focal cartilage defects that is compatible with existing clinical workflows.

The self-organised AC engineered in this study was highly biomimetic in both its composition and structural organisation. It has been demonstrated that bioprinting a high density (100×10^3 cells/microwell) of MSCs results in superior organisation of the collagen network when compared to a lower starting density. In addition, by employing a dynamic culture regime, the richness of ECM composition can be significantly improved, as well as the generation of a collagen architecture with near-native levels of spatial organisation. The concept for using a polymer framework to guide the self-organisation process has been demonstrated previously [41]. Unlike previous reports, the

microwell system described here has a temporary base instead of a solid polymer base, which provides a number of benefits. First, it provides the option for bidirectional tissue growth and nutrient delivery. Removal of such a base from the engineered implant also permits cartilage-bone cross-talk, the importance of which is becoming increasingly apparent for AC homeostasis [10,11,20]. Finally, apposition of a neo-cartilage with subchondral bone has been shown to facilitate *in situ* integration [231,232]. Other improvements over similar attempts are the generation of a consistently thicker tissue (> 1mm compared to ~680 µm in this study and Daly *et al.* respectively) after only 4 weeks of dynamic culture. Importantly, the approach taken in this chapter yielded a far more biomimetic collagen network than that described previously [41], whereby PLM visualisation and quantification revealed a near-native organisation. Other attempts to bioprint a self-organised AC have focused on fusing extruded tissue-strands [214]. More recently, the same group have leveraged the collagen alignment within these cartilage strands to create stratification within a bioprinted cartilage [215]. Although this approach generated a cartilage with native-like mechanical properties, complete fusion between the proximal cartilage strands appeared incomplete, preventing the formation of a homogenous tissue. Additionally, the organisation of the collagen network using this approach did not appear to mimic the Benninghoff arcade structures as effectively as the approach presented in this chapter. In contrast the self-organisation strategy utilised in this study does not require extensive progenitor cell expansion and as such, may be more amenable to engineering AC at a human-clinically relevant scale.

The number of cells inkjetted into each microwell had a significant effect on both the composition and organisation of the resulting tissue. In static conditions, cartilage engineered using a lower cell-density exhibited a significantly richer cartilaginous matrix as well as more pronounced mineralisation. The availability of nutrients within the two cell-density conditions could explain these differences. Specifically, in the higher-density system, limited nutrient availability appears to hinder biosynthesis. However, this higher metabolic consumption within this system would also impact the pO_2. Since oxygen tension is known to be a potent regulator of stem cell fate [191–195], the more cellular engineered cartilage could exhibit a favourable phenotype (less mineralisation) by creating a more hypoxic local environment during culture. Similar observations have been made in hydrogel systems, where chondrogenic gradients can be seen in relation to local oxygen availability [196]. In this study, dynamic culture conditions appeared to enhance tissue development in the higher density group. Interestingly, although bioreactor culture has been shown to interfere with chondrogenesis [188–190], the dynamic conditions employed here resulted in significantly higher amount of matrix components and better organisation within the engineered cartilage. Others have shown similar findings [197], suggesting that carefully implementing dynamic culture can be an effective method for cultivating large engineered cartilages.

While this bioprinting strategy clearly enables the engineering of cartilage that mimics key features of the native tissue, there are still areas for improvement. While the sGAG content of the engineered tissue is reaching native levels, the overall levels of collagen are still noticeably lower. It has previously been shown that a failure to recapitulate the structure-function relationship of native cartilage within engineered analogues creates mechanical mismatches between the implanted neo-cartilage and the host tissue [111,231,235]. Since, recreating native-like mechanical properties is rare [111,231], and a large part of this challenge involves the difficulties associated with recapitulating the collagen content and architecture of native AC in the laboratory [42,45,47,231]. The techniques presented in this study have identified an effective means of recreating feature of native AC's collagen network *in vitro*. Albeit a promising start, further tissue development is be necessary to generate a complete tissue mimic. To this end, the use of remodelling enzymes (chondroitinase-ABC and lysyl oxidase), growth factors and mechanical stimulus have been successfully employed to increase the biochemical and biomechanical properties of self-assembled/self-organised engineered cartilages [45,49–51,117]. Further biomechanical improvements can be made by integrating the efforts outlined in literature with the platform developed in this study. By coupling structural organisation with increases in neo-collagen maturation, content, and cross-linking engineered cartilages with adequate mechanical properties to provide immediate joint resurfacing could be realised in the future. Mechanical testing was not undertaken within this study as the presence of PCL microchambers dominates the mechanical properties of the construct, making assessments of the tissue properties challenging. Nevertheless, further studies will need to fully elucidate the impact of enhanced collagen content and organisation on the biomechanical properties of self-organised engineered cartilages.

4.5 Conclusion

This work has established a strategy to bioprint a self-organised cartilage using an instructive fixation device. Specifically, a novel assembly of a 3D printed polymer implant and temporary base has been used to effectively guide the self-organisation and development of highly-cellular condensations towards a stratified articular cartilage. Dynamic culture conditions were shown to further enhance the quality of this engineered tissue. To this end, bioreactor culture of a high-density cellular condensations enabled the generation of an engineered articular cartilage with near-native levels of matrix components and organisation.

Chapter 5.

5 Engineering High-Quality Cartilage Microtissues

5.1 Introduction

The feasibility of generating a clinically relevant macrotissue *via* microtissue/aggregate engineering, depends on several reciprocal factors. Principally, the size of the microtissue units generated and the number of these units required to generate a construct/fill a particular defect volume is an important balance. As such, engineering high-quality microtissues (with a tissue-specific matrix) of a suitable initial size to feasibly generate a tissue of scale is a significant challenge. Identifying a workable balance between microtissue quality (mitigating diffusion gradients and nutrient limitations), microtissue size (maximising the size of the individual units to minimise the total number required), the number of cells required to generate the microtissues, and ultimately the number of microtissues required to generate a tissue of clinically relevant scale requires considering multiple factors. To date, engineering osteochondral tissues using cellular aggregates or microtissues has predominately focused on the use of undifferentiated mesenchymal stem cell (MSC) aggregates [89,141]. These immature aggregates do not mimic the complex native extracellular matrix (ECM), which may explain why they fail to promote the regeneration of hyaline cartilage when implanted into pre-clinical models for chondral/osteochondral defects [69,236].

Unlike traditional scaffold or hydrogel tissue engineering strategies, scaffold-free approaches are inherently reliant on the cell's own capacity to generate the bulk of the tissue/construct through deposition of ECM macromolecules. Although this follows a developmentally inspired paradigm and facilitates the generation of biomimetic *in vitro* cartilage tissues [43–48,64,81,115,116], in the absence of an interstitial 'bulking' scaffold or hydrogel material, creating tissues of scale can be challenging. Scaling down scaffold-free tissue units can support more robust differentiation, alleviate diffusion gradients, and ultimately improve matrix deposition [54,70,114,130]. Despite the numerous biological benefits associated with scaled-down 3D scaffold-free strategies [42,66,81], microtissues do not yet represent an idealised solution whereby robust ECM biosynthesis is guaranteed. In particular, heterogeneity of cell phenotype within MSC populations can lead to poor chondrogenesis and impact the richness of any cartilage ECM generated *in vitro* [237]. Such donor-to-donor variation is well documented throughout the literature and has been shown to directly affect the *in vivo* performance of engineered cartilages [238]. To date, microtissue/aggregate strategies for engineering clinically relevant osteochondral tissues faces many hurdles. In particular, creating high-quality microtissues as part of a scalable biofabrication process is challenging. Moreover, the ability to generate numerous

ECM rich microtissues in a practical and economical manner can be exacerbated by the common use of mixed MSC populations and their inherently variable chondrogenic capacity.

With this in mind, generating osteochondral tissues of scale using microtissue/aggregate engineering will require the high-throughput production of consistently high-quality cartilage microtissues. In particular, methods capable of consistently delivering quality cartilage microtissues despite the use of diverse donors with different chondrogenic capacity is required. Without well-defined markers for identifying MSCs within primary isolations, many tissue engineers use uncharacterised cohorts of cells for generating tissues, which in turn can reduce the reliability and quality of the engineered cartilages. The identification of a simple method for improving the chondrogenic capacity of uncharacterised MSC populations, isolated from bone marrow, could help to limit the variability seen in cartilage tissue engineering. Specifically, in the context of aggregate engineering, defining a protocol amenable to the novel hydrogel microwell platform would support the generation of high-quality cartilage microtissues. Ultimately, these high-quality cartilage microtissues can be used as building blocks to more efficiently engineer osteochondral tissues of scale. Based on a serendipitous observation that Endothelial Growth Medium (EGM) enhanced MSC aggregation and chondrogenic capacity in animal bone-marrow derived MSCs (BMSCs), this chapter sought to elucidate the driving factor within EGM using human BMSCs. Ultimately, the aim was to improve upon current chondrogenic culture regimes and create a novel platform for engineering high-quality scaffold-free cartilages.

5.2 Materials & Methods

5.2.1 Media Formulations

Expansion Medium "XPAN". XPAN is composed of high glucose Dulbecco's modified eagle's medium (hgDMEM) GlutaMAX supplemented with 10 % v/v FBS, 100 U/mL penicillin, 100 µg/mL streptomycin (all Gibco, Biosciences, Dublin, Ireland) and 5 ng/mL bFGF2 (Prospect Bio).

Endothelial Growth Medium (EGM). EGM is composed of Endothelial Cell Basal Medium-2 (EBM) (Lonza) supplemented with MV Microvascular Endothelial Cell Growth Medium-2 BulletKit™ (Lonza). As the concentration of the supplements added to EBM are proprietary information, the concentrations for each are given as a %v/v. Fetal bovine serum (FBS) was added at 5 %, Hydrocortisone (Hydro) was added at 0.04 %, human FGF-2 (FGF) was added at 0.4 %, vascular endothelial growth factor (VEGF), recombinant human long R3 insulin like growth factor 1 (IGF), ascorbic acid (AA), and human epidermal growth factor (EGF) were all added at 0.1%. Finally, gentamicin sulfate-Amphotericin (GA-1000) was added at 0.1%.

Chondrogenic Differentiation Medium (CDM). hgDMEM GlutaMAX supplemented with 100 U/mL penicillin, 100 µg/mL streptomycin (both Gibco), 100 µg/mL sodium pyruvate, 40 µg/mL L-proline, 50 µg/mL L-ascorbic acid-2-phosphate, 4.7 µg/mL linoleic acid, 1.5 mg/mL bovine serum albumin, 1 X insulin–transferrin–selenium (ITS), 100 nM dexamethasone (all from Sigma), 2.5 µg/mL amphotericin B and 10 ng/mL of human transforming growth factor-b3 (TGF-β) (Peprotech, UK).

5.2.2 Bone Marrow Mesenchymal Stem/Stromal Cell (BMSC) Isolation

Goat BMSC (gBMSC) isolation. gBMSCs were harvested under sterile conditions from the sternum of skeletally mature, female, Saanen goats. Briefly, excised bone marrow was dissected into small pieces using a scalpel. The marrow pieces were then gently rotated for 5 min in XPAN to help liberate the cellular components. The culture medium was then aspirated and passed through a 70 µm cell sieve prior to counting and plating at a density of 57×10^3 cells/cm^2 and expanded under hypoxic conditions (37 °C in a humidified atmosphere with 5 % CO_2 and 5 % pO_2) for chondrogenic differentiation. Following colony formation, gBMSCs were trypsinised using 0.25 % (w/v) Trypsin Ethylenediaminetetraacetic acid (EDTA). gBMSCs for microtissues were expanded from an initial density of 5000 cells/cm^2 in XPAN medium under physioxic conditions until P3.

Human BMSC (hBMSC) isolation. hBMSCs were isolated from unprocessed human bone marrow (Lonza) on the basis of plastic adherence. Briefly, unprocessed bone marrow was plated at 2.5×10^5 cells/cm^2 (estimated approx. 4000 - 5000 MSCs/cm^2) in XPAN medium and expanded under physiological oxygen conditions (37 °C in a humidified atmosphere with 5 % CO_2 and 5 % pO_2). Following colony formation, hBMSCs were trypsinised using 0.25 % (w/v) Trypsin

Ethylenediaminetetraacetic acid (EDTA), hBMSCs were expanded in XPAN under physioxic conditions (5 % pO2) and aggregated into pellets at P3.

5.2.3 Experimental Design

For all studies, microwells were seeded at a density that results in 4 x 10^3 cells/microtissue. Cell expansion and cartilage microtissue cultivation took place at physiological oxygen conditions (37 °C in a humidified atmosphere with 5 % CO_2 and 5 % pO_2). With the exception of the first 24 hours, media was exchanged every 2 days. Initial investigation using gBMSCs involved 21 Days of chondrogenic culture. All studies using hMSCs were carried out over 7 days of chondrogenic cultivation.

Control Group. Here, cartilage microtissues are formed by seeding bMSCs into the microwells in XPAN. The following day, the XPAN medium is carefully aspirated from the wells and replaced with CDM.

EGM Group. EGM was used to soak the agarose hydrogel microwells overnight prior to seeding. As such, cells seeded into the microwells in the 'EGM' group were never directly exposed to EGM. The seeding procedure and following chondrogenic culture was identical to the control group.

Media Component Isolation Groups. By means of determining the prominent factor within EGM that aided in chondrogenesis, a screening study was undertaken. Each of the supplements listed in §2.1 for EGM formulation were added at the correct concentration (%v/v) to both XPAN during pre-soaking and seeding, as well as CDM during differentiation culture. Chondrogenic and experimental EGM supplements were added to the basal media of CDM fresh prior to media exchange. Additionally, blends of XPAN/CDM and EGM were used. In these groups EGM was supplemented as a 1× or 2× formulation and then mixed 50/50 with either XPAN, for soaking and seeding, or with CDM (2×) for chondrogenic differentiation.

Table 5.1 Summary of the components added to each experimental group/media type

Experimental Group/Media type	**FBS**	**FGF-2**	**Hydro**	**VEGF**	**IGF**	**EGF**	**TGF-β**	**ITS**	**Dex**	**AA**
XPAN	Yes (10 %v/v)	Yes (5 ng/mL)	No	No	No	No	No	No	No	No
EGM (%v/v)	Yes (5%)	Yes (0.4%)	Yes (0.04%)	Yes (0.1%)	Yes (0.1%)	Yes (0.1%)	No	No	No	Yes (0.1%)
CDM	No	No	No	No	No	No	Yes (10 ng/mL)	1×	Yes (100 nM)	Yes (50 µg/mL)
50/50 1×	• Yes (7.5% - XPAN/EGM • Yes (2%) - CDM/EGM)	• Yes (2.5 ng/mL + 0.2%) - XPAN/EGM • Yes (0.2%) - CDM/EGM)	Yes (0.02%)	Yes (0.05%)	Yes (0.05%)	Yes (0.05%)	• No – XPAN/EGM • Yes (10 ng/mL) – CDM/EGM	• No – XPAN/EGM • Yes (1×) – CDM/EGM	• No – XPAN/EGM • Yes (100 nM) – CDM/EGM	• Yes (0.05%) – XPAN/EGM • Yes (0.05% + 50 µg/mL) – CDM/EGM
50/50 2×	• Yes (7.5%) XPAN/EGM • Yes (5%) - CDM/EGM)	• Yes (2.5 ng/mL + 0.4%) - XPAN/EGM • Yes (0.4%) - CDM/EGM	Yes (0.04%)	Yes (0.1%)	Yes (0.1%)	Yes (0.1%)	• No – XPAN/EGM • Yes (10 ng/mL) – CDM/EGM	• No – XPAN/EGM • Yes (1×) – CDM/EGM	• No – XPAN/EGM • Yes (100 nM) – CDM/EGM	• Yes (0.1%) – XPAN/EGM • Yes (0.1% + 50 µg/mL) – CDM/EGM
Hydro	• Yes (10%) XPAN/Hydro • No - CDM/Hydro	• Yes (5 ng/mL) – XPAN/Hydro • No – CDM/Hydro	Yes (0.04%)	No	No	No	• No – XPAN/Hydro • Yes (10 ng/mL) – CDM/Hydro	• No – XPAN/EGM • Yes (1×) – CDM/Hydro	• No – XPAN/EGM • Yes (100 nM) – CDM/Hydro	• No – XPAN/Hydro • Yes (50 µg/mL) – CDM/Hydro
FGF	• Yes (10%) XPAN/FGF • No - CDM/FGF	• Yes (5 ng/mL) – XPAN/FGF	No	No	No	No	• No – XPAN/FGF	• No – XPAN/FGF • Yes (1×) – CDM/FGF	• No – XPAN/FGF • Yes (100 nM) – CDM/FGF	• No – XPAN/FGF

		• Yes (0.4%) – CDM/FGF					• Yes (10 ng/mL) – CDM/FGF			• Yes (50 µg/mL) – CDM/FGF
VEGF	• Yes (10%) XPAN/VEGF • No - CDM/VEGF	• Yes (5 ng/mL) – XPAN/VEGF • No – CDM/VEGF	No	Yes (0.1%)	No	No	• No – XPAN/VEGF • Yes (10 ng/mL) – CDM/VEGF	• No – XPAN/VEGF • Yes (1×) – CDM/VEGF	• No – XPAN/VEGF • Yes (100 nM) – CDM/VEGF	• No – XPAN/VEGF • Yes (50 µg/mL) – CDM/VEGF
IGF	• Yes (10%) XPAN/IGF • No - CDM/IGF	• Yes (5 ng/mL) – XPAN/IGF • No – CDM/IGF	No	No	Yes (0.1%)	No	• No – XPAN/IGF • Yes (10 ng/mL) – CDM/IGF	• No – XPAN/IGF • Yes (1×) – CDM/IGF	• No – XPAN/IGF • Yes (100 nM) – CDM/IGF	• No – XPAN/IGF • Yes (50 µg/mL) – CDM/IGF
EGF	• Yes (10%) XPAN/EGF • No - CDM/EGF	• Yes (5 ng/mL) – XPAN/EGF • No – CDM/EGF	No	No	No	Yes (0.1%)	• No – XPAN/EGF • Yes (10 ng/mL) – CDM/EGF	• No – XPAN/EGF • Yes (1×) – CDM/EGF	• No – XPAN/EGF • Yes (100 nM) – CDM/EGF	• No – XPAN/EGF • Yes (50 µg/mL) – CDM/EGF
FBS	• Yes (10%) XPAN/FBS • Yes (5%) - CDM/FBS	• Yes (5 ng/mL) – XPAN/FBS • No – CDM/FBS	No	No	No	No	• No – XPAN/FBS • Yes (10 ng/mL) – CDM/FBS	• No – XPAN/FBS • Yes (1×) – CDM/FBS	• No – XPAN/FBS • Yes (100 nM) – CDM/FBS	• No – XPAN/FBS • Yes (50 µg/mL) – CDM/FBS

Study 1. EGM treatment enhances aggregation & chondrogenic differentiation (gBMSCs)

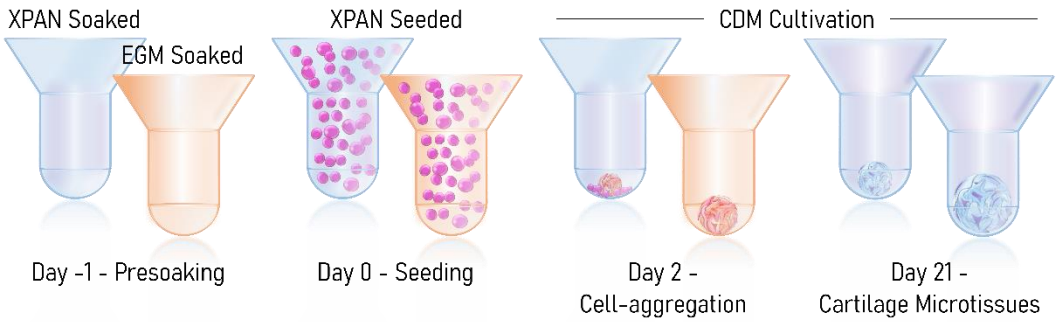

Study 2. Hydrocortisone is the predominant factor driving enhanced chondrogenesis (hBMSCs - Donor 1)

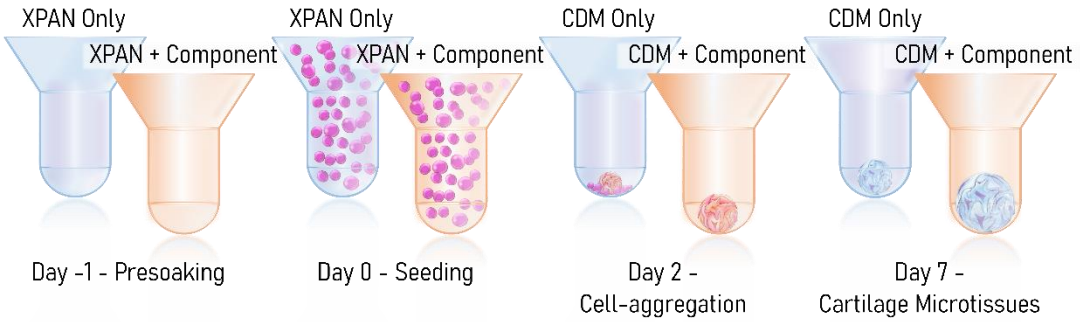

Study 3. Investigation of the effect of EGM and hydrocortisone supplementation on hBMSCs - Donor 2

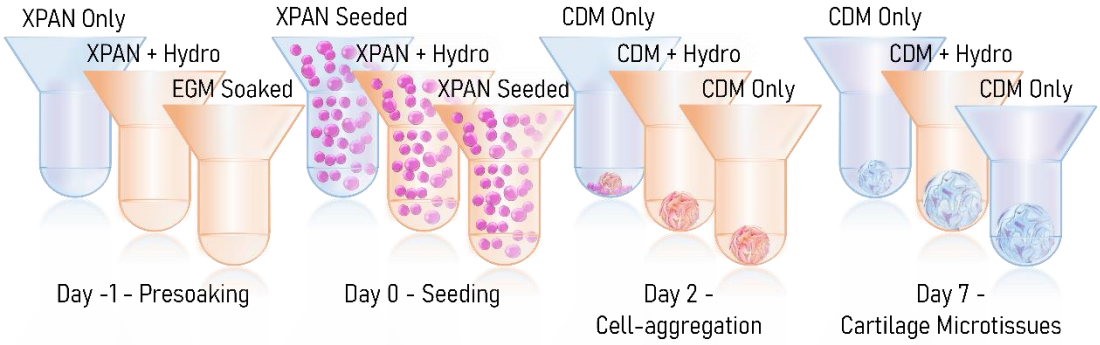

Study 4. Inverstigation of the effect of hydrocortisone exposure time (hMSCs - Donor 2)

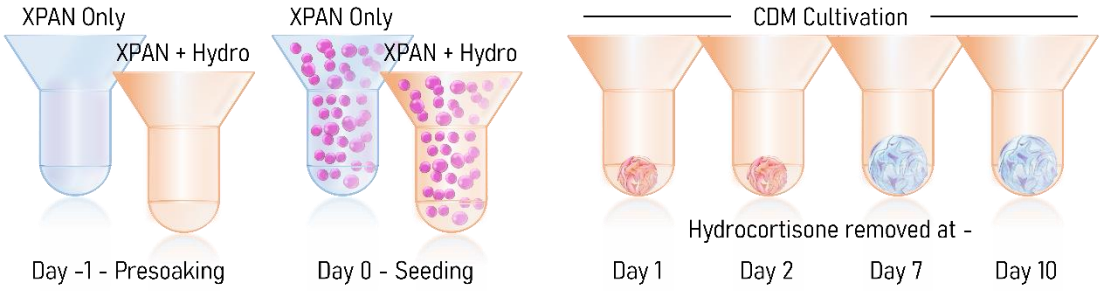

Scheme 5.1 *Schematic of the 4 studies. In study 1) Microwells are soak loaded with EGM, after which a normal chondrogenic protocol is undertaken. Study 2) Factors are soak loaded into the microwells and added to culture medium for the entire culture period. Study 3) Hydrocortisone is added for the entire study, whereas EGM is only soak loaded into the hydrogel microwells prior to seeding. Study 4) Media is supplemented with hydrocortisone until certain time points, after its removal standard chondrogenic cultivation is carried out.*

5.2.4 Histological Analysis

Samples were fixed using 4 % paraformaldehyde (PFA) solution overnight at 4 °C. After fixation, samples were dehydrated in a graded series of ethanol solutions (70 % - 100 %), cleared in xylene, and embedded in paraffin wax (all Sigma-Alrich). Prior to staining tissue sections (5 μm) were rehydrated. Sections were stained with hematoxylin and eosin (H&E), 1 % (w/v) alcian blue 8GX in 0.1 M hydrochloric acid (HCL) (AB) to visualise sulphated glycosaminoglycan (sGAG) content and counter-stained with 0.1 % (w/v) nuclear fast red to determine cellular distribution, 0.1 % (w/v) picrosirius red (PSR) to visualise collagen deposition, and 1 % (w/v) alizarin red (pH 4.1) to determine mineral deposition *via* calcium staining (all from Sigma-Aldrich). Stained sections were imaged using an Aperio ScanScope slide scanner.

5.2.5 Quantitative Biochemical Analysis

Samples were washed in PBS after retrieval and the number of microtissues within each technical replicate counted prior to digestion. A papain enzyme solution, 3.88 U/mL of papain enzyme in 100mM sodium phosphate buffer/5mM Na2EDTA/10mM Lcysteine, pH 6.5 (all from Sigma–Aldrich), was used to digest the samples at 60 °C for 18 hours. DNA content was quantified immediately after digestion using Quant-iT™ PicoGreen ® dsDNA Reagent and Kit (Molecular Probes, Biosciences). The amount of sGAG was determined using the dimethylmethylene blue dye-binding assay (Blyscan, Biocolor Ltd., Northern Ireland), with a chondroitin sulphate standard read using the Synergy HT multi-detection micro-plate reader (BioTek Instruments, Inc) with a wavelength set to 656 nm. Total collagen content was determined using a chloramine-T assay [186] to measure the hydroxyproline content and calculated collagen content using a hydroxyproline-to-collagen ratio of 1:7.69. Briefly, samples were mixed with 38 % HCL (Sigma) and incubated at 110 °C for 18 hours to allow hydrolysis to occur. Samples were subsequently dried in a fume hood and the sediment reconstituted in ultra-pure H_2O. 2.82 % (w/v) Chloramine T and 0.05 % (w/v) 4-(Dimethylamino) benzaldehyde (both Sigma) were added and the hydroxyproline content quantified with a trans-4-Hydroxy-L-proline (Fluka analytical) standard using a Synergy HT multi-detection micro-plate reader at a wavelength of 570 nm (BioTek Instruments, Inc).

5.2.6 Image Quantification & Statistical Analysis

Diameter measurement of growing microtissues were taken from microscope images (4×) using ImageJ software. Statistical analysis was performed using GraphPad Prism software (GraphPad Software, CA, USA). Analysis of differences between two groups at one timepoint was done using a standard two-tailed t-test. For two groups over multiple time-points a one-way analysis of variance (ANOVA) was performed. Numerical and graphical results are presented as mean ± standard deviation unless stated otherwise. Significance was determined when $p < 0.05$.

5.3 Results

5.3.1 Endothelial Growth Media Treatment Enhances Aggregation and Chondrogenesis of goat BMSCs

Soaking the hydrogel microwells with EGM prior to seeding appeared to have a rapid, and potent, effect on the self-organisation of gBMSCs into a spheroid. By day 2, MSC aggregates were significantly larger, and microscopically appeared to include all of the cells which had been seeded into the individual microwells (Figure 5.1A). In contrast, MSC aggregates within XPAN soaked microwells had a smaller average diameter and large numbers of cells, which did not coalesce within the spheroid, were apparent at the bottom of the microwell. These significant differences in size were maintained throughout the culture period, resulting in a final average microtissue diameter of 0.403 ± 0.03 μm and 0.311 ± 0.026 μm for EGM and XPAN soaked microwells respectively. Histologically, both microtissue cohorts exhibited canonical markers for chondrogenic differentiation, with positive matrix staining for sGAG and collagen deposition. In the EGM pre-soak group, the intensity of the staining indicated a richer cartilaginous ECM. Neither group stained positive for calcium deposition, providing evidence that the cartilage has not yet progressed towards a mature hypertrophic phenotype. Biochemical evaluation demonstrated that there were significantly higher levels of DNA, sGAG, and collagen per microtissue when the microwells were soaked with EGM compared to XPAN. Additionally, the levels of sGAG and collagen deposited, normalised to DNA content, demonstrated that EGM treatment resulted in a higher biosynthetic output at a cellular level. Collectively, these results indicated that EGM treatment resulted in the generation of a richer cartilage microtissues. Specifically, the microtissues were initially larger and appeared more cellular. After 21 days of chondrogenic culture, in the EGM group, the bulk composition of each microtissue contained higher levels of key cartilage ECM components. Moreover, the cells within the microtissue demonstrated a higher synthetic output compared to those undergoing a traditional chondrogenic culture regime.

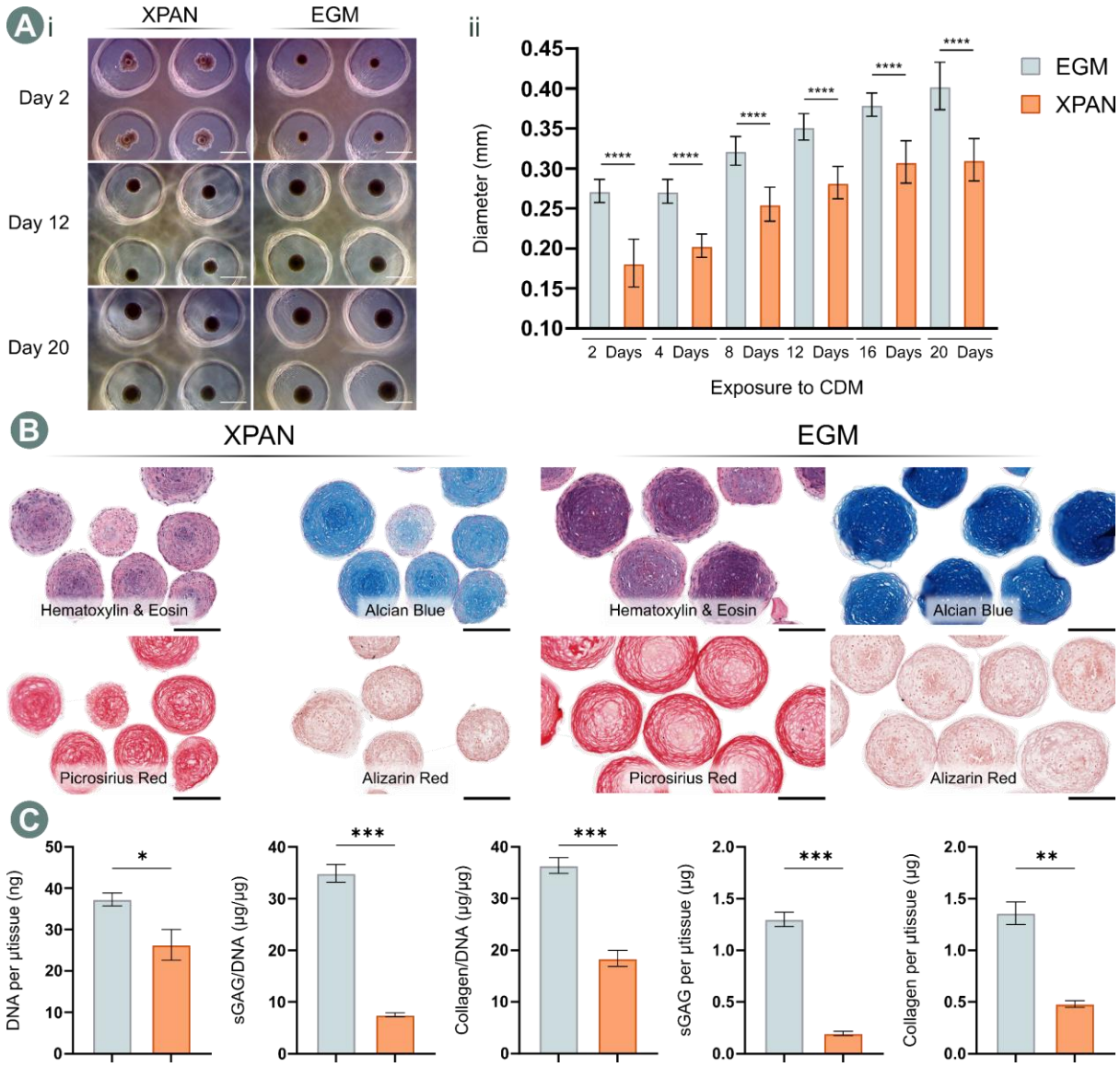

Figure 5.1 *Soaking hydrogel microwells with EGM results in a richer matrix within cartilage microtissues. Ai) Microscopic images at days 2, 12, and 20 during chondrogenic culture (Scale bar = 500 µm), and quantification of diameter (ii) as a non-destructive metric for microtissue development. **** denotes significance when tested using a Šídák's multiple comparisons test, two-way ANOVA, where p < 0.0001, (N = 20, Mean ± SD). B) Histological evaluation of cartilage microtissues after 21 days of chondrogenic culture (Scale bar = 200 µm). C) Biochemical quantification of the cartilage microtissues after 21 days. * denotes significance using a two-tailed, unpaired Welch's t-test, p < 0.05 (N = 3, Mean ± SD).*

5.3.2 Hydrocortisone is the Predominant Factor Driving Enhanced Chondrogenesis in Human BMSCs

EGM contains multiple factors that potentially enhance chondrogenesis in the microtissue model. This motivated an investigation to identify the predominant driving factors within the EGM. Additionally, to improve its clinical relevance, this empirical study was undertaken using hBMSCs. To this end, hBMSCs within the microwell system were cultured in media supplemented with each factor used within the EGM formulation. These factors were added to both the XPAN used during

pre-soaking and seeding, as well as to CDM during chondrogenic induction. A typical chondrogenic culture regime 'control' was also carried out, as well as an EGM pre-soak 'EGM' which, was identical to the protocol shown to be effective in animal derived BMSCs. After 7 days of *in vitro* chondrogenesis, differences in microtissue size was apparent microscopically (Figure 5.2B). Cellular arrangement also appeared to vary within the microtissues depending on which additional EGM supplement was provided (Figure 5.2A). Histologically, archetypal cartilage spheroids were seen in the control, EGM, and hydrocortisone (Hydro) groups. Although other supplements did not entirely suppress chondrogenesis, with disposition of sGAG and collagen detected in all groups at varying levels, they did result in condensed, highly cellular and atypical cartilage spheroids. When compared to a standard chondrogenic culture regime (control), supplementation with hydrocortisone resulted in significantly higher levels of DNA per microtissue as well as a higher deposition of sGAG per cell. Although EGM soaking did not significantly influence the DNA levels within the microtissues in hBMSCs, its effect on biosynthetic output did mirror observations made previously with gBMSCs, and whereby pre-soaking with EGM resulted in a significantly richer cartilaginous ECM profile compared to a standard chondrogenic approach (control). Direct comparison of continuous supplementation with hydrocortisone and EGM pre-soaking of hydrogel microwells indicated that there was a significant benefit to hydrocortisone treatment in terms of sGAG deposition.

By means of consolidating the previous result, a second human donor was investigated. Here, the study was simplified by only testing the effect of an EGM pre-soaking treatment (EGM) or continuous hydrocortisone treatment (Hydro) versus the traditional chondrogenic regime (control). Diameter measurements taken during the 7 days *in vitro* revealed similar responses in terms of microtissue growth in both experimental groups (Figure 5.3A). Although microtissues within these groups remained significantly larger than those under conventional chondrogenic conditions, unlike in the previous study, the diameter of microtissues in the control group also increased over the 7 days. Histologically, all groups appeared to result in robust chondrogenic differentiation and the deposition of cartilage specific ECM components (Figure 5.3B). Biochemical quantification of the cartilage microtissues indicated that significantly higher levels of sGAG/DNA and sGAG/microtissue could be achieved using the EGM pre-soak and hydrocortisone treatments respectively. Despite this, there was no significant benefit in terms of collagen deposition for either experimental group. Interestingly, the baseline chondrogenic capacity of the donor investigated within this study appeared far superior to that of the previous hBMSCs. Under standard conditions (control), the sGAG/DNA was 5.50 ± 0.175, compared to 2.81 ± 0.236, with the previous donor. The difference in collagen deposition per cell was more pronounced, with 25.9 ± 1.13 collagen/DNA for the control group within this study versus 5.83 ± 0.887 collagen/DNA demonstrated previously. This

suggested that the beneficial effects demonstrated in terms of chondrogenesis are more pronounced when the baseline level is relatively low.

Finally, this study considered that prolonged hydrocortisone treatment may not be beneficial for chondrogenic culture. Given the potency of pre-soaking with EGM, and the evidence that hydrocortisone was the driving factor behind this enhanced chondrogenesis, how the length of hydrocortisone treatment influenced chondrogenesis over 10 days was investigated. Biochemically, peak sGAG biosynthesis coincided with a significant downregulation in collagen production at day 7 (Figure 5.4A & B). Although sGAG/DNA appeared to vary over the time course, there was a clear downward trend in collagen/DNA with extended hydrocortisone treatment. Histologically, all groups exhibited normal cell morphology and distribution. Additionally, all groups stained extensively and homogenous for sGAG. Differences in PSR staining was apparent, where 7 and 10 days of hydrocortisone supplementation resulted in apparently lower levels of collagen within the microtissues, corroborating the biochemical data. Although preliminary, this data, coupled with earlier findings, indicates that shorter periods (< 7 days) of hydrocortisone treatment produce better chondrogenic outcomes than prolonged/continuous exposure. However, future studies should look to elucidate this result using other donors. In particular, donors with inherently limited chondrogenic capacity, where we have previously shown hydrocortisone/EGM treatment to be most effective, should be studied to ensure that an extended/continuous treatment regime is not beneficial.

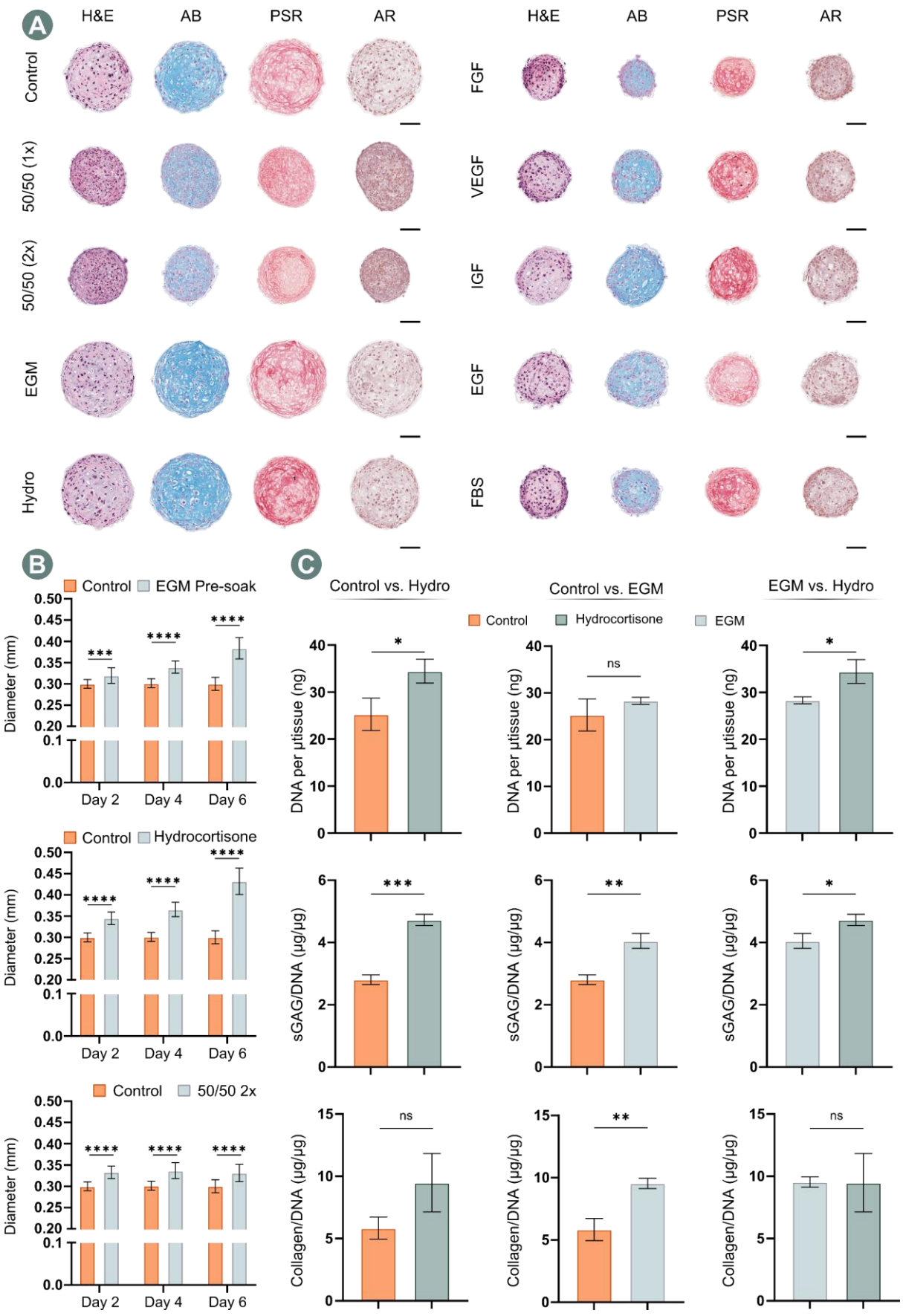

Figure 5.2 *Hydrocortisone is the driving factor in EGM that improved chondrogenesis. A) Histological panel of microtissues, representing each EGM supplement, after 7 days of chondrogenic*

*culture (Scale Bar = 100 µm). B) Diameter measurements during culture, * denotes significance when tested using a Šídák's multiple comparisons test, two-way ANOVA, where p < 0.05, (N = 20, Mean ± SD). C) Biochemical quantification of the cartilage microtissues after 7 days of chondrogenic culture. Hydrocortisone treatment compared to typical chondrogenic conditions (control) and positive control group (EGM) demonstrated a significant increase in DNA content and sGAG deposition. * denotes significance using a two-tailed, unpaired Welch's t-test, p < 0.05 (N = 3, Mean ± SD).*

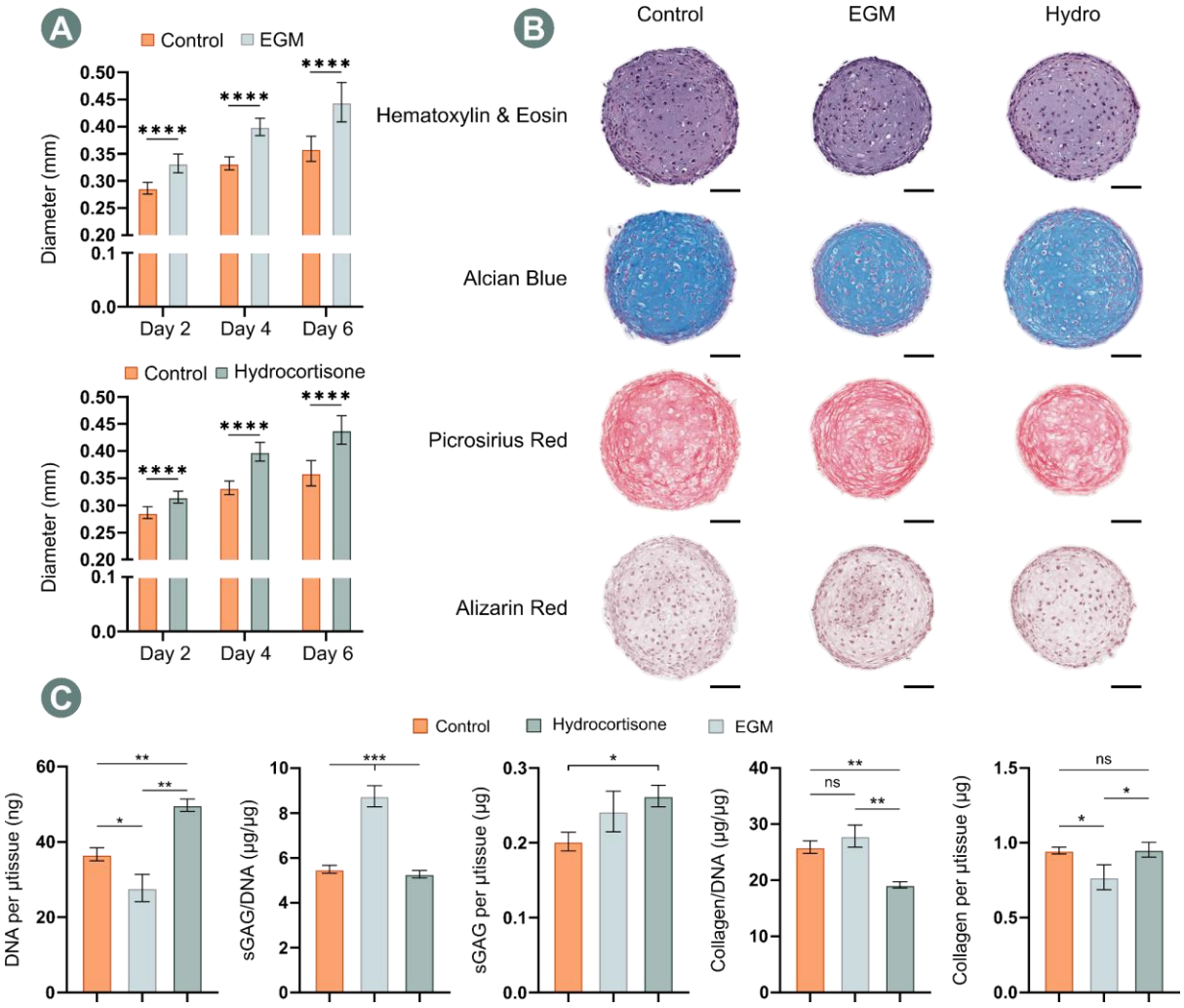

Figure 5.3 *The effect of both EGM pre-soaking and hydrocortisone supplementation is lessened in a more chondrogenic hBMSC population. A) Quantification of microtissue diameter. **** denotes significance when tested using a Šídák's multiple comparisons test, two-way ANOVA, where p < 0.0001, (N = 25, Mean ± SD). B) Histological evaluation of cartilage microtissues after 7 days of chondrogenic culture (Scale bar = 100 µm). C) Biochemical quantification of the cartilage microtissues after 7 days. * denotes significance using a Brown-Forsythe and Welch One-way ANOVA, p < 0.05 (N = 3 for control & Hydro, N = 4 for EGM, Mean ± SD).*

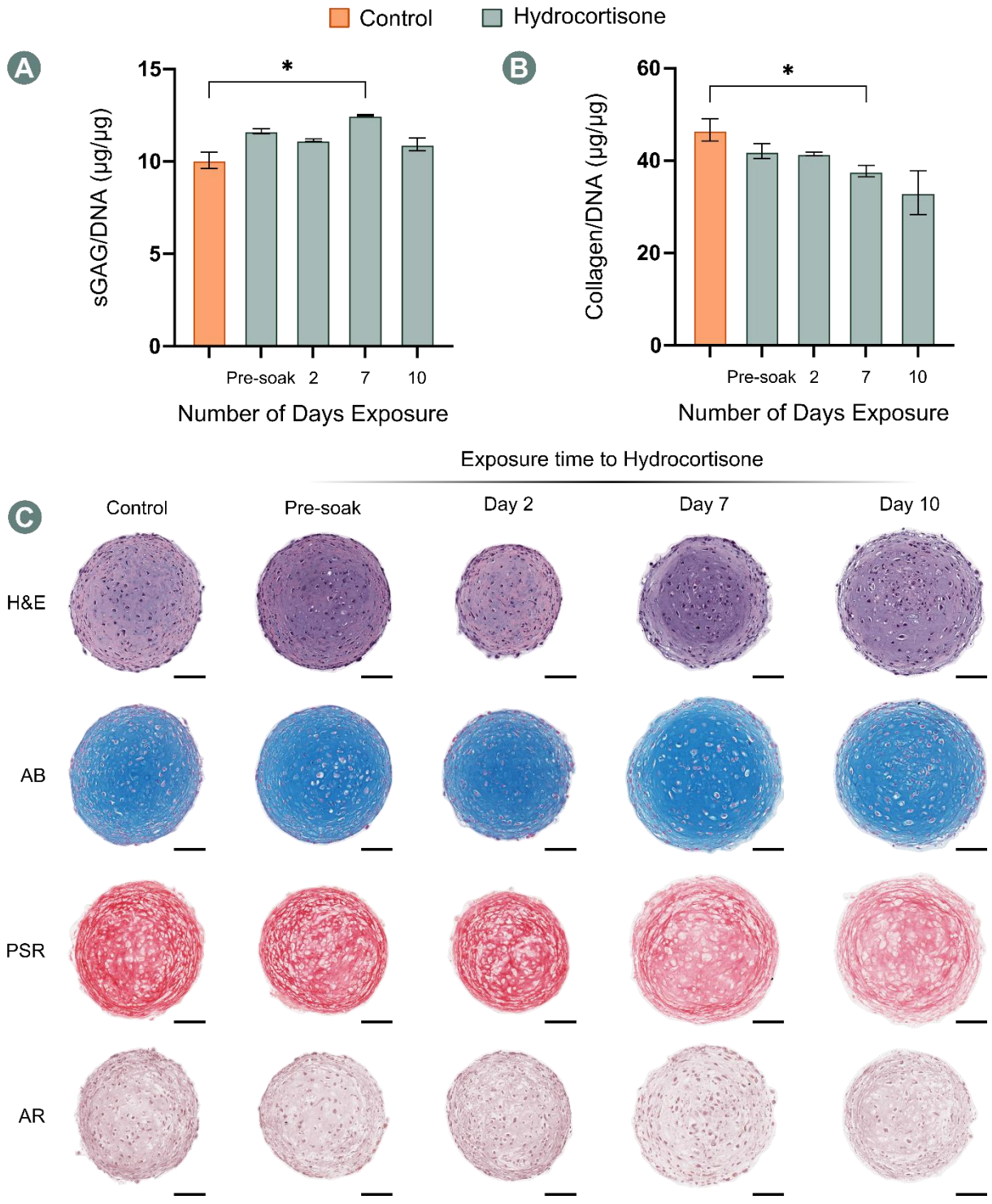

Figure 5.4 *Prolonged hydrocortisone exposure is not beneficial in MSC populations that undergo robust chondrogenic differentiation. Biochemical quantification after 10 days of chondrogenic culture of A) sGAG normalised to DNA, (N = 3, Mean ± SD) and B) collagen normalised to DNA, (N = 3, Mean ± SD). * denotes significance using a Brown-Forsythe and Welch One-way ANOVA, $p < 0.05$. C) Histological evaluation of cartilage microtissues after 10 days of chondrogenic culture (Scale bar = 100 µm)*

5.4 Discussion

This chapter aimed to establish a novel protocol for ensuring the generation of high-quality cartilage microtissues. Soaking the hydrogel microwells in fully supplemented EGM a day prior to seeding gBMSCs was found to enhance cellular aggregation and cause a significant improvement in chondrogenesis. At day 2, all cells within the microwells of the EGM group had coalesced, forming large spherical aggregates. In contrast, a standard chondrogenic protocol yielded relatively small cell aggregates with a large number of unengaged cells surrounding the spheroids. By day 21 of culture, histological and biochemical evaluation indicated that a richer cartilage ECM could be generated by soaking the microwells with EGM prior to seeding. The canonical cartilage matrix markers, sGAG and collagen were more extensively deposited in the EGM group compared to the control condition. Moreover, the increased abundance of ECM proteins was not only due to more cellular microtissues, as evident by higher DNA content after 21 days of culture, but also as a result of the increased biosynthetic output of the resident cell population within the EGM microtissues. Collectively, this preliminary study indicated that factor(s) within EGM provide a potent cue(s) capable of improving the chondrogenic capacity of an uncharacterised gBMSCs population.

Next, this study sought to determine if a single component was responsible for the aforementioned results using more clinically relevant hBMSCs. Within the supplement profile of EGM, basic FGF/FGF-2 (FGF) and insulin-like growth factor (IGF) were potential candidates for driving improved chondrogenesis. FGF is known to maintain MSCs in an immature state, enhance their proliferation during *in vitro* expansion and their subsequent differentiation potential [239]. Additionally, the treatment of hMSCs with FGF during expansion has given rise to enhanced chondrogenesis [240,241]. Specifically, chondrogenic aggregates formed using cells treated with FGF during monolayer expansion were larger and expressed higher proteoglycan content. Additionally, FGF-treated cells have been formed into cartilage spheroids that lacked collagen type I and expressed collagen type II in their periphery [241]. FGF signalling, although not critical for chondrogenesis, has been coupled with improved chondrogenic differentiation of hMSCs [242]. However, prolonged treatment with FGF during MSC condensation and early chondrogenic differentiation has been shown to inhibit chondrogenesis, whereas the addition of other isoforms, such as FGF-9, to chondrogenic media has been shown to marginally increase matrix production during early chondrogenesis [243]. In this study, all MSCs were exposed to FGF during expansion, and we also found that prolonged exposure to FGF (during the first 7 days of chondrogenic differentiation) does not lead to enhanced chondrogenesis and ECM production (Supporting Figure5.1).

IGF, when combined with TGF-β, is commonly discussed as a promoter of chondrogenesis in MSCs [239,244]. IGF alone has been suggested to have similar chondrogenic effects as TGF-β,

stimulating proliferation, regulating apoptosis, and inducing the expression of chondrogenic markers in BMSCs. Moreover, the two growth-factors have demonstrated additive effects, resulting in gene expression analogous to human primary culture chondrocytes [245]. We failed to see a similar results in this study, as there was no discernible benefit associated with supplementing CDM with IGF (Supporting Figure5.1). However, it should be noted that insulin was not removed from CDM in this study. As such, the insulin within ITS could have masked any effects of treating with IGF and potentially explain the failure to recreate findings which have been previously reported using IGF for enhanced chondrogenesis.

In the first human donor, EGM produced a similar result to goat MSCs. More importantly, the growth factor hydrocortisone emerged as the principle driving factor within the EGM supplement capable of promoting more robust chondrogenesis. Intra-articular injection of glucocorticoids, such as hydrocortisone, has been a longstanding means of managing arthritis. Primarily, glucocorticoid therapy aims to provide symptomatic relief, reducing inflammation and pain within an affected joint. However, the use of such steroidal agents has been discouraged for the treatment of OA due to their undesirable effects of cartilage metabolism [246]. Despite this, chondroprotective properties and other putative benefits of glucocorticoid treatment have been suggested. More recently, the chondroprotective capacity of hydrocortisone, has been found to be heavily dose-dependent, with beneficial changes associated with low doses both *in vitro* and *in vivo*, whereas higher doses result in deleterious effects [247]. *In vitro*, the exposure of MSCs to synthetic glucocorticoids for the initiation of chondrogenesis has been well established through the use of dexamethasone (DEX) [213,248]. The role of DEX in promoting chondrogenesis has been elucidated through studies demonstrating that glucocorticoids directly regulate the expression of cartilage ECM genes and/or enhance TGF-β-mediated upregulation of their expression. Specifically, a positive interaction between TGF-β and glucocorticoid signalling pathways, which are mediated by the glucocorticoid receptor, have been demonstrated during chondrogenesis [249]. The impact of hydrocortisone, an adrenocortical hormone, is much less documented. It has been reported to be found in FBS, where it is important in the modulation of MSC functions such as growth and adhesion [250]. As such, it is often included in serum-free medium formulations. Additionally, hydrocortisone has been used to 'activate' multipotent MSCs for adipogenic differentiation and its addition during passaging preserves the self-maintenance capacity of MSCs [251]. In the context of chondrogenesis, hydrocortisone supplementation in 3D culture with human chondrocytes has been shown to optimise the ECM metabolism. In particular, exposure to physiological levels of hydrocortisone was linked with an enhanced capacity to synthesise ECM components (aggrecan, collagen type II, and fibronectin) whilst decreasing the activity of catabolic pathways (suppression of the IL1 catabolic

pathway - reduced intracellular IL1-α and –β and IL1RI) [252]. These results indicate that corticosteroids play a role in the maintenance of normal human cartilage metabolism.

MSCs from a second donor were observed to respond differently to hydrocortisone as they underwent chondrogenesis. Similar potent improvements to chondrogenesis seen in the first two studies by supplementing the media with hydrocortisone were not apparent. Whilst biochemically, hydrocortisone treatment enhanced sGAG deposition per microtissue, no improvement in collagen accumulation was observed. Biochemically and histologically, all conditions using the second donor resulted in robust chondrogenesis after 7 days. Explicitly, the baseline levels (control group) of sGAG/DNA and collagen/DNA detected within the microtissues were 1.96- and 4.44-times higher respectively, in the second human donor compared to the first. This suggested that the potent improvement in chondrogenesis previously observed may be coupled to the basal chondrogenic capacity of the donor. Specifically, donors with limited initial chondrogenic capacity benefit more from EGM/hydrocortisone treatment when compared with donors that would more readily undergo chondrogenic differentiation.

One potential explanation for the donor-to-donor variability in the response to EGM/hydrocortisone treatment could be the heterogeneity of MSC populations. Several surface markers have been suggested as a means of sorting cells with greater chondrogenic potential over other subpopulations. To this end, $CD271^+$ cells have been shown to be more chondrogenic, expressing higher levels of collage type II and aggrecan compared to other subpopulations [253]. Other have corroborated these findings, showing $CD271^+$ BMSCs result in superior cartilage spheroids, and a reduction in CD271 expression during culture correlated with a decrease in chondrogenesis. Importantly, *in vivo*, $CD271^+$ cells were shown to outperform an unsorted MSC population, resulting in improved cartilage repair [254]. MSCs expressing CD105 and CD29 have also been identified as subpopulations with improved chondrogenic differentiation potential [255,256]. Growth factors, such as FGF, have been shown to change the expression of certain surface markers [257,258]. Hydrocortisone may, like FGF, help to active/regulate stem cell populations and could alter the distribution of specific markers which have been coupled to chondrogenic potential. In addition, the varied responses to EGM/hydrocortisone treatment reported here, could be a result of innate differences in relative expression of surface markers within the three cell cohorts tested. However, variances in differentiation potential is not always reflected in changes in stem cell surface marker expression [257], and as such, further investigation would be necessary to clarify the effect of EGM/hydrocortisone on the surface marker profile of heterogeneous MSC populations and the correlation, if any, to the changes observed in chondrogenic potential.

Whilst the mechanism of action remains unclear, evidence within this chapter suggests that EGM/hydrocortisone treatment can improve the chondrogenic potential of heterogeneous MSC populations. Investigation into the full effects of this novel chondrogenic protocol in terms of its regulation/re-activation of MSC subpopulations, and/or its effect on chondrogenic genes that are co-regulated *via* glucocorticoid receptors would provide an interesting insight and could help design enhanced chondrogenic cultures in the future. Given the evidence that selection of superior chondrogenic donors *in vitro* can translate into improved *in vivo* outcomes [254,259], the data presented in this chapter represents a simple alternative method for restoring the chondrogenic capacity of MSC populations that exhibit inherently limited chondrogenesis. As such, effectively implementing this novel protocol can result in the formation of high-quality cartilage microtissues. To this end, preliminary data suggests that prolonged exposure to hydrocortisone may not be beneficial for long term chondrogenic culture. This evidence, coupled with our findings relating to the potency of EGM pre-soaking indicates that a similar pre-soaking, or short-term exposure (<7 days) may be the most effective means of implementing hydrocortisone treatment within a chondrogenic culture regime. Ultimately, this work provides a platform to generate larger engineered cartilage through self-organisation of these high-quality building blocks without the need for additional cells, unfeasible numbers of microtissue units, or compromising the quality of the final construct and its *in vivo* efficacy. The results presented in this chapter were collected after those presented in the subsequent chapters 6 and 7. As such, hydrocortisone/EGM stimulation of developing cartilage microtissues was not employed in the following studies. Alternatively, in chapters 6 and 7, where microtissues are employed to engineer cartilage and osteochondral tissues of scale, novel chondrogenic induction protocols are explored to maximise microtissue growth and macrotissue quality.

5.5 Conclusion

Collectively, the results indicate that pre-treatment *via* EGM pre-soaking or the supplementation of chondrogenic differentiation medium with hydrocortisone can provide a simple and potent means of improving chondrogenesis in heterogeneous MSC cohorts. This work could enable the generation of more scalable engineered cartilages by ensuring the formation of high-quality cartilage microtissue building blocks without the need for extensive cell immunophenotyping.

Chapter 6.

6 Biofabrication of Cartilage Grafts using Engineered Microtissues as Biological Building Blocks

6.1 Introduction

Articular cartilage (AC) has a limited capacity for natural healing [2,111,231]. This has motivated the development of a range of cell- and/or scaffold-based tissue engineering strategies for AC regeneration, including matrix-assisted autologous chondrocyte transplantation (MACI) [111–113]. In general such cartilage repair strategies fail to consistently produce a hyaline repair tissue, fill the entire defect and properly integrate with the surrounding native tissue [111]. While the reasons for such sup-optimal clinical outcomes are not yet fully understood, the failure to engineer tissues that recapitulate the structure, composition and biomechanical properties of native AC is believed to be a predominant contributing factor [5,111,231,260–262]. Scaffold-free tissue engineering is a strategy that moves away from the traditional 'tissue engineering triad' in order to leverage processes that occur during embryonic and post-natal development to improve the quality and biomechanical functionality of an engineered tissue [42,115]. It is believed that scaffold-free approaches can circumvent the limitations of traditional scaffold-based tissue engineering, enabling cells to generate a more biomimetic tissue unencumbered by the constraints of a scaffold material or hydrogel [81,115]. In the context of AC tissue engineering, scaffold-free approaches aim to recapitulate the cellular condensation that occurs during limb bud development, and have been shown to support chondrogenesis of mesenchymal stem/stromal cell (MSC) *in vitro* and the generation of a tissue that is biochemically and biomechanically comparable to that of early developing cartilage [43,44,64,86]. The success of such scaffold-free cartilage tissue engineering strategies can be linked to the increased expression of physiologically relevant cell adhesion proteins (neural cadherin (N-cadherin) and neural cell adhesion molecule (N-CAM)), as well as recapitulation of specific and appropriate cell-ECM interactions and growth factor mediated signalling events associated with limb bud development [64]. Emerging platforms that facilitate such MSC condensation, such as self-assembled cartilage discs or micromasses, have been shown to be more supportive of chondrogenesis compared to traditional models [47,48,116]. Furthermore, self-assembled cartilage discs have been shown to support the development of spatially organised AC when exposed to physiologically inspired cues [45,46,49–51,117].

In spite of promising findings, there are several hurdles facing the translation of self-assembled tissues into preclinical and human clinical applications [111,118]. Fixation of these self-

assembled neo-cartilages *in situ* within damaged synovial joints can be problematic, with insufficient fixation and/or integration with the surrounding host osteochondral tissues known to contribute to graft failure *in vivo* [111,119,231]. Additionally, generating tissues with comparable thickness to human AC has proven to be a challenge, as is scaling the manufacture of highly cellular self-assembled constructs. The challenges of engineering tissues of predefined size and shape can potentially be addressed by using cartilage spheroids or microtissues as building blocks for the biofabrication of larger cartilage grafts [63,68,74,120,148]. For example, immature cartilage spheroids (< 5 days in TGF-β_3) have been fused onto an underlying bone scaffold using external, manual pressure to generate osteochondral constructs of predefined shape [68]. The resultant macro-cartilage exhibited a physiology stratification of matrix components (glycosaminoglycan (GAG), collagen type- II and X, lubricin). Impressively, the cartilage has biomechanical properties approaching those of native AC after only 5 weeks of *in vitro* cultivation [68]. Despite its relative success there are some limitations to this approach. For example, the manual nature of the approach, requiring external pressure to fuse spheroids and create a homogenous tissue, could limit this methods capacity to generate patient-specific geometries in the future. Additionally, whether the reported tissue stratification extended to the formation of a zonal biomimetic collagen network remains unclear. To this end, others have identified that the potent upregulation of numerous chondrogenic markers associated with self-assembled cartilage does not ensure the concomitant formation of a native-like zonal collagen architecture [42,45,47]. Given the interdependence of ACs biomechanical properties and the anisotropy of its collagen network (specifically the Benninghoff arcade structure), identifying a means of reliably recapitulating this macromolecular stratification is essential for the engineering of biomimetic grafts capable of effectively resurfacing articular joints.

Biofabrication using numerous cartilage spheroids or microtissues as 'biological building blocks' appears to be an effective means of scaling scaffold-free tissue engineering strategies. Despite the many benefits of such approaches, generating a tissue with a hierarchical collagen structure within the engineered tissue is not guaranteed. Moreover, identifying a biofabrication method that facilitates spontaneous fusion between adjacent cartilage building blocks, and the fixation of an engineered cartilage within a defect site is essential if scaffold-free cartilages are to have a significant clinical impact in the future. With this in mind, this study aims to identify an effective method for generating stable cartilage microtissues with the capacity to spontaneously fuse and, under appropriate guidance from a supporting polymer framework, self-organise into a stratified engineered cartilage (Figure 6.1A). This study will then combine these microtissues with a novel 3D printed cartilage fixation device (Figure 6.1C), and evaluate their efficacy as a treatment for focal chondral lesions within a preclinical, large animal model of focal chondral defects. In this

chapter, fat-pad stromal cells (FPSCs) were employed *in lieu* of bone marrow derived MSCs. This decision was motivated by challenges associated with isolating sufficient numbers of MSCs from the femoral shaft of skeletally mature goats. Instead, adipose tissues can offer up to a 5 times higher yield of MSCs compared to bone marrow [263] and adequate number of stromal cells have been isolated from infrapatellar fat-pad tissue [165]. Moreover, fat pad derived progenitors have been discussed as having a role in injury response and may contribute to healing within articular joints [264]. Equally, robust *in vitro* chondrogenic differentiation of FPSCs has been previously shown [165,192,210], making them an ideal alternative progenitor cell source to bone marrow.

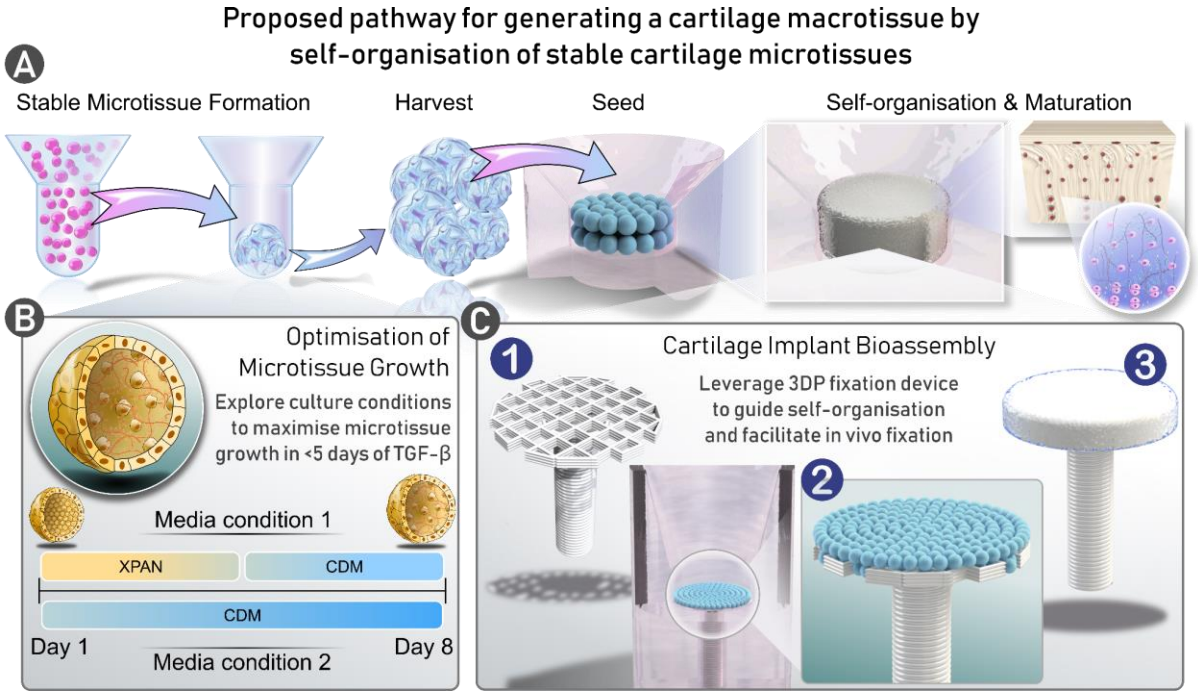

Figure 6.1 *Study schematic for the biofabrication of a stable cartilage for the treatment of focal chondral defects. A) The proposed pathway for forming a homogenous and biomimetic millimetre-scale cartilage via self-organisation of early stable-cartilage microtissues. B) In order to design a scalable process the growth of the cartilage microtissues needed to be optimised. To do so, two media conditions were explored which, varied the length of chondrogenic induction of cell aggregates during microtissue cultivation. C) A novel bioassembly strategy was developed to facilitate guided self-organisation of cartilage microtissues into a spatially organised cartilage macrotissue on a novel 3D printed fixation device.*

6.2 Materials and Methods

Expansion Medium "XPAN". XPAN is composed of high glucose Dulbecco's modified eagle's medium (hgDMEM) GlutaMAX supplemented with 10 % v/v FBS, 100 U/mL penicillin, 100 µg/mL streptomycin (all Gibco, Biosciences, Dublin, Ireland) and 5 ng/mL FGF2 (Prospect Bio).

Chondrogenic Differentiation Medium (CDM). hgDMEM GlutaMAX supplemented with 100 U/mL penicillin, 100 µg/mL streptomycin (both Gibco), 100 µg/mL sodium pyruvate, 40 µg/mL L-proline, 50 µg/mL L-ascorbic acid-2-phosphate, 4.7 µg/mL linoleic acid, 1.5 mg/mL bovine serum albumin, 1 X insulin–transferrin–selenium (ITS), 100 nM dexamethasone (all from Sigma), 2.5 µg/mL amphotericin B and 10 ng/mL of human transforming growth factor-b3 (TGF-β) (Peprotech, UK).

6.2.1 Cell Isolation and Expansion

Goat Fat-pad stromal cell (FPSC) Isolation: Under sterile conditions, infrapatellar fat pad (IFP) tissue was diced into approximately 1-2 mm^3 pieces using a scalpel. The tissue was then weighed and subsequently incubated with high glucose DMEM (Gibco) containing 750U collagenase I (Gibco). For rapid isolation; the tissue was shaken at 2000 RPM at 37°C for 30 minutes (Multi Reax Shaker, Heidolph). After digestion, the cell suspension was neutralised with DMEM containing 20 % fetal bovine serum (FBS - Gibco). Insoluble tissue and residual fat were removed and discarded. The remaining cell suspension was passed through a series of cell strainers with decreasing mesh sizes (100 µm, 70 µm and 40 µm (Fisher Scientific)), centrifuged and washed with saline.

Goat Chondrocyte (CC) Isolation: Cartilage was harvested from the joint surface under sterile conditions, it was rinsed in saline, weighed, and diced finely. Chondrocytes were isolated by digestion in hgDMEM containing 100 U/mL penicillin, 100 µg/mL streptomycin and 350 U/mL of collagenase type II for 12-14 hours with constant rotation at 37 °C. The remaining suspension was passed through a cell filter (40 µm), and the filtrate centrifuged and rinsed with saline. Chondrocytes were expanded in XPAN in physioxic conditions.

6.2.2 Microtissue Formation & Culture Optimisation

The procedure for fabricating the hydrogel microwell platform and the method of generating cellular aggregates and microtissues has been described within chapter 3. The same underpinning methodology was employed herein. Initially, stable cartilage microtissues were form at three cell densities: 1 x 10^3, 2 x 10^3, or 4 x 10^3 cells per microtissue. To dampen the inherent hypertrophic tendencies of MSCs, a co-culture of FPSC and CCs (3:1) was employed throughout.

To ensure that the maximum growth of the cartilage microtissues prior to their bioassembly into a larger macrotissue, two initial growth conditions were explored. The first (Media Condition 1), involved culturing the cell aggregated initially in XPAN for the first 4 days, followed by 4 days in

CDM. The second (Media Condition 2), was 8 days of continuous chondrogenic induction in CDM. In both strategies, microtissues were cultivated in physioxic conditions (37 °C in a humidified atmosphere with 5 % CO_2 and 5 % pO_2). Diameter fold change of the growing microtissues was calculated over the first 4 days of chondrogenic induction. For media condition 1, this described the diameter change from day 2 to day 6 and from day 4 to day 8 in media condition 2.

Table 6.1 *Summary of the media conditions employed for the rapid and robust initial chondrogenic induction of cartilage microtissues*

Media Condition	Days in Expansion Medium (XPAN)	Days in Chondrogenic Differentiation Medium (CDM)
1. Temporal TGF-β	4	4
2. Continuous TGF-β	0	8

6.2.3 Microtissue Self-organisation and Macrotissue Engineering

The capacity for cartilage microtissues to spontaneously self-organise into a macrotissue was determined by seeding microtissues into a custom agarose well. The well was created using sterile 2 % w/v agarose cast into a 12 well plate. The central agarose well was 3 mm in diameter and 1.5 mm in depth. The number of microtissues seeded to create each construct was determined as a function of the microtissue volume and the volume of the final construct. As such, the following equation was used:

$$Number\ of\ microtissues = \frac{Volume\ of\ the\ construct\ \times 0.74}{Volume\ of\ the\ microtissue}$$

Where,

$$Volume\ of\ the\ microtissue = \frac{4}{3}\pi r^3$$

and 0.74 is the packing efficiency, or packing factor. For this study the volume of the construct chosen was determined using 3 mm diameter and a depth of 1 mm.

After seeding the microtissues into the central agarose well, CDM was added slowly to prevent disruption of the microtissues. The developing cartilages were maintained in CDM and physioxic conditioned for 5 weeks. Media was exchanged every 2-3 days.

6.2.4 Biochemical Evaluation

Samples were washed in PBS after retrieval and the number of microtissues within each technical replicate counted prior to digestion. A papain enzyme solution, 3.88 U/mL of papain enzyme in

100mM sodium phosphate buffer/5mM Na2EDTA/10mM Lcysteine, pH 6.5 (all from Sigma–Aldrich), was used to digest the samples at 60 °C for 18 hours. DNA content was quantified immediately after digestion using Quant-iT™ PicoGreen ® dsDNA Reagent and Kit (Molecular Probes, Biosciences). The amount of sGAG was determined using the dimethylmethylene blue dye-binding assay (Blyscan, Biocolor Ltd., Northern Ireland), with a chondroitin sulphate standard read using the Synergy HT multi-detection micro-plate reader (BioTek Instruments, Inc) with a wavelength set to 656 nm. Total collagen content was determined using a chloramine-T assay [186] to measure the hydroxyproline content and calculated collagen content using a hydroxyproline-to-collagen ratio of 1:7.69. Briefly, samples were mixed with 38 % HCL (Sigma) and incubated at 110 °C for 18 hours to allow hydrolysis to occur. Samples were subsequently dried in a fume hood and the sediment reconstituted in ultra-pure H_2O. 2.82 % (w/v) Chloramine T and 0.05 % (w/v) 4-(Dimethylamino) benzaldehyde (both Sigma) were added and the hydroxyproline content quantified with a trans-4-Hydroxy-L-proline (Fluka analytical) standard using a Synergy HT multi-detection micro-plate reader at a wavelength of 570 nm (BioTek Instruments, Inc).

6.2.5 Mechanical Evaluation

Mechanical evaluation was performed using a single column Zwick (Zwick, Roell, Germany). Testing was undertaken in hydrated conditions using saline. A 0.025N pre-load was applied, followed by 10 % strain at a speed of 1 mm/minute. The compressive modulus was taken between 9 % and 10 % strain.

6.2.6 Preclinical Evaluation

Fibronectin coating

To improve the integration of the microtissues with the polymer (polycaprolactone, PCL) implant, the surface of the implant was coated with bovine fibronectin (PromCell) using a protocol modified from Liverani *et al.* [265]. Briefly, the PCL implants were immersed in a 3M sodium hydroxide solution (NaOH) and gently agitated for 12-14 hours at room temperature to improve the hydrophilicity of the polymer. Similar methods of hydrolysing PCL using NaOH have been demonstrated in electrospun scaffolds, where the exposure of hydroxyl and carboxylic groups on the polymer surface can improve hydropillicity and subsequently protein absorption and biocompatibility [266]. After washing in ultra-pure H_2O, implants were immersed in 0.5M N- (3-Dimethylaminopropyl)-N'-ethylcarbodiimide hydrochloride (EDC) (Sigma) and 0.5M N-Hydroxysuccinimide (NHS) in 0.1M 2-(N-Morpholino)ethanesulfonic acid hemisodium salt (MES) buffer at a ratio of 2:1 (EDC:NHS) for 24 hours again with gentle agitation. Implants were rinsed in PBS and immersed in a 50 µg/mL fibronectin solution for 24 hours. After functionalisation with

fibronectin, implants were rinsed and either processed for analysis by Fourier-transform infrared spectroscopy (FTIR) or SEM, or used immediately for tissue culture.

Implant seeding

GBMSCs were isolated as previously described in chapter 5. Briefly, marrow pieces were then gently rotated for 5 min in XPAN to help liberate the cellular components. Cells were initially plated at a density of 57 x 10^3 cells/cm^2 and expanded under hypoxic conditions (37 °C in a humidified atmosphere with 5 % CO_2 and 5 % pO_2) for chondrogenic differentiation. Following colony formation, gBMSCs were trypsinised using 0.25 % (w/v) Trypsin Ethylenediaminetetraacetic acid (EDTA). gBMSCs for microtissues were expanded from an initial density of 5000 cells/cm^2 in XPAN medium under physioxic conditions until P3. As before, stable cartilage microtissues were generated using a co-culture of MSCs and CCs (3:1) at a final density of 2 x 10^3 cells/microtissue, and cultivated using media condition 1. After 8 days, stable cartilage microtissues were seeded manually into the head of fixation device defined in chapter 4. As before, the number of microtissues seeded into the head of the implant was determined by the volume of the microtissues after 8 days of preliminary culture, and the volume of the desired final construct (6 mm ø x 1 mm height). Cartilage was then cultivated for 5 weeks in physioxic conditions prior to implantation.

Surgical Procedure

All animal experiments were approved by the University College Dublin Animal Research Ethics Committee (Approval number – AREC 12-74) and the Irish Health Products Regulatory Authority (Approval number - AE18982/P032). Surgery was performed on skeletally mature female Saanen goats. Goats were sedated using diazepam (0.3–0 0.4 mg/kg IV) and butorphanol (0.2 mg/kg IV). An epidural was administered using morphine (0.2 mg/kg). Anaesthesia was induced with propofol (max. dose 4 mg/kg IV) and maintained with isoflurane. Goats were placed in dorsal recumbency and an arthrotomy of each stifle joint was then performed using the lateral para-patellar approach. Bi-lateral surgery was performed on all animals. 6mm diameter by 1mm deep chondral defects were created in the medial femoral condyles using a 6mm biopsy punch to mark the defect diameter followed by cartilage removal using a curette. Microdrilling was performed in all defects using a Kirschner wire (1.6mm Ø for a central hole). In the treatment group, this central microdrilling hole was populated with the fixation pin, facilitating the implantation of the self-organised cartilage. An in-depth description of the implant design and fabrication can be found in chapter 4. Briefly, the fixation pin was a biodegradable, 3D printed fixation device fabricated using polycaprolactone (PCL, Perstop). The shaft of the fixation device was fabricated to be the same diameter as the central MFX hole (1.6mm Ø) so that the device and scaffold could be push-fit into the defect. Following routine closure of the joint capsule, subcutaneous tissues and skin with

sutures, Carprofen (1.5–2.5 mg/kg subcutaneously) was administered for analgesia. Following surgery, goats were housed in indoor pens and were allowed full weight bearing immediately. NSAIDs and antibiotics Amoxicillin (Noroclav) were administered for 5 days post-surgery. Two weeks post-operatively, following removal of sutures, animals were released to pasture for the remainder of the study period. Tissue repair was evaluated at 6 months post-surgery.

Evaluation of the Repair Tissue

Sections containing the defect site were harvested. Before fixation, gross morphological images were taken using a stereomicroscope (Olympus) for macroscopic evaluation. Macroscopic images were blinded, randomised, and subsequently scored by expert reviewers using a previously described macroscopic scoring system [267,268]. This macroscopic scoring system evaluates the edge integration of the scaffold with the native tissue, the smoothness of the cartilage surface, the degree of defect filling and the colour/opacity of the neo-cartilage in the defect.

6.2.7 Histological Evaluation

In vitro

Samples were fixed using 4 % paraformaldehyde (PFA) solution overnight at 4 °C. After fixation, samples were dehydrated in a graded series of ethanol solutions (70 % - 100 %), cleared in xylene, and embedded in paraffin wax (all Sigma-Alrich). Prior to staining tissue sections (5 µm) were rehydrated. Sections were stained with hematoxylin and eosin (H&E), 1 % (w/v) alcian blue 8GX in 0.1 M hydrochloric acid (HCL) (AB) to visualise sulphated glycosaminoglycan (sGAG) content and counter-stained with 0.1 % (w/v) nuclear fast red to determine cellular distribution, and 0.1 % (w/v) picrosirius red (PSR) to visualise collagen deposition (all from Sigma-Aldrich). Stained sections were imaged using an Aperio ScanScope slide scanner. Polarised-light microscopy (PLM) was used to visualised the orientation of collagen fibres in samples stained with PSR.

In vivo

Prior to histological processing, samples were fixed in 10% neutral buffered formalin solution (Sigma) for 72 hours with gentle agitation. Samples were then decalcified with Decalcifying solution lite (Sigma) until all mineral was removed, which was confirmed by x-ray analysis. Demineralized wax-embedded constructs were sectioned at 10µm and stained with Goldner's Trichrome, picrosirius red stain and safranin-O. Histological scoring was performed using a modified ICRS II scoring system [269].

Immunohistochemisty

Immunohistochemistry was performed for collagen type I (Abcam ab90395 1:400), collagen type II (Santa Cruz sc52658 1:400), and collagen type X (Abcam ab49945 1:200) as previously described [165].

6.2.8 SEM Evaluation

For SEM imaging, samples were prepared for imaging by coating with gold/palladium for 40 s at a current of 40 mA. Imaging was conducted in a Zeiss ULTRA plus SEM using InLens and SE2 detectors with an accelerating voltage of 4 – 5 kV.

6.2.9 Fourier-transform Infrared (FTIR) Measurements

FTIR spectra of samples were recorded using a Spectrum 100 FT-IR spectrometer (PerkinElmer, Waltham, USA) in attenuated total internal reflection mode. The spectra were scanned between 500 and 4000 cm^{-1}. In an attempt to address this concern, the surface of the polymer framework was functionalised with fibronectin (Fn) (Figure 6.5D). Visually, the Fn functionalised PCL appeared to have a considerable, and uniform deposition of the protein on its surface (Figure 6.4Di). FTIR was used to validate that the functionalisation process was effective. In the modified scaffolds, it was possible to detect peaks centred at 1,640 and 1,540 cm^{-1} indicative of amide I and amide II respectively. A clear peak centred around 3,287 cm^{-1} was also detected in the modified group, which correlated to stretching of NH bonds within NH_2 groups (Figure 6.4Dii). Through surface modification with the recognised adhesion protein fibronectin, the aim was to mitigate the risk of poor integration between the developing tissue and the supporting PCL framework.

6.2.10 Image Quantification & Statistical analysis

Diameter measurement of growing microtissues, and engineered macrotissues were taken from microscope images (4x) using ImageJ software. Statistical analysis was performed using GraphPad Prism software (GraphPad Software, CA, USA). Analysis of differences between two groups at one timepoint was done using a standard two-tailed t-test. For two groups over multiple time-points a one-way analysis of variance (ANOVA) was performed. Numerical and graphical results are presented as mean ± standard deviation unless stated otherwise. Significance was determined when $p < 0.05$.

6.3 Results

6.3.1 Maximising Early-Cartilage Microtissue Growth

Engineering a cartilage macrotissue *via* self-organisation of multiple early-cartilage microtissues (Figure 6.1A) requires the engineering of large numbers of such microtissues. Furthermore, conditions to support the rapid growth and chondrogenesis of such microtissues must be identified if scaled-up tissues are to be engineered using practical numbers of cells and tissue building blocks. Therefore, the first objective of this study was to rapidly generate cartilage microtissues of sufficient size (>200 μm in diameter) to simplify their use as biological building blocks for the biofabrication of hyaline cartilage grafts. To optimise the generation of these cartilage microtissues, two media conditions intended to induce rapid and robust chondrogenesis using a co-culture of CCs and FPSCs (Figure 6.1B) were compared, as well as three starting cell densities (with the same 3:1 ratio of FPSCs to CCs). During the 8 days of culture, the continuous exposure to chondrogenic media supplemented with TGF-β (media condition 2) yielded a predictable and linear increase in microtissue diameter. In contrast, 4 days of exposure to expansion media following by 4 days of exposure to chondrogenic media supplemented with TGF-β (media condition 1) resulted in an initial contraction of the microtissues, during the first 4 days, followed by a rapid increase in microtissue diameter upon chondrogenic induction at day 4 (Figure 6.2Ai). Given that prolonged exposure of cartilage spheroids to TGF-β has been reported to reduce their capacity to fusion [68], this study aimed to limit exposure time to this growth factor whilst still ensuring rapid growth. Therefore, the change in diameter of the microtissues after exposure to TGF-β was compared for the two media conditions (Figure 6.2Aii). The fold change in diameter after initial exposure to TGF-β was significantly higher for media condition 1 compared to media condition 2 (Figure 6.2Aii). Collectively, these findings indicated that first culturing cell aggregates in XPAN for 4 days prior to chondrogenic induction primes the microtissues for rapid growth, enabling the engineering of microtissues >200μm in diameter after only 4 days of chondrogenic culture with as little as 1,000 starting cells. To validate that numerous microtissues could be brought together and spontaneously fuse, the microtissues were seeded into a non-adherent agarose wells and cultured under chondrogenic conditions for 35 days (Figure 6.1A). After 2 days all microtissues began to coalesce, and after 7 days a unified tissue with a single, uninterrupted boundary was apparent. Microscopically, no differences between the developing macrotissue formed by microtissues with varied starting cell numbers were apparent within the two groups. However, there were observable differences between the two initial media conditions. As expected, microtissues that had been exposed to TGF-β for 8 days (media condition 2) appeared to fuse less than those that had only undergone a shorter chondrogenic induction (media condition 1). These differences were apparent

after significant culture time (35 days), where the outline of the initial microtissues were still visible in media condition 2 (Figure 6.2B).

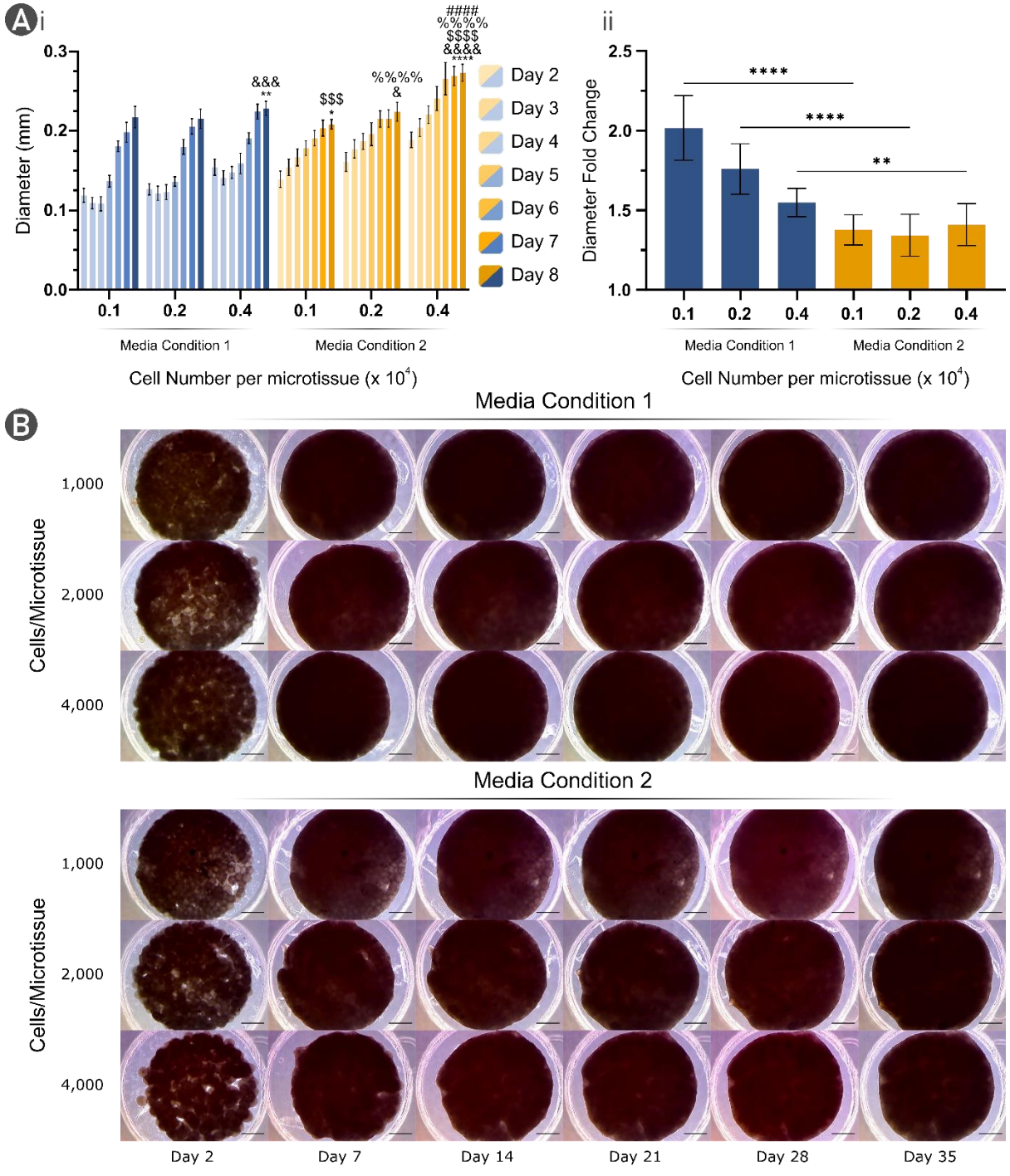

Figure 6.2 *Establishing conditions for cartilage microtissue growth and self-organisation. A) Designing a culture regime for the generation of cartilage microtissues. i) Diameter of cartilage microtissues over 8 days of culture in two media conditions. * Denotes significance for media condition 1 - 1 x 10^3, & for media condition 1 – 2 x 10^3, $ for media condition 1 – 4 x 10^3, % for media condition 2 –1 x 10^3, and # for media condition 2 – 2 x 10^3, when tested using an ordinary two-way ANOVA with Tukey's multiple comparisons test where $p < 0.05$ (N = 25, Mean ± SD). ii) Diameter fold change over the first 4 days of exposure to TGF-β. * Denotes significance when tested using a Brown-Forsythe and Welch One-way ANOVA, where $p < 0.05$ (N = 25, Mean ± SD). B) Representative microscopic images of cartilage microtissues from each condition self-organising over 35 days of chondrogenic culture. (Scale bar = 500 µm)*

6.3.2 Early-cartilage Microtissues Self-organise into a Thick, Homogenous, and Consistent Articular Cartilage

After 5 weeks of chondrogenic culture both cohorts of cartilage microtissues had self-organised into a unified cartilage macrotissue (Figure 6.2B). However, differences in the quality of this macrotissue were apparent histologically (Figure 6.3). Media condition 1 microtissues resulted in the formation of a consistent and homogenous cartilage. All cell densities in this group yielded cartilage that was rich in sGAG and collagen, indicated by diffuse positive alcian blue and picrosirius red staining respectively. Immunohistochemistry revealed that the engineered cartilage exhibited a stable hyaline-like phenotype, with positive DAB staining for collagen type II and negative matrix staining for collagens type I and X. The cartilage generated using the more cellular microtissues (4 x 10^3 cells) in media condition 1 stained weakly for collagen type I, with little or no staining observed using the two lower cell densities (Figure 6.3A). Although the core of the microtissue units were still visible within the self-organised cartilage, a large number of cells and matrix was present between what remained of the initial spheroidal cartilage seeds. This suggests that the more immature microtissue phenotype generated using a shorter chondrogenic induction (media condition 1) period permitted cells to move out from the initial spheroid and facilitated (re)modelling of the engineering tissue.

The gross morphology of the cartilage formed using the more mature microtissues (media condition 2) was more irregular, as evident by the concave surface of the tissue for all initial cell densities. Histologically, the cartilage structure reflected the microscopic observations made during microtissue fusion. Here, the individual tissue units were much more apparent and overall less interstitial tissue (tissue formed between fusing microtissue units) formation was evident (Figure 6.2B & 6.3B). Despite the more punctate appearance of the microtissues, the engineered cartilage appeared to stain more positively for both sGAG and collagen in comparison to that generated using media condition 1 microtissues. However, the final cartilage exhibited a fibrocartilage phenotype, indicated by the presence of collagen types I and II and the absence of collagen type X (Figure 6.3B). Unsurprisingly the more mature phenotype of the cartilage microtissues generated in the second cohort appeared to limit cell motility and (re)modelling of the engineered macro-graft. Although adjacent microtissues had fused to form a macrotissue, the spherical architecture of the microtissue units and limited interstitial matrix and cellularity was more obvious than in the more immature cohort.

The physical properties of the engineered tissue indicated that a thick (~1 mm) macro-scale (mm-diameter) cartilage was generated in all groups. A significantly thicker tissue could be achieved by using microtissues generated in the media condition 1, at a density of 2 x 10^3 and 4 x 10^3 cells/microtissue. Mechanically, the engineered cartilages were relatively stiff with a compressive

modulus of ~0.150 MPa, although there were no statistically significant differences between the groups. Biochemically, there were no differences in DNA content after 5 weeks, while microtissues

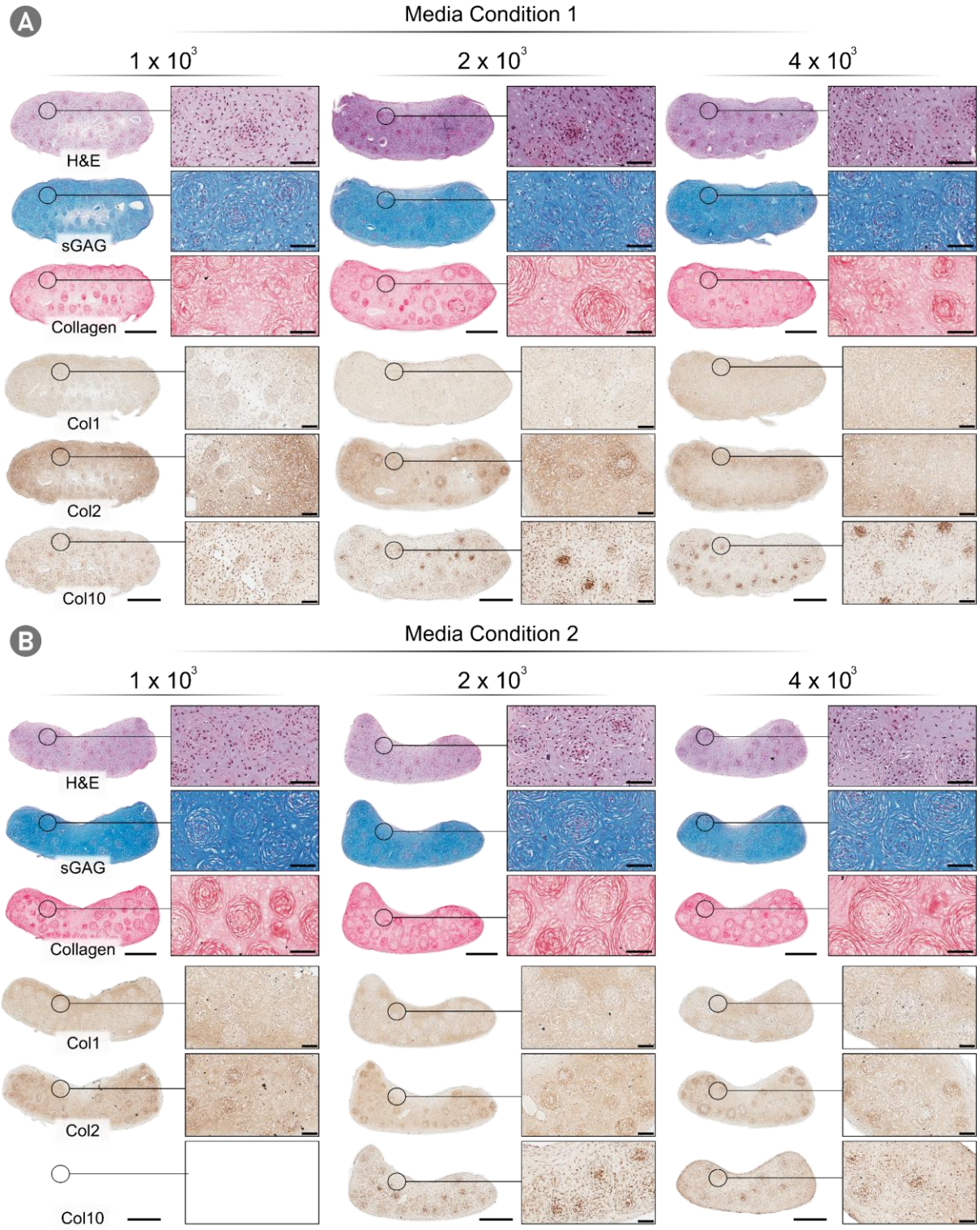

Figure 6.3 *Cartilage microtissues can self-organise into a homogenous cartilage macrotissue. A&B) Histological panels of the cartilage macrotissue formed via the self-organisation of cartilage microtissues units, generated using the two media compositions, after 5 weeks of chondrogenic cultivation. sGAG and collagen deposition stained for by alcian blue and picrosirius red staining respectively. DAB immunohistochemistry for the visualisation of collagen types within the engineered cartilage. (Scale bar: Overview = 500 µm & Zoom = 100 µm)*

engineered in media condition 2 generated a microtissue with higher levels of sGAG and collagen deposition for the 1 x 10^3 cells/microtissue group (Figure 6.4). Collectively, the results indicated that a thick, stable, and mechanically competent millimetre scale cartilage could be consistently engineered by the self-organisation of microtissues with a starting density of 2 x 10^3 cells/microtissue, when the microtissues are cultivated using media condition 1. As such, these conditions were brought forwards for all future studies.

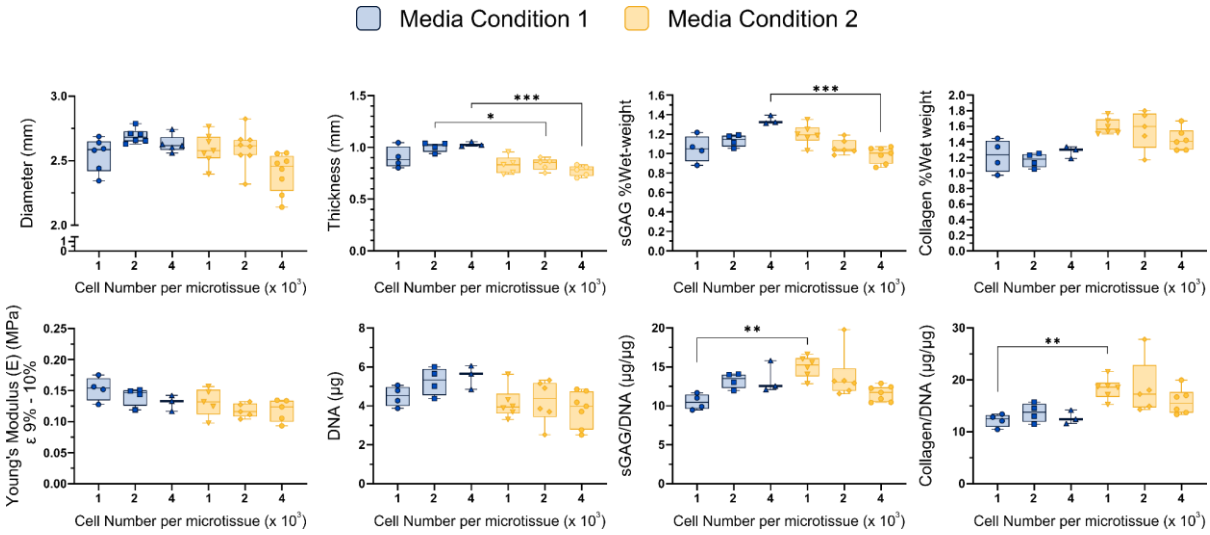

Figure 6.4 *Physical, mechanical, and biochemical evaluation of cartilage macrotissue after 5 weeks. * Denotes significance when tested using a using a Brown-Forsythe and Welch One-way ANOVA, where p < 0.05 (Individual data points provided, Mean ± SD)*

6.3.3 The Self-organisation of Early-cartilage Microtissues can be Guided using a 3D Printed Framework

Since the biomechanical properties of native AC are closely coupled to the zonal organisation of the collagen network, this chapter next attempted to engineer self-organised cartilage with a biomimetic collagen architecture by guiding the fusion and growth of microtissues using a 3D printed framework. Polarised-light microscopy (PLM) was used to visualise the orientation of the collagen fibrils within the engineered cartilage. In unguided conditions, there was limited spatial organisation within the engineered tissue (Figure 6.5A). This lack of organisation was particularly evident with the more mature cartilage microtissues engineered in media condition 2, where the circular collagen alignment was clear indicating that limited remodelling that had taken place post-fusion. This spherical alignment was present to a lesser extent with the less mature cartilage microtissues engineered using media condition 1. Furthermore, discrete microtissues were less obvious in this group and there was some evidence of tissue remodelling and the formation of interstitial collagen. Imparting some level of spatial organisation to the developing collagen

network was identified as a means of improving the quality of the engineered cartilage. To do so, a 3D printed framework was employed (Figure 6.5Bi &ii). By imposing boundary conditions on the developing macrotissue, the growth and subsequent organisation of this tissue could be better guided in comparison to unguided conditions. Importantly, the addition of the 3D printed

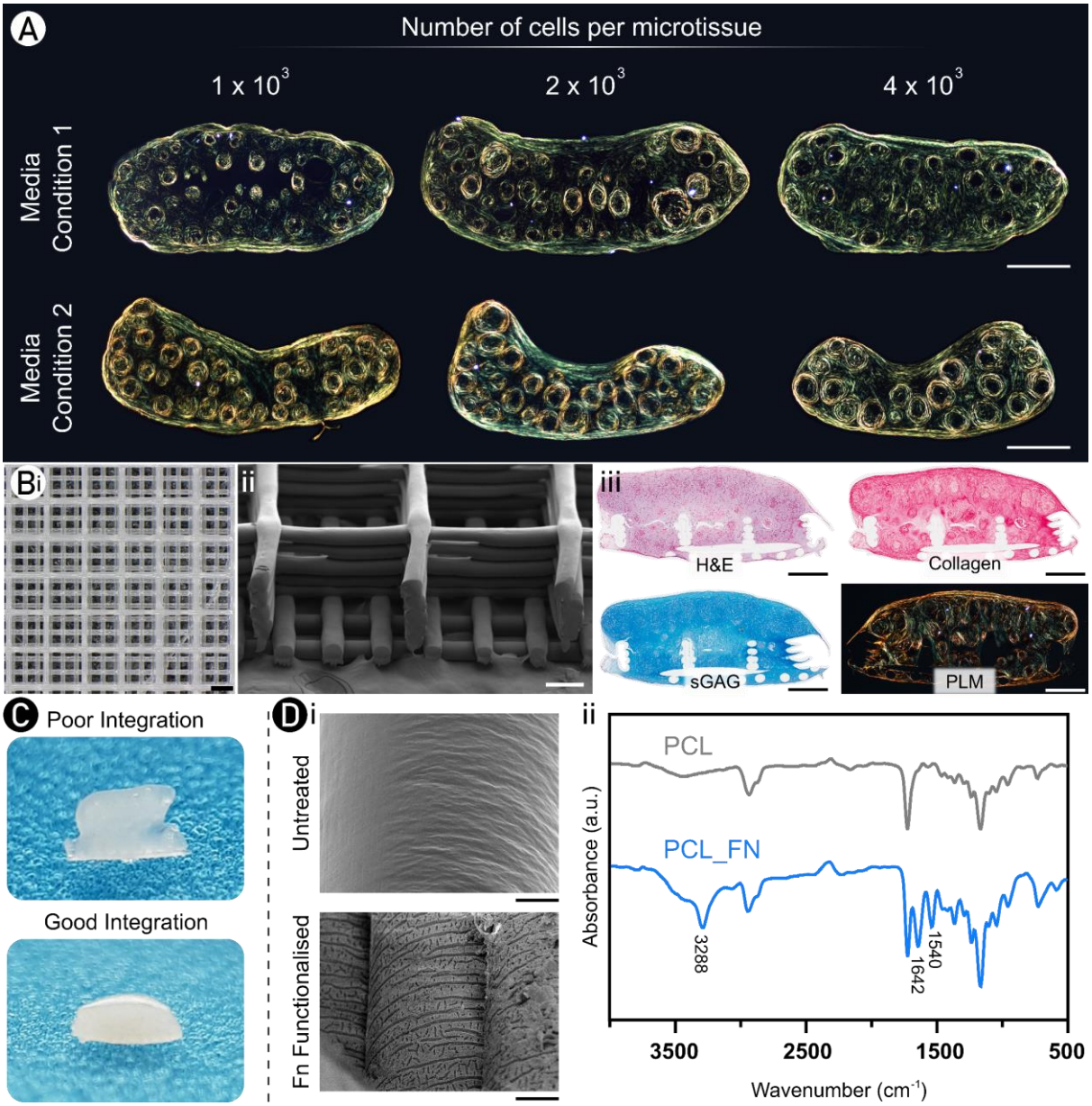

Figure 6.5 *A 3D printed polymer framework can better guide the self-organisation of cartilage microtissues. A) Polarised-light microscopy (PLM) showing the limited spatial organisation of the collagen network that formed within the cartilage macrotissue after 5 weeks of culture. Bi) Microscopic image of the 3D printed polymer framework, ii) SEM of a cross-section of the microwells of the polymer framework, with subjacent catching fibres. iii) Histological staining for cartilage marker, sGAG (alcian blue) and collagen (picrosirius red staining) as well as PLM showing the biomimetic spatial organisation of the collagen network within the engineered cartilage that formed via guided self-organisation of cartilage microtissues. C) Representative macroscopic images of poor & good integration between the engineered cartilage and 3D printed polymer framework. Di) SEM for untreated PCL and fibronectin (Fn) functionalised PCL. ii) FTIR spectrum for the untreated and functionalised PCL (Scale bar: A, Bi & Biii = 500 µm; Bii = 200 µm; Di = 20 µm).*

framework did not negatively impact the microtissues capacity to fuse, undergo chondrogenic differentiation, and form a unified cartilage macrotissue (Figure 6.5Biii). However, the solid polymer walls of the microwell array appeared to provide guidance during tissue growth, resulting in the development of a collagen network which mirrored aspects of the Benninghoff arcade structure seen in normal AC (Figure 6.5Biii). Despite this relative success, it was observed that in some samples the developing macrotissue would pull away from the polymer framework during the fusion process (Figure 6.5C). Although the polymer surface had been hydrolysed to improved hydrophilicity, it appeared that this was not sufficient to guarantee integration between the tissue and scaffold. As such, fibronectin functionalisation was carried out for FDM fabricated frameworks herein.

6.3.4 Evaluation of Cartilage Repair in a Clinically-relevant Large-animal Model

Having established *in vitro* the capacity to generate a robust and biomimetic self-organised cartilage, this chapter next sought to evaluate the efficacy of such engineered cartilage in the treatment of focal chondral defects in a clinically-relevant caprine model of AC repair. To this end, engineered implants (treatment) or micro-drilling (empty) were randomly assigned to the lateral femoral condyle of the rear stifles. After 6 months *in vivo*, the repair tissue was evaluated macroscopically (Figure 6.6) and histologically. Initial quantification of the repair tissue, using a panel of blinded and independent expert scorers, indicated no significant difference between the groups (Figure 6.7). Despite this, high levels of variability in the quality of repair within the empty cohort was seen. As such, in some key metrics the treatment did appear to improve the consistency of the repair tissue generated. For example, a lower standard deviation was noted when quantifying the matrix staining (SD = 1.56 versus 2.69, for treatment and empty respectively), abnormal calcification (SD = 0.981 versus 2.47, treatment and empty respectively), and overall assessment (SD = 1.42 versus 2.54, treatment and empty respectively) of the repair tissue. From the

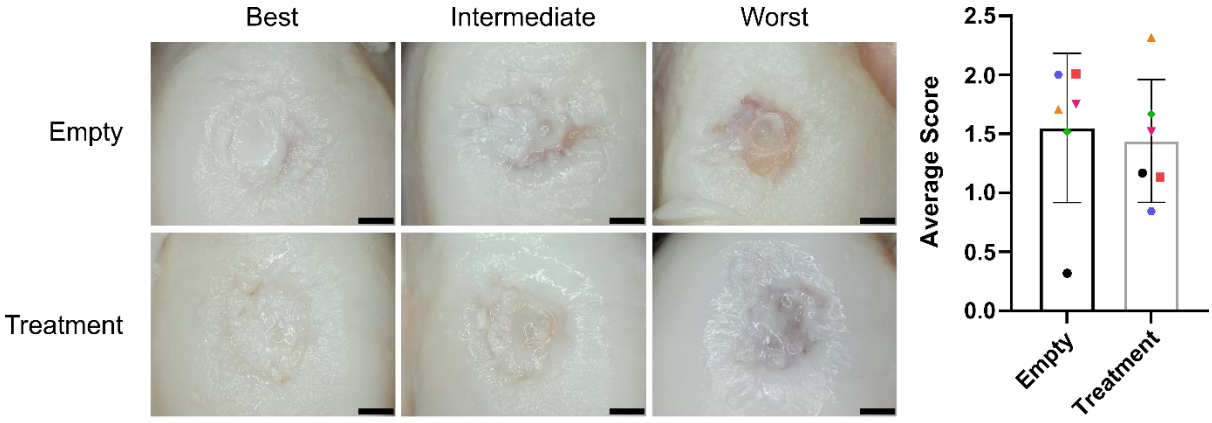

Figure 6.6 *Macroscopic evaluation of the healing response. Panel of the best, intermediate, and worst cases for empty and treatment groups, and graphical representation of macroscopic scoring. Ranks determined from quantification of the macroscopic defect appearance after 6 months. (Scale Bar = 2 mm) (N = 6, Mean ± SD)*

quantification, 3 individuals were identified from each group to represent the 'best', 'intermediate', and 'worst' repair from the empty and treatment groups.

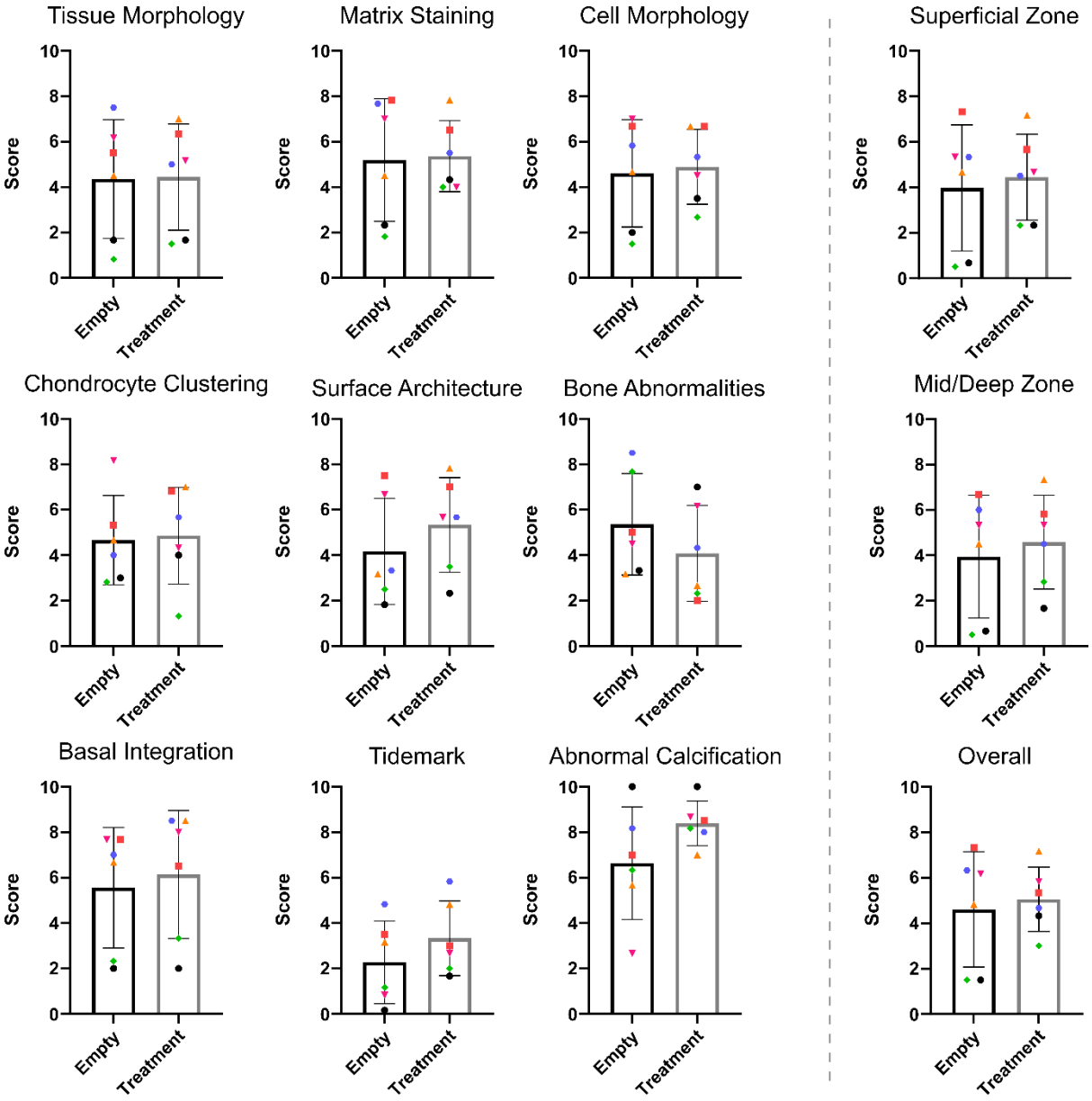

Figure 6.7 *Treatment of a chondral defect with an engineered cartilage does not significantly improve the healing response. Graphical representation of histological scores after 6 month in vivo. Internal controls are represented by data points with matching colour and symbol. (N = 6, Mean ± SD)*

From these cases, only the best-treatment resulted in the restoration of the articular surface with a tissue that was comparable to the surrounding native cartilage. Specifically, in the best-case from the empty group, a thin layer of cartilage which stained positively for both collagen and sGAG was observed. The repair tissue was clearly recessed from the articular surface and there were regions where the repair tissue was not properly integrated with the subchondral bone. Additionally, there were obvious fibrillations at the apical surface of the repair and native tissue. In the best case, the subchondral bone was largely normal, however there was a region of fibrous

tissue subjacent to the defect (Figure 6.8). Expression of collagen type II and absence of collagen type I in the best empty case is indicative of a phenotypically stable repair cartilage (Figure 6.10). In the intermediate group, the repair tissue was largely fibrous with a rough articular surface and significant fibrillations within the repair tissue. Although there was evidence of endochondral bone formation in the subchondral bone, there was also extensive fibrous tissue and trabecular thickening (Figure 6.8). Here, the repair tissue was a mixture of fibrous and stable cartilage, with regions within the defect site rich in collagen type II and more centrally, collagen type I (figure 6.10). Little repair tissue filling was identified in the worst case, leaving the subchondral bone exposed within the defect region. Moreover, significant fibrillations and deterioration of the surrounding native articular tissue were apparent. The extent of the bone abnormalities correlated to the rank of the repair tissue, whereby an extensive replacement of bone with fibrous/fibrotic tissue was found in the worst case (Figure 6.8).

Treatment using a self-organised cartilage appeared to result in better resurfacing of the joint in the best and intermediate cases, although the observed differences did not translate to statistically significant differences in histological scores. In the best case the defect region was filled with a cartilage that stained positively for both collagen and sGAG to a level similar to that of the surrounding native tissue. Additionally, the repair tissue was at a similar height to the surrounding tissue. However, fibrillations in the native cartilage suggested that the deterioration of the articular surface had occurred during the 6 months and the treatment did not provide immediate resurfacing. Although some fibrous tissue was present in the subchondral bone, it appeared to be less extensive and evidence of new bone formation around the implant, *via* an endochondral pathway, was promising. In the intermediate case the repair tissue was more fibrous in nature, with limited staining for sGAG. Additionally, the repair tissue failed to reach a congruent level with the native cartilage, although on average appeared better than the control groups. Fibrous tissue was present in the subchondral bone, to a similar level as seen in the empty group (Figure 6.9). Both the best and worst treatment groups displayed a fibrocartilage repair tissue. The characteristic co-expression of collagen types I & II within the defect site indicated that a stable AC phenotype was not realised (Figure 6.10). In the worst case, there was little joint resurfacing. Despite this, the limited repair tissue did stain positively for sGAG and collagen type II, whilst showing no collagen type I deposition within the defect region (Figure 6.9 & 6.10). Unlike in the empty group, the worst-case treatment did not have exposed subchondral bone and the subchondral-bone abnormalities was far less pervasive. Additionally, new bone formation was noted around the implant, with clear regions of endochondral ossification noted outlining the stem of the 3D printed implant (Figure 6.9).

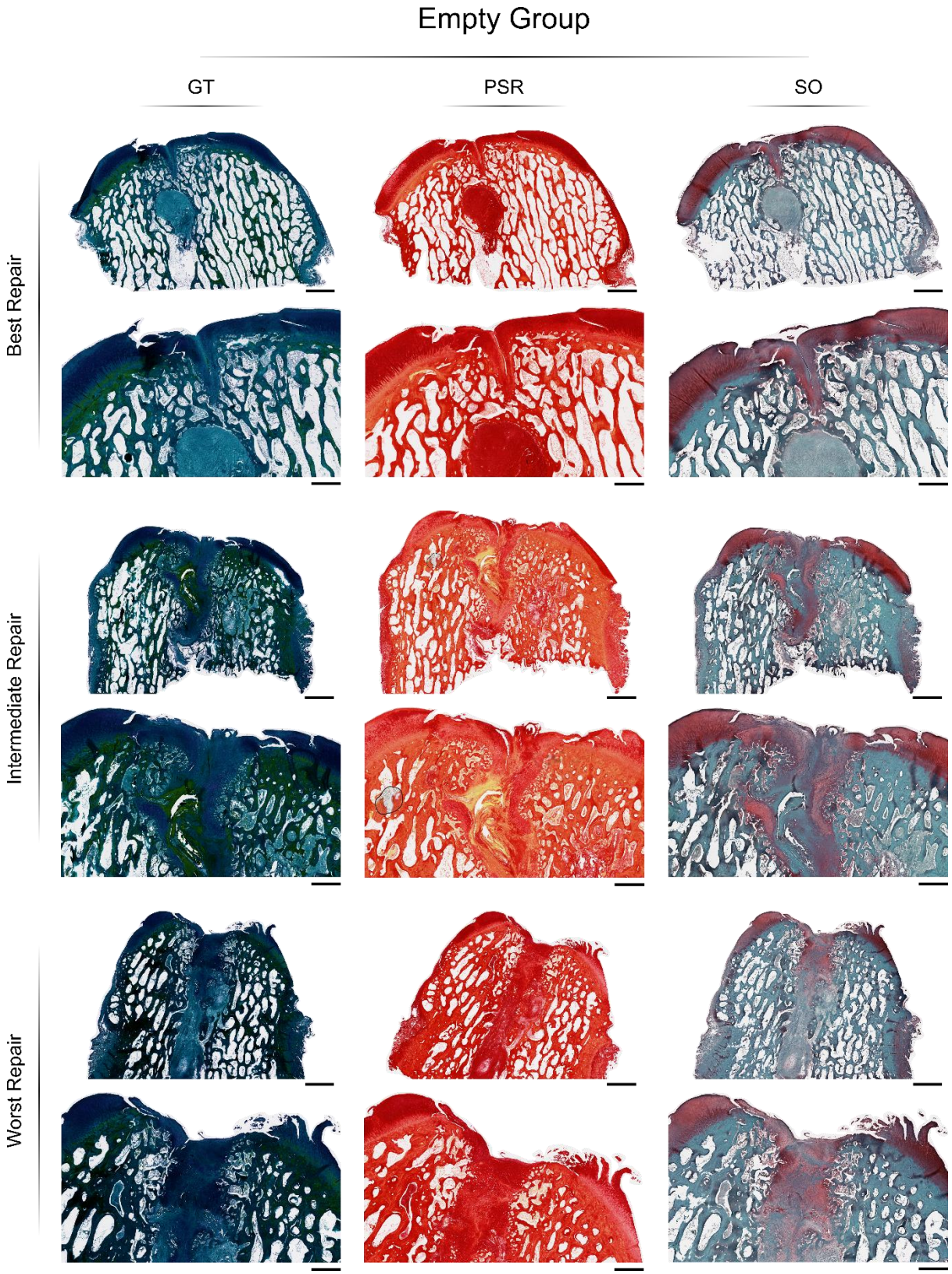

Figure 6.8 *Histological panel for the 'Best', 'Intermediate', and 'Worst' repair response in the empty group. Ranking was determined from the histological scoring. (Scale bars: Overview = 2 mm, Zoom = 1 mm)*

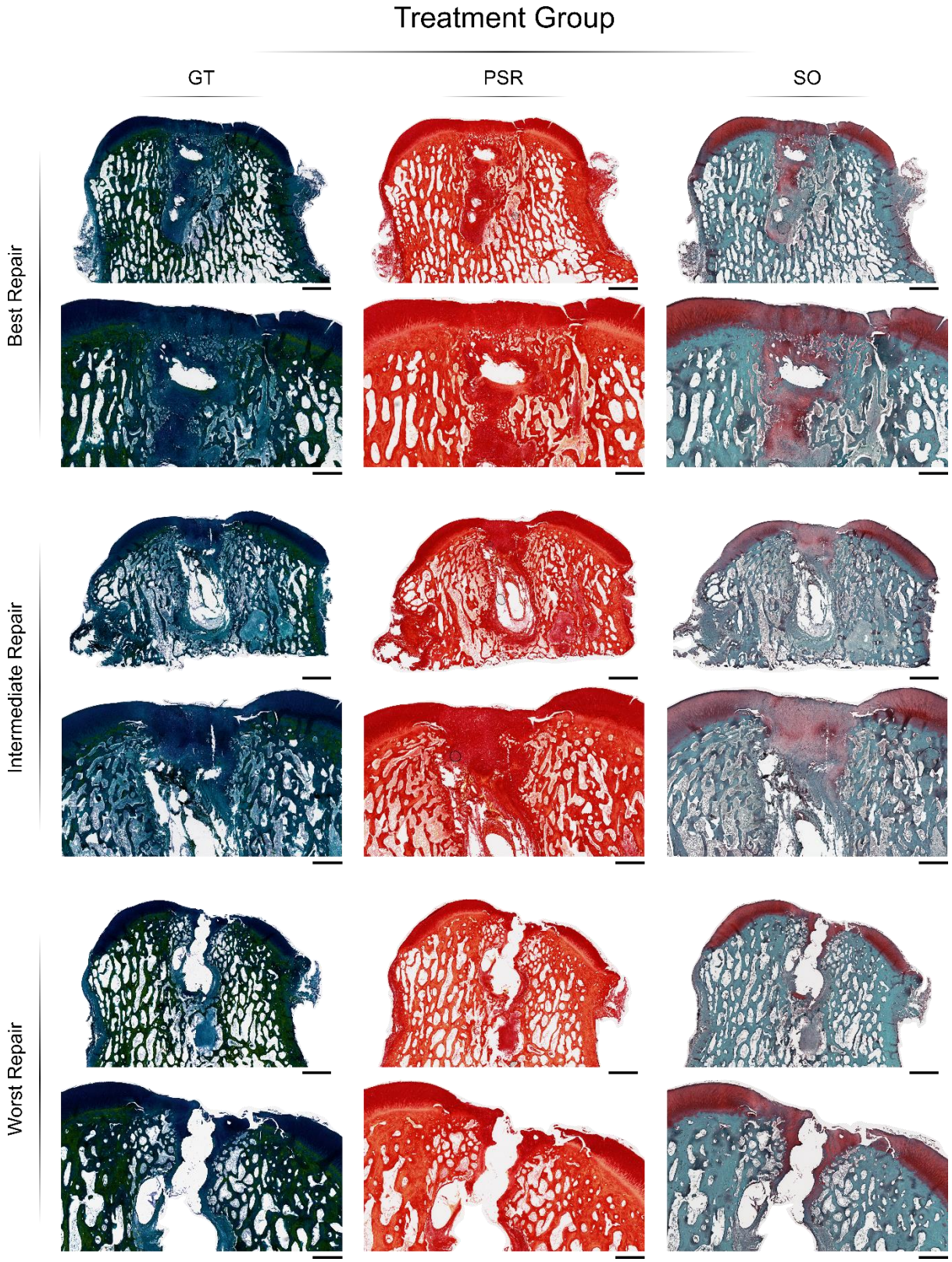

Figure 6.9 *Histological panel for the 'Best', 'Intermediate', and 'Worst' repair response in the treatment group. Ranking was determined from the histological scoring. (Scale bars: Overview = 2 mm, Zoom = 1 mm)*

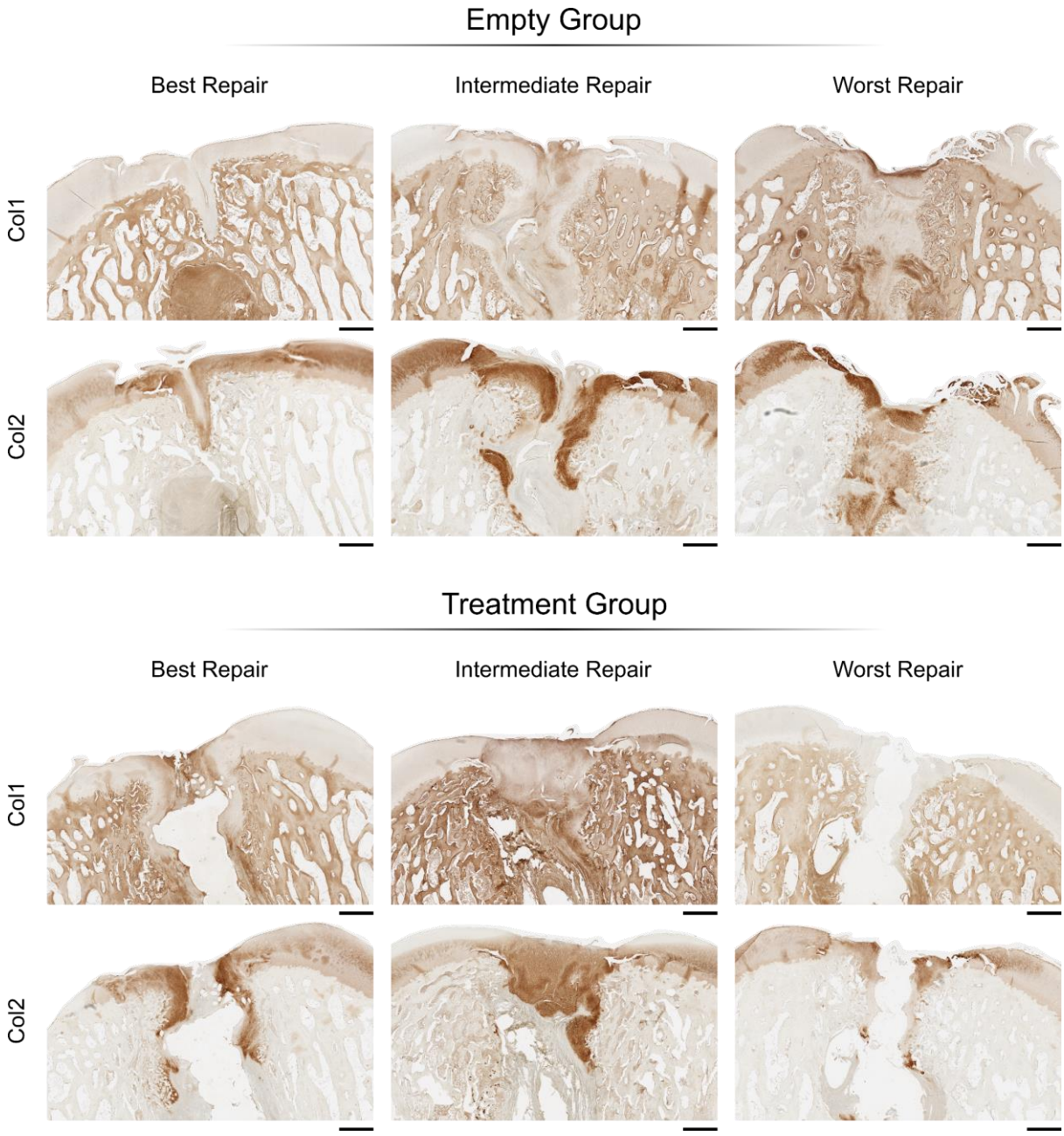

Figure 6.10 *Immunohistological panel for the 'Best', 'Intermediate', and 'Worst' repair response in the treatment group. Staining for collagen types I and II (Col1 and Col2 respectively). Ranking was determined from the histological scoring. (Scale bars = 1 mm)*

6.4 Discussion

The overarching aim of this chapter was to evaluate the efficacy of a stratified cartilage, generated using cartilage microtissue building blocks, as a treatment for focal chondral defects within a preclinical large-animal defect model. To achieve this, an effective method for generating stable cartilage microtissues was defined, and the capacity to spontaneously fuse these initially-discrete tissue units was demonstrated. The resulting self-organised cartilage exhibited a stable phenotype as well as promising biochemical and mechanical properties. A biomimetic organisation of the collagen network within the engineered AC was achieved by guiding the self-organisation process using a 3D printed polymer framework. Ultimately, implantation of the engineered tissue did not significantly enhance healing of a focal chondral defect and potential explanations for this shortcoming are discussed herein.

Cartilage microtissues were observed to spontaneously fuse and form millimetre-scale tissues in the absence of external mechanical forces when they were simply deposited within agarose wells. Previously, in work that generating a similar unified cartilage from spheroidal cartilage building blocks, manual forces were necessary to ensure any fusion between the tissue units [68]. Within this early work, the authors identified 7 days as the maximum permissible exposure time to the chondrogenic growth factor TGF-β_3 before 'boundary setting' occurred within the mesenchymal condensations and prevented homogenous tissue formation. The authors also identified that 3-5 days of chondrogenic induction resulted in tissue homogeneity and near-native mechanical properties. In this chapter, similar behaviour in terms of boundary setting between different cartilage microtissues maturities was observed. Specifically, of two investigated microtissue populations, cells within the early-cartilage microtissues were able to disassociate from the initial spheroid, facilitating proper fusion between proximal spheroids, generate interstitial tissue and better (re)modelling the developing matrix. In contrast, and in agreement with the findings of others [68,138], attempts to fuse more 'mature' cartilage microtissues resulted in the development of an inhomogeneous cartilage macrotissue, with a worse overall morphology and limited interstitial tissue. In spite of this, all cartilage microtissues generated within this study were able to spontaneously fuse and form a macrotissue, even those that had undergone an extended chondrogenic induction (7 days). These findings therefore confirm that prolonged chondrogenic microtissue culture induces boundary setting which, impairs the resident cells capacity to liberate themselves from the dense microtissue matrix and (re)model the developing cartilage. But importantly, that the spontaneous fusion of adjacent cartilage spheroids without the need for external manual force, even in more 'established' cartilage microtissues. This could potentially be linked to the size of the cartilage microtissues engineered in this study, which are considerably smaller and require fewer cells to generate than those presented by other [68].

In the absence of any guiding structures, the fusing microtissues failed to generate a macrotissue with a collagen network mimetic of the AC. Similar observations have been reported whereby scaffold-free cartilages, although biomimetic in composition have not exhibited native-like collagen anisotropy [42,45,47]. Previous attempts to guide self-assembled cartilages have shown that radial confinement can lead to significant increase in biomechanical properties *via* changes in collagen organisation [78]. Having established 3D printed microwells as an effective method for driving the spatial organisation of a self-organised cartilage within chapter 4, this chapter aimed to leverage a similar framework to help guide the self-organisation process of early-cartilage microtissues. Importantly, the introduction of a PCL framework did not hinder the capacity for early-cartilage microtissues to fuse, and produce a rich hyaline cartilage-like matrix. Moreover, the boundary conditions provided by the walls of the microwells appeared to guide tissue development and resulted in the formation of a more biomimetic collagen architecture with a 'Benninghoff' arcade structure. The engineered cartilage was designed to be ~ 1 mm in height including the 0.5 mm tall microwells integrated within the engineered tissue. Despite this significant tissue overgrowth covering the PCL filaments, the entire articular surface of the implant was designed to sit flush with or slightly recessed to the articular surface of the native condyle which is typically 1 – 1.5 mm in height. The novel fixation device in chapter 4 was also leveraged here as a means of initially fixating the self-organised cartilage within a focal chondral defect, facilitating vertical integration between the engineered tissue and the exposed bone within the defect site. Achieving lateral cartilage-cartilage integration is challenging [232]. Instead, subchondral bone can be leveraged in many ways to anchor a neo-cartilage [231,232]. In particular, vertical integration between an implant and the subchondral bone plate is routinely reported [231]. Consequently, interfacing an engineered cartilage with the subjacent bone could provide a means of fixation. However, direct apposition of the implanted cartilage and subchondral bone is required to create a near-native cartilage-bone interface [232]. As such, we investigated whether the novel fixation pin discussed in chapter 4 would provide a means of initially fixating the self-organised cartilage developed in this study within a preclinical model for focal chondral defects, and facilitate vertical integration between the engineered tissue and the exposed bone within the defect site. After 6 months, no evidence of implant loosening observed histologically, and the repair tissue was well integrated with the subchondral bone in most cases. However, some subsidence of the implant into the subchondral bone was noted. This may contributed to the variability in outcomes observed histologically, with evidence of hyaline-like cartilage development observed in some animals, but no significant improvement in term of the quality of repair tissue when compared to an existing cartilage-treatment strategy.

Several limitations of the approach investigated within this chapter could explain the limited *in vivo* success. First, the mechanical properties and biochemical composition of the engineered tissue was not comparable to native AC. Other who have leveraged cartilage spheroids for generating a larger macrotissue have demonstrated enhanced matrix stratification and superior mechanical properties within their engineered tissue [68]. A potential explanation for a higher-quality engineered cartilage in this study, is the use of a decellularised trabecular-bone scaffold. The potent cues, both physical and biochemical, known to be present within bone-ECM scaffolds [270], could explain the development of the physiologic stratification and development of a more mature cartilage. Others have also demonstrated that spatiotemporal delivery of soluble cues that mimic the osteochondral interface *in vitro* can yield a more stable phenotype in a scaffold-free cartilage [46]. Alternatively, the superior biomechanical properties reported (825 ± 197 KPa versus, 153 ± 19.5 KPa, Bhumiratana *et al.* [68] and this study respective) could be explained by a synergistic effect of superior levels of sGAG exhibited (~75 µg/mg sGAG/WW versus 13.4 µg/mg, for Bhumiratana *et al.* and this study respective) and the aforementioned physiologic tissue stratification. Achieving similar levels of matrix production, tissue stratification, and mechanical competency could be achieved by using an alternate MSC source, longer culture periods, and/or the inclusion of other cues during culture. Nevertheless, whether adequate *in vitro* tissue maturation can be achieved within clinically relevant time-frames remains contentious. Hence, whether truly scaffold-free approaches for load-bearing musculoskeletal tissues, such as AC, are realistic is unclear. As such, there may be a need for a scaffold material to temporarily bear load during *in situ* tissue maturation [42,74]. In this vein, the mechanical properties of the tissue at implantation could be improved through the inclusion of a more involved scaffold as opposed to a guiding framework. For example, tubular structures that mimic the macromolecular organisation of native AC can be created within collagen-based scaffolds. Population of this biologically inspired scaffold with microtissues, that support robust chondrogenesis within the scaffold, can result in an engineered cartilage that has compressive properties approaching naïve native AC [121]. In this context, modular biofabrication approaches, such as the self-organisation of tissue units, can yield promising hybrid approaches. However, scaffolds and microstructural devices intended to guide developing tissues must be carefully design and implemented to provide instructive boundaries without compromising the capacity for tissue-unit fusion, and remodelling of the macrotissue [73]. As such, we believe that our approach offers a platform for guiding the self-organisation of early-cartilage microtissues towards a more biomimetic engineered cartilage addressing, in part, a key challenge within the field.

Finally, avoiding post-operative load-bearing has been advised following cartilage repair [222], coupled with the putative need for *in situ* maturation of relatively naïve engineered tissues, could

help to explain the limited benefit seen in this study where the implant was subjected to full biomechanical loading almost immediately. Osteochondral approaches have been discussed as the most likely approach for successfully implementing larger and stiffer engineered AC [111]. Many approaches for generating osteochondral implants have been proposed [271], given that animals are load-bearing days after implantation, and control over post-operative joint motility is limited, an osteochondral approach could provide a more robust platform to treat focal chondral defects. Additionally, the subsidence of the implant observed in this study suggests that the implant design failed to provide sufficient cues for osteointegration in all cases. Similar undesirable bone alterations and formation of a fibrous implant-tissue interface, as opposed to bony ingrowth, has been reported elsewhere when using a biodegradable polymer pin for chondral fixation [272]. Clearly, stabilising the defect site including the subchondral bone is an important feature that has not been realised in this work. To this end, fixating a self-organised cartilage *via* an osteochondral implant, capable of inducing rapid and robust osteointegration and defect stabilisation could address these issues and will be explored in the next chapter of this thesis.

6.5 Conclusion

This work demonstrates that early-cartilage microtissues can spontaneously self-organise into a stable cartilage macrotissue with promising biochemical and biomechanical properties. Furthermore, organisation of the collagen network within this engineered AC can be guided towards a more biomimetic arrangement using a 3D-printed polymer framework. Implantation of the engineered cartilage using a previously developed implant into a preclinical chondral defect model did not result in a significant improvement in healing response when compared to an existing treatment strategy. This failure to properly regenerate the articular surface is likely due to limited osteointegration of the implant in the defect site and implant subsidence. Consequently, this work motivates investigation into alternative fixation strategies, such as osteochondral implantation, which may better stabilise the defect and improve the therapeutic efficacy of the engineered AC.

Chapter 7.

7 Biofabrication of Osteochondral Grafts using Phenotypically Distinct Microtissues for Synovial Joint Repair

7.1 Introduction

Autologous osteochondral transplantation (AOT) has been shown to outperform other clinical joint repair strategies such as microfracture and autologous chondrocyte implantation [24,25]. The success of AOT is associated with the transplantation of a functional unit of bone and cartilage into the defect site. Traditional approaches for engineering the osteochondral unit have failed to fully recapitulate the structure, composition and functional properties of the target tissue. New developmental engineering (DE) strategies have recently emerged which aim to recapitulate key events of embryonic and postnatal development as a means of generating truly biomimetic engineered tissues [79,80]. Typically, DE approaches are 'scaffold-free' and are underpinned by the processes of cellular self-assembly or self-organisation [42,81]. In the absence of a 'bulking' scaffold/hydrogel material, DE seeks to leverage the cell's inherent ability to synthesis a biomimetic extracellular matrix (ECM) under the direction of appropriate exogenous cues. While such processes have successfully been used to engineer bony and cartilaginous tissues [52,115], barriers to their use in synovial joint regeneration remain. A major challenge with DE is fabricating tissues large enough to treat human-scale defects; the engineering of such grafts will typically require large numbers of cells which in turn incurs nutrient transport limitations and compromises the quality, integrity, and therapeutic efficacy of the resulting implant [62,273]. Furthermore, recapitulating key aspects of the OC unit, such as the arcade-like collagen architecture that is integral to the biomechanical functionality of articular cartilage, remains a challenge.

Microtissues have emerged as a means of overcoming these scalability issues, permitting the formation of millimetre-centimetre scale tissues through self-organisation (tissue fusion and remodelling) of initially discrete tissue 'building block' units [54]. Such approaches have been used to engineer grafts for both articular cartilage tissue engineering [68] and large bone defect healing [54,238]. For example, hypertrophic cartilage rudiments have been used as developmentally inspired bone precursors generating bone organs *in vivo* [52,274], and similar hypertrophic phenotypes have been generated in cartilage microtissues [54,275,276]. Cellular aggregates generated using progenitor cells have been combined to biofabricate scaled-up implants [69,139–142] and assessed for their capacity to regenerate osteochondral defects in pre-clinical large animal models [69]. Despite macroscopic and histological evidence indicating improved healing in

response to the treatment, quantification of these differences showed no significant benefit when compared to an untreated osteochondral lesion. This might be attributed, at least in part, to the use of relatively undifferentiated cellular aggregates used in generating such tissue engineered grafts. This raises the question as to whether engineering a more biomimetic cartilaginous tissue using microtissue building blocks would lead to superior joint regeneration.

With this in mind, the objective of this study was to leverage emerging knowledge of DE and microtissue self-organisation to engineer a biphasic osteochondral plug containing a biomimetic layer of engineered articular cartilage. The osseous region of this osteochondral graft was engineered using islands of hypertrophic cartilage microtissues, while the chondral region of the graft was formed by the self-organisation of early-cartilage microtissues into a unified and homogenous cartilage. It is hypothesised that implantation of such an engineered plug into an osteochondral defect would result in effective biological joint resurfacing and prevent the deleterious cascade of events that typically follow an untreated OC injury.

7.2 Materials and Methods

Expansion Medium "XPAN". XPAN is composed of high glucose Dulbecco's modified eagle's medium (hgDMEM) GlutaMAX supplemented with 10 % v/v FBS, 100 U/mL penicillin, 100 µg/mL streptomycin (all Gibco, Biosciences, Dublin, Ireland) and 5 ng/mL FGF2 (Prospect Bio).

Chondrogenic Differentiation Medium (CDM). hgDMEM GlutaMAX supplemented with 100 U/mL penicillin, 100 µg/mL streptomycin (both Gibco), 100 µg/mL sodium pyruvate, 40 µg/mL L-proline, 50 µg/mL L-ascorbic acid-2-phosphate, 4.7 µg/mL linoleic acid, 1.5 mg/mL bovine serum albumin, 1 × insulin–transferrin–selenium (ITS), 100 nM dexamethasone (all from Sigma), 2.5 µg/mL amphotericin B and 10 ng/mL of human transforming growth factor- β3 (TGF-β) (Peprotech, UK).

7.2.1 Cell Isolation and Expansion

Goat Fat-pad Stromal Cell (FPSC) Isolation: Under sterile conditions, infrapatellar fat pad (IFP) tissue was diced into approximately 1-2 mm^3 pieces using a scalpel. The tissue was then weighed and subsequently incubated with high glucose DMEM (Gibco) containing 750 U collagenase I (Gibco). For rapid isolation; the tissue was shaken at 2000 RPM at 37 °C for 30 min (Multi Reax Shaker, Heidolph). After digestion, the cell suspension was neutralised with DMEM containing 20 % fetal bovine serum (FBS - Gibco). Insoluble tissue and residual fat were removed and discarded. The remaining cell suspension was passed through a series of cell strainers with decreasing mesh sizes (100 µm, 70 µm and 40 µm (Fisher Scientific)), centrifuged and washed with saline. FPSCs were expanded in physioxic conditions (37 °C in a humidified atmosphere with 5 % CO_2 and 5 % pO_2) until P3.

Goat Chondrocyte (CC) Isolation: Cartilage was harvested from the joint surface under sterile conditions, it was rinsed in saline, weighed, and diced finely. Chondrocytes were isolated by digestion in hgDMEM containing 100 U/mL penicillin, 100 µg/mL streptomycin and 350 U/mL of collagenase type II for 12-14 h with constant rotation at 37 °C. The remaining suspension was passed through a cell filter (40 µm), and the filtrate centrifuged and rinsed with saline. Chondrocytes were expanded in XPAN in physioxic conditions until P2.

Goat Bone Marrow MSC (gBMSC) Isolation: gBMSCs were isolated as previously described in chapter 5. Briefly, marrow pieces were then gently rotated for 5 min in XPAN to help liberate the cellular components. Cells were initially plated at a density of 5.7×10^4 cells/cm^2 and expanded under hypoxic conditions (37 °C in a humidified atmosphere with 5 % CO_2 and 5 % pO_2) for chondrogenic differentiation. Following colony formation, gBMSCs were trypsinised using 0.25 % (w/v) Trypsin Ethylenediaminetetraacetic acid (EDTA). gBMSCs for microtissues were expanded from an initial density of 5000 cells/cm^2 in XPAN medium under physioxic conditions until P3.

7.2.2 Formation of Hypertrophic Cartilage Microtissues

The procedure for fabricating the hydrogel microwell platform and the method of generating microtissues has been described within chapter 3. The same underpinning methodology was employed herein for the formation of stable and hypertrophic cartilage microtissues. gBMSC were seeded into the microwell array to generate cell aggregates containing 4×10^3 cells/microtissue. For the first 24 h, aggregates were cultivated in XPAN medium in physioxic conditions. After 24 h, chondrogenesis was induced using CDM. Cartilage microtissues were formed over 2 weeks of chondrogenic cultivation (CDM and physioxic conditions). Hypertrophic maturation was initiated by switching to hypertrophic medium (HYP), which was composed of hgDMEM GlutaMAX supplemented with 100 U ml -1 penicillin, 100 µg/mL streptomycin (both Gibco), 1 × insulin–transferrin–selenium, 4.7 µg/ml linoleic acid, 50 nM thyroxine, 100 nM dexamethasone, 250 µM ascorbic acid, 7 mM β-glycerophosphate and 2.5 µg/mL amphotericin B (all from Sigma), and culturing in normoxic conditions (37 °C in a humidified atmosphere with 5 % CO_2 and 20 % pO_2) for 1 week.

7.2.3 Biochemical Evaluation

Samples were washed in PBS after retrieval and the number of microtissues within each technical replicate was counted prior to digestion. 3.88 U/mL of papain enzyme in 100mM sodium phosphate buffer/5mM Na2EDTA/10mM Lcysteine, pH 6.5 (all from Sigma–Aldrich), was used to digest the samples at 60 °C for 18 h. Samples intended for calcium quantification were digested using 1 M HCL at 60 °C. Here, samples were deemed digested by the absence of any precipitate within the lysate. DNA content was quantified immediately after digestion *via* papain enzyme using Quant-iT™ PicoGreen ® dsDNA Reagent and Kit (Molecular Probes, Biosciences). The amount of sGAG was determined using the dimethylmethylene blue dye-binding assay (Blyscan, Biocolor Ltd., Northern Ireland), with a chondroitin sulphate standard read using the Synergy HT multi-detection micro-plate reader (BioTek Instruments, Inc) with a wavelength set to 656 nm. Total collagen content was determined using a chloramine-T assay [186] to measure the hydroxyproline content and calculated collagen content using a hydroxyproline-to-collagen ratio of 1:7.69. Briefly, samples were mixed with 38 % HCL (Sigma) and incubated at 110 °C for 18 h to allow hydrolysis to occur. Samples were subsequently dried in a fume hood and the sediment reconstituted in ultra-pure H_2O. 2.82 % (w/v) Chloramine T and 0.05 % (w/v) 4-(Dimethylamino) benzaldehyde (both Sigma) were added and the hydroxyproline content quantified with a trans-4-Hydroxy-L-proline (Fluka analytical) standard using a Synergy HT multi-detection micro-plate reader at a wavelength of 570 nm (BioTek Instruments, Inc). Calcium content was determined using calcium liquid colorimetric assay (Sentinel Diagnostics). The absorbance of each sample was read using a Synergy HT multi-detection micro-plate reader at a wavelength of 570 nm.

7.2.4 Preclinical Evaluation

Fibronectin coating

To improve the integration of the microtissues with the polymer (polycaprolactone, PCL) implant, the surface of the implant was coated with bovine fibronectin (PromCell) using a protocol modified from Liverani *et al.* [265]. Briefly, the PCL implants were immersed in a 3M sodium hydroxide solution (NaOH) and gently agitated for 12-14 h at room temperature to improve the hydrophilicity of the polymer. Similar methods of hydrolysing PCL using NaOH have been demonstrated in electrospun scaffolds, where the exposure of hydroxyl and carboxylic groups on the polymer surface can improve hydropillicity and subsequently protein absorption and biocompatibility [266]. After washing in ultra-pure H_2O, implants were immersed in 0.5M N- (3-Dimethylaminopropyl)-N'-ethylcarbodiimide hydrochloride (EDC) (Sigma) and 0.5M N-Hydroxysuccinimide (NHS) in 0.1M 2-(N-Morpholino)ethanesulfonic acid hemisodium salt (MES) buffer at a ratio of 2:1 (EDC:NHS) for 24 h again with gentle agitation. Implants were rinsed in PBS and immersed in a 50 µg/mL fibronectin solution for 24 h. After functionalisation with fibronectin, implants were rinsed and used immediately for tissue culture.

Implant seeding

As previously described, stable cartilage microtissues were formed at a cell density of 2×10^3 cells per microtissue. To dampen the inherent hypertrophic tendencies of MSCs, a co-culture of FPSC and CCs (3:1) was employed. To ensure that the maximum growth of the cartilage microtissues prior to their bioassembly into a larger macrotissue, the cells aggregated initially in XPAN for the first 4 days, followed by 4 days in CDM (media Condition 1) as developed in chapter 6. Early-cartilage microtissues were cultivated in CDM under physioxic conditions. The capacity to biofabricate an AC *via* the self-organisation of early-cartilage microtissues within a guiding polymer framework has been demonstrated in chapter 6. The same approach was taken within this study to engineer an AC in the chondral region of an osteochondral implant. Briefly, the number of microtissues seeded to create each construct was determined as a function of the microtissue volume and the volume of the final construct. As such, the following equation was used:

$$Number\ of\ microtissues = \frac{Volume\ of\ the\ construct\ \times 0.74}{Volume\ of\ the\ microtissue}$$

Where,

$$Volume\ of\ the\ microtissue = \frac{4}{3}\pi r^3$$

and 0.74 is the packing efficiency, or packing factor. For this study, the volume of the construct chosen was determined using 6 mm diameter and a depth of 1 mm. After seeding the microtissues into the central agarose well on top of the polymer implant, CDM was added slowly to prevent disruption of the microtissues. The developing cartilages were maintained in CDM and physioxic conditioned for 8 weeks. Media was exchanged every 2-3 days. 24 h before implantation, hypertrophic microtissues were harvested and seeded into the bone region of the implant within a fibrin hydrogel (30 mg/mL).

Surgical Procedure

All animal experiments were approved by the University College Dublin Animal Research Ethics Committee (Approval number – AREC 12-74) and the Irish Health Products Regulatory Authority (Approval number - AE18982/P032). Surgery was performed on skeletally mature female Saanen goats. Goats were sedated using diazepam (0.3–0 0.4 mg/kg IV) and butorphanol (0.2 mg/kg IV). An epidural was administered using morphine (0.2 mg/kg). Anaesthesia was induced with propofol (max. dose 4 mg/kg IV) and maintained with isoflurane. Goats were placed in dorsal recumbency and an arthrotomy of each stifle joint was then performed using the lateral para-patellar approach. Bi-lateral surgery was performed on all animals. 6 mm diameter by 6 mm deep osteochondral defects were created in the femoral trochlear groove using a 6mm drill. In the treatment group, this defect was populated with the engineered osteochondral plug, facilitating the implantation of the self-organised AC. Briefly, the polymer component of hybrid osteochondral implant was a biodegradable, 3D printed framework fabricated using polycaprolactone (PCL, Perstop). The chondral portion of the implant had similar features to those that had previously been shown as an effective means of guiding the self-organisation of microtissues (Chapter 6). The osseous region was a lattice structure with large internal and external porosity. The diameter of the implant was designed so the device could be push-fit into the defect. Following routine closure of the joint capsule, subcutaneous tissues and skin with sutures, Carprofen (1.5–2.5 mg/kg subcutaneously) was administered for analgesia. Following surgery, goats were housed in indoor pens and were allowed full weight bearing immediately. NSAIDs and antibiotics Amoxicillin (Noroclav) were administered for 5 days post-surgery. Two weeks post-operatively, following removal of sutures, animals were released to pasture for the remainder of the study period. Tissue repair was evaluated at 6 months post-surgery.

Evaluation of the Repair Tissue

After 6 months, biopsies containing the entire defect site were harvested. Before fixation, gross morphological images were taken using a stereomicroscope (Olympus) for macroscopic evaluation. Macroscopic images were blinded, randomised, and subsequently scored by expert reviewers using

a previously described macroscopic scoring system [267,268]. This macroscopic scoring system evaluates the edge integration of the scaffold with the native tissue, the smoothness of the cartilage surface, the degree of defect filling and the colour/opacity of the neo-cartilage in the defect.

7.2.5 Histological Evaluation

In vitro

Samples were fixed using 4 % paraformaldehyde (PFA) solution overnight at 4 °C. After fixation, samples were dehydrated in a graded series of ethanol solutions (70 % - 100 %), cleared in xylene, and embedded in paraffin wax (all Sigma-Alrich). Prior to staining tissue sections (5 µm) were rehydrated. Sections were stained with hematoxylin and eosin (H&E), 1 % (w/v) alcian blue 8GX in 0.1 M hydrochloric acid (HCL) (AB) to visualise sulphated glycosaminoglycan (sGAG) content and counter-stained with 0.1 % (w/v) nuclear fast red to determine cellular distribution, 0.1 % (w/v) picrosirius red (PSR) to visualise collagen deposition, and 1 % (w/v) alizarin red (pH 4.1) to determine mineral deposition via calcium staining (all from Sigma-Aldrich). Stained sections were imaged using an Aperio ScanScope slide scanner.

In vivo

Prior to histological processing, samples were fixed in 10% neutral buffered formalin solution (Sigma) for 72 h with gentle agitation. Samples were then decalcified with Decalcifying solution lite (Sigma) until all mineral was removed, which was confirmed by X-ray analysis. Demineralized wax-embedded constructs were sectioned at 10µm and stained with Goldner's Trichrome, picrosirius red stain and safranin-O. Histological scoring was performed using a modified ICRS II scoring system [269].

Immunohistochemistry

Immunohistochemistry was performed for collagen type I (Abcam ab90395 1:400), collagen type II (Santa Cruz sc52658 1:400), and collagen type X (Abcam ab49945 1:200) as previously described [165].

7.2.6 Micro-computed tomography (µCT)

Micro-computed tomography (µCT) scan were performed using a Scanco Medical 40 µCT system (Scanco Medical, Bassersdorf, Switzerland) in order to visualise bone formation within the defect after 6 months. Sampes were scanned in 50% EtOH, at a voxel resolution of 12µm, a voltage of 70 kVp, a current of 114 µA. Reconstructed 3D images and planar X-rays were generated using Dragonfly 3D visualisation and analysis software.

7.2.7 Image Quantification & Statistical analysis

Diameter measurement of growing microtissues, and engineered macrotissues were taken from microscope images (4x) using ImageJ software. Statistical analysis was performed using GraphPad Prism software (GraphPad Software, CA, USA). Analysis of differences between two groups at one timepoint was done using a standard two-tailed t-test. For two groups over multiple time-points, a one-way analysis of variance (ANOVA) was performed. Numerical and graphical results are presented as mean ± standard deviation unless stated otherwise. Significance was determined when $p < 0.05$.

7.3 Results

7.3.1 Forming Bone Precursors using Hypertrophic Cartilage Microtissues

The biofabrication of an osteochondral graft requires the development of distinct implant regions capable of supporting either articular cartilage or subchondral bone regeneration. Motivated by the observation that engineered hypertrophic cartilage can be used as a developmentally inspired template to support endochondral bone formation [52,54,211,274], this study first sought to engineer the osseous region of an osteochondral implant with a population of bone precursor microtissues. As such, this study evaluated if the microwell platform developed previously could facilitate the hypertrophic maturation of cartilage microtissues (Figure 7.1A). Over the 3 weeks of culture, where cells were either continuously exposed to a chondrogenic media supplemented with TGF-β_3 (CDM), or 2 weeks of exposure to CDM followed by 1 week of hypertrophic media (HYP). Greater increases in microtissue diameter were observed in the HYP group (Figure 7.2B). Hypertrophic maturation of microtissues exposed to HYP stimulation was confirmed histologically and biochemically (Figure 7.1C & D). Histologically, both CDM and HYP groups stained positively for canonical markers of cartilage, specifically sGAG and collagen, whereas only microtissues exposed to HYP conditions displayed diffuse mineralisation throughout the cartilaginous matrix, indicative of a hypertrophic cartilage phenotype (Figure 2Cii). These observations were confirmed biochemically, with significantly higher levels of calcium, sGAG and collagen content measured within the hypertrophic microtissues (Figure 2D).

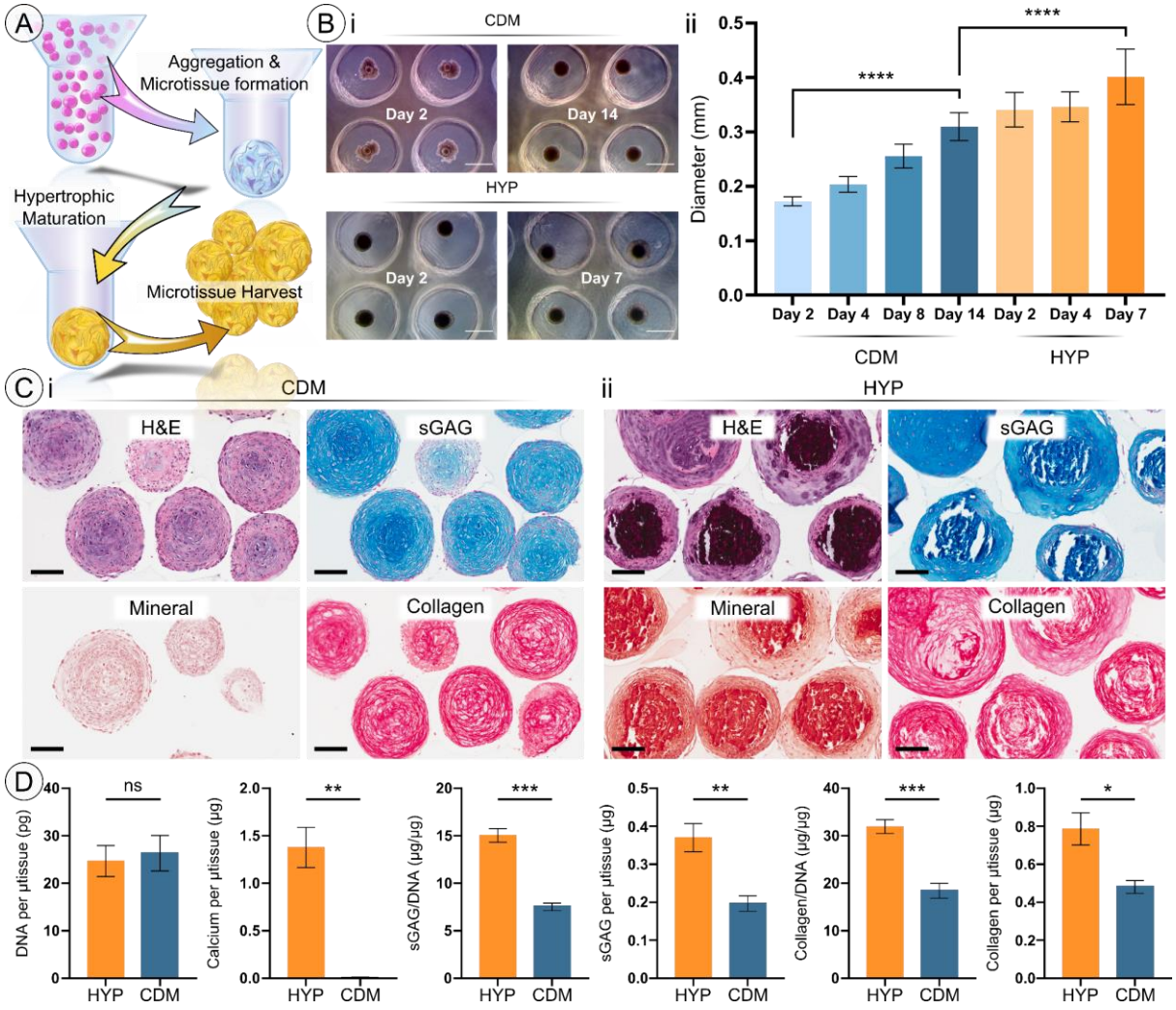

Figure 7.1 *Engineering hypertrophic cartilage microtissues as bone precursors. A) Schematic timeline for the generation of hypertrophic cartilage microtissues within a hydrogel microwell platform. Bi) Microscopic images of hypertrophic cartilage microtissues during cultivation. (Scale Bar = 500 µm). ii) Diameter measurements through cartilage microtissue generation and hypertrophic maturation. * Denotes significance when tested using a Brown-Forsythe and Welch One-way ANOVA, $p < 0.05$ (N = 24, Mean ± SD). C) Histological evaluation of microtissues after 21 days of culture in either a control chondrogenic regime (i) or hypertrophic regime (ii). (Scale Bar = 100 µm). D) Biochemical evaluation of hypertrophic cartilage microtissues compared to a control of standard cartilage microtissues after 21 days of cultivation. * Denotes significance when tested using a two-tailed, unpaired Welch's t-test, $p < 0.05$ (N = 3, Mean ± SD).*

7.3.2 *Bioassembly of an Osteochondral Plug using Phenotypically Distinct Cartilage Microtissues as Biological Building Blocks*

Biofabrication of an osteochondral plug involved spatially localising the two phenotypically distinct cartilage microtissues engineered within a single 3D printed framework. The framework retained design features which proved effective in guiding the zonal organisation of the stable cartilage layer, while the bone region offered lateral porosity to encourage vascular infiltration and the conversion of the hypertrophic cartilage microtissues into bone (Figure 7.2A). Prior to implantation, and having established the stable apical chondral layer, the hypertrophic cartilage microtissues were backfilled into the osseous region of implant within a carrier fibrin hydrogel. Macroscopically, the discrete islands of hypertrophic cartilage could be seen within the osseous region, subjacent to a continuous layer of stable cartilage (Figure 7.2A). Histological evaluation of the final implant clearly demonstrated the two distinct phases, with suitable ECM profiles for the chondral and osseous regions. Macroscopic images from implantation of the engineered plug into a large animal pre-

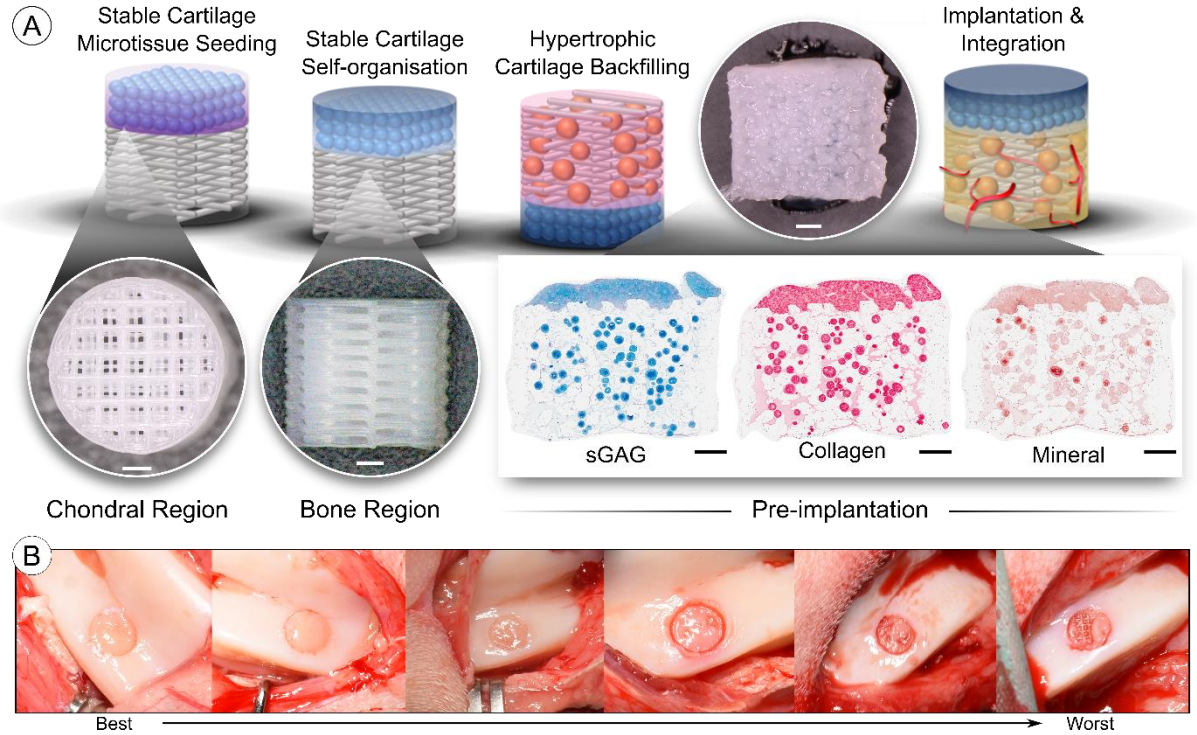

Figure 7.2 *Biofabrication strategy for creating a biphasic osteochondral plug using two phenotypically distinct microtissue populations as cellular building blocks. A) Timeline schematic showing macroscopic and histological images of a representative implant at each stage. From left to right, first stable cartilage microtissues are seeded into the chondral region of the implant. This cartilage is then cultured chondrogenically to engineer a competent articular surface. Prior to implantation, hypertrophic cartilage microtissues are backfilled into the implant. Histologically, two distinct layers are apparent. Both the self-organised apical cartilage and the hypertrophic microtissue units exhibited a cartilaginous matrix. Importantly, mineralisation was only present in the hypertrophic cartilage microtissues situated within the bone region of the implant B) Six macroscopic images at implantation, ranked from best to worse, demonstrating that in the majority of cases the implant provided immediate joint resurfacing. (Scale bar = 1 mm)*

clinical model indicated that in the majority of cases, the engineered AC provided immediate joint resurfacing (Figure 7.2B). In these cases, the apical cartilage of the engineered plugs resembled the surrounding native articular cartilage at the defect site.

7.3.3 Regeneration of Caprine Osteochondral Defects using Tissue Engineered Implants

After 6 months, macroscopic evaluation of the defect site indicated a trend towards an improved healing response in defects treated with the engineered implant ('treatment' group) compared to the empty control. Moreover, treatment using the engineered implant appeared to result in a more consistent healing response (SD = 0.321 vs. 0.592, for treatment and empty respectively) (Figure 7.3).

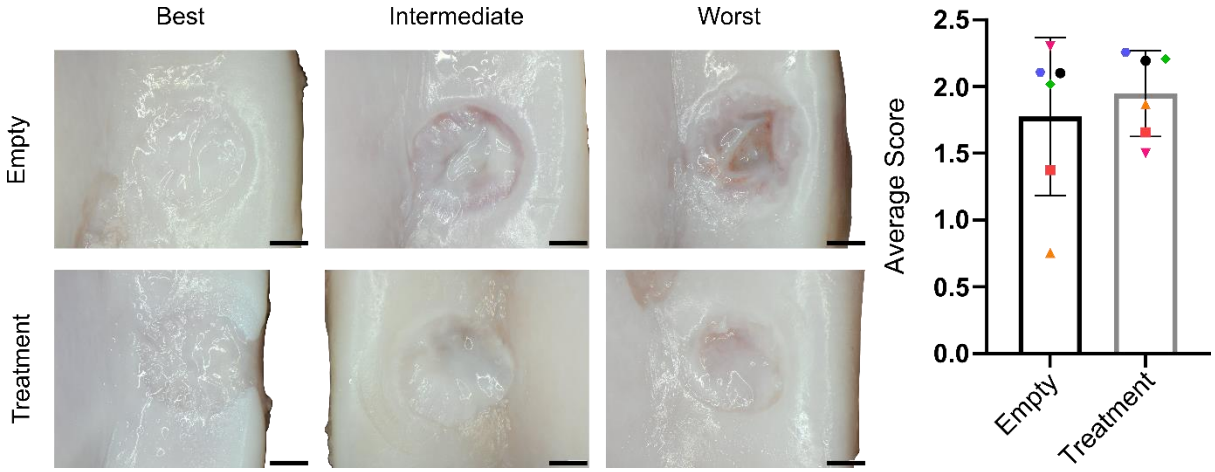

Figure 7.3 *Macroscopic evaluation of the healing response. Panel of the best, intermediate, and worst cases for empty and treatment groups, and graphical representation of macroscopic scoring. Ranks determined from quantification of the macroscopic defect appearance after 6 months. (Scale Bar = 2 mm) (N = 6, Mean ± SD)*

Histological scoring of the repair tissue indicated trends towards improved healing in the treatment group across all metrics (Figure 7.4). From this histological quantification, 'best', 'intermediate', and 'worst' cases of healing in different animals were identified from the empty and treatment groups. Within the empty group, histological sections showed that the articular surface was not restored in any animal (Figure 7.5). Instead, the defect filled with a fibrous repair tissue in both the cartilage and bone regions in all cases. In contrast, the treatment appeared to result in partial-to-full restoration of the joint surface with a near-normal articular tissue (Figure 7.6). In particular, a smooth and congruent articular surface can be seen in the best treatment group. The repair tissue formed within the chondral region was rich in collagen and histologically appeared similar to the surrounding native articular cartilage, although the repair tissue appeared to stain less intensely for sGAG compared to surrounding undamaged articular cartilage. The subchondral bone plate was re-established in this animal, which correlated with what appeared to be a marginal subsidence of the implant. Moreover, evidence of new bone formation in and around the osseous

region of the osteochondral implant was evident. In the intermediate repair group, the repair tissue in the chondral region of the defect was also congruent surface with the native AC. Again, the tissue was rich in collagen, but stained less intensely for sGAG.

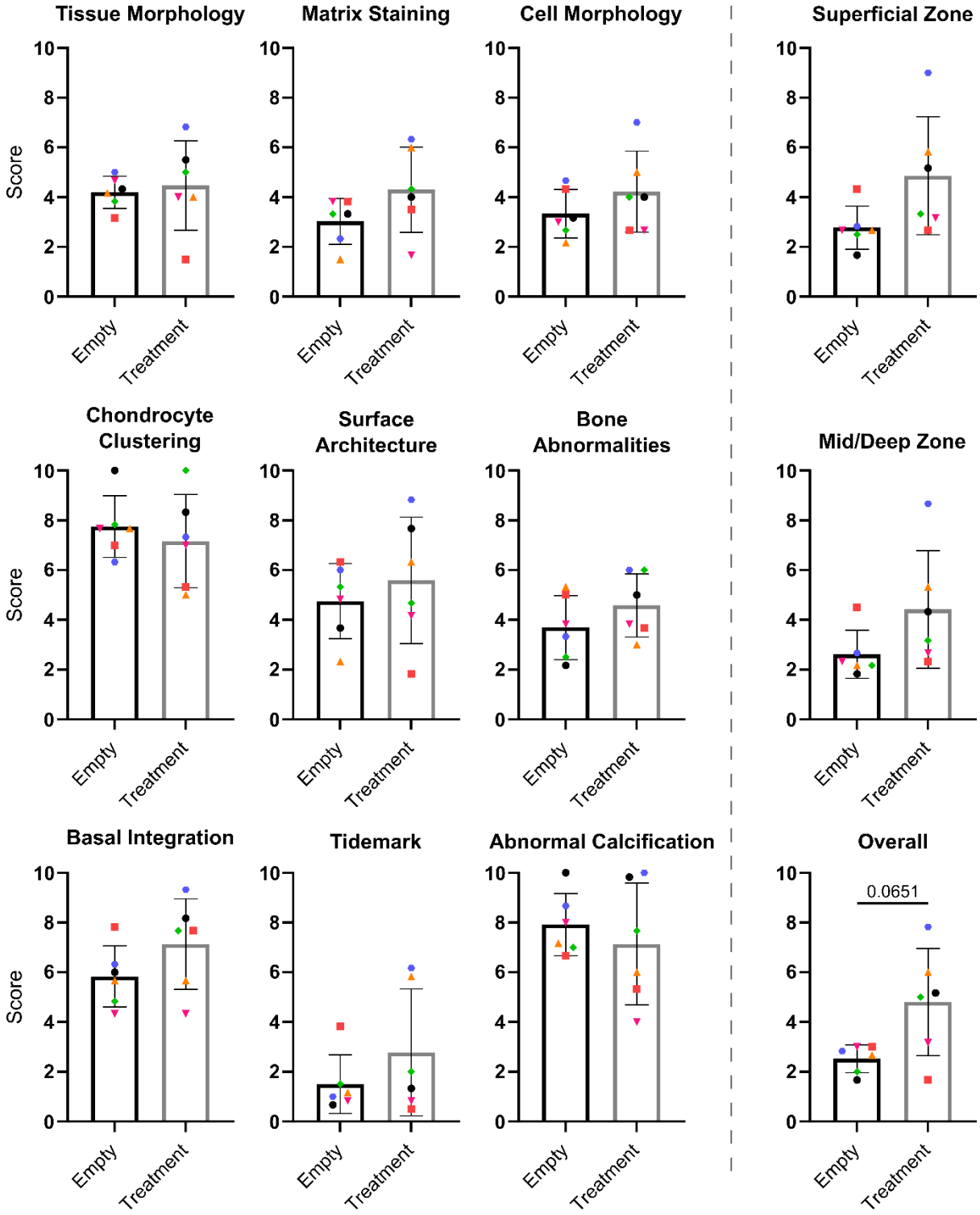

Figure 7.4 *Treatment of an osteochondral defect with an engineered osteochondral plug shows trends towards an improved healing response. Graphical representation of histological scores after 6 month in vivo. Internal controls are represented by data points with matching colour and symbol. (N = 6, Mean ± SD) Statistical differences determined using a paired t-test.*

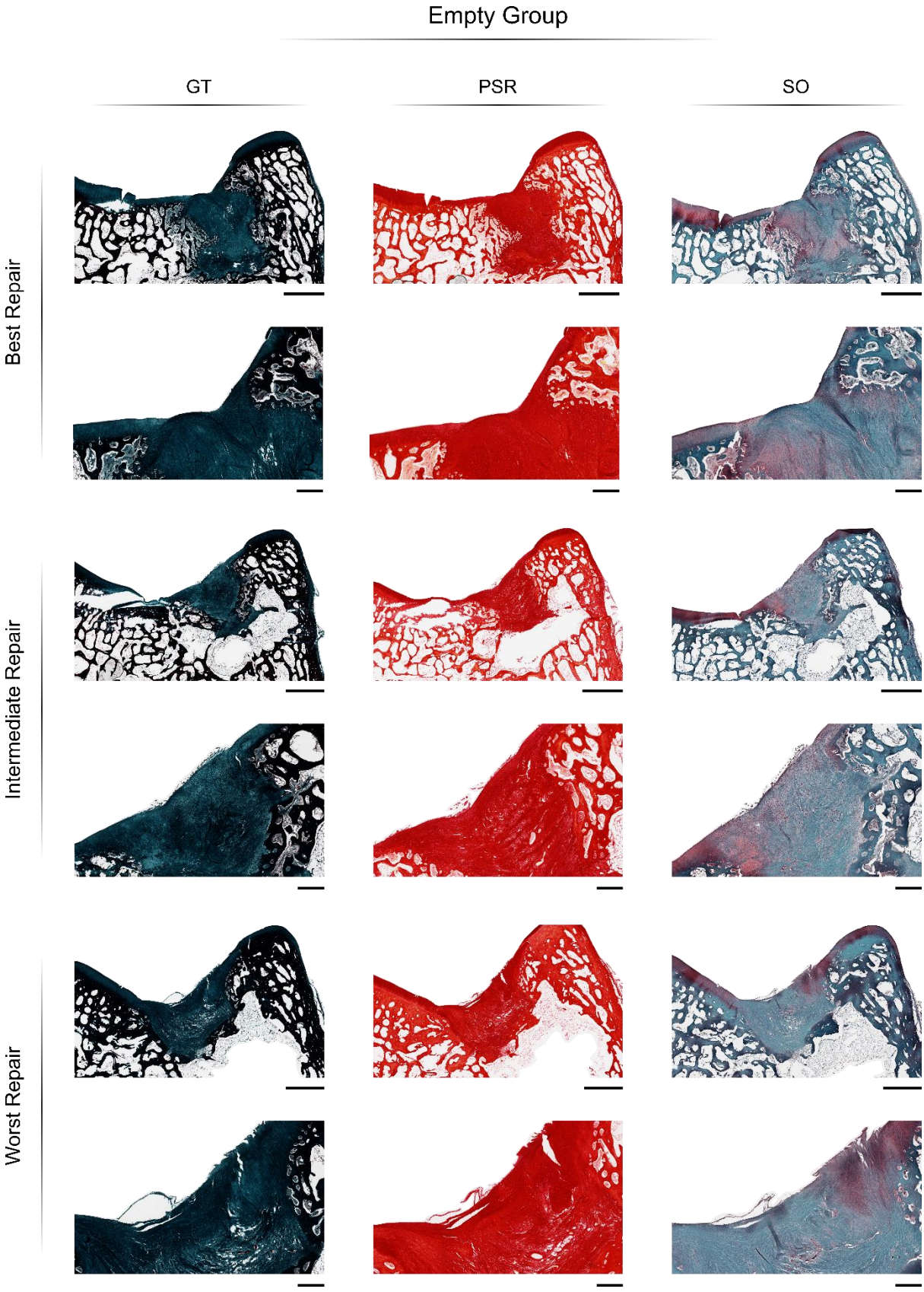

Figure 7.5 *Histological evaluation of; 'best', 'intermediate', and 'worst' healing responses in empty osteochondral defects, as determined from histological scoring. Goldners trichrome (GT), Picrosirius red (PSR), and Safranin-O (SO) staining provided. (Scale Bars; Overview = 2 mm, Zoom = 500 µm)*

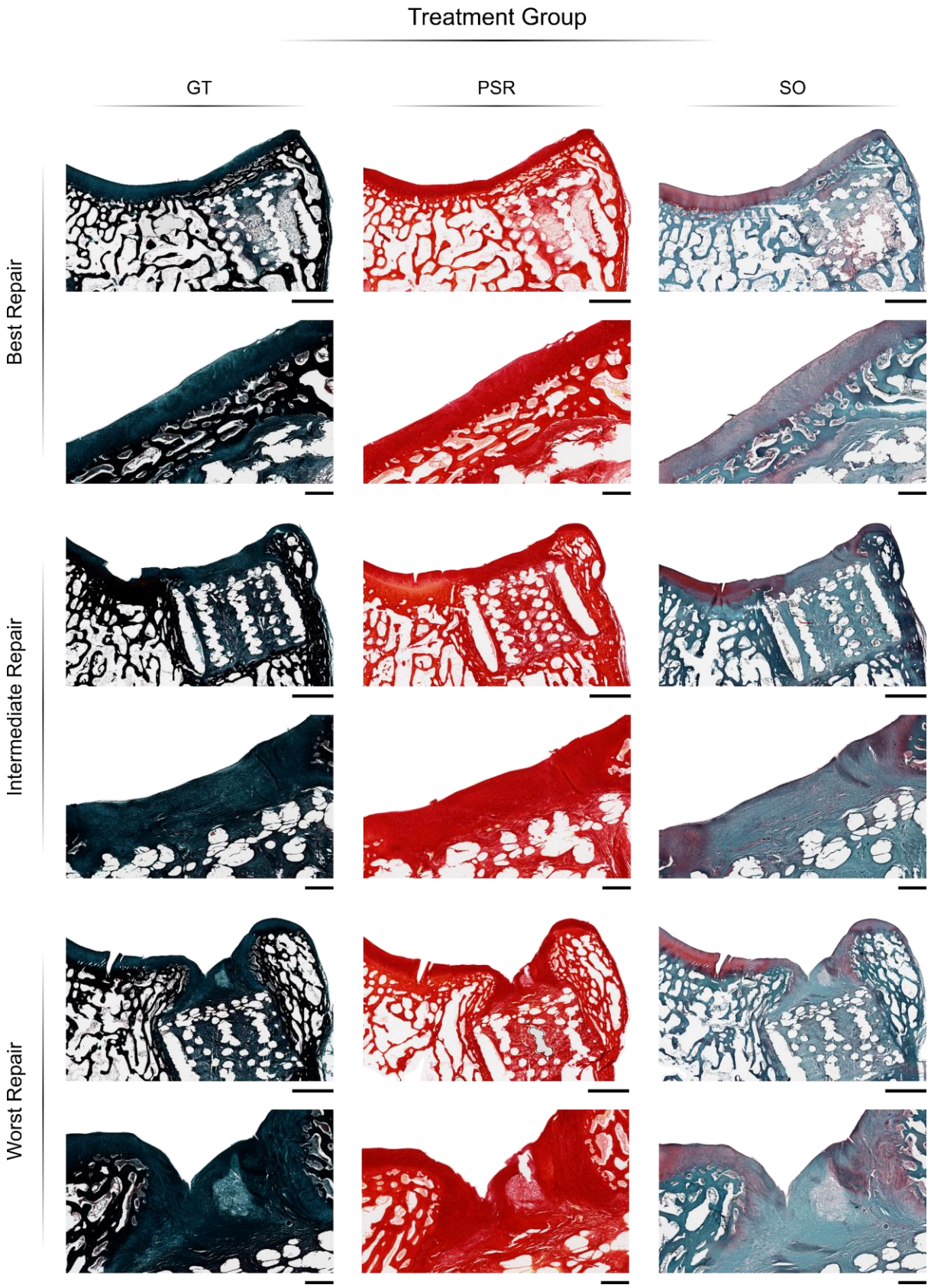

Figure 7.6 *Histological evaluation of; 'best', 'intermediate', and 'worst' healing responses in osteochondral defects treated using an engineered osteochondral plug, as determined from histological scoring. Goldners trichrome (GT), Picrosirius red (PSR), and Safranin-O (SO) staining provided. (Scale Bars; Overview = 2 mm, Zoom = 500 µm)*

Histologically, the repair tissue in this case appeared inferior to that seen in the best case, resembling fibrocartilage at the margins of the defect and fibrous tissue more centrally. Evidence of spicules of bone formation within the osseous region of the implant were seen histologically, although fibrous tissue was also noted in the bone region. In the worst case, the implant had subsided drastically into the subchondral bone. As such, the defect appeared unstable and closely resembled those seen in the untreated groups. Here, the chondral repair tissue was fibrotic and failed to resurface the defect. Moreover, deterioration of the surrounding native AC, as seen in the

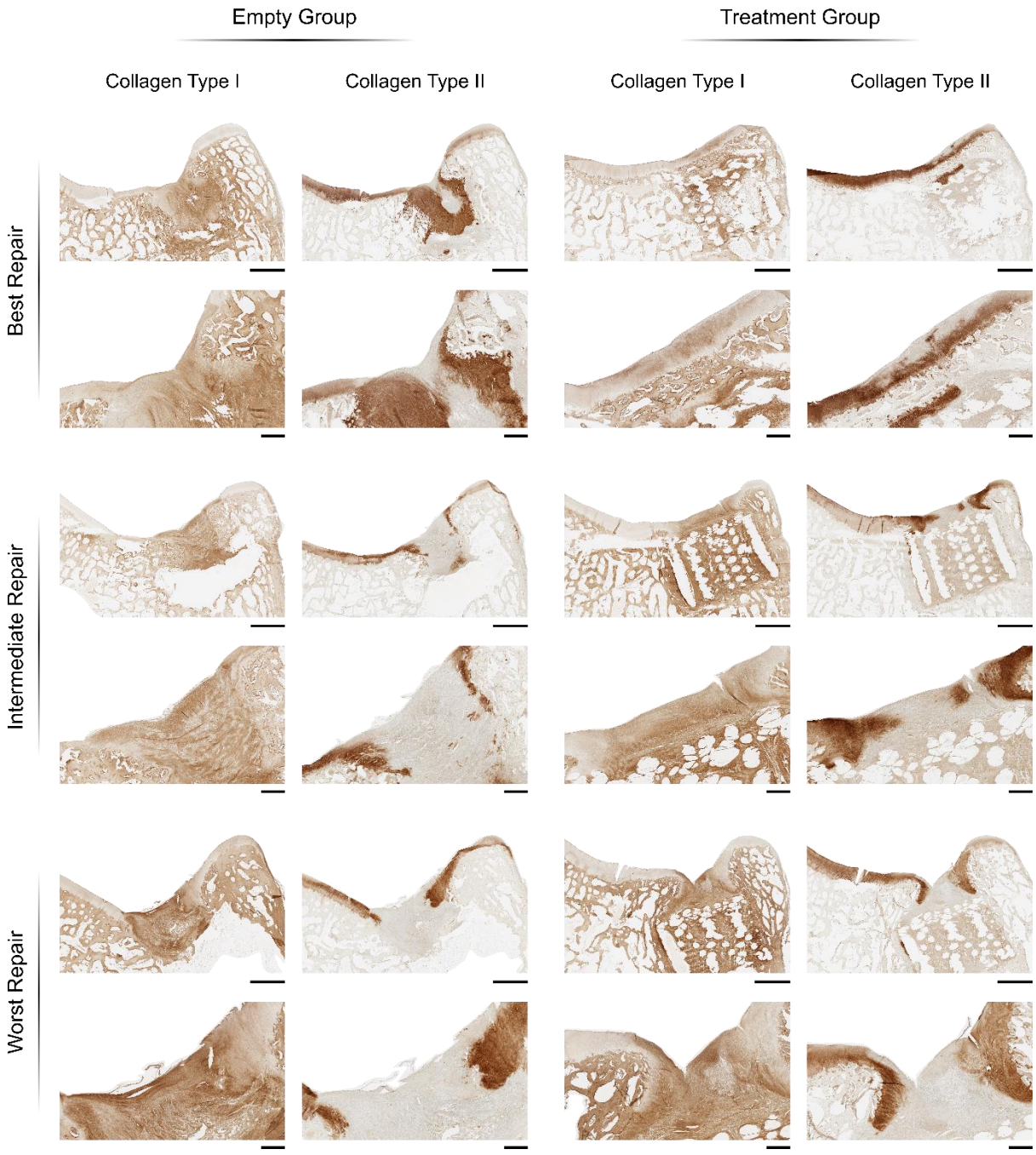

Figure 7.7 *Immunohistological panel for the 'Best', 'Intermediate', and 'Worst' repair response in the empty and treatment groups. Staining for collagen types I and II. Ranking was determined from the histological scoring. (Scale Bars; Overview = 2 mm, Zoom = 500 µm)*

empty defects was also apparent within the worst treatment case. Immunohistochemistry identified positive collagen type II staining in the chondral region of the treatment group, whereas accurate localisation of collagen type II was not detected in any of the empty cases. As expected, collagen type I was present in all groups within the bone region (Figure 7.7).

7.3.4 Defect Stabalistation through Osteointegration of the Implant

3D µCT reconstructions and planar X-ray images were used to visualise the bony repair/remodelling in the defect site after 6 months (Figure 7.8). Empty defects followed an irregular healing response, whereby no correlation between subchondral bone and articular cartilage regeneration is apparent. Generally, large asymetrical vacancies remain in the bone and, in most cases, the defect becomes larger over time. In contrast, treatment appeared to encourage bone ingrowth within the osseous phase of the implant, with bony protusions visable into and around the 3D printed framework. The exception to this was the worst case, where there was no evidence of bone ingrowth into the implant. In the absence of any bony fixation, the implant has subsided into the subchondral bone and the destablaised defect bears resemblance to an equivalent empty.

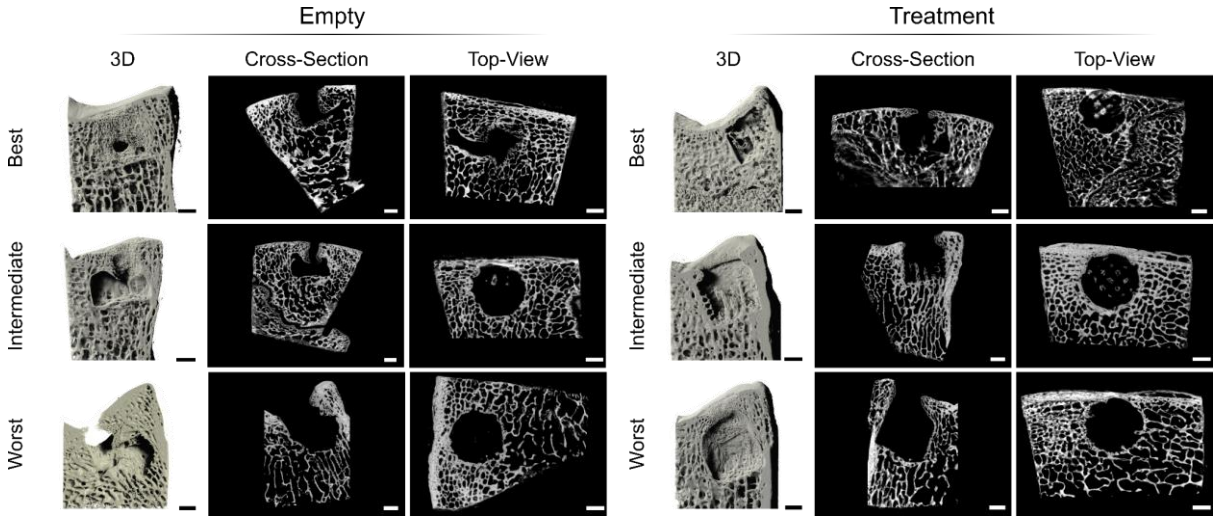

Figure 7.8 *µCT panel for 'Best', 'Intermediate' and 'Worst' repair responses for empty and treatment groups. 3D reconstructions and X-ray images to visualise bone formation within the defect site (Scale Bar = 2 mm)*

7.4 Discussion

As a means of creating a biphasic osteochondral implant, this study leveraged two phenotypically distinct cartilage microtissue populations as biological building blocks. Having previously demonstrated the capacity to engineer early-cartilage microtissues using a hydrogel microwell platform, this work first sought to create hypertrophic cartilage microtissues as rudiments for bone formation using the same platform. Microtissues that exhibited a rich, mineralised cartilage matrix were formed over 21 days of cultivation in hypertrophic culture conditions. This hypertrophic phenotype was primarily a result of the culture regime employed, and not just the inherent instability of chondrogenically differentiated bMSCs in culture. Importantly, engineering the hypertrophic cartilage microtissues required for the bone region, did not directly influence the formation of a stable cartilage phenotype in the chondral region of the implant. This was due to the modular biofabrication strategy employed. Specifically, by using microtissues as building blocks for engineering a larger tissue/organ precursors, it facilitated the creation of two distinct tissues within a single implant. Achieving a similar biphasic construct using non-modular tissue engineering approaches is challenging due to conflicting needs of the constituent tissues. In this way, modular bioassembly could lead to higher-quality engineered implants by removing the interdependence between the components of a hybrid implant, and allowing individual tissue-units to be developed and optimised separately before being combined in the final implant [74]. This study successfully leveraged this model to create individually optimised conditions for engineering a homogenous AC (chapter 6) as well as bone-precursor microtissues. Others have utilised a similar high-throughput modular approach of creating bone and cartilage microtissues, as a means of avoiding the use of an isotropic or cocktail induction media, for engineering a continuous scaffold-free osteochondral tissue [142]. At present, without the use of microtissues or an osteochondral media cocktail, engineering a unified biphasic tissue obligates the use of complex custom-made dual-chamber bioreactors. Such approaches typically involve creating a hermetic seal that prevents media mixing and realises effective simultaneous chondrogenic and osteogenic differentiation of a single stem cell population is challenging [277–281]. However, it should be noted that in spite of the challenges, spatiotemporal exposure of a developing scaffold-free cartilage to physiologically inspired soluble cues within a dual-well system has been demonstrated as a successful way of engineering a stable and biomimetic AC [46]. As such, developing systems capable of bringing together phenotypically distinct cartilage populations, maintaining lineage commitment, whilst encouraging cross-talk between the two tissue cohorts as a means of recapitulating the fluid stratification seen within native osteochondral tissue, is an interesting prospect for the future. Nevertheless, microtissues currently represent a logical method for generating biphasic osteochondral implants, where two phenotypically discrete engineered tissues are required within a single construct. This study successfully implemented a modular biofabrication strategy founded on the generation of two,

independently optimised, tissue-specific microtissue populations. The first of which was intended as biological building blocks for the self-organisation of a stable AC for immediate joint resurfacing, and the second cohort, were developmentally inspired organ-seeds intended for bone regeneration.

In this work, a novel bioassembly strategy for engineering an osteochondral implant was established. This strategy resulted in the fabrication a biphasic construct, consisting of engineered AC overlying an osseous region containing islands of hypertrophic cartilage microtissues. Despite this relative success, at the end of the in vitro culture period, some sample-to-sample variability in the consistency of engineered cartilage layer was observed. Tissue fusion is a collective term used to describe a number of events that take place during native organogenesis, and is a process whereby two initially discrete cellular/tissue-units fuse together and remodel to form a union[83]. Although in the context of tissue engineering, self-organisation describes an open system where order within the tissue appears from the input of external forces/energy, it is still governed by the laws of thermodynamics [81]. As such, the process will tend towards the lowest energy state. In the context of this study, after initial bioassembly, the self-organisation process within the chondral layer was allowed to progress with no further manipulation or constraint (addition of energy). Consequently, the variation seen in the self-organised apical cartilage could be due to the cells within the system organising to minimise free energy. Specifically, in some cases it appears the boundary conditions provided (input energy to direct organisation) by the polymer framework have not been sufficient to effectively guide the process towards an uninterrupted tissue. In these cases, the tissue has pulled from the framework, as a means of minimising the energy within the system, creating a discontinuous surface. Although this was not the case in the majority of implants, and the bioassembly strategy appears to have been relatively successful, the inconsistency within the small cohort of implants indicates there is still room for improvement. To this end, the manual nature of the bioassembly process could be a major contributor to the observed variation, and emphasises the need to establish biofabrication strategies which combine automated systems (bioprinting) and spheroidal self-organisation. Examples where bioprinting and spheroidal biofabrication strategies have been successfully married have been demonstrated in the literature [82,120,146,236,282]. It is easy to envisage how precise spatial positioning of an exact number of microtissues using a technology such as aspiration assisted bioprinting [282] or fluidic-based singularisation [120] could greatly improve reliability of the biofabrication process designed as part of this study and ultimately the therapeutic efficacy of self-organised implants developed here.

After 6 months *in vivo*, treatment using an engineered osteochondral implant resulted in the restoration of a near-normal articular surface. Furthermore, trends towards an improved healing response was determined in almost all the metrics evaluated. It appeared that by leveraging

an osteochondral approach in this study, despite concerns associated with iatrogenic damage to the subchondral bone [10,11,19,283], yielded a more consistent and predictable healing response compared to a chondral only treatment strategy that has been previously attempted in this thesis. In particular, robust osseous integration with an osteochondral implant, and by extension stabilisation of the defect, appears to be central to achieving this level of chondral repair. The observations made in this study suggest that subsidence of the implant within a defect can greatly influence the level of chondral repair. For example, in the best healing case the implant appeared slightly recessed from the articular surface as originally intended, whereas in the worst case severe subsidence had occurred. Although it is difficult to know the contribution towards healing the engineered AC provided in the best-case scenario, it appears that the greatest healing is coupled with the complete regeneration of the subchondral bone plate. In this vein, failure to regenerate chondral lesions has been linked with an absence of an intact subchondral bed [284]. Furthermore, it has been demonstrated in a critically-sized osteochondral defect in a small animal model that a "flow like" migration of the surrounding native subchondral bone into the defect site, over an implanted scaffold, underpinned the restoration of the articular surface [285]. It was demonstrated that it took 1 year for the native subchondral bone to migrate inwards from the margins of the defect and cover the scaffold. Importantly, this complete restoration of the subchondral bone plate was highly correlated to the quality of the repair AC. This led the authors to propose the following as a mechanism for osteochondral repair. Mechanical stimulation present within the articulating joint encouraged the migration of the surrounding subchondral bone into the defect converting a native *in situ* repair cartilage into bone *via* an endochondral pathway. Over time, the cues present within the joint led to the maturation of this bone which in turn supported and protected the formation of a new AC. The pathway of generation of this AC was unclear, with the authors hypothesising that it arose from the maturation of the initial repair cartilage, or the migration of surrounding neighbouring native AC into the defect. Fundamentally, as the reinstated subchondral bone matured further, its mechanical competency prevents secondary changes in the bone surrounding the defect and the uncontrolled deterioration regularly seen in untreated critically-sized defects [285]. These findings, coupled with the observations made in this study, allows for speculation that successful restoration of the articular surface with a native-like AC starts from the bone, although further mechanistic studies would be needed to elucidate this. In the absence of a more osteoinductive/osteogenic biomaterial within the osseous region of the implant, hypertrophic cartilage microtissues were employed as an endochondral template to encourage bone formation and implant fixation. Similar cartilage templates within unmodified PCL frameworks have been used to generate *de novo* bone ectopically [211]. Moreover, hypertrophic microtissues undergo rapid and extensive mineralisation *in vivo* [286], indicating their suitability as a bone precursor. Alternatively, 3D printable bioceramics have shown great potential for stimulating

orthotopic bone formation [287,288]. Additionally, these materials have been co-printed with PCL to form osteochondral constructs [289]. However, the high solubility of the brushite is concerning for prolonged chondrogenic culture, whereby the release of osteogenic minerals (CaP) could significantly compromise the quality and stability of an engineered articular cartilage. Nevertheless, the results from this chapter and the findings of others, suggest that subchondral bone plays a key role in the regeneration of the articular surface in osteochondral defects. Leveraging early and robust osteointegration of an engineered implant, to strategically position it as a bridge/platform to reinstate the subchondral bone plate, facilitate the regeneration of a native AC and restoration of the articular surface is emerging as a viable treatment plan. To this end, work in this chapter helps to establish the bioassembly of cohorts of phenotypically distinct cartilage microtissues as a promising method for realising this strategy.

7.5 Conclusion

This chapter demonstrates that implantation of an engineered biphasic osteochondral plug, composed of two phenotypically distinct, developmentally inspired engineered tissues, can result in the immediate joint resurfacing, contribute towards defect stabilisation and aid in joint restoration. Although further optimisation is required to improve the consistency of this modular bioassembly strategy, the data presented in this chapter supports further exploration of this approach for the treatment of osteochondral defects. Furthermore, when coupled with emerging developments in bioprinting, and further work elucidating mechanisms of action in damaged and diseased joints, suggests that a similar approach could realise complete biological joint resurfacing in the future.

Chapter 8.
8 Discussion

In this thesis, two different biofabrication approaches were explored as means of engineering developmentally inspired and biomimetic cartilages. The first used inkjet bioprinting and a novel scaffold assembly for directed cellular self-organisation. Specifically, a 3D printed polymer framework was used to impose boundary conditions onto a developing cartilage. Through this constraint, it was possible to guide the self-organisation of bioprinted MSCs, and generate near-native spatial organisation within the collagen network of the engineered articular cartilage. Additionally, this work demonstrated that employing dynamic culture conditions could enhance the quality of this *in vitro* cartilage and yield a tissue with a biomimetic composition and matrix stratification. The second biofabrication strategy employed in this thesis was the use of microtissues as biological building blocks. Here, a 3D printed scaffold functioned to guide the fusion and (re)modelling of the cartilage microtissues, resulting in the development of a biomimetic cartilage. This approach formed the basis of tissue engineering strategies that were used to treat chondral and osteochondral defects in preclinical large animal models. Collectively, this work demonstrated how developmentally inspired engineered cartilages can be effective merged with a supporting and instructing 3D printed polymer scaffold. In doing so, this thesis highlights the potential for modular, hybrid biofabrication strategies to generate complex, functional, and highly-biomimetic implants for musculoskeletal regeneration.

Inkjet printing of structurally organised articular cartilage

Creating engineered analogues of native articular cartilage is challenging. Although recreation of an appropriate ECM composition is frequently reported, recapitulation of the zonal arrangement of these matrix components, in particular the unique collagen architecture seen in native hyaline cartilage, remains a challenge [42,45,47]. Complete biomimicry of articular cartilage's composition and structure is central to designing effective treatment strategies [201]. Previous attempts that have come close to this have centred on self-assembly/self-organisation and have been successful in recreating some, but not all, of the necessary tissue features [41,68,115]. In particular, generating tissues of clinically relevant thicknesses and/or fully mirror the 'Benninghoff arcade' structures remains elusive. To address some of these challenges, this thesis used instructive physical cues, provided by 3D printed constraints, to direct cellular self-organisation and the generation of highly-biomimetic tissues [73]. As such, this work has created a biofabrication strategy/platform to bioprint highly-biomimetic hyaline cartilage. As part of this chapter, the effect of varying initial cell

density was observed in terms of matrix accumulation and organisation. Tissue engineering has trialled a vast range of initial seeding densities ranging from 10 – 130 million cells/mL [290]. In young native articular cartilage, the cell density typically varies with depth from 240 – 100 million cells/mL superficial to deep [290]. In the context of this work, the printed cell densities were 145 and 290 million cells/mL for the low-density (50×10^3 cells/microwell) and high-density (100×10^3 cells/microwell) groups respectively. Given that superior cartilage was engineered using more than double those typically employed in tissue engineering indicates that this novel, highly cellular self-organisation biofabrication strategy represents a significant development in the field. Despite this, the study was not without its limitations. The differentiation potential of hMSCs is known to diminish with donor age and the progression of joint disease [291–293], as well as with increased passage numbers during expansion [294]. As such, the feasibility of recreating the quality of tissue seen using young porcine-derived BMSCs in this study with clinically relevant human cells remains unclear. To combat the challenges associated with limited clonogenic and chondrogenic capacity of MSCs, new progenitor cell sources from synovial joints are being explored [135]. In particular, a putative source of cartilage progenitor cells have been identified in the superficial zone of articular cartilage and have been shown to respond to chondral injury [295–297]. Articular cartilage progenitor cells (APCs) have the potential to revolutionise cartilage tissue engineering by generating exceptional engineered cartilages after prolonged expansion [136], making them an ideal candidate for highly cellular strategies like the one employed in study.

Near-native levels of collagen organisation were demonstrated using the novel biofabrication approach presented in chapter 4. The impact of the enhanced biomimicry exhibited in the engineered cartilage on its biomechanical properties is also unclear. There have been reports that by confining a developing self-assembled cartilage, the spatial alignment of collagen fibres can be altered and a concomitant increase in collagen content and mechanical strength is achievable [78]. It is reasonable to envisage that similar results could be seen in the self-organised cartilage formed in this study. However, determining a method for creating a 'homogeneous collagen' control as well as effectively decoupling the contribution of the polymer framework would be necessary to fully elucidate this. Other methods to improve the biomechanical properties of engineered cartilages have focused on shifting the ratio of sGAG to collagen to favour a more collagen rich tissues. Native articular cartilage is predominantly collagen [2], however, as this thesis has identified reaching these levels *in vitro* is challenging. Promising methods to match these levels of collagen content and maturity use enzymatic treatment [45,50,117]. In the context of this work, coupling the use of remodelling enzymes with the biofabrication strategy for imparting biomimetic spatial collagen organisation will be an interesting avenue for the future. Despite some shortcomings, the work presented in chapter 4 successfully identified a biofabrication strategy for

effectively capturing key compositional and structural features of native articular cartilage within an engineered tissue analogue. This approach could be implemented within future biofabrication strategies to generate truly biomimetic cartilage grafts for the treatment of chondral defects.

Biofabrication of cartilage and osteochondral grafts using cartilage microtissues as biological building blocks

The second biofabrication strategy employed in this thesis was the use of microtissues as biological building blocks. Here, an effective microwell system for generating suitable microtissues for musculoskeletal tissue engineering was developed. The fabrication method was simple, easily implemented and reused. Importantly, the developed platform satisfied the key criteria discussed in literature for a spheroid biofabrication strategy [152]. Specifically, the methodology produces high fidelity hydrogel microwells and this accuracy translated into the biofabrication of highly reproducible spheroids. These spheroids could be cultivated in various induction protocols to produce different phenotypes and maturities ranging from initial cell condensations/aggregates to mature hypertrophic cartilage microtissues. The spheroid phenotypes explored within this thesis were conceived as ideal precursor-tissues for tissues/organs of the musculoskeletal system, such as cartilage, vasculature, and bone. Importantly, spheroids were capable of undergoing key tissue-specific processes after biofabrication and harvest, confirming their utility for tissue engineering applications. As part of this work, the capacity to fuse early cartilage microtissues into a thick and homogenous macro-tissue was substantiated. Furthermore, it was identified that using smaller microtissue in greater number lead to a superior cartilage macro-tissue. As part of this early validation work, this thesis developed vascular spheroids, with the capacity to spontaneously form a pervasive prevascularise network within a commonly used fibrin-based bioink [164]. Collectively demonstrating that the microwell system developed represents an ideal platform technology for emerging aggregate-engineering strategies.

Despite this relative success, efforts to enhance the scalability of this approach using dynamic culture were less efficacious. While the target here was to generate high-quality cartilage microtissues over prolonged cultivation, dynamic cultivation appeared to support an osteogenic phenotype. Changes in the oxygen tension or excessive shear stresses could explain this suppression of chondrogenesis [188–191,193,195]. Nevertheless, the more osteogenic phenotype could be valuable for bone tissue engineering as an alternative to the hypertrophic cartilage rudiments employed herein. Alternatively, modulating environmental oxygen tension is an effective way of facilitating dynamic culture conditions for chondrogenesis [197] and could be a simple solution to engineering higher quality cartilage microtissues in bioreactor culture. In spite of

these challenges, the novel stirred-tank bioreactor designed in this thesis represents a simple and accessible means of dynamically cultivating microtissues. Given the difficulties associated with maintaining robust chondrogenesis in dynamic conditions, the hydrogel platform emerged a suitable method for generating phenotypically distinct microtissue populations in sufficient numbers to enable the biofabrication of osteochondral tissues/implants at a clinically relevant scale. As such, the novel methods designed and developed in this thesis represent a platform for generating biological building blocks for musculoskeletal tissue engineering in a medium-high throughput fashion. A serendipitous discovery that endothelial growth medium (EGM) enhanced the aggregation and chondrogenic capacity of animal-derived MSCs was also made using this microwell platform. From this initial observation, hydrocortisone was identified as the principle factor driving the enhanced chondrogenesis in human-derived MSCs. In this study, the biosynthetic output of MSCs within cartilage microtissues could be significantly enhanced by supplementation of chondrogenic medium with hydrocortisone, yielding high-quality microtissues with a rich cartilaginous ECM profile. As part of chapter 5, it was identified that the effects of EGM/hydrocortisone were most pronounced in donors with limited chondrogenic capacity. As such, hydrocortisone could function to alter the surface marker expression of heterogeneous MSC populations, 'reactivating' subsets of cells which would otherwise not undergo robust chondrogenic differentiation. Alternative, hydrocortisone could directly regulate the expression of cartilage ECM genes and/or enhance TGF-β-mediated upregulation of their expression in a similar fashion to dexamethasone, a glucocorticoid commonly used in chondrogenic differentiation of MSCs. Finally, given hydrocortisones anti-inflammatory role, the enhanced chondrogenesis noted in chapter 5 could be a feature of the suppression of inflammation related catabolic pathways such as IL1. While the mechanism of action remains unclear, the evidence presented in chapter 5 strongly indicates a benefit to the modification of traditional chondrogenic differentiation regimes with EGM/hydrocortisone. However, this discovery was made after the studies presented in chapters 6 & 7 and as such, alternate methods of inducing rapid and robust chondrogenesis in MSC microtissues have been utilised therein. The capacity to heal chondral defects using a self-organised articular cartilage was also investigated. As part of this work, a mechanically competent cartilage that expressed a hyaline-like phenotype was engineered by spontaneous self-organisation of early cartilage microtissues. Optimisation of the chondrogenic induction protocol for the microtissues, initially investigated in chapter 3, resulted in maximum microtissue growth during limited exposure to TGF-β. Minimising exposure to this chondrogenic growth factor has been demonstrated as important to mitigate spheroid boundary-setting and maximise the likelihood of successful tissue fusion [68]. The optimised conditions yielded standardised microtissues which, when brought together, fused to form a consistently thick and homogenous articular cartilage. This represented a significant progression in the field, as fusion between cartilage subunits had been challenging and

resulted in an inhomogeneous tissue [138,215], or required the use of manual forces to achieve fusion between the tissue subunits [68]. Since spontaneous fusion was possible, this study was also able to leverage a 3D printed framework to better guide the self-organisation process and generate better spatial organisation of the collagen network as the macro-cartilage (re)modelled. The 3D printed framework also served as a means of implanting the engineered tissue within a preclinical chondral defect model. Here, the novel fixation device and implantation strategy devised in chapter 4 was employed to secure the engineer cartilage *in situ*. Although there was no evidence of implant loosening after 6 months, the therapeutic impact of the engineered cartilage was negligible compared to treatment using an existing chondral treatment strategy (micro-drilling).

Histological evaluation indicated that implant subsidence had occurred in the 'chondral only' treatment strategy. This prompted investigation into an alternative method of securing an engineered cartilage in place. Chapter 7 investigated the biofabrication of an osteochondral plug *via* the spatial assembly of two phenotypically distinct populations of cartilage microtissues. In this work, novel bioassembly strategies were employed to fabricate a biphasic osteochondral plug. Specifically, the implant comprised of an overlying stable articular cartilage layer, similar to the one developed in chapter 6, and an osseous region filled with islands of hypertrophic cartilage microtissues. After *in vitro* cultivation, the majority of implants provided immediate joint resurfacing with an engineered cartilage that, macroscopically, closely resembled the surrounding native tissue. However, the surface integrity of some of the implants was sub-optimal, and this natural variation was most likely due to the cells trying to minimise free-energy during self-organisation. Although the bioassembly method employed within this thesis is a promising start, in the context of engineering human clinically-relevant implants improvements are necessary. As demonstrated in chapter 4, bioprinting can be an effective method of accurately positioning biologics for self-organisation. The manual nature of the approach taken in chapters 7 could explain, in part, the differences seen in the chondral regions of the implants. Hence, bioprinting the cartilage microtissues would aid in controlling their position and number in a more reproducible manner. Emerging bioprinting technologies such as aspiration-assisted bioprinting and fluidic-based singularisation methods have been shown to be an effect method of precisely controlling the position of spheroids for hierarchical osteochondral applications [120,282]. Furthermore, bioprinting is known to facilitate the formation of complex multi-material implants [298]. As such, leveraging bioprinting in future versions of the implant could permit the inclusion of additional components, such as vascular spheroids for prevascularisation of the osseous region and the fabrication of larger implants. Similar strategies of forming microvascular networks have also been shown to correlate with bone formation and as such, could also enhance the therapeutic efficacy of the osteochondral implant by encouraging rapid osteointegration [164].

Learnings from chapters 6 and 7 have implicated subchondral bone as having a central role in the restoration of articular cartilage. In both the 6 month *in vivo* studies of chondral and osteochondral lesions, cases of 'best repair' correlated with re-establishing the subchondral bone plate. This was particularly evident in the osteochondral study, whereby treatment resulted in the restoration of a near-normal articular surface in cases where the implant stabilised the defect and acted as a platform for the regeneration of the subchondral bone and thus the overlying cartilage. Similar findings have been reported in literature, where time-course studies have shown that subchondral bone restoration predicates cartilage regeneration [285]. Moreover, stabilisation of an osteochondral defect alone, using a solid and inert polymer implant, can prevent secondary changes and joint deterioration [299]. In contrast, failure to stabilise critically-sized defects results in aberrant subchondral bone remodelling and the collapse of the subchondral bone plate inwards [19]. As such, collective evidence indicates that to provide successful joint resurfacing an implant must; 1) stabilise the defect, preventing secondary changes and mechanical collapse, 2) provide a platform from which the subchondral bone can be reinstated, and 3) facilitate the restoration of the articular cartilage, either through the *in situ* maturation of an engineered tissue or *via* native healing mechanisms. Taking this knowledge forwards has the potential to aid in designing joint regeneration strategies which synergistically leverage native healing mechanisms with developmentally inspired precursor tissues. Specifically, future joint resurfacing treatments should focus on designing implants that induce rapid and robust osteointegration and are positioned *in situ* to act as a bridge/platform for the regeneration of the subchondral bone plate *via* endochondral conversion of a hypertrophic portion of a stratified engineered cartilage. To this end, replacement of the thermo-polymer framework with a more osteoinductive/conductive material which can be 3D structured, such as a metal [300,301] or ceramic [287–289], could be a means of improving the clinical efficacy of the approaches developed.

Considerations for clinical translation

In chapters 6 & 7, preclinical evaluation of engineered grafts for chondral and osteochondral repair has been undertaken. For both studies, an allogeneic cell source was selected. With a view to clinical translation, an autologous source of cells would be ideal. However, limited cell numbers, the need for two surgeries, and donor site morbidity are well documented limitations associated with using autologous cells [42,302]. In the absence of bulking hydrogels/biomaterial scaffold, developmentally inspired approaches for engineering cartilages often require large cell numbers making the use of allogeneic cell sources commonplace [42]. Allogeneic sources can also be considered a more 'off-the-shelf' product, as banks of cells can be stored until needed. Moreover,

allogeneic MSC sources allow for greater control, consistency, and higher quality tissues when compared to autologous counterparts as they can be isolated from healthy and/or juvenile sources [303,304]. In this context, batch criteria can be defined for each donor whereby cell cohorts are screened for optimal proliferation, differentiation, as well as immunogenicity [42,305]. Despite the numerous benefits, there are some drawbacks associated with allogeneic cells which could have contributed to some of the suboptimal outcomes observed in the preclinical evaluation undertaken in this thesis. Due to its avascular nature, cartilage has been suggested to be immunologically privileged [302,306,307]. In spite of this, implantation of allogeneic cells into the joint could invoke an immune response. As part of this, inflammatory cytokines, known to inhibit chondrogenesis and progress osteoarthritis [308–310], could be released and inhibit *in situ* cartilage maturation and defect repair. In this context, negative immune reactions associated with allogeneic cells would likely be seen to a greater extent in the osteochondral model presented in chapter 7 where immune cell invasion from the vascularised subchondral bone could play a larger role. However, the superior results in chapter 7 are not indicative of a more inflammatory state. The emerging role of MSCs as potent signalling cells could explain the suitability of the autologous cells employed in this thesis. Specifically, there is accumulating evidence that the therapeutic effects *in vivo* of MSCs may not only be due to their differentiation into chondrocytes. But, also *via* modulations of the host immune response and anabolic/chondrogenic stimulation of resident chondrocytes and MSCs through numerous paracrine effects and symbiotic feedback loops [305]. In the context of this thesis, the contribution of the implanted MSCs/CCs remains unclear. In order to elucidate their involvement, follow-up studies should look at earlier time points and assess the acute immune responses to implanting and engineered tissue. Additionally, methods of cell labelling and tracking could be employed to help determine the persistence and distribution of implanted MSCs to help clarify their contribution to healing.

Many of the concepts presented in this thesis required considerable cell expansion and *in vitro* priming regimes. As part of this, challenges and concerns associate with clinical translation of the approaches presented in this thesis arise. Specifically, the use of animal-derived serums for the expansion of stem/stromal as well as primary cells is widely considered as a predominant limiting factor in human clinical translation of current engineered cartilages [311]. In view of human clinical translation, exploring the biofabrication strategies employed herein using alternatives to animal-serum based media is necessary. Currently, human plasma lysate (HPL) has been successfully implemented as an alternative to fetal bovine serum (FBS) for the expansion of human MSCs whilst retaining their multipotency [312–314]. Equally, serum-free cultures are being developed as a potential route towards the clinic [315,316]. The ultimate goal of tissue engineering should be to move away from animal-derived serums in the interest of designing standardised and clinically

relevant cell-based strategies. Given that as the long-term goal of the broader field, short-to-medium term targets for the approaches identified in this thesis should focus on reifying the reproducibility of the two main biofabrication strategies. Demonstrating similar levels of cartilage quality using various batches of FBS would help to confirm the efficacy of the approaches independent of the ill-defined serum.

9 Future Outlook

At present, the work presented in this thesis offers an excellent nucleus for the development of chondral and osteochondral implants capable of making a significant clinical impact. To realise that goal, some limitation of the current work should be addressed. First, achieving reliable chondrogenesis from heterogeneous populations of MSCs can be challenging. This thesis leveraged a serendipitous discovery that endothelial growth medium could significantly improve the initial aggregation and chondrogenic potential of heterogeneous MSC populations. Specifically, hydrocortisone was identified as a novel factor capable of improving current chondrogenic induction protocols and consistently engineering high-quality cartilage. Since engineering high-quality cartilage *in vitro* have been shown to yield superior results for bone and cartilage *in vivo* [46,238], this work, albeit preliminary, has the potential to impact both bone and cartilage tissue engineering. Hence, future efforts should seek to clarify the mechanism of action as part of designing and implementing novel factors into *in vitro* chondrogenic induction and cartilage cultivation protocols.

Second, significant effort should be made to improve the mechanical strength of the engineered articular cartilage. Several approaches, such as advanced chondrogenic culture regimes and mechanical stimulation have been discussed as reasonable methods for achieving this. Amalgamating these approaches with the biofabrication strategies employed within this thesis has the potential to generate physiologic levels of matrix components, structure organisation, and biomechanical properties. In this vein, elucidating the mechanical properties of the articular cartilage engineered within the guiding polymer framework is necessary in the future. In particular, determining the effect, if any, of the enhanced collagen organisation observed in chapters 4 and 6 on the engineered cartilages functional properties. At present, mechanical evaluation of the engineered biocomposites was not undertaken as the polymer component dominates the mechanical properties and masks the influence of tissue structure. However, the use of micro/nano-indentation could offer a means of quantifying any tissue structure-function relationships present in the hybrid implants by testing only the engineered cartilage. In spite of best efforts, achieving sufficient functional properties from an engineered tissue may be unobtainable *in vitro* [42,74,185]. In which case, employing an *in vivo* bioreactor, that have principally been used for critically-sized bone grafts [317–322] but also cartilage [323], to vascularise and mature an engineered precursor osteochondral tissues could facilitate the formation of a truly functional engineered graft, suited to immediate load-bearing applications [185].

Finally, the microenvironment within biocomposite structures such as those created in this thesis from self-organised tissues and polymer frameworks could play an influential role in directing

cell phenotype and tissue development. Specifically, generation of a hypoxic microenvironment at the bottom of culture wells and within the core of hydrogel constructs is well documented [33,324]. It stands to reason that a local hypoxic environment forms within the polymer microwells and that this microenvironment likely favours chondrogenic differentiation and accumulation of GAGs. Moreover, the cellular consumption of nutrients, such as glucose, within the PCL microwells is likely to generate nutrient gradients which could encourage the upward tissue growth out of the microwell. Coupling these microenvironmental factors with the physical constraint on the growing cartilage provided by the PCL microwells can help to explain the enhanced tissue quality seen when self-organising cartilages are combined with the 3D printed framework. Probing these microenvironments to better understand their evolution during key phases such as; lineage commitment, matrix accumulation, and tissue maturation can help to inform biofabrication strategies. Specifically, identifying favourable conditions for creating specific tissue phenotypes could be highly beneficial in designing unique multi-phasic microenvironments to guide the development of complex target tissues and interfaces commonplace in the musculoskeletal system. To this end, microphsyiological systems [325,326], non-invasive biosensing [327], direct measurement methods [324,328,329], and *in-silico* models [329,330] have all been employed to quantify and understand key environmental conditions within 3D tissue models. In the context of cartilage tissue engineering, coupling direct measurement of oxygen consumption rates with numerical modelling has identified oxygen concentrations which favour either sGAG deposition or collagen synthesis [324]. Equally, computational models have been used to predict the glucose requirements of large chondrogenic constructs. These predictions identified culture conditions (media volume) and construct architectures (number of nutrient channels) conducive to maintaining adequate glucose levels for cartilage matrix synthesis [331]. Since this thesis took steps towards the biofabrication of cartilages grafts at a clinically-relevant scale, incorporating current techniques to quantify environmental changes within engineered tissues would be a logical next step. Mapping changes in nutrient diffusion, cell consumption rates, and matrix synthesis as a means of designing adaptive cultivation strategies, engineering effective constructs, and creating accurate predictive simulations could further the quality of the engineered tissues developed in this thesis and/or the scalability of the biofabrication approaches employed.

10 Conclusions

- A strategy to bioprint biomimetic self-organised cartilage using a supportive joint fixation device has been developed. Specifically, a novel assembly of 3D printed polymer implant and temporary base has been shown to be an effective method for guiding the self-organisation and development of high-density cellular condensations towards a stratified articular cartilage. The quality of this engineered cartilage could be enhanced using dynamic culture conditions. In particular, bioreactor culture resulted in near-native levels of cartilage matrix components and structural stratification.

- A novel hydrogel microwell platform has been developed for the biofabrication of cellular spheroids in a medium-high throughput fashion. This technology satisfies the key criteria for a spheroid biofabrication platform, producing standardised spheroids, which can have various phenotypes and suitable degrees of maturity, in a scalable manner, and are capable of tissue-fusion and the formation of larger macro-tissues.

- Leveraging this platform, early-cartilage microtissues have been generated as 'biological building blocks' for the biofabrication of a thick and homogenous stable cartilage analogue *via* spontaneous self-organisation. Employing optimised initial culture conditions results in rapid growth of early-cartilage microtissues, to sizes suited to designing a scalable approach. The stable cartilage macro-tissue exhibited promising biochemical and biomechanical properties. Moreover, a hybrid biofabrication approach, coupling a 3D printed polymer framework with cartilage microtissues, aided in guiding the self-organisation process. This process resulted in superior structural organisation within the collagen network of the engineered cartilage.

- Treatment of focal chondral defects did not result in significant improvement when compared to a current clinical treatment. Failure to suitably stabilise the implant within the defect prompted investigation into an osteochondral strategy. Here, two populations of phenotypically distinct, developmentally inspired, cartilage microtissues were used to biofabricate a biphasic osteochondral plug. When assessed in large animal, preclinical osteochondral defect model, this engineered implant demonstrated immediate joint

resurfacing, and restoration of an almost near-native articular surface after 6 months. Histological and μCT evaluation of the defect revealed a trend towards improved healing response in almost all metrics quantified, and implicated regeneration of the subchondral bone plate as important for effective joint resurfacing.

- Developmentally inspired strategies, such as scaffold-free and self-organisation approaches, have demonstrated the capacity to generate highly-biomimetic cartilages that have otherwise been unobtainable using traditional 'top-down' methods. Although, mirroring key developmental stages *in vitro* often results in the deposition of a rich and mimetic ECM profile, it does not guarantee tissue functionality. As such, modular hybrid approaches which seek to merge traditional biomaterial scaffolds with developmentally engineered tissues without negatively impacting tissue development are rapidly emerging as a promising means of improving their functionality. This thesis presents two strategies which successfully marry a developmentally inspired cartilage engineering strategy with a traditional 3D printed polymer framework. Collectively, this work highlights the capacity of instructive scaffolds to guide and enhance the development of self-organising tissues *in vitro*, demonstrating the potential of modular, hybrid biofabrication strategies to regenerate complex musculoskeletal tissues.

11 Supporting Information

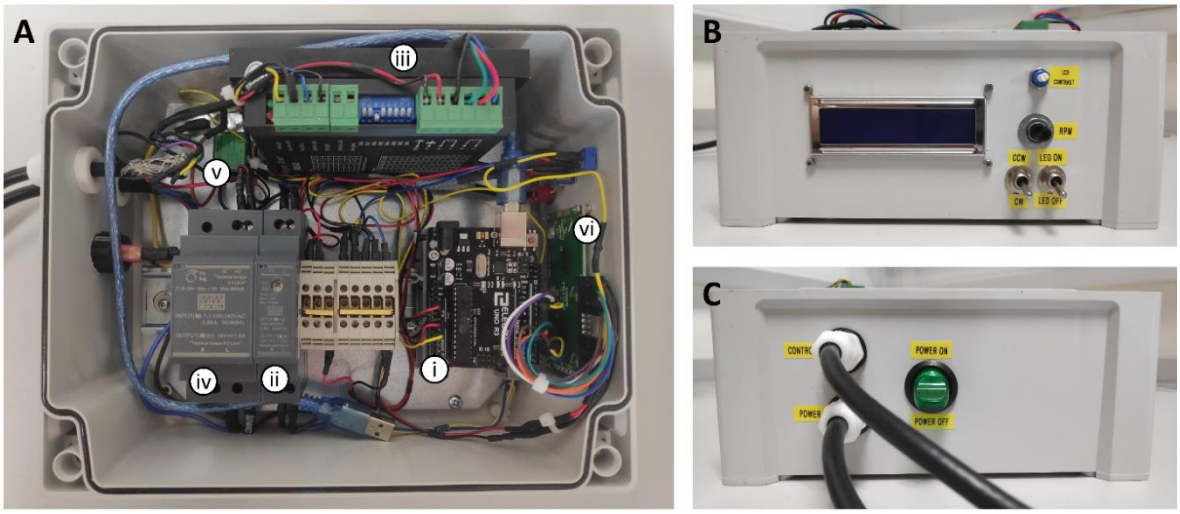

Figure s3.1 A) interior of control box illustrating main components for controlling the bioreactor. B) Front panel of the control box. C) Rear panel of the control box.

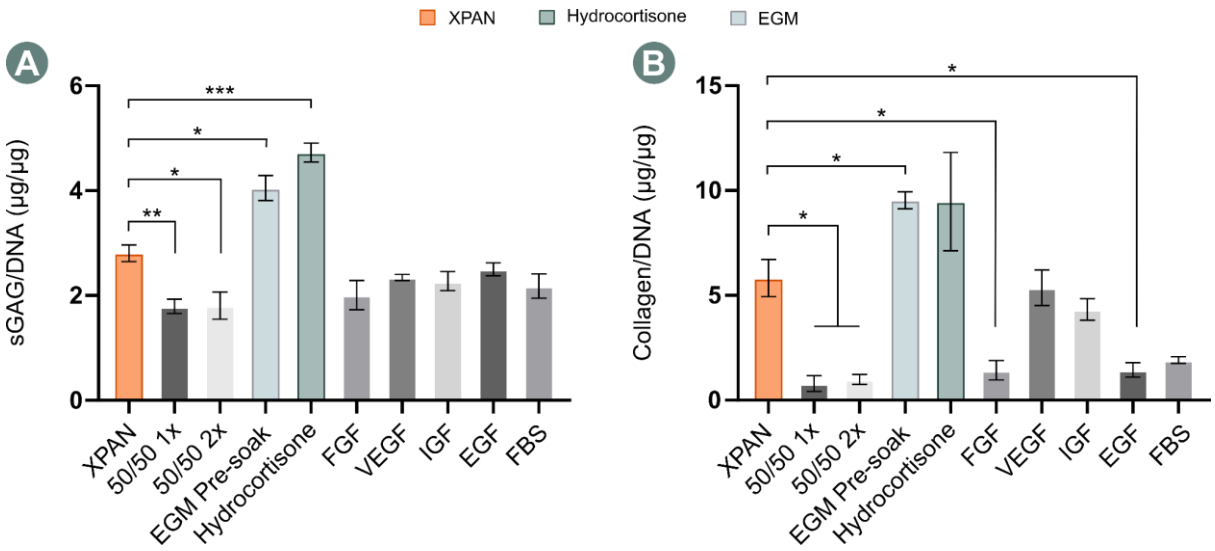

Supporting Figure 5.1 *Determining the driving factor in EGM. Biochemical quantification after 7 days of chondrogenic culture of A) sGAG normalised to DNA, (N = 3, Mean ± SD) and B) collagen normalised to DNA, (N = 3, Mean ± SD). * denotes significance using a Brown-Forsythe and Welch One-way ANOVA, $p < 0.05$*

12 References

[1] E.N. Marieb, K. Hoehn, Joints, in: Hum. Anat. Physiol., 9th ed., 2013: pp. 249–273.

[2] S.A.J. Fox, A. Bedi, S.A. Rodeo, The basic science of articular cartilage: Structure, composition, and function, Sports Health. 1 (2009) 461–468. https://doi.org/10.1177/1941738109350438.

[3] V.C. Mow, A. Ratcliffe, R.A. Poole, Cartilage and diarthrodial joints as paradigms for hierarchical materials and structures, Biomaterials. 13 (1992) 67–97. https://doi.org/10.1016/0142-9612(92)90001-5.

[4] A.M. Bhosale, J.B. Richardson, Articular cartilage: Structure, injuries and review of management, Br. Med. Bull. 87 (2008) 77–95. https://doi.org/10.1093/bmb/ldn025.

[5] E.B. Hunziker, K. Lippuner, M.J.B. Keel, N. Shintani, An educational review of cartilage repair: Precepts & practice - myths & misconceptions - progress & prospects, Osteoarthr. Cartil. 23 (2015) 334–350. https://doi.org/10.1016/j.joca.2014.12.011.

[6] G. Li, J. Yin, J. Gao, T.S. Cheng, N.J. Pavlos, C. Zhang, M.H. Zheng, Subchondral bone in osteoarthritis: Insight into risk factors and microstructural changes, Arthritis Res. Ther. 15 (2013) 223. https://doi.org/10.1186/ar4405.

[7] T.J. Lyons, S.F. McClure, R.W. Stoddart, J. McClure, The normal human chondro-osseous junctional region: Evidence for contact of uncalcified cartilage with subchondral bone and marrow spaces, BMC Musculoskelet. Disord. 7 (2006) 52. https://doi.org/10.1186/1471-2474-7-52.

[8] J. Pan, X. Zhou, W. Li, J.E. Novotny, S.B. Doty, L. Wang, In situ measurement of transport between subchondral bone and articular cartilage, J. Orthop. Res. 27 (2009) 1347–1352. https://doi.org/10.1002/jor.20883.

[9] D.L. Johnson, W.P. Urban, D.N. Caborn, W.J. Vanarthos, C.S. Carlson, Articular cartilage changes seen with magnetic resonance imaging-detected bone bruises associated with acute anterior cruciate ligament rupture., Am. J. Sports Med. 26 (1998) 409–14. https://doi.org/10.1177/03635465980260031101.

[10] S.R. Goldring, M.B. Goldring, Changes in the osteochondral unit during osteoarthritis: Structure, function and cartilage bone crosstalk, Nat. Rev. Rheumatol. 12 (2016) 632–644. https://doi.org/10.1038/nrrheum.2016.148.

[11] D. Lajeunesse, P. Reboul, Subchondral bone in osteoarthritis: A biologic link with articular cartilage leading to abnormal remodeling, Curr. Opin. Rheumatol. 15 (2003) 628–633. https://doi.org/10.1097/00002281-200309000-00018.

[12] S.I.M. Lepage, N. Robson, H. Gilmore, O. Davis, A. Hooper, S. St John, V. Kamesan, P. Gelis, D. Carvajal, M. Hurtig, T.G. Koch, Beyond Cartilage Repair: The Role of the Osteochondral Unit in Joint Health and Disease, Tissue Eng. - Part B Rev. 25 (2019) 114–125. https://doi.org/10.1089/ten.teb.2018.0122.

[13] J.S. Day, M. Ding, J.C. Van Der Linden, I. Hvid, D.R. Sumner, H. Weinans, A decreased subchondral trabecular bone tissue elastic modulus is associated with pre-arthritic cartilage damage, J. Orthop. Res. 19 (2001) 914–918. https://doi.org/10.1016/S0736-0266(01)00012-2.

[14] J. Day, J. Van Der Linden, R. Bank, M. Ding, I. Hvid, D. Sumner, H. Weinans, Adaptation of subchondral bone in osteoarthritis., Biorheology. 41 (2004) 359–68. http://www.ncbi.nlm.nih.gov/pubmed/23142725.

[15] P. Rahnamay Moshtagh, N.M. Korthagen, S.G. Plomp, B. Pouran, A. Zadpoor, H. Weinans, Bone Remodeling is an Early Sign of Biomechanically Induced Pre-Osteoarthritis, Osteoarthr. Cartil. 25 (2017) S295–S296. https://doi.org/10.1016/J.JOCA.2017.02.498.

[16] D. Muratovic, F. Cicuttini, A. Wluka, D. Findlay, Y. Wang, S. Otto, D. Taylor, J. Humphries, Y. Lee, A. Labrinidis, R. Williams, J. Kuliwaba, Bone marrow lesions detected by specific combination of MRI sequences are associated with severity of osteochondral degeneration, Arthritis Res. Ther. 18 (2016) 54. https://doi.org/10.1186/s13075-016-0953-x.

[17] R.J. Lories, F.P. Luyten, The bone-cartilage unit in osteoarthritis, Nat. Rev. Rheumatol. 7 (2011) 43–49. https://doi.org/10.1038/nrrheum.2010.197.

[18] X.L. Yuan, H.Y. Meng, Y.C. Wang, J. Peng, Q.Y. Guo, A.Y. Wang, S.B. Lu, Bone-cartilage interface crosstalk in osteoarthritis: Potential pathways and future therapeutic strategies, Osteoarthr. Cartil. 22 (2014) 1077–1089. https://doi.org/10.1016/j.joca.2014.05.023.

[19] D.W. Jackson, P.A. Lalor, H.M. Aberman, T.M. Simon, Spontaneous repair of full-thickness defects of articular cartilage in a goat model - A preliminary study, J. Bone Jt. Surg. 83 (2001) 53–64.

[20] M.B. Goldring, S.R. Goldring, Articular cartilage and subchondral bone in the pathogenesis of osteoarthritis, in: Ann. N. Y. Acad. Sci., Wiley/Blackwell (10.1111), 2010: pp. 230–237. https://doi.org/10.1111/j.1749-6632.2009.05240.x.

[21] D.K. Bae, K.H. Yoon, S.J. Song, Cartilage Healing After Microfracture in Osteoarthritic Knees, Arthrosc. - J. Arthrosc. Relat. Surg. 22 (2006) 367–374. https://doi.org/10.1016/j.arthro.2006.01.015.

[22] G. Knutsen, V. Isaksen, O. Johansen, L. Engebretsen, T.C. Ludvigsen, J.O. Drogset, T. Grøntvedt, E. Solheim, T. Strand, S. Roberts, Autologous Chondrocyte Implantation Compared with Microfracture in the Knee: A Randomized Trial, J. Bone Jt. Surg. - Ser. A. 86 (2004) 455–464. https://doi.org/10.2106/00004623-200403000-00001.

[23] D. Goyal, S. Keyhani, E.H. Lee, J.H.P. Hui, Evidence-based status of microfracture technique: A systematic review of Level I and II studies, Arthrosc. - J. Arthrosc. Relat. Surg. 29 (2013) 1579–1588. https://doi.org/10.1016/j.arthro.2013.05.027.

[24] U. Horas, D. Pelinkovic, G. Herr, T. Aigner, R. Schnettler, Autologous chondrocyte implantation and osteochondral cylinder transplantation in cartilage repair of the knee joint. A prospective, comparative trial, J. Bone Jt. Surg. - Ser. A. 85 (2003) 185–192. https://doi.org/10.2106/00004623-200302000-00001.

[25] R. Gudas, R.J. Kalesinskas, V. Kimtys, E. Stankevičius, V. Toliušis, G. Bernotavičius, A. Smailys, A prospective randomized clinical study of mosaic osteochondral autologous transplantation versus microfracture for the treatment of osteochondral defects in the knee joint in young athletes, Arthrosc. - J. Arthrosc. Relat. Surg. 21 (2005) 1066–1075. https://doi.org/10.1016/j.arthro.2005.06.018.

[26] T.M. Simon, D.W. Jackson, Articular Cartilage: Injury Pathways and Treatment Options, Sports Med. Arthrosc. 14 (2006) 146–154. https://doi.org/10.1097/JSA.0000000000000182.

[27] K.W. Ng, G.A. Ateshian, C.T. Hung, Zonal chondrocytes seeded in a layered agarose hydrogel create engineered cartilage with depth-dependent cellular and mechanical inhomogeneity., Tissue Eng. Part A. 15 (2009) 2315–2324. https://doi.org/10.1089/ten.tea.2008.0391.

[28] D. Zhu, P. Trinh, E. Liu, F. Yang, Biochemical and Mechanical Gradients Synergize to Enhance Cartilage Zonal Organization in 3D, ACS Biomater. Sci. Eng. 4 (2018) 3561–3569. https://doi.org/10.1021/acsbiomaterials.8b00775.

[29] D. Zhu, X. Tong, P. Trinh, F. Yang, Mimicking Cartilage Tissue Zonal Organization by Engineering Tissue-Scale Gradient Hydrogels as 3D Cell Niche, Tissue Eng. - Part A. 24 (2018) 1–10. https://doi.org/10.1089/ten.tea.2016.0453.

[30] L.H. Nguyen, A.K. Kudva, N.S. Saxena, K. Roy, Engineering articular cartilage with spatially-varying matrix composition and mechanical properties from a single stem cell population using a multi-layered hydrogel, Biomaterials. 32 (2011) 6946–6952. https://doi.org/10.1016/j.biomaterials.2011.06.014.

[31] L.H. Nguyen, A.K. Kudva, N.L. Guckert, K.D. Linse, K. Roy, Unique biomaterial compositions direct bone marrow stem cells into specific chondrocytic phenotypes corresponding to the various zones of articular cartilage, Biomaterials. 32 (2011) 1327–1338. https://doi.org/10.1016/j.biomaterials.2010.10.009.

[32] S. Camarero-Espinosa, B. Rothen-Rutishauser, C. Weder, E.J. Foster, Directed cell growth in multi-zonal scaffolds for cartilage tissue engineering, Biomaterials. 74 (2016) 42–52. https://doi.org/10.1016/j.biomaterials.2015.09.033.

[33] S.D. Thorpe, T. Nagel, S.F. Carroll, D.J. Kelly, Modulating Gradients in Regulatory Signals within Mesenchymal Stem Cell Seeded Hydrogels: A Novel Strategy to Engineer Zonal Articular Cartilage, PLoS One. 8 (2013) 60764. https://doi.org/10.1371/journal.pone.0060764.

[34] I.S. Park, W.H. Choi, D.Y. Park, S.R. Park, S.H. Park, B.H. Min, Effect of joint mimicking loading system on zonal organization into tissue-engineered cartilage, PLoS One. 13 (2018) 1–12. https://doi.org/10.1371/journal.pone.0202834.

[35] R. Burdis, D.J. Kelly, 3D Bioprinting Hardware, in: D.M. Devine (Ed.), Polym. Addit. Manuf. Biomed. Appl., Springer International Publishing, Cham, 2019: pp. 161–186. https://doi.org/10.1007/978-3-030-24532-0_8.

[36] J. Nulty, R. Schipani, R. Burdis, D.J. Kelly, Bioinks and Their Applications in Tissue Engineering, in: D.M. Devine (Ed.), Polym. Addit. Manuf. Biomed. Appl., Springer International Publishing, Cham, 2019: pp. 187–218. https://doi.org/10.1007/978-3-030-24532-0_9.

[37] A.C. Daly, F.E. Freeman, T. Gonzalez-Fernandez, S.E. Critchley, J. Nulty, D.J. Kelly, 3D Bioprinting for Cartilage and Osteochondral Tissue Engineering, Adv. Healthc. Mater. 6 (2017) 1700298. https://doi.org/10.1002/adhm.201700298.

[38] P. Abdollahiyan, F. Oroojalian, A. Mokhtarzadeh, M. de la Guardia, Hydrogel-Based 3D Bioprinting for Bone and Cartilage Tissue Engineering, Biotechnol. J. 15 (2020) 1–16. https://doi.org/10.1002/biot.202000095.

[39] R. Levato, W.R. Webb, I.A. Otto, A. Mensinga, Y. Zhang, M. van Rijen, R. van Weeren, I.M. Khan, J. Malda, The bio in the ink: cartilage regeneration with bioprintable hydrogels and articular cartilage-derived progenitor cells, Acta Biomater. 61 (2017) 41–53.

https://doi.org/10.1016/j.actbio.2017.08.005.

[40] X. Ren, F. Wang, C. Chen, X. Gong, L. Yin, L. Yang, Engineering zonal cartilage through bioprinting collagen type II hydrogel constructs with biomimetic chondrocyte density gradient, BMC Musculoskelet. Disord. 17 (2016). https://doi.org/10.1186/s12891-016-1130-8.

[41] A.C. Daly, D.J. Kelly, Biofabrication of spatially organised tissues by directing the growth of cellular spheroids within 3D printed polymeric microchambers, Biomaterials. 197 (2019) 194–206. https://doi.org/10.1016/j.biomaterials.2018.12.028.

[42] G.D. DuRaine, W.E. Brown, J.C. Hu, K.A. Athanasiou, Emergence of Scaffold-Free Approaches for Tissue Engineering Musculoskeletal Cartilages, Ann. Biomed. Eng. 43 (2015) 543–554. https://doi.org/10.1007/s10439-014-1161-y.

[43] M. Centola, B. Tonnarelli, S. Schären, N. Glaser, A. Barbero, I. Martin, Priming 3D Cultures of Human Mesenchymal Stromal Cells Toward Cartilage Formation Via Developmental Pathways, Stem Cells Dev. 22 (2013) 2849–2858. https://doi.org/10.1089/scd.2013.0216.

[44] G. Ofek, C.M. Revell, J.C. Hu, D.D. Allison, K.J. Grande-Allen, K.A. Athanasiou, Matrix development in self-assembly of articular cartilage, PLoS One. 3 (2008). https://doi.org/10.1371/journal.pone.0002795.

[45] D.J. Responte, B. Arzi, R.M. Natoli, J.C. Hu, K.A. Athanasiou, Mechanisms underlying the synergistic enhancement of self-assembled neocartilage treated with chondroitinase-ABC and TGF-β1, Biomaterials. 33 (2012) 3187–3194. https://doi.org/10.1016/j.biomaterials.2012.01.028.

[46] J.J. Ng, Y. Wei, B. Zhou, J. Bernhard, S. Robinson, A. Burapachaisri, X.E. Guo, G. Vunjak-Novakovic, Recapitulation of physiological spatiotemporal signals promotes in vitro formation of phenotypically stable human articular cartilage, Proc. Natl. Acad. Sci. 114 (2017) 2556–2561. https://doi.org/10.1073/pnas.1611771114.

[47] A.D. Murdoch, L.M. Grady, M.P. Ablett, T. Katopodi, R.S. Meadows, T.E. Hardingham, Chondrogenic Differentiation of Human Bone Marrow Stem Cells in Transwell Cultures: Generation of Scaffold-Free Cartilage, Stem Cells. 25 (2007) 2786–2796. https://doi.org/10.1634/stemcells.2007-0374.

[48] W.D. Lee, M.B. Hurtig, R.A. Kandel, W.L. Stanford, Membrane Culture of Bone Marrow Stromal Cells Yields Better Tissue Than Pellet Culture for Engineering Cartilage-Bone Substitute Biphasic Constructs in a Two-Step Process, Tissue Eng. Part C Methods. 17 (2011) 939–948. https://doi.org/10.1089/ten.tec.2011.0147.

[49] B.D. Elder, K.A. Athanasiou, Systematic assessment of growth factor treatment on biochemical and biomechanical properties of engineered articular cartilage constructs, Osteoarthr. Cartil. 17 (2009) 114–123. https://doi.org/10.1016/j.joca.2008.05.006.

[50] R.M. Natoli, D.J. Responte, B.Y. Lu, K.A. Athanasiou, Effects of multiple chondroitinase ABC applications on tissue engineered articular cartilage, J. Orthop. Res. 27 (2009) 949–956. https://doi.org/10.1002/jor.20821.

[51] B.D. Elder, K.A. Athanasiou, Effects of temporal hydrostatic pressure on tissue-engineered bovine articular cartilage constructs, Tissue Eng. - Part A. 15 (2009) 1151–1158. https://doi.org/10.1089/ten.tea.2008.0200.

[52] C. Scotti, B. Tonnarelli, A. Papadimitropoulos, A. Scherberich, S. Schaeren, A. Schauerte, J. Lopez-Rios, R. Zeller, A. Barbero, I. Martin, Recapitulation of endochondral bone formation

using human adult mesenchymal stem cells as a paradigm for developmental engineering, Proc. Natl. Acad. Sci. 107 (2010) 7251–7256. https://doi.org/10.1073/pnas.1000302107.

[53] C. Scotti, E. Piccinini, H. Takizawa, A. Todorov, P. Bourgine, A. Papadimitropoulos, A. Barbero, M.G. Manz, I. Martin, Engineering of a functional bone organ through endochondral ossification, Proc. Natl. Acad. Sci. 110 (2013) 3997–4002. https://doi.org/10.1073/pnas.1220108110.

[54] G. Nilsson Hall, L.F. Mendes, C. Gklava, L. Geris, F.P. Luyten, I. Papantoniou, Developmentally Engineered Callus Organoid Bioassemblies Exhibit Predictive In Vivo Long Bone Healing, Adv. Sci. 7 (2020) 1–16. https://doi.org/10.1002/advs.201902295.

[55] J. van der Stok, M. Koolen, H. Jahr, N. Kops, J. Waarsing, H. Weinans, O. van der Jagt, Chondrogenically differentiated mesenchymal stromal cell pellets stimulate endochondral bone regeneration in critical-sized bone defects, Eur. Cells Mater. 27 (2014) 137–148. https://doi.org/10.22203/eCM.v027a11.

[56] K.C. Murphy, A.I. Hoch, J.N. Harvestine, D. Zhou, J.K. Leach, Mesenchymal Stem Cell Spheroids Retain Osteogenic Phenotype Through α 2 β 1 Signaling, Stem Cells Transl. Med. 5 (2016) 1229–1237. https://doi.org/10.5966/sctm.2015-0412.

[57] A.I. Hoch, V. Mittal, D. Mitra, N. Vollmer, C.A. Zikry, J.K. Leach, Cell-secreted matrices perpetuate the bone-forming phenotype of differentiated mesenchymal stem cells, Biomaterials. 74 (2016) 178–187. https://doi.org/10.1016/j.biomaterials.2015.10.003.

[58] S.S. Ho, A.T. Keown, B. Addison, J.K. Leach, Cell Migration and Bone Formation from Mesenchymal Stem Cell Spheroids in Alginate Hydrogels Are Regulated by Adhesive Ligand Density, Biomacromolecules. 18 (2017) 4331–4340. https://doi.org/10.1021/acs.biomac.7b01366.

[59] S. Rumiński, I. Kalaszczyńska, A. Długosz, M. Lewandowska-Szumieł, Osteogenic differentiation of human adipose-derived stem cells in 3D conditions - comparison of spheroids and polystyrene scaffolds, Eur. Cell. Mater. 37 (2019) 382–401. https://doi.org/10.22203/eCM.v037a23.

[60] S.S. Ho, B.P. Hung, N. Heyrani, M.A. Lee, J.K. Leach, Hypoxic Preconditioning of Mesenchymal Stem Cells with Subsequent Spheroid Formation Accelerates Repair of Segmental Bone Defects, Stem Cells. 36 (2018) 1393–1403. https://doi.org/10.1002/stem.2853.

[61] F.G. Lyons, A.A. Al-Munajjed, S.M. Kieran, M.E. Toner, C.M. Murphy, G.P. Duffy, F.J. O'Brien, The healing of bony defects by cell-free collagen-based scaffolds compared to stem cell-seeded tissue engineered constructs, Biomaterials. 31 (2010) 9232–9243. https://doi.org/10.1016/j.biomaterials.2010.08.056.

[62] M. Bhattacharjee, J. Coburn, M. Centola, S. Murab, A. Barbero, D.L. Kaplan, I. Martin, S. Ghosh, Tissue engineering strategies to study cartilage development, degeneration and regeneration, Adv. Drug Deliv. Rev. 84 (2015) 107–122. https://doi.org/10.1016/j.addr.2014.08.010.

[63] V. Mironov, R.P. Visconti, V. Kasyanov, G. Forgacs, C.J. Drake, R.R. Markwald, Organ printing: Tissue spheroids as building blocks, Biomaterials. 30 (2009) 2164–2174. https://doi.org/10.1016/j.biomaterials.2008.12.084.

[64] A.M. DeLise, L. Fischer, R.S. Tuan, Cellular interactions and signaling in cartilage development, Osteoarthr. Cartil. 8 (2000) 309–334.

https://doi.org/10.1053/joca.1999.0306.

[65] B.J. Huang, J.C. Hu, K.A. Athanasiou, Effects of passage number and post-expansion aggregate culture on tissue engineered, self-assembled neocartilage, Acta Biomater. 43 (2016) 150–159. https://doi.org/10.1016/j.actbio.2016.07.044.

[66] M. Sarem, O. Otto, S. Tanaka, V.P. Shastri, Cell number in mesenchymal stem cell aggregates dictates cell stiffness and chondrogenesis, Stem Cell Res. Ther. 10 (2019) 10. https://doi.org/10.1186/s13287-018-1103-y.

[67] M.W. Laschke, M.D. Menger, Life is 3D: Boosting Spheroid Function for Tissue Engineering, Trends Biotechnol. 35 (2017) 133–144. https://doi.org/10.1016/j.tibtech.2016.08.004.

[68] S. Bhumiratana, R.E. Eton, S.R. Oungoulian, L.Q. Wan, G.A. Ateshian, G. Vunjak-Novakovic, Large, stratified, and mechanically functional human cartilage grown in vitro by mesenchymal condensation, Proc. Natl. Acad. Sci. 111 (2014) 6940–6945. https://doi.org/10.1073/pnas.1324050111.

[69] D. Murata, S. Akieda, K. Misumi, K. Nakayama, Osteochondral Regeneration with a Scaffold-Free Three-Dimensional Construct of Adipose Tissue-Derived Mesenchymal Stromal Cells in Pigs, Tissue Eng. Regen. Med. 15 (2018) 101–113. https://doi.org/10.1007/s13770-017-0091-9.

[70] L. De Moor, E. Beyls, H. Declercq, Scaffold Free Microtissue Formation for Enhanced Cartilage Repair, Ann. Biomed. Eng. (2019). https://doi.org/10.1007/s10439-019-02348-4.

[71] L. De Moor, S. Fernandez, C. Vercruysse, L. Tytgat, M. Asadian, N. De Geyter, S. Van Vlierberghe, P. Dubruel, H. Declercq, Hybrid Bioprinting of Chondrogenically Induced Human Mesenchymal Stem Cell Spheroids, Front. Bioeng. Biotechnol. 8 (2020) 1–20. https://doi.org/10.3389/fbioe.2020.00484.

[72] L. De Moor, I. Merovci, S. Baetens, J. Verstraeten, P. Kowalska, D. V. Krysko, W.H. De Vos, H. Declercq, High-throughput fabrication of vascularized spheroids for bioprinting, Biofabrication. 10 (2018) 35009. https://doi.org/10.1088/1758-5090/aac7e6.

[73] J. Laurent, G. Blin, F. Chatelain, V. Vanneaux, A. Fuchs, J. Larghero, M. Théry, Convergence of microengineering and cellular self-organization towards functional tissue manufacturing, Nat. Biomed. Eng. 1 (2017) 939–956. https://doi.org/10.1038/s41551-017-0166-x.

[74] B.S. Schon, G.J. Hooper, T.B.F. Woodfield, Modular Tissue Assembly Strategies for Biofabrication of Engineered Cartilage, Ann. Biomed. Eng. 45 (2017) 100–114. https://doi.org/10.1007/s10439-016-1609-3.

[75] I. Martin, J. Malda, N.C. Rivron, Organs by design, Curr. Opin. Organ Transplant. 24 (2019) 562–567. https://doi.org/10.1097/MOT.0000000000000679.

[76] I.T. Ozbolat, Scaffold-Based or Scaffold-Free Bioprinting: Competing or Complementing Approaches?, J. Nanotechnol. Eng. Med. 6 (2015) 1–6. https://doi.org/10.1115/1.4030414.

[77] R. Burdis, D.J. Kelly, Biofabrication and bioprinting using cellular aggregates, microtissues and organoids for the engineering of musculoskeletal tissues, Acta Biomater. 126 (2021) 1–14. https://doi.org/10.1016/j.actbio.2021.03.016.

[78] B.D. Elder, K.A. Athanasiou, Effects of confinement on the mechanical properties of self-assembled articular cartilage constructs in the direction orthogonal to the confinement surface, J. Orthop. Res. 26 (2008) 238–246. https://doi.org/10.1002/jor.20480.

[79] P. Lenas, M. Moos, F.P. Luyten, Developmental Engineering: A New Paradigm for the Design and Manufacturing of Cell-Based Products. Part I: From Three-Dimensional Cell Growth to Biomimetics of In Vivo Development, Tissue Eng. Part B Rev. 15 (2009) 395–422. https://doi.org/10.1089/ten.teb.2009.0461.

[80] P. Lenas, M. Moos, F.P. Luyten, Developmental engineering: A new paradigm for the design and manufacturing of cell-based products. Part II. from genes to networks: Tissue engineering from the viewpoint of systems biology and network science, Tissue Eng. - Part B Rev. 15 (2009) 395–422. https://doi.org/10.1089=ten.teb.2009.0461.

[81] K.A. Athanasiou, R. Eswaramoorthy, P. Hadidi, J.C. Hu, Self-Organization and the Self-Assembling Process in Tissue Engineering, Annu. Rev. Biomed. Eng. 15 (2013) 115–136. https://doi.org/10.1146/annurev-bioeng-071812-152423.

[82] J.A. Brassard, M. Nikolaev, T. Hübscher, M. Hofer, M.P. Lutolf, Recapitulating macro-scale tissue self-organization through organoid bioprinting, Nat. Mater. In Press (2020). https://doi.org/10.1038/s41563-020-00803-5.

[83] J.M. Pérez-Pomares, R.A. Foty, Tissue fusion and cell sorting in embryonic development and disease: Biomedical implications, BioEssays. 28 (2006) 809–821. https://doi.org/10.1002/bies.20442.

[84] E.J. Sheehy, D.J. Kelly, F.J. O'Brien, Biomaterial-based endochondral bone regeneration: a shift from traditional tissue engineering paradigms to developmentally inspired strategies, Mater. Today Bio. 3 (2019) 100009. https://doi.org/10.1016/j.mtbio.2019.100009.

[85] E.M. Thompson, A. Matsiko, E. Farrell, D.J. Kelly, F.J. O'Brien, Recapitulating endochondral ossification: a promising route to in vivo bone regeneration, J. Tissue Eng. Regen. Med. 9 (2015) 889–902. https://doi.org/10.1002/term.1918.

[86] B. Johnstone, T.M. Hering, A.I. Caplan, V.M. Goldberg, J.U. Yoo, In vitro chondrogenesis of bone marrow-derived mesenchymal progenitor cells., Exp. Cell Res. 238 (1998) 265–272. https://doi.org/10.1006/excr.1997.3858.

[87] E.J. Sheehy, T. Vinardell, C.T. Buckley, D.J. Kelly, Engineering osteochondral constructs through spatial regulation of endochondral ossification, Acta Biomater. 9 (2013) 5484–5492. https://doi.org/10.1016/j.actbio.2012.11.008.

[88] J. van der Stok, M.K.E. Koolen, H. Jahr, N. Kops, J.H. Waarsing, H. Weinans, O.P. van der Jagt, Chondrogenically differentiated mesenchymal stromal cell pellets stimulate endochondral bone regeneration in critical-sized bone defects, Eur. Cells Mater. 27 (2014) 137–148. https://doi.org/10.22203/eCM.v027a11.

[89] A.M. McDermott, S. Herberg, D.E. Mason, J.M. Collins, H.B. Pearson, J.H. Dawahare, R. Tang, A.N. Patwa, M.W. Grinstaff, D.J. Kelly, E. Alsberg, J.D. Boerckel, Recapitulating bone development through engineered mesenchymal condensations and mechanical cues for tissue regeneration, Sci. Transl. Med. 11 (2019) 1–16. https://doi.org/10.1126/scitranslmed.aav7756.

[90] N.C. Rivron, C.C. Raiss, J. Liu, A. Nandakumar, C. Sticht, N. Gretz, R. TruckenmuÏler, J. Rouwkema, C.A. Van Blitterswijk, Sonic Hedgehog-activated engineered blood vessels enhance bone tissue formation, Proc. Natl. Acad. Sci. U. S. A. 109 (2012) 4413–4418. https://doi.org/10.1073/pnas.1117627109.

[91] S.H. Bhang, S.W. Cho, W.G. La, T.J. Lee, H.S. Yang, A.Y. Sun, S.H. Baek, J.W. Rhie, B.S. Kim, Angiogenesis in ischemic tissue produced by spheroid grafting of human adipose-derived

stromal cells, Biomaterials. 32 (2011) 2734–2747. https://doi.org/10.1016/j.biomaterials.2010.12.035.

[92] K. Mineda, J. Feng, H. Ishimine, H. Takada, K. Doi, S. Kuno, K. Kinoshita, K. Kanayama, H. Kato, T. Mashiko, I. Hashimoto, H. Nakanishi, A. Kurisaki, K. Yoshimura, Therapeutic Potential of Human Adipose-Derived Stem/Stromal Cell Microspheroids Prepared by Three-Dimensional Culture in Non-Cross-Linked Hyaluronic Acid Gel, Stem Cells Transl. Med. 4 (2015) 1511–1522. https://doi.org/10.5966/sctm.2015-0037.

[93] S.H. Kwon, S.H. Bhang, H.K. Jang, T. Rhim, B.S. Kim, Conditioned medium of adipose-derived stromal cell culture in three-dimensional bioreactors for enhanced wound healing, J. Surg. Res. 194 (2015) 8–17. https://doi.org/10.1016/j.jss.2014.10.053.

[94] M.W. Laschke, M.D. Menger, Adipose tissue-derived microvascular fragments: Natural vascularization units for regenerative medicine, Trends Biotechnol. 33 (2015) 442–448. https://doi.org/10.1016/j.tibtech.2015.06.001.

[95] M.W. Laschke, T.E. Schank, C. Scheuer, S. Kleer, S. Schuler, W. Metzger, D. Eglin, M. Alini, M.D. Menger, Three-dimensional spheroids of adipose-derived mesenchymal stem cells are potent initiators of blood vessel formation in porous polyurethane scaffolds, Acta Biomater. 9 (2013) 6876–6884. https://doi.org/10.1016/j.actbio.2013.02.013.

[96] D.N. Heo, M. Hospodiuk, I.T. Ozbolat, Synergistic interplay between human MSCs and HUVECs in 3D spheroids laden in collagen/fibrin hydrogels for bone tissue engineering, Acta Biomater. 95 (2019) 348–356. https://doi.org/10.1016/j.actbio.2019.02.046.

[97] B. Ayan, D.N. Heo, Z. Zhang, M. Dey, A. Povilianskas, C. Drapaca, I.T. Ozbolat, Aspiration-assisted bioprinting for precise positioning of biologics, Sci. Adv. 6 (2020) 1–17. https://doi.org/10.1126/sciadv.aaw5111.

[98] T.M. Achilli, J. Meyer, J.R. Morgan, Advances in the formation, use and understanding of multi-cellular spheroids, Expert Opin. Biol. Ther. 12 (2012) 1347–1360. https://doi.org/10.1517/14712598.2012.707181.

[99] J. Rouwkema, J. De Boer, C.A. Van Blitterswijk, Endothelial cells assemble into a 3-dimensional prevascular network in a bone tissue engineering construct, Tissue Eng. 12 (2006) 2685–2693. https://doi.org/10.1089/ten.2006.12.2685.

[100] L.A. Kunz-Schughart, J.A. Schroeder, M. Wondrak, F. Van Rey, K. Lehle, F. Hofstaedter, D.N. Wheatley, Potential of fibroblasts to regulate the formation of three-dimensional vessel-like structures from endothelial cells in vitro, Am. J. Physiol. - Cell Physiol. 290 (2006) 1385–1399. https://doi.org/10.1152/ajpcell.00248.2005.

[101] A. Wenger, A. Stahl, H. Weber, G. Finkenzeller, H.G. Augustin, G.B. Stark, U. Kneser, Modulation of In Vitro Angiogenesis in a Three-Dimensional Spheroidal Coculture Model for Bone Tissue Engineering, Tissue Eng. 10 (2004) 1536–1547. https://doi.org/10.1089/ten.2004.10.1536.

[102] A. Alajati, A.M. Laib, H. Weber, A.M. Boos, A. Bartol, K. Ikenberg, T. Korff, H. Zentgraf, C. Obodozie, R. Graeser, S. Christian, G. Finkenzeller, G.B. Stark, M. Héroult, H.G. Augustin, Spheroid-based engineering of a human vasculature in mice, Nat. Methods. 5 (2008) 439–445. https://doi.org/10.1038/nmeth.1198.

[103] J.M. Kelm, V. Djonov, L.M. Ittner, D. Fluri, W. Born, S.P. Hoerstrup, M. Fussenegger, Design of custom-shaped vascularized tissues using microtissue spheroids as minimal building units, Tissue Eng. 12 (2006) 2151–2160. https://doi.org/10.1089/ten.2006.12.2151.

[104] M.A. Skylar-Scott, S.G.M. Uzel, L.L. Nam, J.H. Ahrens, R.L. Truby, S. Damaraju, J.A. Lewis, Biomanufacturing of organ-specific tissues with high cellular density and embedded vascular channels, Sci. Adv. 5 (2019). https://doi.org/10.1126/sciadv.aaw2459.

[105] T.A. Gwyther, J.Z. Hu, A.G. Christakis, J.K. Skorinko, S.M. Shaw, K.L. Billiar, M.W. Rolle, Engineered vascular tissue fabricated from aggregated smooth muscle cells, Cells Tissues Organs. 194 (2011) 13–24. https://doi.org/10.1159/000322554.

[106] B.C. Dash, K. Levi, J. Schwan, J. Luo, O. Bartulos, H. Wu, C. Qiu, T. Yi, Y. Ren, S. Campbell, M.W. Rolle, Y. Qyang, Tissue-Engineered Vascular Rings from Human iPSC-Derived Smooth Muscle Cells, Stem Cell Reports. 7 (2016) 19–28. https://doi.org/10.1016/j.stemcr.2016.05.004.

[107] R. Gauvin, T. Ahsan, D. Larouche, P. Lévesque, J. Dubé, F.A. Auger, R.M. Nerem, L. Germain, A novel single-step self-assembly approach for the fabrication of tissue-engineered vascular constructs, Tissue Eng. - Part A. 16 (2010) 1737–1747. https://doi.org/10.1089/ten.tea.2009.0313.

[108] N. L'Heureux, S. Pâquet, R. Labbé, L. Germain, F.A. Auger, A completely biological tissue-engineered human blood vessel, FASEB J. 12 (1998) 47–56. https://doi.org/10.1096/fsb2fasebj.12.1.47.

[109] Y. Haraguchi, T. Shimizu, T. Sasagawa, H. Sekine, K. Sakaguchi, T. Kikuchi, W. Sekine, S. Sekiya, M. Yamato, M. Umezu, T. Okano, Fabrication of functional three-dimensional tissues by stacking cell sheets in vitro, Nat. Protoc. 7 (2012) 850–858. https://doi.org/10.1038/nprot.2012.027.

[110] C. Norotte, F.S. Marga, L.E. Niklason, G. Forgacs, Scaffold-free vascular tissue engineering using bioprinting, Biomaterials. 30 (2009) 5910–5917. https://doi.org/10.1016/j.biomaterials.2009.06.034.

[111] B.J. Huang, J.C. Hu, K.A. Athanasiou, Cell-based tissue engineering strategies used in the clinical repair of articular cartilage, Biomaterials. 98 (2016) 1–22. https://doi.org/10.1016/j.biomaterials.2016.04.018.

[112] A. Bistolfi, R. Ferracini, C. Galletta, F. Tosto, V. Sgarminato, E. Digo, E. Vernè, A. Massè, Regeneration of articular cartilage: Scaffold used in orthopedic surgery. A short handbook of available products for regenerative joints surgery, Clin. Sci. Res. Reports. 1 (2017) 1–7. https://doi.org/10.15761/csrr.1000101.

[113] X. Li, J. Ding, J. Wang, X. Zhuang, X. Chen, Biomimetic biphasic scaffolds for osteochondral defect repair, Regen. Biomater. 2 (2015) 221–228. https://doi.org/10.1093/rb/rbv015.

[114] M. Bhattacharjee, J. Coburn, M. Centola, S. Murab, A. Barbero, D.L. Kaplan, I. Martin, S. Ghosh, Tissue engineering strategies to study cartilage development, degeneration and regeneration, Adv. Drug Deliv. Rev. 84 (2015) 107–122. https://doi.org/10.1016/j.addr.2014.08.010.

[115] J.C. Hu, K.A. Athanasiou, A Self-Assembling Process in Articular Cartilage Tissue Engineering, Tissue Eng. 12 (2006) 969–979. https://doi.org/10.1089/ten.2006.12.969.

[116] L. Zhang, P. Su, C. Xu, J. Yang, W. Yu, D. Huang, Chondrogenic differentiation of human mesenchymal stem cells: A comparison between micromass and pellet culture systems, Biotechnol. Lett. 32 (2010) 1339–1346. https://doi.org/10.1007/s10529-010-0293-x.

[117] E.A. Makris, R.F. MacBarb, N.K. Paschos, J.C. Hu, K.A. Athanasiou, Combined use of chondroitinase-ABC, TGF-β1, and collagen crosslinking agent lysyl oxidase to engineer

functional neotissues for fibrocartilage repair, Biomaterials. 35 (2014) 6787–6796. https://doi.org/10.1016/j.biomaterials.2014.04.083.

[118] R.A. Kandel, M. Grynpas, R. Pilliar, J. Lee, J. Wang, S. Waldman, P. Zalzal, M. Hurtig, Repair of osteochondral defects with biphasic cartilage-calcium polyphosphate constructs in a Sheep model, Biomaterials. 27 (2006) 4120–4131. https://doi.org/10.1016/j.biomaterials.2006.03.005.

[119] P.B. Lewis, L.P. McCarty, J.Q. Yao, J.M. Williams, R. Kang, B.J. Cole, Fixation of tissue-engineered human neocartilage constructs with human fibrin in a caprine model., J. Knee Surg. 22 (2009) 196–204. https://doi.org/10.1055/s-0030-1247749.

[120] N. V. Mekhileri, K.S. Lim, G.C.J. Brown, I. Mutreja, B.S. Schon, G.J. Hooper, T.B.F. Woodfield, Automated 3D bioassembly of micro-tissues for biofabrication of hybrid tissue engineered constructs, Biofabrication. 10 (2018). https://doi.org/10.1088/1758-5090/aa9ef1.

[121] M. Younesi, V.M. Goldberg, O. Akkus, A micro-architecturally biomimetic collagen template for mesenchymal condensation based cartilage regeneration, Acta Biomater. 30 (2016) 212–221. https://doi.org/10.1016/j.actbio.2015.11.024.

[122] M.A. Gionet-Gonzales, J.K. Leach, Engineering principles for guiding spheroid function in the regeneration of bone, cartilage, and skin, Biomed. Mater. 13 (2018). https://doi.org/10.1088/1748-605X/aab0b3.

[123] A. Jauković, D. Abadjieva, D. Trivanović, E. Stoyanova, M. Kostadinova, S. Pashova, S. Kestendjieva, T. Kukolj, M. Jeseta, E. Kistanova, M. Mourdjeva, Specificity of 3D MSC Spheroids Microenvironment: Impact on MSC Behavior and Properties, Stem Cell Rev. Reports. 16 (2020) 853–875. https://doi.org/10.1007/s12015-020-10006-9.

[124] K.C. Murphy, B.P. Hung, S. Browne-Bourne, D. Zhou, J. Yeung, D.C. Genetos, J.K. Leach, Measurement of oxygen tension within mesenchymal stem cell spheroids, J. R. Soc. Interface. 14 (2017). https://doi.org/10.1098/rsif.2016.0851.

[125] R. Grantab, S. Sivananthan, I.F. Tannock, The penetration of anticancer drugs through tumor tissue as a function of cellular adhesion and packing density of tumor cells, Cancer Res. 66 (2006) 1033–1039. https://doi.org/10.1158/0008-5472.CAN-05-3077.

[126] B.A. Wagner, S. Venkataraman, G.R. Buettner, The rate of oxygen utilization by cells, Free Radic. Biol. Med. 51 (2011) 700–712. https://doi.org/10.1016/j.freeradbiomed.2011.05.024.

[127] K.C. Murphy, S.Y. Fang, J.K. Leach, Human mesenchymal stem cell spheroids in fibrin hydrogels exhibit improved cell survival and potential for bone healing, Cell Tissue Res. 357 (2014) 91–99. https://doi.org/10.1007/s00441-014-1830-z.

[128] L. De Moor, E. Beyls, H. Declercq, Scaffold Free Microtissue Formation for Enhanced Cartilage Repair, Ann. Biomed. Eng. 48 (2019) 298–311. https://doi.org/10.1007/s10439-019-02348-4.

[129] L.S. Moreira Teixeira, J.C.H. Leijten, J. Sobral, R. Jin, A.A. van Apeldoorn, J. Feijen, C. van Blitterswijk, P.J. Dijkstra, M. Karperien, High throughput generated micro-aggregates of chondrocytes stimulate cartilage formation in vitro and in vivo, Eur. Cells Mater. 23 (2012) 387–399. https://doi.org/10.22203/eCM.v023a30.

[130] J. Leijten, L.S. Moreira Teixeira, J. Bolander, W. Ji, B. Vanspauwen, J. Lammertyn, J. Schrooten, F.P. Luyten, Bioinspired seeding of biomaterials using three dimensional

microtissues induces chondrogenic stem cell differentiation and cartilage formation under growth factor free conditions, Sci. Rep. 6 (2016) 1–12. https://doi.org/10.1038/srep36011.

[131] J. Libera, K. Ruhnau, P. Baum, U. Lüthi, T. Schreyer, U. Meyer, H.P. Wiesmann, A. Herrmann, T. Korte, O. Pullig, V. Siodla, Cartilage Engineering, in: U. Meyer, J. Handschel, H.P. Wiesmann, T. Meyer (Eds.), Fundam. Tissue Eng. Regen. Med., Springer Berlin Heidelberg, Berlin, Heidelberg, 2009: pp. 233–242. https://doi.org/10.1007/978-3-540-77755-7_18.

[132] E.A. Makris, A.H. Gomoll, K.N. Malizos, J.C. Hu, K.A. Athanasiou, Repair and tissue engineering techniques for articular cartilage, Nat. Rev. Rheumatol. 11 (2015) 21–34. https://doi.org/10.1038/nrrheum.2014.157.

[133] J. Ng, Y. Wei, B. Zhou, A. Burapachaisri, E. Guo, G. Vunjak-Novakovic, Extracellular matrix components and culture regimen selectively regulate cartilage formation by self-assembling human mesenchymal stem cells in vitro and in vivo, Stem Cell Res. Ther. 7 (2016) 1–12. https://doi.org/10.1186/s13287-016-0447-4.

[134] H. Fan, C. Zhang, J. Li, L. Bi, L. Qin, H. Wu, Y. Hu, Gelatin microspheres containing TGF-β3 enhance the chondrogenesis of mesenchymal stem cells in modified pellet culture, Biomacromolecules. 9 (2008) 927–934. https://doi.org/10.1021/bm7013203.

[135] M.E. Candela, R. Yasuhara, M. Iwamoto, M. Enomoto-Iwamoto, Resident mesenchymal progenitors of articular cartilage, Matrix Biol. 39 (2014) 44–49. https://doi.org/10.1016/j.matbio.2014.08.015.

[136] D.E. Anderson, B.D. Markway, K.J. Weekes, H.E. McCarthy, B. Johnstone, Physioxia Promotes the Articular Chondrocyte-Like Phenotype in Human Chondroprogenitor-Derived Self-Organized Tissue, Tissue Eng. Part A. 24 (2018) 264–274. https://doi.org/10.1089/ten.tea.2016.0510.

[137] A.J. Hayes, S. MacPherson, H. Morrison, G. Dowthwaite, C.W. Archer, The development of articular cartilage: evidence for an appositional growth mechanism., Anat. Embryol. (Berl). 203 (2001) 469–479. https://doi.org/10.1007/s004290100178.

[138] M. Lehmann, F. Martin, K. Mannigel, K. Kaltschmidt, U. Sack, U. Anderer, Three-dimensional scaffold-free fusion culture: The way to enhance chondrogenesis of in vitro propagated human articular chondrocytes, Eur. J. Histochem. 57 (2013) 206–216. https://doi.org/10.4081/ejh.2013.e31.

[139] D. Murata, S. Tokunaga, T. Tamura, H. Kawaguchi, N. Miyoshi, M. Fujiki, K. Nakayama, K. Misumi, A preliminary study of osteochondral regeneration using a scaffold-free three-dimensional construct of porcine adipose tissue-derived mesenchymal stem cells, J. Orthop. Surg. Res. 10 (2015) 1–12. https://doi.org/10.1186/s13018-015-0173-0.

[140] T. Oshima, J. Nakase, T. Toratani, H. Numata, Y. Takata, K. Nakayama, H. Tsuchiya, A Scaffold-Free Allogeneic Construct From Adipose-Derived Stem Cells Regenerates an Osteochondral Defect in a Rabbit Model, Arthrosc. - J. Arthrosc. Relat. Surg. 35 (2019) 583–593. https://doi.org/10.1016/j.arthro.2018.08.033.

[141] A. Yamasaki, Y. Kunitomi, D. Murata, T. Sunaga, T. Kuramoto, T. Sogawa, K. Misumi, Osteochondral regeneration using constructs of mesenchymal stem cells made by bio three-dimensional printing in mini-pigs, J. Orthop. Res. 37 (2019) 1398–1408. https://doi.org/10.1002/jor.24206.

[142] B.K. Babur, K. Futrega, W.B. Lott, T.J. Klein, J. Cooper-White, M.R. Doran, High-throughput

bone and cartilage micropellet manufacture, followed by assembly of micropellets into biphasic osteochondral tissue, Cell Tissue Res. 361 (2015) 755–768. https://doi.org/10.1007/s00441-015-2159-y.

[143] J. Malda, J. Visser, F.P. Melchels, T. Jüngst, W.E. Hennink, W.J.A. Dhert, J. Groll, D.W. Hutmacher, 25th Anniversary Article: Engineering Hydrogels for Biofabrication, Adv. Mater. 25 (2013) 5011–5028. https://doi.org/10.1002/adma.201302042.

[144] A. McCormack, C.B. Highley, N.R. Leslie, F.P.W. Melchels, 3D Printing in Suspension Baths: Keeping the Promises of Bioprinting Afloat, Trends Biotechnol. 38 (2020) 584–593. https://doi.org/10.1016/j.tibtech.2019.12.020.

[145] T. Bhattacharjee, C.J. Gil, S.L. Marshall, J.M. Urueña, C.S. O'Bryan, M. Carstens, B. Keselowsky, G.D. Palmer, S. Ghivizzani, C.P. Gibbs, W.G. Sawyer, T.E. Angelini, Liquid-like Solids Support Cells in 3D, ACS Biomater. Sci. Eng. 2 (2016) 1787–1795. https://doi.org/10.1021/acsbiomaterials.6b00218.

[146] O. Jeon, Y. Bin Lee, H. Jeong, S.J. Lee, D. Wells, E. Alsberg, Individual cell-only bioink and photocurable supporting medium for 3D printing and generation of engineered tissues with complex geometries, Mater. Horizons. 6 (2019) 1625–1631. https://doi.org/10.1039/C9MH00375D.

[147] N. Noor, A. Shapira, R. Edri, I. Gal, L. Wertheim, T. Dvir, 3D Printing of Personalized Thick and Perfusable Cardiac Patches and Hearts, Adv. Sci. 6 (2019) 1900344. https://doi.org/10.1002/advs.201900344.

[148] B. Ayan, Y. Wu, V. Karuppagounder, F. Kamal, I.T. Ozbolat, Aspiration-assisted bioprinting of the osteochondral interface, Sci. Rep. 10 (2020) 1–12. https://doi.org/10.1038/s41598-020-69960-6.

[149] N.I. Moldovan, N. Hibino, K. Nakayama, Principles of the kenzan method for robotic cell spheroid-based three-dimensional bioprinting, Tissue Eng. - Part B Rev. 23 (2017) 237–244. https://doi.org/10.1089/ten.teb.2016.0322.

[150] M. Itoh, K. Nakayama, R. Noguchi, K. Kamohara, K. Furukawa, K. Uchihashi, S. Toda, J.I. Oyama, K. Node, S. Morita, Scaffold-free tubular tissues created by a bio-3D printer undergo remodeling and endothelialization when implanted in rat aortae, PLoS One. 10 (2015) 1–15. https://doi.org/10.1371/journal.pone.0136681.

[151] S.P. Grogan, E.W. Dorthé, N.E. Glembotski, F. Gaul, D.D. D'Lima, Cartilage tissue engineering combining microspheroid building blocks and microneedle arrays, Connect. Tissue Res. 61 (2020) 229–243. https://doi.org/10.1080/03008207.2019.1617280.

[152] V. Mironov, R.P. Visconti, V. Kasyanov, G. Forgacs, C.J. Drake, R.R. Markwald, Organ printing: Tissue spheroids as building blocks, Biomaterials. 30 (2009) 2164–2174. https://doi.org/10.1016/j.biomaterials.2008.12.084.

[153] Y. Lu, W. Zhang, J. Wang, G. Yang, S. Yin, T. Tang, C. Yu, X. Jiang, Recent advances in cell sheet technology for bone and cartilage regeneration: from preparation to application, Int. J. Oral Sci. 11 (2019). https://doi.org/10.1038/s41368-019-0050-5.

[154] V. Mironov, V. Kasyanov, R.R. Markwald, Organ printing: From bioprinter to organ biofabrication line, Curr. Opin. Biotechnol. 22 (2011) 667–673. https://doi.org/10.1016/j.copbio.2011.02.006.

[155] A.N. Leberfinger, D.J. Ravnic, A. Dhawan, I.T. Ozbolat, Concise Review: Bioprinting of Stem Cells for Transplantable Tissue Fabrication, Stem Cells Transl. Med. 6 (2017) 1940–1948.

https://doi.org/10.1002/sctm.17-0148.

[156] R.Z. Lin, H.Y. Chang, Recent advances in three-dimensional multicellular spheroid culture for biomedical research, Biotechnol. J. 3 (2008) 1172–1184. https://doi.org/10.1002/biot.200700228.

[157] J.M. Karp, J. Yeh, G. Eng, J. Fukuda, J. Blumling, K.Y. Suh, J. Cheng, A. Mahdavi, J. Borenstein, R. Langer, A. Khademhosseini, Controlling size, shape and homogeneity of embryoid bodies using poly(ethylene glycol) microwells, Lab Chip. 7 (2007) 786–794. https://doi.org/10.1039/b705085m.

[158] H. Tekin, M. Anaya, M.D. Brigham, C. Nauman, R. Langer, A. Khademhosseini, Stimuli-responsive microwells for formation and retrieval of cell aggregates, Lab Chip. 10 (2010) 2411–2418. https://doi.org/10.1039/c004732e.

[159] B.C. Kim, J.H. Kim, H.J. An, W. Byun, J.H. Park, I.K. Kwon, J.S. Kim, Y.S. Hwang, Microwell-mediated micro cartilage-like tissue formation of adipose-derived stem cell, Macromol. Res. 22 (2014) 287–296. https://doi.org/10.1007/s13233-014-2044-7.

[160] G.S. Jeong, Y. Jun, J.H. Song, S.H. Shin, S.H. Lee, Meniscus induced self organization of multiple deep concave wells in a microchannel for embryoid bodies generation, Lab Chip. 12 (2012) 159–166. https://doi.org/10.1039/c1lc20619b.

[161] A.P. Napolitano, D.M. Dean, A.J. Man, J. Youssef, D.N. Ho, A.P. Rago, M.P. Lech, J.R. Morgan, Scaffold-free three-dimensional cell culture utilizing micromolded nonadhesive hydrogels, Biotechniques. 43 (2007) 494–500. https://doi.org/10.2144/000112591.

[162] L. Zhao, S. Mok, C. Moraes, Micropocket hydrogel devices for all-in-one formation, assembly, and analysis of aggregate-based tissues, Biofabrication. (2019). https://doi.org/10.1088/1758-5090/ab30b4.

[163] H.W. Kang, S.J. Lee, I.K. Ko, C. Kengla, J.J. Yoo, A. Atala, A 3D bioprinting system to produce human-scale tissue constructs with structural integrity, Nat. Biotechnol. 34 (2016) 312–319. https://doi.org/10.1038/nbt.3413.

[164] J. Nulty, F.E. Freeman, D.C. Browe, R. Burdis, D.P. Ahern, P. Pitacco, Y. Bin Lee, E. Alsberg, D.J. Kelly, 3D Bioprinting of prevascularised implants for the repair of critically-sized bone defects, Acta Biomater. (2021). https://doi.org/10.1016/j.actbio.2021.03.003.

[165] C.T. Buckley, T. Vinardell, S.D. Thorpe, M.G. Haugh, E. Jones, D. McGonagle, D.J. Kelly, Functional properties of cartilaginous tissues engineered from infrapatellar fat pad-derived mesenchymal stem cells, J. Biomech. 43 (2010) 920–926. https://doi.org/10.1016/j.jbiomech.2009.11.005.

[166] H.K. Heywood, D.L. Bader, D.A. Lee, Rate of oxygen consumption by isolated articular chondrocytes is sensitive to medium glucose concentration, J. Cell. Physiol. 206 (2006) 402–410. https://doi.org/10.1002/jcp.20491.

[167] M.J. Farrell, J.I. Shin, L.J. Smith, R.L. Mauck, Functional consequences of glucose and oxygen deprivation onengineered mesenchymal stem cell-based cartilage constructs, Osteoarthr. Cartil. 23 (2015) 134–142. https://doi.org/10.1016/j.joca.2014.09.012.

[168] H.A. Leddy, H.A. Awad, F. Guilak, Molecular diffusion in tissue-engineered cartilage constructs: Effects of scaffold material, time, and culture conditions, J. Biomed. Mater. Res. - Part B Appl. Biomater. 70 (2004) 397–406. https://doi.org/10.1002/jbm.b.30053.

[169] S. Razaq, R.J. Wilkins, J.P.G. Urban, The effect of extracellular pH on matrix turnover by

cells of the bovine nucleus pulposus, Eur. Spine J. 12 (2003) 341–349. https://doi.org/10.1007/s00586-003-0582-3.

[170] W.L. Murphy, C.A. Simmons, D. Kaigler, D.J. Mooney, Bone regeneration via a mineral substrate and induced angiogenesis., J. Dent. Res. 83 (2004) 204–10. https://doi.org/10.1177/154405910408300304.

[171] D.H.R. Kempen, L. Lu, A. Heijink, T.E. Hefferan, L.B. Creemers, A. Maran, M.J. Yaszemski, W.J.A. Dhert, Effect of local sequential VEGF and BMP-2 delivery on ectopic and orthotopic bone regeneration, Biomaterials. 30 (2009) 2816–2825.

[172] W. Zhang, C. Zhu, Y. Wu, D. Ye, S. Wang, D. Zou, X. Zhang, D.L. Kaplan, X. Jiang, VEGF and BMP-2 promote bone regeneration by facilitating bone marrow stem cell homing and differentiation, Eur. Cells Mater. 27 (2014) 1–12.

[173] W. Zhang, L.S. Wray, J. Rnjak-Kovacina, L. Xu, D. Zou, S. Wang, M. Zhang, J. Dong, G. Li, D.L. Kaplan, X. Jiang, Vascularization of hollow channel-modified porous silk scaffolds with endothelial cells for tissue regeneration, Biomaterials. 56 (2015) 68–77. https://doi.org/10.1016/J.BIOMATERIALS.2015.03.053.

[174] C. Feng, W. Zhang, C. Deng, G. Li, J. Chang, Z. Zhang, X. Jiang, C. Wu, 3D Printing of Lotus Root-Like Biomimetic Materials for Cell Delivery and Tissue Regeneration, Adv. Sci. 4 (2017) 1700401. https://doi.org/10.1002/advs.201700401.

[175] A.C. Daly, P. Pitacco, J. Nulty, G.M. Cunniffe, D.J. Kelly, 3D printed microchannel networks to direct vascularisation during endochondral bone repair, Biomaterials. 162 (2018) 34–46. https://doi.org/10.1016/J.BIOMATERIALS.2018.01.057.

[176] M.W. Laschke, H. Mussawy, S. Schuler, A. Kazakov, M. Rücker, D. Eglin, M. Alini, M.D. Menger, Short-Term Cultivation of *In Situ* Prevascularized Tissue Constructs Accelerates Inosculation of Their Preformed Microvascular Networks After Implantation into the Host Tissue, Tissue Eng. Part A. 17 (2011) 841–853. https://doi.org/10.1089/ten.tea.2010.0329.

[177] X. Liu, W. Chen, C. Zhang, W. Thein-Han, K. Hu, M.A. Reynolds, C. Bao, P. Wang, L. Zhao, H.H.K. Xu, Co-Seeding Human Endothelial Cells with Human-Induced Pluripotent Stem Cell-Derived Mesenchymal Stem Cells on Calcium Phosphate Scaffold Enhances Osteogenesis and Vascularization in Rats., Tissue Eng. Part A. 23 (2017) 546–555. https://doi.org/10.1089/ten.tea.2016.0485.

[178] D. Egger, C. Tripisciano, V. Weber, M. Dominici, C. Kasper, Dynamic cultivation of mesenchymal stem cell aggregates, Bioengineering. 5 (2018) 1–15. https://doi.org/10.3390/bioengineering5020048.

[179] C. Hildebrandt, H. Büth, H. Thielecke, A scaffold-free in vitro model for osteogenesis of human mesenchymal stem cells, Tissue Cell. 43 (2011) 91–100. https://doi.org/10.1016/j.tice.2010.12.004.

[180] J.M. Cha, E.K. Shin, J.H. Sung, G.J. Moon, E.H. Kim, Y.H. Cho, H.D. Park, H. Bae, J. Kim, O.Y. Bang, Efficient scalable production of therapeutic microvesicles derived from human mesenchymal stem cells, Sci. Rep. 8 (2018) 1–16. https://doi.org/10.1038/s41598-018-19211-6.

[181] P.R. Baraniak, T.C. McDevitt, Scaffold-free culture of mesenchymal stem cell spheroids in suspension preserves multilineage potential, Cell Tissue Res. 347 (2012) 701–711. https://doi.org/10.1007/s00441-011-1215-5.

[182] S.K. Kapur, X. Wang, H. Shang, S. Yun, X. Li, G. Feng, M. Khurgel, A.J. Katz, Human adipose

stem cells maintain proliferative, synthetic and multipotential properties when suspension cultured as self-assembling spheroids, Biofabrication. 4 (2012) 025004. https://doi.org/10.1088/1758-5082/4/2/025004.

[183] D. Egger, I. Schwedhelm, J. Hansmann, C. Kasper, Hypoxic three-dimensional scaffold-free aggregate cultivation of mesenchymal stem cells in a stirred tank reactor, Bioengineering. 4 (2017). https://doi.org/10.3390/bioengineering4020047.

[184] L.M. Allen, J. Matyas, M. Ungrin, D.A. Hart, A. Sen, Serum-Free Culture of Human Mesenchymal Stem Cell Aggregates in Suspension Bioreactors for Tissue Engineering Applications, Stem Cells Int. 2019 (2019). https://doi.org/10.1155/2019/4607461.

[185] M. Stephenson, W. Grayson, Recent advances in bioreactors for cell-based therapies, F1000Research. 7 (2018) 517. https://doi.org/10.12688/f1000research.12533.1.

[186] W. Kafienah, T.J. Sims, Biochemical Methods for the Analysis of Tissue-Engineered Cartilage, in: Biopolym. Methods Tissue Eng., Humana Press, New Jersey, 2004: pp. 217–230. https://doi.org/10.1385/1-59259-428-X:217.

[187] C.T. Buckley, S.D. Thorpe, D.J. Kelly, Engineering of large cartilaginous tissues through the use of microchanneled hydrogels and rotational culture, Tissue Eng. - Part A. 15 (2009) 3213–3220. https://doi.org/10.1089/ten.tea.2008.0531.

[188] E.J. Sheehy, C.T. Buckley, D.J. Kelly, Chondrocytes and bone marrow-derived mesenchymal stem cells undergoing chondrogenesis in agarose hydrogels of solid and channelled architectures respond differentially to dynamic culture conditions, J. Tissue Eng. Regen. Med. 5 (2011) 747–758. https://doi.org/10.1002/term.385.

[189] L.M. Kock, J. Malda, W.J.A. Dhert, K. Ito, D. Gawlitta, Flow-perfusion interferes with chondrogenic and hypertrophic matrix production by mesenchymal stem cells, J. Biomech. 47 (2014) 2122–2129. https://doi.org/10.1016/j.jbiomech.2013.11.006.

[190] A. Gonalves, P. Costa, M.T. Rodrigues, I.R. Dias, R.L. Reis, M.E. Gomes, Effect of flow perfusion conditions in the chondrogenic differentiation of bone marrow stromal cells cultured onto starch based biodegradable scaffolds, Acta Biomater. 7 (2011) 1644–1652. https://doi.org/10.1016/j.actbio.2010.11.044.

[191] E.G. Meyer, C.T. Buckley, S.D. Thorpe, D.J. Kelly, Low oxygen tension is a more potent promoter of chondrogenic differentiation than dynamic compression, J. Biomech. 43 (2010) 2516–2523. https://doi.org/10.1016/j.jbiomech.2010.05.020.

[192] C.T. Buckley, T. Vinardell, D.J. Kelly, Oxygen tension differentially regulates the functional properties of cartilaginous tissues engineered from infrapatellar fat pad derived MSCs and articular chondrocytes, Osteoarthr. Cartil. 18 (2010) 1345–1354. https://doi.org/10.1016/j.joca.2010.07.004.

[193] J. Leijten, N. Georgi, L.M. Teixeira, C.A. Van Blitterswijk, J.N. Post, M. Karperien, Metabolic programming of mesenchymal stromal cells by oxygen tension directs chondrogenic cell fate, Proc. Natl. Acad. Sci. U. S. A. 111 (2014) 13954–13959. https://doi.org/10.1073/pnas.1410977111.

[194] E.J. Koay, K.A. Athanasiou, Hypoxic chondrogenic differentiation of human embryonic stem cells enhances cartilage protein synthesis and biomechanical functionality, Osteoarthr. Cartil. 16 (2008) 1450–1456. https://doi.org/10.1016/j.joca.2008.04.007.

[195] E.J. Sheehy, C.T. Buckley, D.J. Kelly, Oxygen tension regulates the osteogenic, chondrogenic and endochondral phenotype of bone marrow derived mesenchymal stem cells, Biochem.

Biophys. Res. Commun. 417 (2012) 305–310. https://doi.org/10.1016/j.bbrc.2011.11.105.

[196] C.T. Buckley, E.G. Meyer, D.J. Kelly, The influence of construct scale on the composition and functional properties of cartilaginous tissues engineered using bone marrow-derived mesenchymal stem cells, Tissue Eng. - Part A. 18 (2012) 382–396. https://doi.org/10.1089/ten.tea.2011.0145.

[197] A.C. Daly, B.N. Sathy, D.J. Kelly, Engineering large cartilage tissues using dynamic bioreactor culture at defined oxygen conditions, J. Tissue Eng. 9 (2018). https://doi.org/10.1177/2041731417753718.

[198] W.L. Grayson, S. Bhumiratana, P.H. Grace Chao, C.T. Hung, G. Vunjak-Novakovic, Spatial regulation of human mesenchymal stem cell differentiation in engineered osteochondral constructs: Effects of pre-differentiation, soluble factors and medium perfusion, Osteoarthr. Cartil. 18 (2010) 714–723. https://doi.org/10.1016/j.joca.2010.01.008.

[199] D. Chen, J.Y. Wu, K.M. Kennedy, K. Yeager, J.C. Bernhard, J.J. Ng, B.K. Zimmerman, S. Robinson, K.M. Durney, C. Shaeffer, O.F. Vila, C. Takawira, J.M. Gimble, X. Edward Guo, G.A. Ateshian, M.J. Lopez, S.B. Eisig, G. Vunjak-Novakovic, Tissue engineered autologous cartilage-bone grafts for temporomandibular joint regeneration, Sci. Transl. Med. 12 (2020) 1–16. https://doi.org/10.1126/scitranslmed.abb6683.

[200] Y. Yamaguchi, J. Ohno, A. Sato, H. Kido, T. Fukushima, Mesenchymal stem cell spheroids exhibit enhanced in-vitro and in-vivo osteoregenerative potential, BMC Biotechnol. 14 (2014) 1–10. https://doi.org/10.1186/s12896-014-0105-9.

[201] C.P. Neu, K. Komvopoulos, A.H. Reddi, The Interface of Functional Biotribology and Regenerative Medicine in Synovial Joints, Tissue Eng. Part B Rev. 14 (2008) 235–247. https://doi.org/10.1089/ten.teb.2008.0047.

[202] D. Eyre, M. Weis, J.-J. Wu, Articular cartilage collagen: an irreplaceable framework?, Eur. Cells Mater. 12 (2006) 57–63. https://doi.org/10.22203/eCM.v012a07.

[203] Y. Krishnan, A.J. Grodzinsky, Cartilage diseases, Matrix Biol. (2018). https://doi.org/10.1016/j.matbio.2018.05.005.

[204] N.P. Cohen, R.J. Foster, V.C. Mow, Composition and Dynamics of Articular Cartilage: Structure, Function, and Maintaining Healthy State, Jounal Orthop. Sport Phys. Ther. 28 (1998) 203–215. www.jospt.org (accessed September 20, 2018).

[205] D. Eyre, Collagen of articular cartilage, Arthritis Res. 4 (2002) 30–35. https://doi.org/10.1186/ar380.

[206] C. a Poole, S. Ayad, R.T. Gilbert, Chondrons from articular cartilage. V. Immunohistochemical evaluation of type VI collagen organisation in isolated chondrons by light, confocal and electron microscopy., J. Cell Sci. 103 (Pt 4 (1992) 1101–1110. https://doi.org/10.1016/S0021-9290(99)00175-X.

[207] C. Poole, Articular Cartilage chondrons - form, function and failure, J. Anat. (1997) 1–13. https://onlinelibrary.wiley.com/doi/pdf/10.1046/j.1469-7580.1997.19110001.x (accessed August 15, 2018).

[208] S. Söder, L. Hambach, R. Lissner, T. Kirchner, T. Aigner, Ultrastructural localization of type VI collagen in normal adult and osteoarthritic human articular cartilage, Osteoarthr. Cartil. 10 (2002) 464–470. https://doi.org/10.1053/joca.2002.0512.

[209] P.J. Roughley, The structure and function of cartilage proteoglycans, Eur. Cells Mater. 12

(2006) 92–101. https://doi.org/10.22203/eCM.v012a11.

[210] L. Luo, J.Y.J. Chu, R. Eswaramoorthy, K.J. Mulhall, D.J. Kelly, Engineering Tissues That Mimic the Zonal Nature of Articular Cartilage Using Decellularized Cartilage Explants Seeded with Adult Stem Cells, ACS Biomater. Sci. Eng. 3 (2017) 1933–1943. https://doi.org/10.1021/acsbiomaterials.6b00020.

[211] A.C. Daly, G.M. Cunniffe, B.N. Sathy, O. Jeon, E. Alsberg, D.J. Kelly, 3D Bioprinting of Developmentally Inspired Templates for Whole Bone Organ Engineering, Adv. Healthc. Mater. 5 (2016) 2353–2362. https://doi.org/10.1002/adhm.201600182.

[212] M. Castilho, V. Mouser, M. Chen, J. Malda, K. Ito, Bi-layered micro-fibre reinforced hydrogels for articular cartilage regeneration, Acta Biomater. 95 (2019) 297–306. https://doi.org/10.1016/j.actbio.2019.06.030.

[213] B. Johnstone, T.M. Hering, A.I. Caplan, V.M. Goldberg, J.U. Yoo, In VitroChondrogenesis of Bone Marrow-Derived Mesenchymal Progenitor Cells, Exp. Cell Res. 238 (1998) 265–272. https://doi.org/10.1006/excr.1997.3858.

[214] Y. Yu, K.K. Moncal, J. Li, W. Peng, I. Rivero, J.A. Martin, I.T. Ozbolat, Three-dimensional bioprinting using self-Assembling scalable scaffold-free “tissue strands” as a new bioink, Sci. Rep. 6 (2016) 1–11. https://doi.org/10.1038/srep28714.

[215] Y. Wu, B. Ayan, K.K. Moncal, Y. Kang, A. Dhawan, S. V. Koduru, D.J. Ravnic, F. Kamal, I.T. Ozbolat, Hybrid Bioprinting of Zonally Stratified Human Articular Cartilage Using Scaffold-Free Tissue Strands as Building Blocks, Adv. Healthc. Mater. 9 (2020) 1–15. https://doi.org/10.1002/adhm.202001657.

[216] H. Gudapati, M. Dey, I. Ozbolat, A comprehensive review on droplet-based bioprinting: Past, present and future, Biomaterials. 102 (2016) 20–42. https://doi.org/10.1016/j.biomaterials.2016.06.012.

[217] T. Xu, K.W. Binder, M.Z. Albanna, D. Dice, W. Zhao, J.J. Yoo, A. Atala, Hybrid printing of mechanically and biologically improved constructs for cartilage tissue engineering applications, Biofabrication. 5 (2013). https://doi.org/10.1088/1758-5082/5/1/015001.

[218] X. Cui, K. Breitenkamp, M.G. Finn, M. Lotz, D.D. D’Lima, Direct Human Cartilage Repair Using Three-Dimensional Bioprinting Technology, Tissue Eng. Part A. 18 (2012) 1304–1312. https://doi.org/10.1089/ten.tea.2011.0543.

[219] M. Sittinger, D.W. Hutmacher, M. V Risbud, Current strategies for cell delivery in cartilage and bone regeneration, Curr. Opin. Biotechnol. 15 (2004) 411–418. https://doi.org/10.1016/j.copbio.2004.08.010.

[220] S. Knecht, C. Erggelet, M. Endres, M. Sittinger, C. Kaps, E. Stüssi, Mechanical testing of fixation techniques for scaffold-based tissue-engineered grafts, J. Biomed. Mater. Res. - Part B Appl. Biomater. 83 (2007) 50–57. https://doi.org/10.1002/jbm.b.30765.

[221] T. Efe, C. Theisen, S. Fuchs-Winkelmann, T. Stein, A. Getgood, M.B. Rominger, J.R.J. Paletta, M.D. Schofer, Cell-free collagen type I matrix for repair of cartilage defects-clinical and magnetic resonance imaging results, Knee Surgery, Sport. Traumatol. Arthrosc. 20 (2012) 1915–1922. https://doi.org/10.1007/s00167-011-1777-5.

[222] M. Drobnič, D. Radosavljevič, D. Ravnik, V. Pavlovčič, M. Hribernik, Comparison of four techniques for the fixation of a collagen scaffold in the human cadaveric knee, Osteoarthr. Cartil. 14 (2006) 337–344. https://doi.org/10.1016/j.joca.2005.11.007.

[223] D. Enea, S. Cecconi, S. Calcagno, A. Busilacchi, S. Manzotti, C. Kaps, A. Gigante, Single-stage cartilage repair in the knee with microfracture covered with a resorbable polymer-based matrix and autologous bone marrow concentrate, Knee. 20 (2013) 562–569. https://doi.org/10.1016/j.knee.2013.04.003.

[224] J. Gille, E. Schuseil, J. Wimmer, J. Gellissen, A.P. Schulz, P. Behrens, Mid-term results of Autologous Matrix-Induced Chondrogenesis for treatment of focal cartilage defects in the knee, Knee Surgery, Sport. Traumatol. Arthrosc. 18 (2010) 1456–1464. https://doi.org/10.1007/s00167-010-1042-3.

[225] L. De Girolamo, G. Bertolini, M. Cervellin, G. Sozzi, P. Volpi, Treatment of chondral defects of the knee with one step matrix-assisted technique enhanced by autologous concentrated bone marrow: In vitro characterisation of mesenchymal stem cells from iliac crest and subchondral bone, Injury. 41 (2010) 1172–1177. https://doi.org/10.1016/j.injury.2010.09.027.

[226] T. Zantop, W. Petersen, Arthroscopic Implantation of a Matrix to Cover Large Chondral Defect During Microfracture, Arthrosc. - J. Arthrosc. Relat. Surg. 25 (2009) 1354–1360. https://doi.org/10.1016/j.arthro.2009.04.077.

[227] W. Petersen, S. Zelle, T. Zantop, Arthroscopic implantation of a three dimensional scaffold for autologous chondrocyte transplantation, Arch. Orthop. Trauma Surg. 128 (2008) 505–508. https://doi.org/10.1007/s00402-007-0348-1.

[228] J.E.J. Bekkers, A.I. Tsuchida, J. Malda, L.B. Creemers, R.J.M. Castelein, D.B.F. Saris, W.J.A. Dhert, Quality of scaffold fixation in a human cadaver knee model, Osteoarthr. Cartil. 18 (2010) 266–272. https://doi.org/10.1016/j.joca.2009.09.001.

[229] R. Rezakhaniha, A. Agianniotis, J.T.C. Schrauwen, A. Griffa, D. Sage, C.V.C. Bouten, F.N. Van De Vosse, M. Unser, N. Stergiopulos, Experimental investigation of collagen waviness and orientation in the arterial adventitia using confocal laser scanning microscopy, Biomech. Model. Mechanobiol. 11 (2012) 461–473. https://doi.org/10.1007/s10237-011-0325-z.

[230] A.R. Gannon, T. Nagel, A.P. Bell, N.C. Avery, D.J. Kelly, Postnatal changes to the mechanical properties of articular cartilage are driven by the evolution of its Collagen network, Eur. Cells Mater. 29 (2015) 105–123. https://doi.org/10.22203/eCM.v029a09.

[231] D.J. Huey, J.C. Hu, K.A. Athanasiou, Unlike Bone, Cartilage Regeneration Remains Elusive, Science (80-.). 338 (2012) 917–921. https://doi.org/10.1126/science.1222454.

[232] I.M. Khan, S.J. Gilbert, S.K. Singhrao, V.C. Duance, C.W. Archer, Cartilage integration: Evaluation of the reasons for failure of integration during cartilage repair. A review, Eur. Cells Mater. 16 (2008) 26–39. https://doi.org/10.22203/eCM.v016a04.

[233] S. Parithimarkalaignan, T. V Padmanabhan, Osseointegration: An Update, J. Indian Prosthodont. Soc. 13 (2013) 2–6. https://doi.org/10.1007/s13191-013-0252-z.

[234] A.B. Novaes, S.L.S. de Souza, R.R.M. de Barros, K.K.Y. Pereira, G. Iezzi, A. Piattelli, Influence of implant surfaces on osseointegration, Braz. Dent. J. 21 (2010) 471–481. https://doi.org/10.1590/s0103-64402010000600001.

[235] Y. Liu, G. Zhou, Y. Cao, Recent Progress in Cartilage Tissue Engineering—Our Experience and Future Directions, Engineering. 3 (2017) 28–35. https://doi.org/10.1016/J.ENG.2017.01.010.

[236] A. Yamasaki, Y. Kunitomi, D. Murata, T. Sunaga, T. Kuramoto, T. Sogawa, K. Misumi, Osteochondral regeneration using constructs of mesenchymal stem cells made by bio

three-dimensional printing in mini-pigs, J. Orthop. Res. 37 (2019) 1398–1408. https://doi.org/10.1002/jor.24206.

[237] C.M. McLeod, R.L. Mauck, On the origin and impact of mesenchymal stem cell heterogeneity: New insights and emerging tools for single cell analysis, Eur. Cells Mater. 34 (2017) 217–231. https://doi.org/10.22203/eCM.v034a14.

[238] J. van der Stok, M.K.E. Koolen, H. Jahr, N. Kops, J.H. Waarsing, H. Weinans, O.P. van der Jagt, Chondrogenically differentiated mesenchymal stromal cell pellets stimulate endochondral bone regeneration in critical-sized bone defects, Eur. Cells Mater. 27 (2014) 137–148. https://doi.org/10.22203/eCM.v027a11.

[239] X. Tang, L. Fan, M. Pei, L. Zeng, Z. Ge, Evolving concepts of chondrogenic differentiation: History, state-of-the-art and future perspectives, Eur. Cells Mater. 30 (2015) 12–27. https://doi.org/10.22203/eCM.v030a02.

[240] R.A. Somoza, J.F. Welter, D. Correa, A.I. Caplan, Chondrogenic differentiation of mesenchymal stem cells: Challenges and unfulfilled expectations, Tissue Eng. - Part B Rev. 20 (2014) 596–608. https://doi.org/10.1089/ten.teb.2013.0771.

[241] L.A. Solchaga, K. Penick, J.D. Porter, V.M. Goldberg, A.I. Caplan, J.F. Welter, FGF-2 enhances the mitotic and chondrogenic potentials of human adult bone marrow-derived mesenchymal stem cells, J. Cell. Physiol. 203 (2005) 398–409. https://doi.org/10.1002/jcp.20238.

[242] F. Ng, S. Boucher, S. Koh, K.S.R. Sastry, L. Chase, U. Lakshmipathy, C. Choong, Z. Yang, M.C. Vemuri, M.S. Rao, V. Tanavde, PDGF, tgf- 2. And FGF signaling is important for differentiation and growth of mesenchymal stem cells (mscs): Transcriptional profiling can identify markers and signaling pathways important in differentiation of MSCs into adipogenic, chondrogenic, and ost, Blood. 112 (2008) 295–307. https://doi.org/10.1182/blood-2007-07-103697.

[243] C.A. Hellingman, W. Koevoet, N. Kops, E. Farrell, H. Jahr, W. Liu, R.J.B. De Jong, D.A. Frenz, G.J.V.M. Van Osch, Fibroblast growth factor receptors in in vitro and in vivo chondrogenesis: Relating tissue engineering using adult mesenchymal stem cells to embryonic development, Tissue Eng. - Part A. 16 (2010) 545–556. https://doi.org/10.1089/ten.tea.2008.0551.

[244] S. Boeuf, W. Richter, Chondrogenesis of mesenchymal stem cells: Role of tissue source and inducing factors, Stem Cell Res. Ther. 1 (2010) 1–9. https://doi.org/10.1186/scrt31.

[245] L. Longobardi, L. O'Rear, S. Aakula, B. Johnstone, K. Shimer, A. Chytil, W.A. Horton, H.L. Moses, A. Spagnoli, Effect of IGF-I in the chondrogenesis of bone marrow mesenchymal stem cells in the presence or absence of TGF-β signaling, J. Bone Miner. Res. 21 (2006) 626–636. https://doi.org/10.1359/jbmr.051213.

[246] M. Ulrich-Vinther, M.D. Maloney, E.M. Schwarz, R. Rosier, R.J. O'Keefe, Articular Cartilage Biology, J. Am. Acad. Orthop. Surg. 11 (2003) 421–430. https://doi.org/10.5435/00124635-200311000-00006.

[247] C. Wernecke, H.J. Braun, J.L. Dragoo, The effect of intra-articular corticosteroids on articular cartilage: A systematic review, Orthop. J. Sport. Med. 3 (2015) 1–7. https://doi.org/10.1177/2325967115581163.

[248] T. Li, B. Liu, K. Chen, Y. Lou, Y. Jiang, D. Zhang, Small molecule compounds promote the proliferation of chondrocytes and chondrogenic differentiation of stem cells in cartilage

tissue engineering, Biomed. Pharmacother. 131 (2020) 110652. https://doi.org/10.1016/j.biopha.2020.110652.

[249] A. Derfoul, G.L. Perkins, D.J. Hall, R.S. Tuan, Glucocorticoids Promote Chondrogenic Differentiation of Adult Human Mesenchymal Stem Cells by Enhancing Expression of Cartilage Extracellular Matrix Genes, Stem Cells. 24 (2006) 1487–1495. https://doi.org/10.1634/stemcells.2005-0415.

[250] L.R. Devireddy, M. Myers, R. Screven, Z. Liu, L. Boxer, A serum-free medium formulation efficiently supports isolation and propagation of canine adipose-derived mesenchymal stem/stromal cells, PLoS One. 14 (2019) 1–21. https://doi.org/10.1371/journal.pone.0210250.

[251] N.N. Shipunova, N.A. Petinati, N.I. Drize, Effect of hydrocortisone on multipotent human mesenchymal stromal cells, Bull. Exp. Biol. Med. 155 (2013) 159–163. https://doi.org/10.1007/s10517-013-2102-8.

[252] J. Wang, D. Elewaut, I. Hoffman, E.M. Veys, G. Verbruggen, Physiological levels of hydrocortisone maintain an optimal chondrocyte extracellular matrix metabolism, Ann. Rheum. Dis. 63 (2004) 61–66. https://doi.org/10.1136/ard.2002.005298.

[253] M.C. Arufe, A. De La Fuente, I. Fuentes, F.J. De Toro, F.J. Blanco, Chondrogenic potential of subpopulations of cells expressing mesenchymal stem cell markers derived from human synovial membranes, J. Cell. Biochem. 111 (2010) 834–845. https://doi.org/10.1002/jcb.22768.

[254] Y. Mifune, T. Matsumoto, S. Murasawa, A. Kawamoto, R. Kuroda, T. Shoji, T. Kuroda, T. Fukui, Y. Kawakami, M. Kurosaka, T. Asahara, Therapeutic superiority for cartilage repair by CD271-positive marrow stromal cell transplantation, Cell Transplant. 22 (2013) 1201–1211. https://doi.org/10.3727/096368912X657378.

[255] T. Rada, R.L. Reis, M.E. Gomes, Distinct Stem Cells Subpopulations Isolated from Human Adipose Tissue Exhibit Different Chondrogenic and Osteogenic Differentiation Potential, Stem Cell Rev. Reports. 7 (2011) 64–76. https://doi.org/10.1007/s12015-010-9147-0.

[256] T. Jiang, W. Liu, X. Lv, H. Sun, L. Zhang, Y. Liu, W.J. Zhang, Y. Cao, G. Zhou, Potent in vitro chondrogenesis of CD105 enriched human adipose-derived stem cells, Biomaterials. 31 (2010) 3564–3571. https://doi.org/10.1016/j.biomaterials.2010.01.050.

[257] B. Gharibi, F.J. Hughes, Effects of Medium Supplements on Proliferation, Differentiation Potential, and In Vitro Expansion of Mesenchymal Stem Cells, Stem Cells Transl. Med. 1 (2012) 771–782. https://doi.org/10.5966/sctm.2010-0031.

[258] S. Hagmann, B. Moradi, S. Frank, T. Dreher, P.W. Kämmerer, W. Richter, T. Gotterbarm, FGF-2 addition during expansion of human bone marrow-derived stromal cells alters MSC surface marker distribution and chondrogenic differentiation potential, Cell Prolif. 46 (2013) 396–407. https://doi.org/10.1111/cpr.12046.

[259] L. Jiang, A. Ma, L. Song, Y. Hu, H. Dun, P. Daloze, Y. Yu, J. Jiang, M. Zafarullah, H. Chen, Cartilage regeneration by selected chondrogenic clonal mesenchymal stem cells in the collagenase-induced monkey osteoarthritis model, J. Tissue Eng. Regen. Med. 8 (2014) 896–905. https://doi.org/10.1002/term.1676.

[260] A.R. Armiento, M.J. Stoddart, M. Alini, D. Eglin, Biomaterials for articular cartilage tissue engineering: Learning from biology, Acta Biomater. 65 (2018) 1–20. https://doi.org/10.1016/J.ACTBIO.2017.11.021.

[261] K.L. Caldwell, J. Wang, Cell-based articular cartilage repair: The link between development and regeneration, Osteoarthr. Cartil. 23 (2015) 351–362. https://doi.org/10.1016/j.joca.2014.11.004.

[262] D. Correa, S.A. Lietman, Articular cartilage repair: Current needs, methods and research directions, Semin. Cell Dev. Biol. 62 (2017) 67–77. https://doi.org/10.1016/j.semcdb.2016.07.013.

[263] A.N. Leberfinger, D.J. Ravnic, A. Dhawan, I.T. Ozbolat, Concise Review: Bioprinting of Stem Cells for Transplantable Tissue Fabrication, Stem Cells Transl. Med. 6 (2017) 1940–1948. https://doi.org/10.1002/sctm.17-0148.

[264] M.E. Candela, R. Yasuhara, M. Iwamoto, M. Enomoto-Iwamoto, Resident mesenchymal progenitors of articular cartilage, Matrix Biol. 39 (2014) 44–49. https://doi.org/10.1016/j.matbio.2014.08.015.

[265] L. Liverani, M.S. Killian, A.R. Boccaccini, Fibronectin functionalized electrospun fibers by using benign solvents: Best way to achieve effective functionalization, Front. Bioeng. Biotechnol. 7 (2019) 1–12. https://doi.org/10.3389/fbioe.2019.00068.

[266] L.A. Bosworth, W. Hu, Y. Shi, S.H. Cartmell, Enhancing Biocompatibility without Compromising Material Properties: An Optimised NaOH Treatment for Electrospun Polycaprolactone Fibres, J. Nanomater. 2019 (2019). https://doi.org/10.1155/2019/4605092.

[267] A.M.J. Getgood, S.J. Kew, R. Brooks, H. Aberman, T. Simon, A.K. Lynn, N. Rushton, Evaluation of early-stage osteochondral defect repair using a biphasic scaffold based on a collagen-glycosaminoglycan biopolymer in a caprine model, Knee. 19 (2012) 422–430. https://doi.org/10.1016/j.knee.2011.03.011.

[268] T.J. Levingstone, A. Ramesh, R.T. Brady, P.A.J. Brama, C. Kearney, J.P. Gleeson, F.J. O'Brien, Cell-free multi-layered collagen-based scaffolds demonstrate layer specific regeneration of functional osteochondral tissue in caprine joints, Biomaterials. 87 (2016) 69–81. https://doi.org/10.1016/j.biomaterials.2016.02.006.

[269] P. Mainil-Varlet, B. Van Damme, D. Nesic, G. Knutsen, R. Kandel, S. Roberts, A new histology scoring system for the assessment of the quality of human cartilage repair: ICRS II, Am. J. Sports Med. 38 (2010) 880–890. https://doi.org/10.1177/0363546509359068.

[270] K.E.M. Benders, P.R. van Weeren, S.F. Badylak, D.B.F. Saris, W.J.A. Dhert, J. Malda, Extracellular matrix scaffolds for cartilage and bone regeneration, Trends Biotechnol. 31 (2013) 169–176. https://doi.org/10.1016/j.tibtech.2012.12.004.

[271] A.M. Yousefi, M.E. Hoque, R.G.S.V. Prasad, N. Uth, Current strategies in multiphasic scaffold design for osteochondral tissue engineering: A review, J. Biomed. Mater. Res. - Part A. 103 (2015) 2460–2481. https://doi.org/10.1002/jbm.a.35356.

[272] L. Vikingsson, M. Sancho-Tello, A. Ruiz-Saurí, S.M. Díaz, J.A. Gómez-Tejedor, G.G. Ferrer, C. Carda, J.C. Monllau, J.L.G. Ribelles, Implantation of a Polycaprolactone Scaffold with Subchondral Bone Anchoring Ameliorates Nodules Formation and Other Tissue Alterations, Int. J. Artif. Organs. 38 (2015) 659–666. https://doi.org/10.5301/ijao.5000457.

[273] F.G. Lyons, A.A. Al-Munajjed, S.M. Kieran, M.E. Toner, C.M. Murphy, G.P. Duffy, F.J. O'Brien, The healing of bony defects by cell-free collagen-based scaffolds compared to stem cell-seeded tissue engineered constructs, Biomaterials. 31 (2010) 9232–9243. https://doi.org/10.1016/j.biomaterials.2010.08.056.

[274] C. Scotti, E. Piccinini, H. Takizawa, A. Todorov, P. Bourgine, A. Papadimitropoulos, A. Barbero, M.G. Manz, I. Martin, Engineering of a functional bone organ through endochondral ossification, Proc. Natl. Acad. Sci. 110 (2013) 3997–4002. https://doi.org/10.1073/pnas.1220108110.

[275] A. Muraglia, A. Corsi, M. Riminucci, M. Mastrogiamcomo, R. Cancedda, P. Bianco, R. Quarto, Formation of a chondro-osseous rudiment in micromass cultures of human bone-marrow stromal cells, J. Cell Sci. 116 (2003) 2949–2955. https://doi.org/10.1242/jcs.00527.

[276] K. Futrega, J.S. Palmer, M. Kinney, W.B. Lott, M.D. Ungrin, P.W. Zandstra, M.R. Doran, The microwell-mesh: A novel device and protocol for the high throughput manufacturing of cartilage microtissues, Biomaterials. 62 (2015) 1–12. https://doi.org/10.1016/j.biomaterials.2015.05.013.

[277] P.B. Malafaya, R.L. Reis, Bilayered chitosan-based scaffolds for osteochondral tissue engineering: Influence of hydroxyapatite on in vitro cytotoxicity and dynamic bioactivity studies in a specific double-chamber bioreactor, Acta Biomater. 5 (2009) 644–660. https://doi.org/10.1016/j.actbio.2008.09.017.

[278] D. Wendt, M. Jakob, I. Martin, Bioreactor-based engineering of osteochondral grafts: From model systems to tissue manufacturing, J. Biosci. Bioeng. 100 (2005) 489–494. https://doi.org/10.1263/jbb.100.489.

[279] Y. Pei, J.J. Fan, X.Q. Zhang, Z.Y. Zhang, M. Yu, Repairing the osteochondral defect in goat with the tissue-engineered osteochondral graft preconstructed in a double-chamber stirring bioreactor, Biomed Res. Int. 2014 (2014). https://doi.org/10.1155/2014/219203.

[280] X. guo Liu, H. kui Jiang, Preparation of an osteochondral composite with mesenchymal stem cells as the single-cell source in a double-chamber bioreactor, Biotechnol. Lett. 35 (2013) 1645–1653. https://doi.org/10.1007/s10529-013-1248-9.

[281] N. Mahmoudifar, P.M. Doran, Osteogenic differentiation and osteochondral tissue engineering using human adipose-derived stem cells, Biotechnol. Prog. 29 (2013) 176–185. https://doi.org/10.1002/btpr.1663.

[282] B. Ayan, D.N. Heo, Z. Zhang, M. Dey, A. Povilianskas, C. Drapaca, I.T. Ozbolat, Aspiration-assisted bioprinting for precise positioning of biologics, Sci. Adv. 6 (2020) 1–17. https://doi.org/10.1126/sciadv.aaw5111.

[283] M.B. Goldring, S.R. Goldring, Articular cartilage and subchondral bone in the pathogenesis of osteoarthritis, in: Ann. N. Y. Acad. Sci., Wiley/Blackwell (10.1111), 2010: pp. 230–237. https://doi.org/10.1111/j.1749-6632.2009.05240.x.

[284] A.H. Gomoll, H. Madry, G. Knutsen, N. van Dijk, R. Seil, M. Brittberg, E. Kon, The subchondral bone in articular cartilage repair: Current problems in the surgical management, Knee Surgery, Sport. Traumatol. Arthrosc. 18 (2010) 434–447. https://doi.org/10.1007/s00167-010-1072-x.

[285] W. Zhang, Q. Lian, D. Li, K. Wang, D. Hao, W. Bian, J. He, Z. Jin, Cartilage repair and subchondral bone migration using 3d printing osteochondral composites: A one-year-period study in rabbit trochlea, Biomed Res. Int. 2014 (2014). https://doi.org/10.1155/2014/746138.

[286] J. Nulty, R. Burdis, D.J. Kelly, Biofabrication of Prevascularised Hypertrophic Cartilage Microtissues for Bone Tissue Engineering, Front. Bioeng. Biotechnol. 9 (2021) 1–16. https://doi.org/10.3389/fbioe.2021.661989.

[287] R.V. Bolaños, M. Castilho, J. De Grauw, S. Cokelaere, S. Plomp, J. Groll, P.R. Van Weeren, U. Gbureck, J. Malda, Long-Term in Vivo Performance of Low-Temperature 3D-Printed Bioceramics in an Equine Model, ACS Biomater. Sci. Eng. 6 (2020) 1681–1689. https://doi.org/10.1021/acsbiomaterials.9b01819.

[288] P. Diloksumpan, R.V. Bolaños, S. Cokelaere, B. Pouran, J. de Grauw, M. van Rijen, R. van Weeren, R. Levato, J. Malda, Orthotopic Bone Regeneration within 3D Printed Bioceramic Scaffolds with Region-Dependent Porosity Gradients in an Equine Model, Adv. Healthc. Mater. 9 (2020) 1–11. https://doi.org/10.1002/adhm.201901807.

[289] P. Diloksumpan, M. ne De Ruijter, M. Castilho, U. Gbureck, T. Vermonden, P.R. Van Weeren, J. Malda, R. Levato, Combining multi-scale 3D printing technologies to engineer reinforced hydrogel-ceramic interfaces, Biofabrication. 12 (2020). https://doi.org/10.1088/1758-5090/ab69d9.

[290] R.L. Mauck, C.C.B. Wang, E.S. Oswald, G.A. Ateshian, C.T. Hung, The role of cell seeding density and nutrient supply for articular cartilage tissue engineering with deformational loading, Osteoarthr. Cartil. 11 (2003) 879–890. https://doi.org/10.1016/j.joca.2003.08.006.

[291] M. Maredziak, K. Marycz, K.A. Tomaszewski, K. Kornicka, B.M. Henry, The Influence of Aging on the Regenerative Potential of Human Adipose Derived Mesenchymal Stem Cells, Stem Cells Int. 2016 (2016). https://doi.org/10.1155/2016/2152435.

[292] M.S. Choudhery, M. Badowski, A. Muise, J. Pierce, D.T. Harris, Donor age negatively impacts adipose tissue-derived mesenchymal stem cell expansion and differentiation, J. Transl. Med. 12 (2014) 1–14. https://doi.org/10.1186/1479-5876-12-8.

[293] J.M. Murphy, K. Dixon, S. Beck, D. Fabian, A. Feldman, F. Barry, Reduced chondrogenic and adipogenic activity of mesenchymal stem cells from patients with advanced osteoarthritis, Arthritis Rheum. 46 (2002) 704–713. https://doi.org/10.1002/art.10118.

[294] A.I. Hoch, J.K. Leach, Concise Review: Optimizing Expansion of Bone Marrow Mesenchymal Stem/Stromal Cells for Clinical Applications, Stem Cells Transl. Med. 4 (2015) 412–412. https://doi.org/10.5966/sctm.2013-0196erratum.

[295] E. Kozhemyakina, M. Zhang, A. Ionescu, U.M. Ayturk, N. Ono, A. Kobayashi, H. Kronenberg, M.L. Warman, A.B. Lassar, Identification of a Prg4-expressing articular cartilage progenitor cell population in mice, Arthritis Rheumatol. 67 (2015) 1261–1273. https://doi.org/10.1002/art.39030.

[296] G.P. Dowthwaite, J.C. Bishop, S.N. Redman, I.M. Khan, P. Rooney, D.J.R. Evans, L. Haughton, Z. Bayram, S. Boyer, B. Thomson, M.S. Wolfe, C.W. Archer, The surface of articular cartilage contains a progenitor cell population, J. Cell Sci. 117 (2004) 889–897. https://doi.org/10.1242/jcs.00912.

[297] D. Seol, D.J. McCabe, H. Choe, H. Zheng, Y. Yu, K. Jang, M.W. Walter, A.D. Lehman, L. Ding, J.A. Buckwalter, J.A. Martin, Chondrogenic progenitor cells respond to cartilage injury, Arthritis Rheum. 64 (2012) 3626–3637. https://doi.org/10.1002/art.34613.

[298] A.C. Daly, F.E. Freeman, T. Gonzalez-Fernandez, S.E. Critchley, J. Nulty, D.J. Kelly, 3D Bioprinting for Cartilage and Osteochondral Tissue Engineering, Adv. Healthc. Mater. 6 (2017) 1–20. https://doi.org/10.1002/adhm.201700298.

[299] D.W. Jackson, H.M. Aberman, D.H. Kunishima, T.M. Simon, Surface Restoration of Large Medial Femoral Condyle Articular Cartilage Lesions using a Laminated Polymer Plug - An Experimental Study in Goats, 2001. https://www.ors.org/Transactions/50/0672.pdf

(accessed September 7, 2018).

[300] K.C. Wong, P. Scheinemann, Additive manufactured metallic implants for orthopaedic applications, Sci. China Mater. 61 (2018) 440–454. https://doi.org/10.1007/s40843-017-9243-9.

[301] Y. Katsuura, S.A. Qureshi, Additive Manufacturing for Metal Applications in Orthopaedic Surgery, J. Am. Acad. Orthop. Surg. 28 (2020) E349–E355. https://doi.org/10.5435/JAAOS-D-19-00420.

[302] E.B. Hunziker, Articular cartilage repair: Basic science and clinical progress. A review of the current status and prospects, Osteoarthr. Cartil. 10 (2002) 432–463. https://doi.org/10.1053/joca.2002.0801.

[303] H.D. Adkisson, J.A. Martin, R.L. Amendola, C. Milliman, K.A. Mauch, A.B. Katwal, M. Seyedin, A. Amendola, P.R. Streeter, J.A. Buckwalter, The Potential of Human Allogeneic Juvenile Chondrocytes for Restoration of Articular Cartilage, Am. J. Sports Med. 38 (2010) 1324–1333. https://doi.org/10.1177/0363546510361950.

[304] J.M. Pestka, H. Schmal, G. Salzmann, J. Hecky, N.P. Südkamp, P. Niemeyer, In vitro cell quality of articular chondrocytes assigned for autologous implantation in dependence of specific patient characteristics, Arch. Orthop. Trauma Surg. 131 (2011) 779–789. https://doi.org/10.1007/s00402-010-1219-8.

[305] E.D. Aldrich, X. Cui, C.A. Murphy, K.S. Lim, G.J. Hooper, C.W. McIlwraith, T.B.F. Woodfield, Allogeneic mesenchymal stromal cells for cartilage regeneration: A review of in vitro evaluation, clinical experience, and translational opportunities, Stem Cells Transl. Med. (2021) 1–16. https://doi.org/10.1002/sctm.20-0552.

[306] D. a Grande, M.I. Pitman, L. Peterson, D. Menche, M. Klein, The repair of experimentally produced defects in rabbit articular cartilage by autologous chondrocyte transplantation, J. Orthop. Res. 7 (2005) 208–218. https://doi.org/10.1002/jor.1100070208.

[307] X. Nie, Y.J. Chuah, W. Zhu, P. He, Y. Peck, D.A. Wang, Decellularized tissue engineered hyaline cartilage graft for articular cartilage repair, Biomaterials. 235 (2020) 119821. https://doi.org/10.1016/j.biomaterials.2020.119821.

[308] S.J. Gilbert, C.S. Bonnet, P. Stadnik, V.C. Duance, D.J. Mason, E.J. Blain, Inflammatory and degenerative phases resulting from anterior cruciate rupture in a non-invasive murine model of post-traumatic osteoarthritis, J. Orthop. Res. 36 (2018) 2118–2127. https://doi.org/10.1002/jor.23872.

[309] P. Patwari, M.N. Cook, M.A. DiMicco, S.M. Blake, I.E. James, S. Kumar, A.A. Cole, M.W. Lark, A.J. Grodzinsky, Proteoglycan degradation after injurious compression of bovine and human articular cartilage in vitro: Interaction with exogenous cytokines, Arthritis Rheum. 48 (2003) 1292–1301. https://doi.org/10.1002/art.10892.

[310] M. Kondo, K. Yamaoka, K. Sonomoto, S. Fukuyo, K. Oshita, Y. Okada, Y. Tanaka, IL-17 inhibits chondrogenic differentiation of human mesenchymal stem cells, PLoS One. 8 (2013). https://doi.org/10.1371/journal.pone.0079463.

[311] S.L. Francis, C. Di Bella, G.G. Wallace, P.F.M. Choong, Cartilage Tissue Engineering Using Stem Cells and Bioprinting Technology—Barriers to Clinical Translation, Front. Surg. 5 (2018) 1–12. https://doi.org/10.3389/fsurg.2018.00070.

[312] K. Bieback, A. Hecker, A. Kocaömer, H. Lannert, K. Schallmoser, D. Strunk, H. Klüter, Human alternatives to fetal bovine serum for the expansion of mesenchymal stromal cells from

bone marrow, Stem Cells. 27 (2009) 2331–2341. https://doi.org/10.1002/stem.139.

[313] K. Schallmoser, C. Bartmann, E. Rohde, A. Reinisch, K. Kashofer, E. Stadelmeyer, C. Drexler, G. Lanzer, W. Linkesch, D. Strunk, Human platelet lysate can replace fetal bovine serum for clinical-scale expansion of functional mesenchymal stromal cells, Transfusion. 47 (2007) 1436–1446. https://doi.org/10.1111/j.1537-2995.2007.01220.x.

[314] H. Hemeda, B. Giebel, W. Wagner, Evaluation of human platelet lysate versus fetal bovine serum for culture of mesenchymal stromal cells, Cytotherapy. 16 (2014) 170–180. https://doi.org/10.1016/j.jcyt.2013.11.004.

[315] B. Lindroos, S. Boucher, L. Chase, H. Kuokkanen, H. Huhtala, R. Haataja, M. Vemuri, R. Suuronen, S. Miettinen, Serum-free, xeno-free culture media maintain the proliferation rate and multipotentiality of adipose stem cells in vitro, Cytotherapy. 11 (2009) 958–972. https://doi.org/10.3109/14653240903233081.

[316] L.G. Chase, U. Lakshmipathy, L.A. Solchaga, M.S. Rao, M.C. Vemuri, A novel serum-free medium for the expansion of human mesenchymal stem cells, Stem Cell Res. Ther. 1 (2010) 1–11. https://doi.org/10.1186/scrt8.

[317] P. Warnke, I. Springer, P.J. Wiltfang, P.Y. Acil, P.H. Eufinger, M. Wehmöller, P. Russo, H. Bolte, E. Sherry, E. Behrens, P.H. Terheyden, Growth and transplantation of a custom vascularised bone graft in a man, Lancet. 364 (2004) 766–770. https://doi.org/10.1016/S0140-6736(04)16935-3.

[318] M.M. Stevens, R.P. Marini, D. Schaefer, J. Aronson, R. Langer, V.P. Shastri, In vivo engineering of organs: The bone bioreactor, Proc. Natl. Acad. Sci. 102 (2005) 11450–11455. https://doi.org/10.1073/pnas.0504705102.

[319] A. Kaempfen, A. Todorov, S. Güven, R.D. Largo, C. Jaquiéry, A. Scherberich, I. Martin, D.J. Schaefer, Engraftment of prevascularized, tissue engineered constructs in a novel rabbit segmental bone defect model, Int. J. Mol. Sci. 16 (2015) 12616–12630. https://doi.org/10.3390/ijms160612616.

[320] J. Wiltfang, M. Rohnen, J.H. Egberts, U. Lützen, H. Wieker, Y. Açil, H. Naujokat, Man as a Living Bioreactor: Prefabrication of a Custom Vascularized Bone Graft in the Gastrocolic Omentum, Tissue Eng. - Part C Methods. 22 (2016) 740–746. https://doi.org/10.1089/ten.tec.2015.0501.

[321] A.M. Tatara, S.R. Shah, N. Demian, T. Ho, J. Shum, J.J.J.P. van den Beucken, J.A. Jansen, M.E. Wong, A.G. Mikos, Reconstruction of large mandibular defects using autologous tissues generated from in vivo bioreactors, Acta Biomater. 45 (2016) 72–84. https://doi.org/10.1016/j.actbio.2016.09.013.

[322] R.L. Huang, E. Kobayashi, K. Liu, Q. Li, Bone Graft Prefabrication Following the In Vivo Bioreactor Principle, EBioMedicine. 12 (2016) 43–54. https://doi.org/10.1016/j.ebiom.2016.09.016.

[323] P.J. Emans, L.W. van Rhijn, T.J.M. Welting, A. Cremers, N. Wijnands, F. Spaapen, J.W. Voncken, V.P. Shastri, Autologous engineering of cartilage, Proc. Natl. Acad. Sci. 107 (2010) 3418–3423. https://doi.org/10.1073/pnas.0907774107.

[324] S.F. Carroll, C.T. Buckley, D.J. Kelly, Measuring and Modeling Oxygen Transport and Consumption in 3D Hydrogels Containing Chondrocytes and Stem Cells of Different Tissue Origins, Front. Bioeng. Biotechnol. 9 (2021) 1–14. https://doi.org/10.3389/fbioe.2021.591126.

[325] H. Lin, T.P. Lozito, P.G. Alexander, R. Gottardi, R.S. Tuan, Stem cell-based microphysiological osteochondral system to model tissue response to interleukin-1B, Mol. Pharm. 11 (2014) 2203–2212. https://doi.org/10.1021/mp500136b.

[326] P. Occhetta, A. Mainardi, E. Votta, Q. Vallmajo-Martin, M. Ehrbar, I. Martin, A. Barbero, M. Rasponi, Hyperphysiological compression of articular cartilage induces an osteoarthritic phenotype in a cartilage-on-a-chip model, Nat. Biomed. Eng. 3 (2019) 545–557. https://doi.org/10.1038/s41551-019-0406-3.

[327] H. Zirath, M. Rothbauer, S. Spitz, B. Bachmann, C. Jordan, B. Müller, J. Ehgartner, E. Priglinger, S. Mühleder, H. Redl, W. Holnthoner, M. Harasek, T. Mayr, P. Ertl, Every breath you take: Non-invasive real-time oxygen biosensing in two- and three-dimensional microfluidic cell models, Front. Physiol. 9 (2018) 1–12. https://doi.org/10.3389/fphys.2018.00815.

[328] L. Figueiredo, R. Pace, C. D'Arros, G. Réthoré, J. Guicheux, C. Le Visage, P. Weiss, Assessing glucose and oxygen diffusion in hydrogels for the rational design of 3D stem cell scaffolds in regenerative medicine, J. Tissue Eng. Regen. Med. 12 (2018) 1238–1246. https://doi.org/10.1002/term.2656.

[329] J. Malda, J. Rouwkema, D.E. Martens, E.P. Comte, F.K. Kooy, J. Tramper, C.A. Van Blitterswijk, J. Riesle, Oxygen Gradients in Tissue-Engineered PEGT / PBT Cartilaginous Constructs : Measurement and Modeling, Biotechnol. Bioeng. 86 (2004) 9–18. https://doi.org/10.1002/bit.20038.

[330] E.E. McDonnell, C.T. Buckley, Investigating the physiological relevance of ex vivo disc organ culture nutrient microenvironments using in silico modeling and experimental validation, JOR Spine. 4 (2021) 1–16. https://doi.org/10.1002/jsp2.1141.

[331] R.J. Nims, A.D. Cigan, M.B. Albro, G. Vunjak-Novakovic, C.T. Hung, G.A. Ateshian, Matrix Production in Large Engineered Cartilage Constructs Is Enhanced by Nutrient Channels and Excess Media Supply, 2015. https://doi.org/10.1089/ten.tec.2014.0451.